

Cytochrome P450 2J2: Potential role in drug metabolism and cardiotoxicity

Thesis submitted for the degree of

Doctor of Philosophy

at the University of Leicester

By

Meetal Solanki BSc (Hons)

Department of Cardiovascular Sciences

University of Leicester

2018



UNIVERSITY OF
LEICESTER

Abstract

Drug-induced cardiotoxicity may be modulated by protective endogenous arachidonic acid (AA) derived metabolites known as epoxyeicosatrienoic acids (EETs) synthesised by cytochrome P450 2J2 (CYP2J2). In addition, CYP2J2 metabolises both exogenous and endogenous substrates and is involved in phase I metabolism of a variety of structurally diverse compounds. This project addresses the hypothesis that CYP2J2 influences drug-induced cardiotoxicity through potentially conflicting effects on the production of protective EETs and metabolism of drugs.

An *in vitro* model was established in human cardiac myocytes and EA.hy926 cells which was shown to be good predictor of astemizole drug toxicity. sEH inhibitor t-AUCB and exogenous EETs protected cells from toxicity and CYP2J2 inhibitor, MSSPOH and the PLA₂ inhibitors quinacrine dihydrochloride and LY311727 also showed a preservation of or an increase in ATP in toxicity compared to cells treated with astemizole alone. Expression of CYP2J2 and sEH was present in both cell types with higher expression in HCM. Astemizole increased CYP2J2 and decreased sEH gene expression. MSSPOH or t-AUCB in conjunction with astemizole modulated gene and protein expression of both enzymes. Investigation of astemizole metabolism by CYP2J2 showed concentration dependent metabolism to its o-demethylated product which was inhibited by endogenous CYP2J2 substrate AA in a recombinant bactosome system. Further study into the mechanism of astemizole toxicity showed a concentration dependent increase in exosomes compared to the non-toxic drug loratadine.

This data suggests that CYP2J2 may protect in *in vitro* drug induced toxicity and changes in the expression or activity of this enzyme may alter drug and EET concentrations leading to modulation of drug induced toxicity. Understanding more widely the role and possible protection by CYP2J2 in the heart is worthy of further study.

Acknowledgements

I would like to thank my supervisors Dr Karl E. Herbert, Dr Don Jones, Dr Amy Pointon and Dr Barry Jones for their guidance, support and enthusiasm throughout this entire project.

I am particularly grateful to Laurence Hall for his assistance in designing primers for PCR, Dr Rajinder Singh for his assistance with mass-spectrometry and Dr Marcin Wozniak for his help with the Nanosight machine.

I would like to give a special thanks to my colleagues both past and present and my friends and family for their support and encouragement.

Table of Contents

| | |
|---|-----|
| Abstract..... | i |
| Acknowledgements..... | ii |
| Table of Contents..... | iv |
| Table of figures..... | ix |
| Table of tables..... | xii |
| List of abbreviations | 1 |
| Chapter 1 Introduction..... | 1 |
| 1.1 Role of CYP2J2 in cardiovascular biology..... | 3 |
| 1.2 Genetic variation in human CYP2J2..... | 1 |
| 1.3 CYP2J2/EETs in the maintenance of cardiovascular health- a potential role in cardiotoxicity? | 3 |
| 1.3.1 Vascular Inflammation | 3 |
| 1.3.2 Vascular tone | 4 |
| 1.3.3 Ischaemia reperfusion injury | 5 |
| 1.3.4 Cardiac Hypertrophy..... | 6 |
| 1.4 Animal homologues of CYP2J2 to investigate pre-clinical drug-induced cardiotoxicity | 6 |
| 1.4.1 The disadvantages of using animals and advantages of <i>in vitro</i> models .. | 10 |
| 1.4.2 Current <i>in vitro</i> models for drug testing | 12 |
| 1.5 Role of CYP2J2 in xenobiotic metabolism..... | 13 |
| 1.6 Modulation of CYP2J2 activity by drugs..... | 18 |
| 1.7 Potential role of EETs in mitigating drug induced cardiotoxicity | 19 |
| CYP2J2 substrate..... | 20 |
| FDA approval package cardiac warnings | 20 |
| Mechanism contributing to cardiotoxicity..... | 20 |

| | |
|---|----|
| Circumstantial evidence for mitigation of cardiotoxicity by EETs | 20 |
| 1.8 Role of CYP2J2 in doxorubicin induced cardiotoxicity | 21 |
| 1.9 The search for the ideal cell type for <i>in vitro</i> cardiotoxicity testing | 25 |
| 1.9.1 HepG2 cells..... | 25 |
| 1.9.2 iPSC-CMs | 26 |
| 1.9.3 Human cardiac myocytes..... | 27 |
| 1.9.4 EA.hy926 cells..... | 28 |
| 1.10 Candidate cardiotoxic drugs | 28 |
| 1.10.1 Astemizole | 28 |
| 1.10.2 Doxorubicin | 29 |
| 1.10.3 Sunitinib..... | 31 |
| 1.11 Pharmacological inhibitors of the EET pathway..... | 33 |
| 1.11.1 MS-PPOH | 33 |
| 1.11.2 Quinacrine..... | 34 |
| 1.11.3 LY311727 | 35 |
| 1.12 Pharmacological facilitators of the EET pathway | 35 |
| 1.12.1 t-AUCB..... | 35 |
| 1.13 Conclusions | 36 |
| Chapter 2 Hypothesis and Aims | 38 |
| Chapter 3 Materials and Methods..... | 39 |
| 3.1 Cell culture and treatment reagents..... | 39 |
| 3.1.1 Cell lines and primary cells | 39 |
| 3.1.2 Cell culture and treatment method..... | 41 |
| 3.1.3 Treatments | 44 |
| 3.1.4 Markers of cell viability..... | 44 |
| 3.1.5 Molecular biology techniques..... | 50 |
| 3.1.6 Metabolomics..... | 65 |

| | | |
|-----------|--|-----|
| 3.1.7 | Isolation and quantification of exosomes by Nanosight..... | 68 |
| 3.2 | Equipment | 69 |
| Chapter 4 | Establishing an <i>in vitro</i> cell model to investigate the role of Cytochrome P450 2J2 in drug cardiotoxicity | 70 |
| 4.1 | Background | 71 |
| 4.1.1 | A suitable cell model to investigate the role of CYP2J2 in drug cardiotoxicity | 71 |
| 4.2 | Aims | 71 |
| 4.3 | Results | 72 |
| 4.3.1 | Concentration response of a panel of a drugs to relevant cell types..... | 72 |
| 4.3.2 | Concentration and time dependent toxicity response: astemizole..... | 75 |
| 4.3.3 | Effect of EET synthesis inhibitors on astemizole toxicity..... | 77 |
| 4.3.4 | Effect PLA ₂ and CYP2J2 inhibitors on astemizole toxicity in EA.hy926 cells and human cardiac myocytes..... | 79 |
| 4.3.5 | Effect of EET facilitators on astemizole toxicity..... | 86 |
| 4.4 | Discussion | 90 |
| Chapter 5 | Investigating the molecular mechanism of EET protection against astemizole induced toxicity | 94 |
| 5.1 | Background | 95 |
| 5.2 | Aims | 96 |
| 5.3 | Results..... | 97 |
| 5.3.1 | Expression of sEH in EA.hy926 and the human cardiac myocyte cell line | 97 |
| 5.3.2 | Effect of astemizole on sEH mRNA and protein expression..... | 101 |
| 5.3.3 | Effect of sEH and CYP epoxygenase inhibition on sEH mRNA and protein expression | 102 |
| 5.3.4 | Effect of sEH knockdown on astemizole-induced cytotoxicity in EA.hy926 cells..... | 105 |
| 5.4 | Discussion | 107 |

| | | |
|-----------|---|-----|
| Chapter 6 | Investigating the possible role of cytochrome P450 2J2 in astemizole induced cytotoxicity..... | 111 |
| 6.1 | Background | 112 |
| 6.2 | Aims | 114 |
| 6.3 | Results | 115 |
| 6.3.1 | Expression of CYP2J2 mRNA in EA.hy926 cells and human cardiac myocytes: expression studies with TaqMan and SYBR Green qPCR..... | 115 |
| 6.3.2 | Effect of astemizole on CYP2J2 mRNA expression | 118 |
| 6.3.3 | Effect of sEH and CYP epoxygenase inhibitors on expression of CYP2J2 mRNA and protein..... | 120 |
| 6.3.4 | Optimisation of siRNA knockdown of CYP2J2 mRNA | 122 |
| 6.3.5 | Effect of knockdown of CYP2J2 mRNA and CYP2J2 and sEH inhibitors on astemizole-induced cytotoxicity | 123 |
| 6.3.6 | Metabolism of astemizole by cells and recombinant CYP2J2 | 125 |
| 6.3.7 | Metabolism of astemizole by recombinant CYP2J2 in bacosomes..... | 125 |
| 6.4 | Discussion | 127 |
| Chapter 7 | Investigation of biomarkers of astemizole induced cardiotoxicity..... | 132 |
| 7.1 | Background | 133 |
| 7.2 | Aims | 135 |
| 7.3 | Results | 135 |
| 7.3.1 | The effect of serum free media on EA.hy926 cells treated with astemizole | 135 |
| 7.3.2 | The effect of serum free media on EA.hy926 cells treated with doxorubicin | 140 |
| 7.3.3 | The effect of serum free media on EA.hy926 cells treated with loratadine | 145 |
| 7.4 | Discussion | 148 |
| Chapter 8 | General discussion and future work..... | 151 |

| | | |
|-----|--|-----|
| 8.1 | EA.hy926 cells and human cardiac myocytes (HCM) as an <i>in vitro</i> model to study the cellular effects of drug toxicity | 151 |
| 8.2 | Mechanism of CYP2J2/ EETs in regulating astemizole induced toxicity | 154 |
| 8.3 | Exosomes and future biomarkers of drug induced cardiotoxicity | 155 |
| | Bibliography | 156 |

Table of figures

| | |
|---|----|
| Figure 1-1 Overview of hypothesised CYP2J2 functions in the heart. | 2 |
| Figure 1-2 Relative mRNA expression of CYPs in human cardiomyocytes and human heart tissue and cardiomyocytes. | 4 |
| Figure 1-3 The formation of EETs by CYP2J2. | 6 |
| Figure 1-4 <i>In vitro</i> cardiotoxicity approaches within the drug development pipeline.... | 11 |
| Figure 1-5 Table showing the common causes of attrition. | 12 |
| Figure 1-6 Chromatographic data showing the differences in products formed by recombinant CYP3A4 and CYP2J2. | 17 |
| Figure 1-7 Chemical structure of astemizole (Alghamdi, 2008) | 29 |
| Figure 1-8 Chemical structure of doxorubicin (Senes-Lopes et al., 2018)..... | 31 |
| Figure 1-9 Chemical structure of sunitinib malate (Hao and Sadek, 2016) | 33 |
| Figure 1-10 Chemical structure of MS-PPOH (Campbell and Fleming, 2010) | 34 |
| Figure 1-11 Chemical structure of quinacrine dihydrochloride (image courtesy of CAMEO online)..... | 34 |
| Figure 1-12 Chemical structure of LY311727 (Om, 2018)..... | 35 |
| Figure 1-13 Chemical structure of t-AUCB (Iyer et al., 2012)..... | 36 |
| Figure 3-1 The format of a haemocytometer. | 42 |
| Figure 3-2 Timeline showing how iPS-CMs are cultured. | 44 |
| Figure 3-3 Brief diagram showing the reaction to produce luminescence, proportional to caspase 3/7 activity. | 46 |
| Figure 3-4 Mechanism of detection of viable cells using the MT cell viability substrate. | 48 |
| Figure 3-5 Leaked LDH from damaged cells react with lactate and NAD^+ to create Pyruvate and NADH. | 49 |
| Figure 3-6 A typical nanodrop graph plot showing the significance of the peaks in the purity of the RNA | 53 |
| Figure 3-7 Procedure for metabolite isolation from cultured cells. | 66 |
| Figure 4-1 Effect of cardiotoxic compounds on ATP levels in HepG2 cells (A-C) and iPSC-CMs (D-F). | 74 |
| Figure 4-2 Effect of astemizole on ATP levels in EA.hy926 cells and HCM after incubation at 3 time points. | 76 |

Figure 4-3 Effect of Quinacrine dihydrochloride (A,D), MSPPOH (B,E) and LY311727 (C,F) on cell viability..... 78

Figure 4-4 Effect of CYP epoxygenase inhibitor MSPPOH and PLA2 inhibitors quinacrine dihydrochloride and LY311727 on astemizole toxicity (ATP). 80

Figure 4-5 Investigation of the effect of LY311727 on ATP reagent luminescence..... 81

Figure 4-6 Effect of CYP epoxygenase inhibitor MSPPOH and PLA2 inhibitors quinacrine dihydrochloride and LY311727 on astemizole toxicity (Caspase 3/7)..... 82

Figure 4-7 Effect of CYP epoxygenase inhibitor MSPPOH and PLA2 inhibitors quinacrine dihydrochloride and LY311727 on astemizole toxicity measured using the MTS assay in EA.hy926 cells..... 83

Figure 4-8 The effect of different concentrations of astemizole on cell viability through Hoechst 33342 staining..... 84

Figure 4-9 Effect of inhibitors of the EET pathway on astemizole toxicity..... 85

Figure 4-10 Effect of sEH inhibitor t-AUCB on astemizole toxicity assessed by measuring ATP concentrations..... 87

Figure 4-11 Effect of sEH inhibition on cell viability after astemizole treatment. 88

Figure 4-12 Effect of exogenous EETs on astemizole toxicity in EA.hy926 cells. 89

Figure 4-13 Proposed mechanism for how the CYP2J2/EET pathway may play a role in astemizole related cell death. 91

Figure 5-1. PCR products were amplified using gradient gel PCR as described in section 3.3.4. 98

Figure 5-2 Validation of primers designed to housekeepers using gradient gel PCR. ... 99

Figure 5-3 Expression of sEH mRNA in EA.hy926 cells and HCM as determined by qPCR with SYBR green detection..... 100

Figure 5-4 Gene expression of sEH in EA.hy926 cells (A,B) and HCM (D,E) after treatment with 25µM astemizole for 6h (A,D) and 24h (B,E)..... 101

Figure 5-5 Expression of sEH in EA.hy926 cells (A and B) and human cardiac myocytes (HCM) (C and D) after treatment with 25 µM astemizole and/or inhibitors for 6 hr. 104

Figure 5-6 sEH gene and protein expression via RT-PCR and western blot in EA.hy926 cells. 105

Figure 5-7 Effect of sEH knockdown and sEH and CYP2J2 inhibitor on astemizole induced cytotoxicity..... 106

Figure 6-1 Expression of CYP2J2 mRNA in EA.hy926 cells and HCM as determined by qPCR with TaqMan and SYBR green detection. 116

Figure 6-2 TaqMan PCR amplification. 117

Figure 6-3 PCR products were amplified using gradient PCR and run on a gel as described in 3.1.5.3 118

Figure 6-4 mRNA expression of CYP2J2 in EA.hy926 cells (A,B) and HCM (D,E) after treatment with 25µM astemizole for 6h (A,D) and 24h (B,E)..... 119

Figure 6-5 Expression of CYP2J2 mRNA in EA.hy926 cells (A and B) and human cardiac myocytes (HCM) (C and D) after treatment with 25 µM astemizole and/or inhibitors for 6 hr. 121

Figure 6-6 CYP2J2 mRNA knockdown in EA.hy926 cells. 122

Figure 6-7 Effect of CYP2J2 knockdown and sEH and CYP2J2 inhibitors on astemizole-induced cytotoxicity. 124

Figure 6-8 Metabolism of astemizole by EA.hy926 cells. 126

Figure 6-9 Metabolism of astemizole by recombinant CYP2J2 bacosomes. 126

Figure 6-10 EA.hy926 cells treated with cell death siRNA after 3 days. X100 magnification. 129

Figure 7-1 The effect of serum free media on EA.hy926 cells..... 136

Figure 7-2 The effect of astemizole on EA.hy926 cell viability 137

Figure 7-3 Particle size distribution (A) and particle concentration (B) in cells treated with varying concentrations of astemizole for 24hr. 138

Figure 7-4 Particle size distribution and particle concentration in cells treated with astemizole and untreated EA.hy926 cells. 140

Figure 7-5 The effect of doxorubicin on EA.hy926 cell viability 141

Figure 7-6 Particle size distribution (A) and particle concentration (B) in cells treated with varying concentrations of doxorubicin for 24hr. 142

Figure 7-7 Particle size distribution and particle concentration in cells treated with dox and untreated EA.hy926 cells. 145

Figure 7-8 The effect of loratadine on EA.hy926 cells over different concentrations at 24hr. 146

Figure 7-9 Particle size distribution (A) and particle concentration (B) in cells treated with varying concentrations of loratadine for 24hr. 147

Figure 8-1 High content biology used to analyse structure and function. 153

Table of tables

| | |
|---|----|
| Table 1-1 Families of human P450 enzymes, thier function and thier association with disease with a particular emphasis on heart failure. N/D – not detected. | 1 |
| Table 1-2 CYP2J2 allelic variations in humans known to have changes in activity <i>in vitro</i> | 2 |
| Table 1-3 Amino acid sequence homology between human CYP2J2 and mammalian CYP2Js. | 7 |
| Table 1-4 CYP2J gene expressions in human and other mammalian tissues. | 8 |
| Table 1-5 The range of substrates for CYP2J2 and the metabolic pathways by which they are formed. | 15 |
| Table 1-6 Proposed mechanisms of protection by EETs against selected cardiotoxic drugs. | 20 |
| Table 1-7 CYP2J2 next generation sequencing data | 27 |
| Table 3-1 The components required to make 10ml of a standard reaction solution. | 45 |
| Table 3-2 Reagents supplied in the kit for measuring caspase release. | 46 |
| Table 3-3 Reagents supplied in the kit for measuring metabolism of cells. | 47 |
| Table 3-4 Reagents supplied in the kit for measuring LDH release. | 49 |
| Table 3-5 The components provided in the RNeasy mini kit needed for the RNA extraction of cells. | 51 |
| Table 3-6 The DNase I reagents required for DNase treatment. | 51 |
| Table 3-7 Thermal cycler conditions for RT step. | 54 |
| Table 3-8 Composition of 2X cDNA mastermix. | 54 |
| Table 3-9 Recipes for 10X TAE electrophoresis buffer | 55 |
| Table 3-10 CYP2J2 primer gene sequences, combinations for PCR, predicted PCR product size and annealing temperature gradient | 55 |
| Table 3-11 sEH variant primer sequences, combinations for PCR and annealing temperature gradient. | 56 |
| Table 3-12 Housekeeper primer sequences, combinations for PCR and annealing temperature gradient. | 57 |
| Table 3-13 An example of strip tube samples for PCR run in duplicate. | 58 |
| Table 3-14 Composition of PCR mixture. | 58 |

| | |
|--|----|
| Table 3-15 PCR 96 well plate with selected sEH, CY2P2J2 and housekeeping primers including non-template controls (NTC) and water controls. Gap GAPDH; β 2 micro β 2 microglobulin..... | 59 |
| Table 3-16 PCR mixture per well. | 60 |
| Table 3-17 Components of protein standards used for the DC Bio-Rad protein assay.. | 61 |
| Table 3-18 Gel preparation of resolving and stacking gel..... | 62 |
| Table 3-19 Components of 1X SDS-PAGE running buffer | 63 |
| Table 3-20 Components of transfer buffer | 63 |
| Table 3-21 Components of ECL reagent | 64 |
| Table 3-22 Reagents included in the NADPH generation system (Promega, Southampton, UK)..... | 66 |

List of abbreviations

| | |
|--------|--|
| AA | Arachidonic acid |
| AEPU | 1-adamantan-3-(5-(2-(2-ethylethoxy)ethoxy) pentyl)urea |
| AMPK | Adenosinemonophosphate-activated protein kinase |
| Ang II | Angiotensin II |
| ANP | Atrial natriuretic peptide |
| Apo E | Apolipoprotein E |
| APS | Ammonium persulfate |
| ATP | Adenosine triphosphate |
| AUDA | 2-(3-adamantan-1-yl-ureido)-dodecanoic acid |
| BKca | Calcium activated potassium channel |
| BMP | Bone morphogenetic protein |
| BNP | Beta natriuretic peptide |
| CARP | Cardiac ankyrin repeat protein |
| CaSR | Calcium sensing receptor |
| cDNA | Complementary Deoxyribonucleic acid |
| CHO | Chinese hamster ovary |
| CK | Creatinine kinase |
| c-KIT | Stem cell factor receptor |
| COPD | Chronic obstructive pulmonary disorder |
| CPC | Cardiac progenitor cells |
| CSFR-1 | Colony stimulating factor-1 receptor |
| CT | Cycle threshold |
| CYP3A4 | Cytochrome P450 3A4 |
| CYP2E1 | Cytochrome P450 2E1 |
| CYP2J2 | Cytochrome P450 2J2 |
| CYP2J3 | Cytochrome P450 2J3 |
| CYP2J4 | Cytochrome P450 2J4 |
| CYP2J5 | Cytochrome P450 2J5 |

| | |
|------------|---|
| CYP2J6 | Cytochrome P450 2J6 |
| CYP2J8 | Cytochrome P450 2J8 |
| CYP2J9 | Cytochrome P450 2J9 |
| CYP2J11 | Cytochrome P450 2J11 |
| CYP2J12 | Cytochrome P450 2J12 |
| CYP2J13 | Cytochrome P450 2J13 |
| CYP4A3 | Cytochrome P450 4A3 |
| CYP4F1 | Cytochrome P450 4F1 |
| CYP4F5 | Cytochrome P450 4F5 |
| DHA | Docosahexaenoic acid |
| DHET | Dihydroxyeicosatrienoic acids |
| DMEM | Dulbecco's Modified Eagle's Medium |
| DMSO | Dimethyl Sulfoxide |
| DNA | Deoxyribonucleic acid |
| dNTP | Deoxyribonucleotide triphosphate |
| Dox | Doxorubicin |
| DOXol | Doxorubicinol |
| DPBS | Dulbecco's phosphate buffered saline |
| DTT | Dithiothreitol |
| ECG | Electrocardiogram |
| ECL | Enhanced chemiluminescence |
| ECM | Extracellular matrix |
| EDHF | Endothelial derived hyperpolarising factors |
| EDTA | Ethylenediaminetetraacetic acid |
| EETs | Epoxyeicosatrienoic acids |
| 14,15-EEZE | 14,15-Epoxyeicosa-5(Z)-enoic Acid |
| eNOS | Endothelial nitric oxide synthase |
| EPA | Eicosapentaenoic acid |
| ESI | Electrospray ionization |
| EV | Extracellular vesicles |
| FBS | Foetal bovine serum |
| FCS | Foetal calf serum |

| | |
|-------------------------------|--|
| FLIPR | Fluorescence imaging plate reader |
| FOXO1 | Forkhead box protein 01 |
| GAPDH | Glyceraldehyde3-phosphate dehydrogenase |
| Gnb21 | Beta polypeptide 2-like 1 |
| G protein | Guanine nucleotide binding protein |
| H1 | Histamine |
| HCl | Hydrochloric acid |
| HCM | Human cardiac myocytes |
| HDL | High density lipoprotein |
| hERG | Human Ether-à-go-go-Related Gene |
| hESC-CMs | Human embryonic stem cell- derived cardio myocytes |
| 20-HETE | 20-hydroxyeicosatetraenoic acid |
| HF | Heart failure |
| hiPS-CMs | Human induced pluripotent stem cells |
| H ₂ O ₂ | Hydrogen Peroxide |
| HPLC | High performance liquid chromatography |
| HUVEC | Human umbilical vein endothelial cells |
| ICAM | Intracellular adhesion molecule |
| IKr | Delayed rectifier K ⁺ channel |
| IL-6 | Interleukin 6 |
| IL-10 | Interleukin-10 |
| ILV | Intraluminal vesicles |
| iPS-CMs | Induced pluripotent stem cells derived cardiomyocytes |
| Kca | Calcium activated potassium channels |
| LA | Linoleic acid |
| LC/MS | Liquid chromatography/mass spectrometry |
| LDH | Lactate dehydrogenase |
| LPS | Lipopolysaccharide |
| LVDP | Left ventricular developed pressure |

| | |
|------------------|--|
| LVEF | Left ventricular ejection fraction |
| MCP-1 | Monocyte chemoattractant protein 1 |
| MEC | Microvascular endothelial cells |
| MHC | Major histocompatibility complex |
| miRNA | Micro ribonucleic acid |
| mPTP | Mitochondrial membrane permeability pore |
| mRNA | Messenger ribonucleic acid |
| MSPPOH | (N-(methylsulfonyl)-2-(2-propynyloxy)-benzenehexanamide) |
| MVE | Multi vesicular endosomes |
| NaCl | Sodium chloride |
| NADPH | Nicotinamide adenine dinucleotide phosphate |
| NaOH | Sodium hydroxide |
| NDBD | <i>N</i> -desbutyl-dronedarone |
| NF-κB | Nuclear factor kappa B |
| Oct | Octamer-binding transcription factor |
| PDGFR | Platelet derived growth factor receptor |
| PI3K | Phosphoinositide 3 kinase |
| PLA ₂ | Phospholipase A2 |
| PPAR | Peroxisome proliferator-activated receptor |
| PVDF | Polyvinylidene difluoride |
| PYGB | Glycogen phosphorylase |
| RBp4 | Retinol binding protein |
| RDT | Repeat dose testing |
| RLU | Relative light units per second |
| RIPA | Radio immune precipitation assay |
| RNA | Ribonucleic acid |
| ROS | Reactive oxygen species |
| RT | Reverse transcriptase |
| RT-PCR | Reverse-transcription polymerase chain reaction |

| | |
|-------------------|--|
| SDS-PAGE | Sodiumdodecylsulfate polyacrylamide gel electrophoresis |
| sEH | Soluble epoxide hydrolase |
| SEM | Standard error mean |
| SERCA2a | Sarco/endoplasmic reticulum Ca^{2+} -ATPase, |
| SiI-6R | Soluble interleukin 6 receptor |
| siRNA | Small interfering ribonucleic acid |
| SNP | Single nucleotide polymorphisms |
| Sox2 | (Sex determining region Y)-box 2, |
| sPLA ₂ | Soluble phospholipase A2 |
| SRM | Selected reaction monitoring |
| SRS | Standard reaction solution |
| STAT3 | Signal transducer and activator of transcription 3 |
| sTRAIL | TNF-related apoptosis-inducing ligand |
| TAE | Tris-acetate-EDTA |
| t-AUCB | (4-[[<i>trans</i> -4-[[tricyclo[3.3.1.1 ^{3,7}]dec-1ylamino)carbonyl]amino]cyclohexyl]oxy]-benzoic acid) |
| TBP | TATA-binding protein |
| TBST | Tris-buffered saline tween-20 |
| TdP | Torsades de pointes |
| TEM | Transmission electron microscopy |
| TEMED | N,N,N',N'-tetramethylethane-1,2-diamine |
| TGF- β | Transforming growth factor beta |
| TKI | Tyrosine kinase inhibitor |
| TLR | Toll-like receptor |
| Tm | Temperature |
| TNF- α | Tumour necrosis factor alpha |
| Tris | Tris(hydroxymethyl)aminomethane |
| VCAM-1 | Vascular cell adhesion molecule-1 |
| VEGFR | Vascular endothelial cells growth factor |

| | |
|------|--------------------------------|
| VILI | receptor |
| VLDL | Ventilator induced lung injury |
| vWF | Very low density lipoproteins |
| | Von willibrand factor |

Chapter 1 **Introduction**

Drug-induced cardiotoxicity affects all components and functions of the cardiovascular system. It is characterized by changes in ECG waveform morphology, haemodynamics, pathological damage to the myocardium and vasculature and changes in blood function (Lavery et al., 2011). Cardiotoxicity is a major cause of attrition in preclinical and clinical drug development, and may be attributed to a number of mechanisms (Pointon et al., 2013). Drug exerting effects on the cardiovascular system have been shown to change heart contractility, cardiac rhythm, blood pressure and ischaemia (Feenstra et al., 1999). Anti-histamines such as astemizole and terfenadine cause abnormalities in ECG wave intervals such as an increase in QT interval leading to Torsades de Pointes (Z. Zhou et al., 1999, Lu et al., 2012). The anti-cancer drug doxorubicin however causes oxidative stress resulting in structural damage to the heart leading to heart failure (Chatterjee et al., 2010). Whereas astemizole primarily exerts its effect on cardiomyocytes, doxorubicin (dox) also affects ancillary cells such as fibroblasts, endothelial cells and vascular smooth muscle cells, disrupting the structure and function of vascular smooth muscle cells and inducing a pro-fibrotic phenotype in fibroblasts (Chatterjee et al., 2010).

This PhD focuses on cytochrome P450 2J2 (CYP2J2) which has been shown to modulate drug-induced cardiotoxicity (Y. Zhang et al., 2009). The biological role of CYP2J2 appears to relate primarily to its metabolism of arachidonic acid (AA) to cardio-protective epoxyeicosatrienoic acids (EETs). Evidence is presented within this thesis to support the proposal that a complex interplay between EET synthesis and drug metabolism by CYP2J2 exists. It is likely that EET synthesis often predominates and largely protects the cardiovascular system but that drugs might inhibit EET synthesis in a competitive or non-competitive manner; or else drug metabolism by CYP2J2, in the heart or elsewhere, might liberate cardiotoxic drug metabolites.

EETs possess multiple biological activities and are involved in pathways leading to stimulation of angiogenesis, vasodilation, inhibition of vascular smooth muscle cell migration, protection against hypoxia-reperfusion injury, increased endothelial nitric oxide synthase (eNOS) expression and activity, and protection against doxorubicin (dox)-induced cardiotoxicity (Larsen et al., 2007, Spector and Norris, 2007, S. Yang et

al., 2009, Y. Zhang et al., 2009, Campbell and Fleming, 2010). Given these wide-ranging effects on the cardiovascular system it is not surprising that EETs and CYP2J2 might modulate the pathogenesis of cardiovascular disease. However, the understanding behind the protective role of EETs during cardiotoxicity is relatively unexplored suggesting that further studies on a range of cardiotoxic agents are worthwhile. CYP2J2 is also a drug metabolising enzyme and has been implicated in the biotransformation of a variety of drugs in the liver and other tissues (M. Xu et al., 2013, Michaud et al., 2010). We also highlight how the balance between drug metabolism and protective EET formation may influence cardiotoxicity (Figure 1.1).

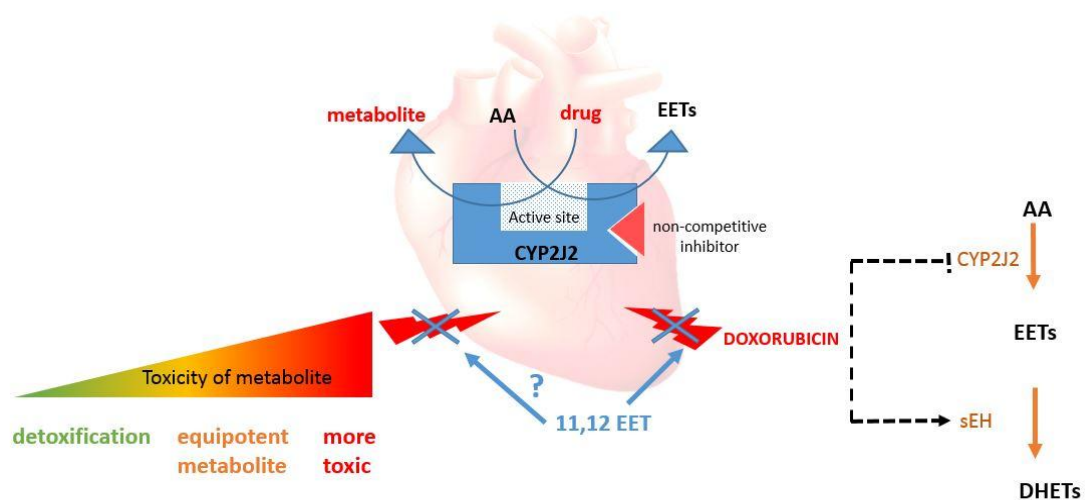


Figure 1-1 Overview of hypothesised CYP2J2 functions in the heart.

CYP2J2 has a role in drug metabolism in the heart which may lead to either detoxification of drugs or cardiotoxicity. This could be counteracted by its epoxygenase activity by which it produces several protective molecules including EETs. Doxorubicin inhibits production of EETs through inhibiting epoxygenase enzymes and increasing sEH mRNA production in rats. However, addition of exogenous EETs protects against dox toxicity in H9c2 cells (Y. Zhang et al., 2009). It may be proposed that the CYP2J2/EET pathway has a role in protecting against other drug-related toxicities within the heart. Furthermore, although there is little evidence regarding drug-AA interactions, the competition between drug substrates and AA may alter the balance of protective EETs and cardiotoxic compounds. Drugs such as dronedarone have been shown to inhibit CYP2J2 in a non-competitive way and so inhibit EET formation in an *in vitro* system (Karkhanis et al., 2016, Karkhanis et al., 2017) epoxyeicosatrienoic acids EETs; soluble epoxygenase sEH; arachidonic acid AA.

1.1 Role of CYP2J2 in cardiovascular biology

The mRNA expression of CYP2J2 in humans is mainly confined to the cardiovascular system and liver, with predominant expression in the right ventricle of the heart (Michaud et al., 2010). However mRNA has also been demonstrated in the kidney (Enayetallah et al., 2004), mRNA and protein in the lung (D. C. Zeldin et al., 1996), brain (Dutheil et al., 2009), GI tract (D. Zeldin et al., 1997), pancreas (D. C. Zeldin et al., 1997) and some human carcinoma tissues at lower levels (Jiang et al., 2005). Discrepancies between CYP2J2 mRNA and protein expression have been found in the liver (Gaedigk et al., 2006), the consequence for the heart remains unknown. Additionally, multiple immunoreactive bands on Western blotting from extracts of adult human liver and heart have been reported. It has been hypothesised that these are uncharacterised isoforms of CYP2J2 (S. Wu et al., 1996, Gaedigk et al., 2006). These isoforms may possess similar or alternate activities to the main isoform of CYP2J2 and so warrant further study. Despite its elevated expression in the cardiovascular system compared to other tissues, the role of CYP2J2 in the metabolism of drugs in the heart is, to an extent, still unknown.

Results from a cytochrome P450 mRNA screen showed that CYP2J2 is the predominant isoenzyme expressed in cardiomyocytes and human heart tissue (Figure 1.2) (Evangelista et al., 2013). Furthermore, in line with these high levels of mRNA expression, CYP2J2 protein levels in human heart microsomes were approximately 50 fold higher than other P450 enzymes (Evangelista et al., 2013, Bylund et al., 2001). Evangelista also established mRNA levels of the P450 enzyme CYP4F12 in human heart. Cytochrome P450 enzymes belonging to the CYP4A and 4F subfamily produce 20-hydroxyeicosatetraenoic acid (20-HETE) from AA (Miyata et al., 2005, Harmon et al., 2006, Tang et al., 2010) and show increased expression in cardiovascular disease. 20-HETE has antagonistic effects towards EETs, exacerbating disease processes (Jenkins et al., 2009). However, it is largely unknown how these other enzymes contribute to cardiovascular function and whether they have a role in cardiotoxicity.

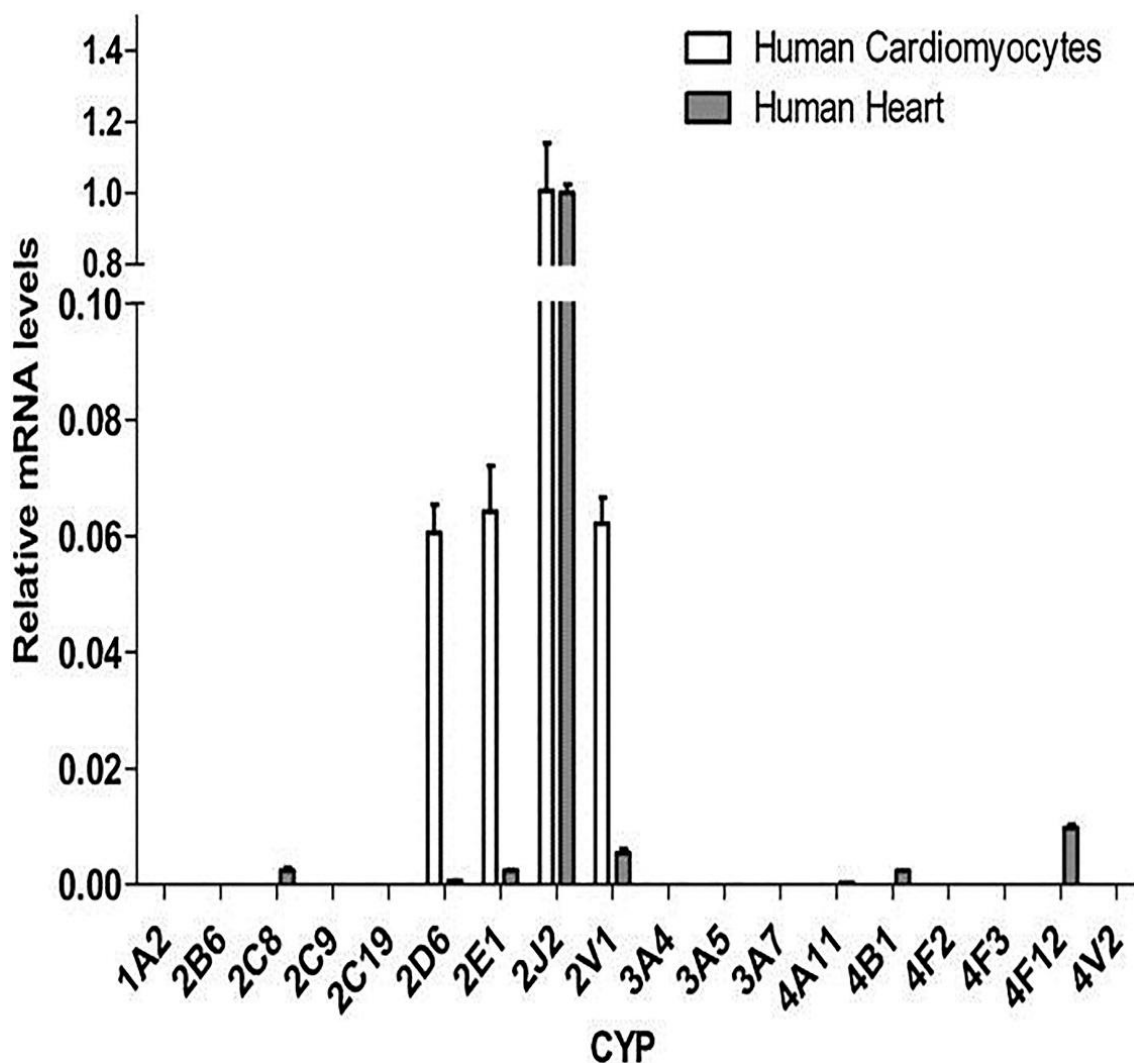


Figure 1-2 Relative mRNA expression of CYPs in human cardiomyocytes and human heart tissue and cardiomyocytes.

Total RNA was extracted from human heart tissue and adult-derived human cardiomyocytes (celprogen) and reverse-transcription polymerase chain reaction (RT-PCR) was carried out using Taqman reporter primer to various P450s. The house keeper *GusB* was used as a housekeeper gene. $2^{\Delta\Delta CT}$ calculation was used to quantitate CYP2J2 mRNA expression. 10 P450 enzymes were investigated of which CYP2J2 had the highest expression. (Evangelista et al., 2013).

In addition to cardiomyocytes, CYP2J2 expression has also been observed in other cardiovascular cells. CYP2J2 is expressed in endothelial cells in a variety of vascular beds including coronary artery, aorta (Delozier et al., 2007) and in varicose veins (Bertrand-Thiebault et al., 2004). The presence of CYP2J2 in a variety of tissues and specific expression in the heart leads to the hypothesis that CYP2J2 could contribute to endogenous tissue function. Although it is not well explored, the expression of CYP2J2 in endothelial cells, fibroblasts and smooth muscle cells (Deb and Ubil, 2014, Brutsaert, 2003) could contribute to cardiotoxicity through drug metabolism as well as protective effects through the formation of EETs.

In endothelial cells, mRNA for another epoxygenase, CYP2C9 is highly expressed compared to CYP2J2 (Delozier et al., 2007). Moreover, CYP2C9 mRNA was higher both in human aorta and coronary artery than CYP2J2 and CYP2C8. Protein analysis further reflected this, as CYP2C9 expression was dominant compared to CYP2J2 and expression of CYP2C8 was not observed (Delozier et al., 2007). Although CYP2C9 can produce EETs, it has also been reported to generate damaging reactive oxygen species (ROS). ROS are regarded as pro-inflammatory mediators, increasing NF- κ B activity (Fleming, 2001) presumably leading to increased expression of pro-inflammatory cytokines, growth factors and adhesion molecules, inducing an inflammatory phenotype and opposing the effects of CYP2J2 (Taniyama and Griendling, 2003).

CYP2J2 catalyses the epoxidation of the double bonds of endogenous cellular AA to generate EETs (Figure 1.3) (D. Zeldin et al., 1997). Due to the four double bonds of AA and the stereochemistry and regiochemistry associated with these bonds, 8 EET isomers are possible: 5,6-EET (R/S), 8,9-EET(R/S), 11,12-EET(R/S) and 14,15-EET(R/S) (M. Xu et al., 2013) . *In vivo* EETs are rapidly metabolised by soluble epoxide hydrolase (sEH) to dihydroxyeicosatrienoic acids (DHETs) which are less biologically active (G. Zhang et al., 2014). In addition to DHET formation, re-esterification of EETs and incorporation into the phospholipid membrane for storage can occur allowing release and distribution (Bernstrom et al., 1992). Other relatively minor metabolism pathways of EETs have been described involving cyclooxygenase, lipoxygenase and CYP ω -oxidase activities (Spector et al., 2004).

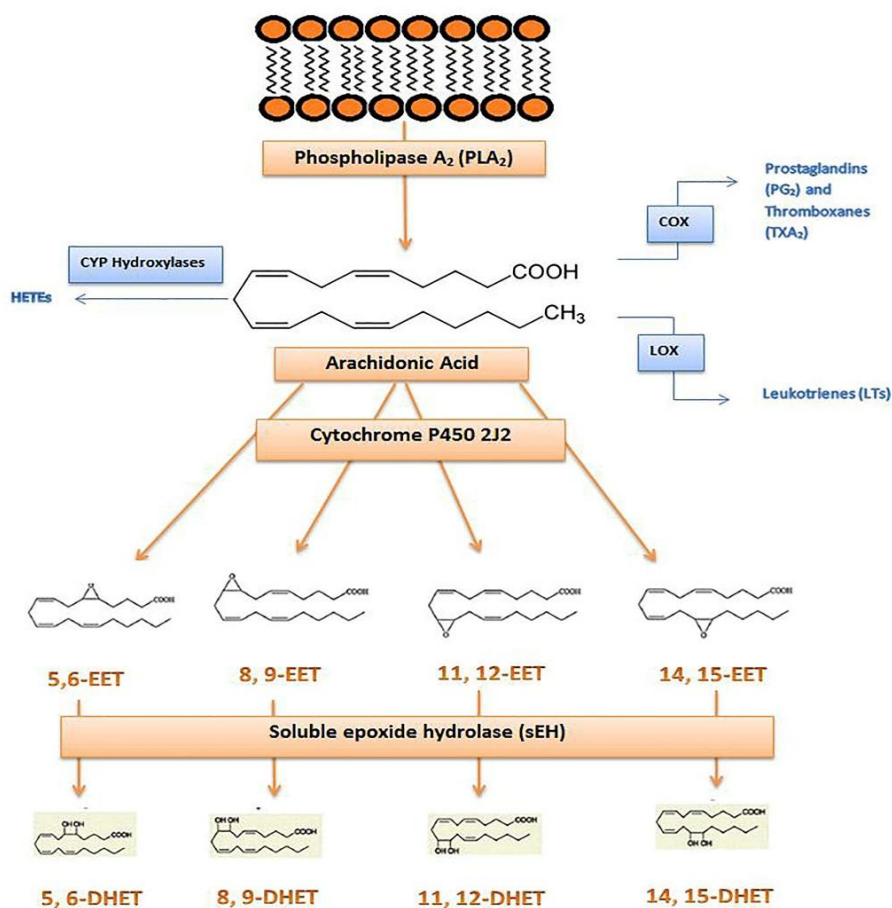


Figure 1-3 The formation of EETs by CYP2J2.

AA is hydrolysed from the phospholipid bilayer by PLA₂ and is the precursor for eicosanoids including prostaglandins, leukotrienes and HETEs. Epoxidation by CYP2J2 leads to production of 4 different EETs which can be deactivated by sEH to form DHETs. Arachidonic acid AA; phospholipase A₂ PLA₂; hydroxyeicosatrienoic acids HETEs; dihydroxyeicosatrienoic acids DHETs;

Soluble epoxide hydrolase may have significant biological activity in a variety of tissues including the liver, kidney, heart, spleen, endothelium and mammary gland (Newman et al., 2005). Its deactivation of biologically protective EETs has led to the development of pharmacological inhibitors of sEH (J. Y. Liu et al., 2009, Hwang et al., 2013). This resulted in the first sEH inhibitor, AR9281, to begin phase IIa trials for the treatment of type 2 diabetes (Anandan et al., 2011) as well as the recent introduction of sEH inhibitor, GSK225629, which is currently in phase I trials for the treatment of hypertension (Lazaar et al., 2016) and chronic obstructive pulmonary disorder (COPD) (L. Yang et al., 2017). Furthermore, several studies have shown that sEH plays an

influential role in the development of myocardial hypertrophy (D. Xu et al., 2006) and atherosclerosis (L. N. Zhang et al., 2009).

Investigation of the CYP2J2 epoxidation pathway in various tissues has provided evidence to support the theory that CYP2J2, and thus EETs, have a biologically protective role and this is emphasised by the growing potential of sEH inhibitors. The investigation of these small molecule inhibitors suggests a link between sEH inhibition and improved cardiovascular health and given the high expression of CYP2J2 in the human heart, suggest a possible protective role for CYP2J2 in drug-induced cardiotoxicity.

In addition to CYP2J2 there are a wealth of other P450 enzymes in humans which contribute to both endogenous and exogenous metabolism and dysfunction may be causal in clinical disease (see table 1.1)

Table 1-1 Families of human P450 enzymes, their function and their association with disease with a particular emphasis on heart failure. N/D – not detected.

| P450 family | Function | Disease associations | Cytochrome P450 enzyme | Expression in human liver (pmol/mg) | Percentage of hepatic pool | Expression present in heart | Expression changes in models of heart failure | | | References |
|-------------|--|-------------------------------------|------------------------|-------------------------------------|----------------------------|-----------------------------|---|---|------------------------------|---|
| | | | | | | | expression | model | change | |
| CYP1 | Metabolism of eicosanoids and drugs, major drug metabolism pathways: | Primary congenital glaucoma | CYP1A1 | <3 | <1 | mRNA | mRNA | Isoproterenol-induced cardiac hypertrophy-rat | Increased | (Zordoky and El-Kadi, 2008, Nebert et al., 2013, Zanger and Schwab, 2013) |
| | | | | | | | mRNA | Spontaneous hypertension in rats | Increased | (Thum and Borlak, 2002) |
| | | | CYP1A2 | 17.7-65 | 4.4-16.3 | N/D | mRNA | Spontaneous hypertension in rats | Increased | (Thum and Borlak, 2002, Zanger and Schwab, 2013) |
| | | | CYP1B1 | N/D | 0 | mRNA | mRNA | Isoproterenol-induced cardiac hypertrophy-rat | Increased | (Zordoky and El-Kadi, 2008, Zanger and Schwab, 2013) |
| CYP2 | Metabolism of eicosanoids and drugs, major drug metabolism pathways: | Vitamin D 25-hydroxylase deficiency | CYP2A6 | 14-56 | 3.5-14 | N/D | mRNA | Hypertrophic hearts-human | Increased | (Thum and Borlak, 2002, Nebert et al., 2013, Zanger and Schwab, 2013) |
| | | | CYP2B6 | 6.9-21 | 1.7-5.3 | mRNA | | | | (Zanger and Schwab, 2013) |
| | | | CYP2C8 | 29.3-30 | ~7.5 | mRNA,protein and activity | | | | (Zanger and Schwab, 2013) |
| | | | CYP2C9 | 18-116 | 4.5-29 | mRNA | | | | (Zanger and Schwab, 2013) |
| | | | CYP2C19 | 3.6-15 | 0.9-3.8 | | | | | (Zanger and Schwab, 2013) |
| | | | CYP2D6 | 5-17 | 1.3-4.3 | | | | | (Zanger and Schwab, 2013) |
| | | | CYP2E1 | 22-66 | 5.5-16.5 | mRNA | mRNA | Isoproterenol-induced cardiac hypertrophy-rat | Decreased | (Zordoky and El-Kadi, 2008, Zanger and Schwab, 2013) |
| | | | | | | | | Protein | Dilated cardiomyopathy-Human | Increased |
| CYP2J2 | 1-2 | <1 | mRNA,protein | mRNA | Failing hearts - human | Increased | (Tan et al., 2002, Zanger and Schwab, 2013) | | | |
| CYP3 | Metabolism of eicosanoids, sex steroids and drugs, major drug | | CYP3A4 | 58-146 | 14.5-37 | N/D | | | | (Nebert et al., 2013, Zanger and Schwab, 2013) |
| | | | CYP3A5 | 3.5-4 | ~1 | N/D | | | | (Zanger and Schwab, 2013) |

| | | | | | | | | | | |
|------|--|---|--------------------------------------|-----|-----|------|------|---------------------------|-----------|--|
| | metabolism pathways: | | | | | | | | | |
| CYP4 | Metabolism of eicosanoids, long chain fatty acids and drugs, major drug metabolism pathways: | Lamellar ichthyosis type-3 Bietti crystalline comeoretinal dystrophy | CYP4A11 CYP4F22 CYP4V2 | N/D | N/D | mRNA | mRNA | Hypertrophic hearts-human | Increased | (Nebert et al., 2013, Thum and Borlak, 2002) |
| CYP5 | Eicosanoid metabolism , platelet aggregation | Ghosal haemato-diaphyseal syndrome | CYP5A1 | N/D | N/D | N/D | | | | (Nebert et al., 2013) |
| CYP7 | Cholesterol 7 α -hydroxylase, oxysterol 7 α -hydroxylase | Neonatal cholestasis | CYP7B1 | N/D | N/D | N/D | | | | (Nebert et al., 2013) |
| CYP8 | Eicosanoid metabolism , platelet aggregation | Essential hypertension | CYP8A1 | N/D | N/D | N/D | | | | (Nebert et al., 2013) |

1.2 Genetic variation in human CYP2J2

Epidemiologic studies conducted to examine variants in many cytochrome P450 genes have found over 2000 single nucleotide polymorphisms (SNPs) (Preissner et al., 2013). A number of these have been associated with disease. Within the Chinese population, a proximal promoter polymorphism (-50G>T), rs890293 (CYP2J2*7), has been shown to alter CYP2J2 expression (Table 1.3). This mutation has been shown to decrease binding of Sp1 transcription factor to the promoter region of CYP2J2. As Sp1 is responsible for regulating transcriptional basal activity, blocking it results in a ~50% reduction in promoter activity and decreased expression of the CYP2J2 gene (Spiecker et al., 2004). This polymorphism may be involved in the pathogenesis of type 2 diabetes (C. Wang et al., 2010), Alzheimer's disease (Yan et al., 2015), chronic kidney disease and was shown to be negatively associated with cardiovascular diseases including myocardial infarction (Jie et al., 2010), coronary artery disease (Zhu et al., 2013) and hypertension (S. Wu et al., 2007) within this population. Contrary to this, studies conducted in the Swedish and German populations looking at cardiovascular risk found no susceptibility to hypertension, coronary artery disease or stroke in carriers of the rs890293 polymorphism, (Fava et al., 2010, Hoffmann et al., 2007) indicating more association studies may be required to elucidate the risk of this CYP2J2 polymorphism for cardiovascular disease. None of the other SNPs in CYP2J2 has been shown to be associated with disease (Table 1.1). Furthermore, there have been no reported associations between any CYP2J2 polymorphisms and cardiotoxicity despite some of the variants having profound effects on enzyme expression or activity *in vitro*. Without further study it is unknown whether CYP2J2 polymorphisms may be important in cardiotoxicity.

Table 1-2 CYP2J2 allelic variations in humans known to have changes in activity *in vitro*.

Currently only a variation in the CYP2J2*7 allele has been shown to have associations with disease. AA arachidonic acid; LA linoleic acid. Adapted from: (Berlin et al., 2011).

| Allele | cDNA/Gene | Enzyme activity <i>in vitro</i> | Association with disease | References |
|-----------|-----------|---|---|---|
| CYP2J2*2 | 427A>G | Reduced AA and LA metabolism | No known association with disease | (King et al., 2002) |
| CYP2J2*3 | 472C>T | Reduced AA and LA metabolism | No known association with disease | (King et al., 2002) |
| CYP2J2*4 | 575T>A | Reduced AA metabolism | No known association with disease | (King et al., 2002) |
| CYP2J2*5 | 1024G>A | Produced wild type levels of AA and LA metabolites | No known association with disease | (King et al., 2002) |
| CYP2J2*6 | 1210A>T | Reduced AA and LA metabolism | No known association with disease | (King et al., 2002) |
| CYP2J2*7 | -50G>T | Reduced transcription due to loss of Sp1 binding site | type 2 diabetes Alzheimer's disease, coronary artery disease Ischaemic stroke | (King et al., 2002, Spiecker et al., 2004, C. Wang et al., 2010, Yan et al., 2015, Zhu et al., 2013, S. Y. Wang et al., 2017) |
| CYP2J2*8 | 934G>A | Complete loss of enzymatic activity | No known association with disease | (S. S. Lee et al., 2005) |
| CYP2J2*9 | 1052C>T | Enzymatic activity comparable to wild type | No known association with disease | (S. S. Lee et al., 2005) |
| CYP2J2*10 | 344C>T | Reduced function protein | No known association with disease | (Gaedigk et al., 2006) |

1.3 CYP2J2/EETs in the maintenance of cardiovascular health- a potential role in cardiotoxicity?

Cardiotoxicity can be viewed as a continuum of physiological states that shares characteristics with cardiovascular disease. Consequently, understanding the role of CYP2J2 and EETs in cardiovascular disease can provide insight into their role in cardiotoxicity. It is widely recognised that many cytochrome P450 enzymes, are upregulated in failing hearts (El-Kadi and Zordoky, 2008). The up-regulation of CYP2J2 and EETs has been shown to be protective in the heart. In the following sections we discuss how CYP2J2 may play a role in modulation of vascular inflammation, vascular tone, ischaemia reperfusion injury and cardiac hypertrophy.

1.3.1 Vascular Inflammation

Infiltration of inflammatory cells, particularly monocytes/macrophages has been shown to be an early event and causal in the development of cardiovascular pathologies. Potent anti-inflammatory effects of CYP2J2 and EETs have been demonstrated both *in vivo* and *in vitro*. *In vitro*, synthetic EETs can reduce expression of many pro-inflammatory genes which are involved in activation and adhesion of endothelial cells to leukocytes and leukocyte transmigration across the endothelium (X. Xu et al., 2011). For example, 11,12-EET suppresses expression of adhesion molecules, E-selectin and vascular cell adhesion molecule-1 (VCAM-1), in tumour necrosis factor alpha (TNF- α) induced human endothelial cells (Node et al., 1999). In addition to blocking the actions of TNF- α , EETs (11, 12- and 8, 9-EET) have also been shown to inhibit basal TNF- α production in THP-1 cells, a model monocytic cell line (Bystrom et al., 2011). EETs inhibit lipopolysaccharide (LPS)-induced macrophage polarisation and reduce expression of many proinflammatory cytokines whilst at the same time upregulating anti-inflammatory cytokine (interleukin-10) IL-10 in HEK293 cells over-expressing recombinant CYP2J2; these effects are likely mediated through downregulating NF- κ B and activation of peroxisome proliferator-activated receptor (PPAR) (Dai et al., 2015).

Studies in mouse models have further validated the effects of transgenic CYP2J2 and EETs in inflammation. Continuous infusion of 11,12-EET inhibited TNF- α -induced endothelial VCAM-1 expression and mononuclear cell rolling and adhesion in mouse

coronary arteries. In addition, in a CYP2J2 transgenic mouse model expression of CYP2J2 in mice significantly reduced LPS-induced production of pro-inflammatory mediators, IL-6, monocyte chemoattractant protein-1 (MCP-1), E-selectin, and IL-1 β , as well as nuclear factor kappa B (NF- κ B) activation and invasion of inflammatory cells in lung tissues (Potente et al., 2003). EETs inhibited phosphorylation of the NF- κ B complex preventing its translocation to the nucleus and hence transcriptional effects (Node et al., 1999). Transgenic CYP2J2 was also found to reduce angiotensin (Ang II)-induced cardiac fibrosis and inflammation in mice possibly through the inhibition of the NF- κ B pathway (L. Yang et al., 2015).

Inflammatory processes have been implicated in the development of atherosclerosis. CYP2J2 has also been found to protect against the production of atherosclerotic plaques in a transgenic mouse model of atherosclerosis (W. Liu et al., 2016). Apolipoprotein E (Apo-E) deficient mice and CYP2J2 transgenic mice were given a high fat diet for 25 weeks. Histological analysis of aorta samples identified fewer plaques on the luminal surface of the aorta when mice had been injected with CYP2J2 vector compared to wild type. Analysis of lipids showed lower circulating triglyceride and cholesterol levels in the transgenic mice. 11,12-EET was also shown to inhibit TNF- α induced apoptosis in human umbilical vein endothelial cells (HUVECs) through the activation of AKT and forkhead box protein 01 (FOXO1) which is down regulated in atherosclerotic aorta (W. Liu et al., 2016). However it is challenging to ascertain whether these results are a direct outcome of CYP2J2 derived EETs or other protective molecules, for example, metabolites of eicosapentaenoic acid (EPA) and docosahexaenoic acid (DHA); moreover, to ascertain which of the EETs may be responsible for the protective action.

Likewise, one of the hallmarks of some drug-induced cardiotoxicities is the increase in production of inflammatory mediators. For example epirubicin, known to alter cardiac morphology, increases IL-6 and its soluble receptor sIL-6R which have been shown to contribute to the pathophysiology of cardiomyopathy (Mercuro et al., 2007). It is possible that the anti-inflammatory effects of EETs could attenuate some of the myocardial damage mediated by elevated levels of these inflammatory mediators.

1.3.2 Vascular tone

Maintenance of vascular tone is critical for cardiovascular function, particularly contributing to blood pressure regulation. EETs, in particular 11,12-EET, are also

known as endothelial derived hyperpolarising factors (EDHFs) and have been shown to cause relaxation of rat coronary arteries as well as renal and cerebral arteries of rats and rabbits (Larsen et al., 2006, J. D. Imig et al., 2001, Fisslthaler et al., 1999, Dimitropoulou et al., 2007, Campbell et al., 1996). EETs have been shown to reduce vascular tone by attenuating calcium entry via voltage-sensitive channels leading to hyperpolarization of vascular smooth muscle cells. However, EETs may also increase intracellular calcium concentration in endothelial cells by activation of K_{Ca} channels.

Although an increase in EETs has been shown to reduce vascular tone and protect against cardiovascular disease in animal models, it is still unknown how this protective pathway may influence cardiotoxicity

1.3.3 Ischaemia reperfusion injury

Ischaemia–reperfusion injury can lead to accumulation of protective EETs following the release of fatty acids by membrane bound phospholipases (J. Seubert et al., 2004). Increasing EETs in a sEH null mouse model showed limited mitochondrial damage following ischaemia compared to wild type (Akhnokh et al., 2016). EETs can enforce their cardioprotective effects through the activation of mitoK (ATP) and opening of the mitochondrial membrane permeability pore (mPTP) (Barau et al., 2015). Activation of this protective pathway by EETs has been shown to maintain mitochondrial structure and function in CYP2J2 transgenic mice (J. Seubert et al., 2004). It is well known that mitochondrial ischaemia reperfusion injury can activate apoptosis. EETs have been shown to inhibit pro-apoptotic pathways through the pro-survival enzyme phosphoinositide 3 kinase (PI3K) in rat cardiomyocytes (Isomoto et al., 2006).

Transgenic mice with endothelial cell specific CYP2J2 expression identified that endothelial-derived EETs did not protect against cardiac ischaemia; moreover, transgenic mice with enhanced endothelial expression of sEH showed no changes in left ventricular developed pressure (LVDP) and infarct size. However, transgenic mice with myocardial specific expression of CYP2J2 had increased recovery of LVDP and decreased infarct size after ischaemia-reperfusion compared to wild type. Furthermore, transgenic mice with expression of myocardial sEH showed no changes in LVDP and infarct size (Edin et al., 2011). This provides a further layer of complexity to the protective capabilities of EETs and how EETs produced from different areas and cell types of the cardiovascular system may have varying effects.

1.3.4 Cardiac Hypertrophy

Cardiac hypertrophy is a prominent risk factor for heart failure and a strong predictor of adverse cardiovascular events (El-Kadi and Zordoky, 2008). It is normally characterised by an increase in cardiomyocyte size, increased synthesis of beta natriuretic peptide (BNP), atrial natriuretic peptide (ANP), myosin and actin accompanied by fibrosis and remodelling (Alsaad et al., 2013). Animal models have shown that during isoproterenol-induced cardiac hypertrophy there is a decrease in protective EETs. Modulation of this process, that is, increasing EET half-life by use of sEH inhibitors, protected against the detrimental effects of cardiac hypertrophy although the exact mechanism for this is yet to be determined. (El-Kadi and Zordoky, 2008).

1.4 Animal homologues of CYP2J2 to investigate pre-clinical drug-induced cardiotoxicity

Prior to first time in human, novel small molecules have to be tested in both rodent and non-rodent *in vivo* models to assess for potential safety liabilities in major organs including the heart. Many mammals possess homologs of the human CYP2J2 protein with varying sequence similarities including the commonly used species for regulatory safety pharmacology and toxicology studies (rodent, dog and monkey) (Table 1.2 and Table 1.3).

Table 1-3 Amino acid sequence homology between human CYP2J2 and mammalian CYP2Js.

Many mammals possess homologs of the human CYP2J2 protein with varying sequence similarities including the commonly used species for regulatory safety pharmacology and toxicology studies. Humans, monkey and dog all have single isoforms for CYP2J2 whereas rodents such as rat have multiple isoforms, CYP2J3 and 2J4 being the most similar to human. Values are percent sequence homology.

| % sequence homology | | | | | |
|---------------------|-------|--------|-----|-----|-----|
| | Human | Monkey | Dog | Rat | |
| | 2J2 | 2J2 | 2J2 | 2J3 | 2J4 |
| Human 2J2 | 100 | 95 | 79 | 72 | 76 |
| Monkey 2J2 | | 100 | 81 | 74 | 76 |
| Dog 2J2 | | | 100 | 72 | 72 |
| Rat 2J3 | | | | 100 | 79 |
| Rat 2J4 | | | | | 100 |

Table 1-4 CYP2J gene expressions in human and other mammalian tissues.

RNA and protein expression are quantified, whereby (+) is low expression, (++) is moderate expression and (+++) is high expression. Within the heart human CYP2J2 has the highest RNA and protein expression. Rat CYP2J3 is expressed highly at the protein level and mouse CYP2J11 has high RNA expression in the heart indicating that there are often discrepancies between RNA and protein expression in different homologues. (Adapted from Xu et al., 2013).

| | Human | Mouse | | | | | | | Monkey | Rat | | |
|-----------------|---------|-------|-----|-----|-----|------|------|------|--------|-----|-----|-----|
| | 2J2 | 2J5 | 2J6 | 2J8 | 2J9 | 2J11 | 2J12 | 2J13 | 2J2 | 2J3 | 2J4 | |
| Liver | RNA | ++ | + | ++ | + | | ++ | | | ++ | +++ | ++ |
| | Protein | ++ | ++ | | | | | | | | +++ | ++ |
| Heart | RNA | +++ | | + | | | +++ | | + | | + | |
| | Protein | +++ | | | | | + | | | + | +++ | |
| Small intestine | RNA | ++ | | +++ | | | + | + | + | | + | +++ |
| | Protein | + | | | | | | | | +++ | | +++ |
| Lung | RNA | + | + | + | | + | | | + | ++ | + | |
| | Protein | + | | | | | | | | | + | + |
| Kidney | RNA | + | +++ | ++ | +++ | ++ | +++ | | +++ | | + | |
| | Protein | ++ | +++ | | ++ | | +++ | | | | + | |
| Brain | RNA | + | | ++ | + | +++ | | +++ | + | | | |
| | Protein | + | | | ++ | +++ | | | | | | |
| Pancreas | RNA | + | | | | | | | + | | | |
| | Protein | + | | | | | | | | | ++ | |
| Stomach | RNA | | | | | | | | + | | + | |
| | Protein | | | | | | | | | | + | |
| Spleen | RNA | | | | | | + | + | + | | | |
| | Protein | | | | | | | | | | | |
| Skeletal muscle | RNA | | | | | | | | | | | |
| | Protein | ++ | | | | | | | | | | |

Compared to the single CYP2J2 gene in humans, mice have a cluster of CYP2J isoform genes. This subfamily is highly homologous with 62-84% sequence homology at the amino acid level compared to human. Mice CYP2J isoforms are distributed in the liver, kidneys, intestine, brain, lung and abundantly in the heart (Graves et al., 2013). All enzymes produced from the CYP2J cluster have similar substrate preferences but the products produced have a unique profile (Nelson et al., 2004). Compared with recombinant CYP2J2 microsomes, all isoforms have been shown to metabolise AA albeit at a lower rate (Graves et al., 2013).

Mouse models are used to investigate cytochrome P450-dependent metabolism. Knockout and transgenic mice are used to study the metabolism pathways pertaining to a specific enzyme leading to toxicity. For example, knockout and humanised mouse models for CYP2E1 have been used to characterise acetaminophen hepatotoxicity (Gonzalez et al., 2015). Currently, transgenic mouse models for CYP2J have been created to understand the biological significance of EETs in disease. However, studies specifically addressing the role of CYP2J in the induction of toxicity have not yet been described. *In vitro*, mouse derived HL-1 cell lines have limited cardiac morphological, biochemical and electrophysiological properties compared to human adult cardiomyocytes. However, their expression of P450 enzymes has not been clearly investigated and so may offer a potential *in vitro* cardiac model to study CYP2J.

The main rat homologues, CYP2J3 and CYP2J4, have 72% and 76% sequence similarity to human CYP2J2 and have a similar tissue distribution to human. Furthermore, CYP2J3 is reported to be found primarily within atrial and ventricular myocytes. (S. Wu et al., 1997, Q. Zhang et al., 1997), while increased expression of CYP2J3 in the heart following ischemic postconditioning significantly increased EET generation (H. Wang et al., 2012) suggesting CYP2J3 may have epoxygenase activity analogous to CYP2J2. Therefore, rat CYP2J3 may be the closest homologous enzyme to CYP2J2 in terms of distribution and epoxygenase activity and may be applicable to investigations of cardiotoxicity. Also, rat cardiac cell lines such as rat myoblast H9c2 cells have been used to investigate cardiac biology and toxicology, however they lack key functional features of cardiomyocytes, exhibit a mainly skeletal muscle phenotype and do not respond to electrical stimulation (Kimes and Brandt, 1976). However, they have recently been used to investigate cardioprotective effects of drugs following

oxidative damage (J. Zhou et al., 2016), thus suggesting the potential use of these cells in investigating mechanisms of cardioprotection from drug induced cardiotoxicity.

In both dog and monkey, a single CYP2J isoform (CYP2J2) has been identified (Nelson, 2009). Monkey CYP2J2 has the greatest sequence similarity (95%) to CYP2J2 in humans (Uno et al., 2007). Immunoquantification of cynomolgus CYP2J2 identified higher levels of protein in monkey liver compared with human (Uehara et al., 2015). This was reflected in activity where there was a higher hepatic clearance of astemizole (Nishimuta et al., 2011) which has been shown to be a drug substrate for CYP2J2 (Uehara et al., 2015). However, to our knowledge, expression of CYP2J2 at the mRNA or protein level has not yet been quantified in the monkey or dog heart.

Cardiotoxicity encompass a variety of features including changes in pathology, ECG and haemodynamics. Therefore, some animal models may be recommended for investigating functional changes whereas other models may be more suited to look at pathological changes. For example, rats which reflect the protective capabilities of CYP2J would be acceptable for studying EETs, however their use in predicting cardiotoxicity associated with ion channel inhibition is limited. Consequently, when selecting a suitable preclinical model system both the potential ability to modulate CYP2J2 and the expected cardiac effects being risk assessed should be taken into consideration in selecting the most appropriate approach and species. Furthermore, although dog has a single CYP2J2 isoform with high sequence similarity more studies are required to fully determine if dog is the best model to study CYP2J2, from both a cardiovascular biology and CYP2J2 perspective.

1.4.1 The disadvantages of using animals and advantages of *in vitro* models

The use of animal models in drug testing is vital in order to show the extensive cell type and tissue interactions which are part of the mammalian system. However, the physiological relevance of animals is sometimes overestimated. Many species differences between animal and man hinder the ability to use these models to assess the probable toxicological outcome in patients (Hartung and Daston, 2009). In regards, specifically to drug metabolism and drug transformation, although many human CYP 450 enzymes have been found to have a homologue in other test animals, differences in genetic makeup and consequently protein structure, as well as tissue distribution has meant that animals can never be a true representation of toxicity in man.

In addition to the obvious ethical issues, there can also be difficulties in the functionality and assessment of the animal paradigm, particularly for high throughput testing as models require large amounts of test substance, increasing the expense for pharmaceutical companies. As well as this, the assessment of data can sometimes be difficult to interpret due to the complexity of interactions and because the experiments rely on a pathological outcome (Hartung and Daston, 2009).

However, where *in vivo* models fail to deliver, *in vitro* toxicity models have been shown to prosper. Although structurally less complex, they are amenable to automated high throughput (as seen in fig 1.4) as they are relatively inexpensive to run owing to the fact that little test substance is needed. Furthermore as cell models are available for nearly all tissues and laboratory animal species, species differences are eradicated (Hartung and Daston, 2009). Despite these advantages, there are some fundamental problems with *in vitro* models. These are mainly to do with the artificial growth conditions cells are maintained in. For example they may not reflect the body temperature of animals, the blood-electrolyte concentration of species, the extracellular matrix (ECM) or the extent of cell contacts, which is maximally 15% of normal in monolayer cultures. Additionally, cell densities in normal monocultures are less than 1% of physiological tissue which may impair cell signalling (Hartung and Daston, 2009).

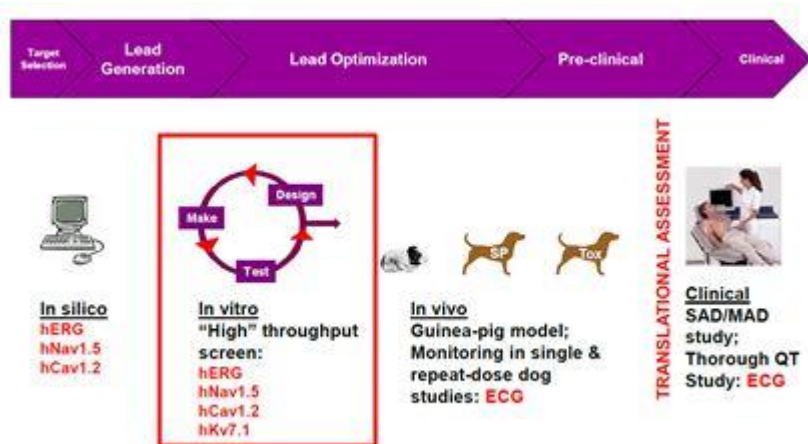


Figure 1-4 *In vitro* cardiotoxicity approaches within the drug development pipeline.

Once a new compound has been identified, selection occurs through a series of safety assessments which most commonly test for functional toxicity through *in silico* and *in vitro* models of ion channel inhibition. *In vivo* ECG recordings are taken from both a rodent and non-rodent animals after variable dose exposures. Similarly, single ascending dose (SAD) and multiple ascending dose (MAD) are used in clinical testing to ascertain a non-toxic therapeutic dose for each drug. hERG human ether-à-go-go-related potassium channel; (Figure kindly given by Dr Amy Pointon, AstraZeneca).

1.4.2 Current *in vitro* models for drug testing

Cardio toxic drug effects are a common cause of attrition and are responsible for many of the drugs that are withdrawn in the early stages and also in later clinical stages of toxicity testing. This causes pharmaceutical drug companies millions of pounds as seen in fig 1.5 (Redfern et al., 2010).

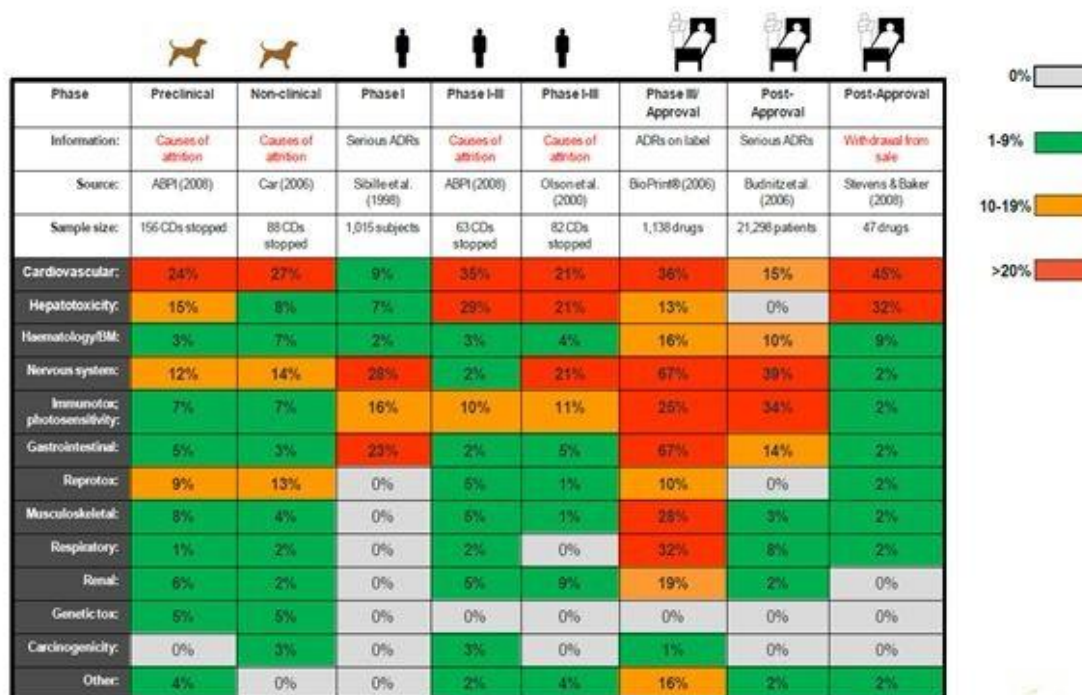


Figure 1-5 Table showing the common causes of attrition.

Cardiovascular side effects account for a large degree of attrition at most stages of the drug development pipeline with many drugs reaching post approval before patients exhibit cardiotoxic side effects. (Redfern et al., 2010)

Because of this, many companies have a driving interest in reducing costs through identifying a reliable human cell model which can be manipulated for study. Drugs exerting effects on the cardiovascular system have been shown to change heart contractility, cardiac rhythm, blood pressure and ischaemia (Laustriat et al., 2010). A great deal of these side effects includes abnormalities in contraction such as an increase in QT interval leading to Torsades de Pointes as well as increases in heart rate and pressure and damage to cardiac structure all of which can lead to heart failure. Many of the current cardiac safety testing procedures involve high-throughput ECG and molecular screens for many of the responsible ion channels such as human Ether-à-go-go-Related Gene (hERG).

However only a small fraction of non-ECG risks are covered in this way. Other *in vitro* tests include the use of Chinese hamster ovary (CHO) cells expressing human hERG channel which have also been used for the purposes of automated patch clamping to identify compounds that block this channel. As well as this cellular and molecular assays are highly influential factors in determining cardiomyocyte damage and death. Assays including cell viability, ROS generation, apoptosis and mitochondrial membrane potential allow structural analysis of a range of parameters (Pointon et al., 2013).

1.5 Role of CYP2J2 in xenobiotic metabolism

In the human liver, CYP2J2 protein comprises of 1 to 2% of total P450 content similar to that in the small intestine (1.4%) (Paine et al., 2006) compared with CYP3A4 that makes up ~30% of total P450 content (Michaels and Wang, 2014). However as CYP3A4 expression is low in cardiac tissue it is unlikely to contribute to drug metabolism within the heart (Chaudhary et al., 2009). Although not the most highly expressed cytochrome P450 in the liver and intestine CYP2J2 has been shown to mediate drug biotransformation reactions with a number of exogenous substances. CYP2J2 has been shown to be the primary enzyme involved in several metabolic reactions including amiodarone 4-hydroxylation, astemizole O-demethylation and ebastine hydroxylation (Matsumoto et al., 2002, Matsumoto and Yamazoe, 2001, K. H. Liu et al., 2006). For ebastine, CYP2J2 plays a superior role in first-pass intestinal metabolism to its pharmacologically active metabolite and less toxic carebastine. All three of these compounds are known cardiotoxins. Both astemizole and ebastine block the Kv11.1 (hERG) potassium channel, causing torsades de pointes and QT prolongation arrhythmias. However both amiodarone and astemizole metabolites are as toxic as the primary compound when metabolised (Matsumoto et al., 2002). Thus the individual product profile of a compound due to CYP2J2 metabolism may lead to less toxic or equipotent metabolites and altered toxicity of these drugs within the heart.

A study in human liver microsomes identified 8 novel substrates for CYP2J2 after screening 139 compounds including marketed therapeutic agents. These chemical entities had wide structural diversity and ranged from small molecules like albendazole to larger complex structures such as cyclosporine (C. A. Lee et al., 2010). This diversity in drug substrates highlights how CYP2J2 may be vital in mediating drug responses and gives a glimpse into the similarity between CYP2J2 and other P450 enzymes of similar

function. CYP2J2 and CYP3A4 share a number of substrates including anti-histamines (terfenadine, astemizole and ebastine), anticancer drugs (doxorubicin and tamoxifen) and immunosuppressants (cyclosporine); a list of known CYP2J2 substrates is shown in Table 1.4. *In silico* approaches suggest structural similarity between CYP2J2 and CYP3A4 and a comparison of active sites showed homology; however further examination shows slight differences in structural geometry. CYP2J2 has a more cylindrical shape and is narrower than CYP3A4 as the β -4 part of the protein is smaller and has a loop which inserts into the active site restricting metabolism (C. A. Lee et al., 2010).

Table 1-5 The range of substrates for CYP2J2 and the metabolic pathways by which they are formed.

Substrates for CYP2J2 include both endogenous compounds (a) and exogenous drugs (b) and the main metabolic pathways which are hydroxylation and epoxygenation. Some K_m and V_{max} values remain unknown and this is indicated by shaded cells. * Metabolic pathway used solely by CYP2J2 (Adapted from Xu et al., 2013)

| <u>Substrate</u> | <u>Metabolic pathway</u> | <u>K_m (μM)</u> | <u>V_{max} /turnover number (nmol/min/nmol)</u> |
|-----------------------|--|---|--|
| a) Endogenous | | | |
| Arachidonic acid | Epoxygenation | | 0.065 |
| Linoleic acid | Epoxygenation | | 0.105 |
| Docosahexaenoic acid | Epoxygenation (major) ω -1/ ω Hydroxylation (minor) | | 0.228 \pm 0.008 |
| Eicosapentaenoic acid | Epoxygenation (major) ω -1/ ω Hydroxylation (minor) | | 0.943 \pm 0.017 |
| Vitamin D3 | 25-Hydroxylation | 7.7 \pm 1.2 | 0.087 \pm 0.013 |
| Vitamin D2 | 25-Hydroxylation | 2.0 \pm 0.3 | 0.16 \pm 0.03 |
| 1 α (OH)D3 | 25-Hydroxylation | 4.4 \pm 0.7 | 2.2 |

| | | | |
|-----------------|---|----------|-----------------|
| a) Drugs | | | |
| Albendazole | ω -Hydroxylation Sulfoxidation | | |
| Amiodarone | 3-Hydroxylation 4-Hydroxylation | 5 | 4.6 |
| Apixaban | O-demethylation | | 0.27 \pm 0.06 |
| Astemizole* | O-demethylation | 0.65 | 1.129 |
| Benzphetamine | N-demethylation | | 0.08 |
| Bufuralol | | | 0.17 |
| Cyclosporine A | Hydroxylation | | |
| Danazol | Hydroxylation | | |
| Ebastin * | Hydroxylation | 1.3/18.3 | 40.6/8.2 |
| Eperisone | ω - Hydroxylation ω -1 Hydroxylation | | 0.0266 |
| Hydroxyebastine | Carboxylation | 0.75 | 9.86 |
| Terfenadine | Hydroxylation | 0.4 | 20 |
| Thioridazine | Sulfoxidation | | |
| Vorapaxar | Hydroxylation | | 0.0306 |

Biotransformation studies looking at the metabolism profile of CYP2J2 and CYP3A4 showed that CYP2J2 produced numerous metabolites, many of which were also observed with CYP3A4 (Figure 1.6). However, indications of differences in the regioselectivity in metabolites from albendazole, amiodarone thioridazine, mesoridazine, danazol and astemizole, after incubation with the two enzymes were found. There was also evidence some metabolites were produced exclusively by CYP2J2. (A. C. Lee and Murray, 2010). Further investigation by Kaspera et al. (2014) showed the significant contribution of CYP2J2 to ritonavir metabolism in the liver, with a unique metabolism profile when compared with CYP3A4/5. CYP2J2 was shown to produce specific metabolites from the oxidation of the thiazole rings on different sides of the molecule. This study found that CYP2J2 had a higher affinity for ritonavir (K_m 0.016 μ M) compared to CYP3A4 (K_m 0.068 μ M) and CYP3A5 (K_m 0.047 μ M) in liver microsomes (Kaspera et al., 2014). In addition, CYP2J2 and CYP2C19 were found to be the major enzymes responsible for the metabolism of albendazole and fenbendazole in human liver microsomes. Both of these drugs can be transformed to their sulfoxide and hydroxyl metabolites (Z. Wu et al., 2013). CYP3A4 and flavin-containing monooxygenase are thought to be major enzymes in producing sulfoxide metabolites (Virkel et al., 2004). However, Zhexue *et al.*, (2013) demonstrated that CYP2J2 was the primary enzyme mediating albendazole hydroxylation; CYP2C19 and CYP2E1 also contributed to this hydroxylation but to a lesser extent. (Z. Wu et al., 2013). The consequences of the formation of these specific metabolites by CYP2J2 has yet to be fully determined.

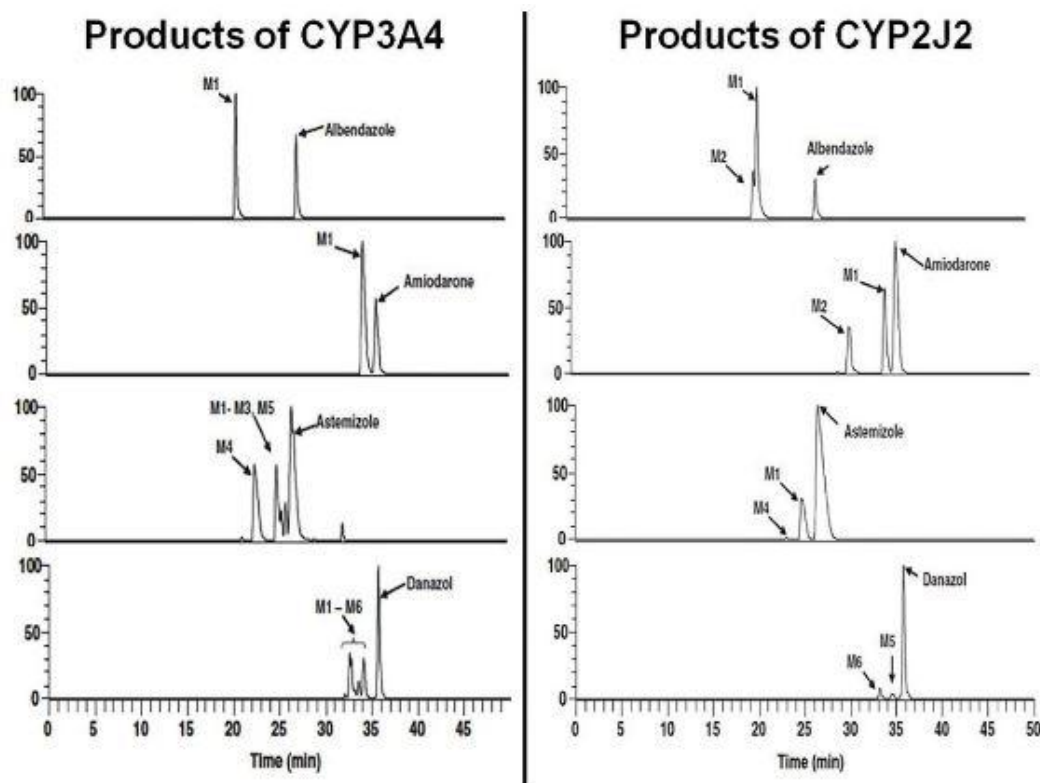


Figure 1-6 Chromatographic data showing the differences in products formed by recombinant CYP3A4 and CYP2J2.

Recombinant CYP2J2 (40pmol/ml) and CYP3A4 (20pmol/ml) were incubated with 50 μ M drug for 20 mins and metabolites were separated via reverse phase chromatography. Albendazole metabolism by both CYP3A4 and CYP2J2 produced the same metabolite, however an additional metabolite was observed for CYP2J2 indicating hydroxylation. CYP2J2 and CYP3A4 produced similar peaks indicating hydroxylation. Chromatographic data of astemizole metabolism showed CYP3A4 produced the hydroxylated product whereas metabolism by CYP2J2 resulted in both the O-dealkylated metabolite and some N-dealkylated product. When danazol was incubated with both enzymes similar metabolites were produced. (C. A. Lee et al., 2010).

Several CYP2J2 substrates are known to have pharmacological effects in the heart and may be metabolised in this tissue (Evangelista et al., 2013). Applying this logic, CYP2J2 may be able to regulate the local concentrations of these compounds and therefore modulate cardiotoxicity. Studies in heart microsomes incubated with verapamil led to the formation of nine CYP metabolites. As verapamil is an L-type calcium channel blocker, which is commonly prescribed for heart conditions such as angina and arrhythmias, CYP2J2 may be able to regulate functional activity of the drug (Michaud et al., 2010). Furthermore, in isolated rat heart hydroxylation of the H1 receptor antagonist, ebastine to hydroxyebastine and carebastine was detected which when compared to human liver microsomes showed a similar metabolism profile.

However, as there was no comparison to metabolism in the human heart it is difficult to ascertain comparative activity between CYP2J2 and CYP2J3. It is also unclear whether other P450 enzymes could be responsible, in part, for ebastine metabolism (Kang et al., 2011). Overall, the metabolic activity of CYP2J2 in the liver and its ability to metabolise a wide array of drugs, coupled with its high expression in the heart, warrant further studies to clarify the significance of cardiac CYP2J2 in drug metabolism in physiological relevant systems.

1.6 Modulation of CYP2J2 activity by drugs

Evangelista et al. (2013) investigated the role of different drugs in the induction and inhibition of CYP2J2 in adult primary human cardiomyocytes. That the cells used in this study are able to divide and are morphologically and functionally different compared with freshly isolated cells is a major limitation of this research. CYP2J2 activity was measured via terfenadine hydroxylation at two different inhibitor concentrations. The most potent inhibitor of CYP2J2 tested was danazol which reduced activity by ~95%; other less potent inhibitors included ketoconazole and astemizole (Evangelista et al., 2013).

A more recent study highlighted the reversible mixed-mode inhibition of recombinant CYP2J2 by dronedarone ($K_i = 0.034\mu\text{M}$), amiodarone ($K_i = 4.8\mu\text{M}$) and their active metabolites, *N*-desbutyldronedarone (NDBD) ($K_i = 0.55\mu\text{M}$) and *N*-desethylamiodarone (NDEA) ($K_i = 7.4\mu\text{M}$) and further irreversible inhibition by dronedarone and NDBD (Karkhanis et al., 2016). Both of these drugs are multi-ion channel blockers designed to reduce cardiac arrhythmias but paradoxically are potentially also cardiotoxic resulting in bradycardia, hypotension, congestive heart failure and ventricular tachycardia (Dixon et al., 2013). Dronedarone has been demonstrated to cause a reduction in a recurrent atrial fibrillation in patients compared to amiodarone (Piccini et al., 2009) but can lead to QT prolongation and subsequently torsades de pointes (TdP) in some instances (Heijman et al., 2013). As both amiodarone and dronedarone are substrates for CYP2J2, the interaction between these drugs and CYP2J2 may modulate cardiac side effects and drug-drug interactions leading to further toxicity. Dronedarone, amiodarone and their respective metabolites have been shown to inhibit CYP2J2 mediated arachidonic acid metabolism and production of EETs NDBD being the most potent (Karkhanis et al., 2017). Due to the protective role of CYP2J2 in cardiac function it is feasible that the

inhibition of CYP2J2 may block epoxygenase activity and reduce protective EETs, although our understanding of the interplay between drug metabolism and EET formation is rudimentary. In addition, it is possible that modulation of CYP2J2 activity may lead to altered levels of toxic parent compound or toxic metabolite and changes in the toxicity profile observed. These concepts are worthy of further study and analysis.

1.7 Potential role of EETs in mitigating drug induced cardiotoxicity

The mechanisms by which compounds cause cardiotoxicity resulting in changes in ECG waveforms/intervals, hemodynamics or cardiac pathology are diverse and compound specific. Each of these outcomes can be further defined both in terms of the physiological and pathological state and the molecular mechanism and or pathways by which perturbations arise. Currently the level of molecular understanding varies considerably depending on the physiological or pathological perturbation. For example, the ion channels behind the cardiac action potential and thus changes in the ECG are well defined. In contrast, multiple mechanisms are proposed for changes in cardiac pathology. For example, the anti-cancer tyrosine kinase inhibitor sunitinib causes oxidative stress (Aparicio-Gallego et al., 2011) and cardiac hypertrophy (Maayah et al., 2014); whether these perturbations are linked and if upstream unidentified mechanisms exist still remains to be determined. However, with this diversity of molecular mechanisms responsible for cardiotoxicity, the role of EETs in cardio-protection is just as diverse (table 1.5). In an animal model of isoproterenol-induced cardiac hypertrophy, use of sEH inhibitors increased levels of EETs and decreased the induction of ANP and BNP and *EPHX2* mRNA (Althurwi et al., 2013). Furthermore, increased circulating EETs reduced oxidative stress and increased expression of antioxidant enzymes (X. Wang et al., 2014). Therefore there is some evidence to suggest protection against sunitinib (and other drug) toxicity may be achieved by an upregulation of these epoxygenases with resultant promotion of EET formation.

Table 1-6 Proposed mechanisms of protection by EETs against selected cardiotoxic drugs.

The listed compounds are known substrates for CYP2J2 which cause cardiotoxicity through a variety of mechanisms. EETs have been shown to manipulate cellular processes to protect against cardiac pathologies and therefore may mitigate the cardiotoxic effects of drugs on the heart.

| CYP2J2 substrate | FDA approval package cardiac warnings | Mechanism contributing to cardiotoxicity | Circumstantial evidence for mitigation of cardiotoxicity by EETs |
|---|---|---|---|
| cyclosporine A (Tang et al., 2011) | Hypertension, tachycardia, myocardial infarction | Oxidative stress and/or mitochondrial dysfunction | In a CYP2J2 transgenic mouse, heart failure-induced oxidative stress was mitigated by EETs; EETs increased expression of antioxidant enzymes and reduced reactive oxygen species levels (X. Wang et al., 2014, Akhnokh et al., 2016). |
| doxorubicin (Zhang et al., 2009b) | ECG abnormalities, tachyarrhythmias, reduction in LVEF and congestive heart failure | | In a CYP2J2 transgenic mouse, doxorubicin-induced ROS levels were reduced compared with wild type. CYP2J2 transgenic mice had preserved mitochondrial structure and membrane potential (Zhang et al., 2009b) |
| sunitinib (Aparicio-Gallego et al., 2011) | Decreased LVEF and HF, QT interval prolongation and TdP, cardiomyopathy. | | In sEH null mice, increased circulating EETs limited mitochondrial damage following ischaemia (Akhnokh et al., 2016) |
| amiodarone (Isomoto et al., 2006) | Ventricular fibrillation, ventricular tachycardia, QTc prolongation. | Activation of apoptotic pathways and caspases | EETs inhibited pro-apoptotic pathways through increasing activity of the pro-survival enzyme phosphoinositide 3 kinase (PI3K) in mouse primary cardiomyocytes (Dhanasekaran et al., 2008) |
| sunitinib (Aparicio-Gallego et al., 2011) | As above | | |
| astemizole (Minotti, 2010) | QTc interval prolongation in a dose related manner. Cardiac dysrhythmia. | Changes in electrophysiology | No evidence to date |
| terfenadine (Minotti, 2010) | | | |
| thioridazine (Minotti, 2010, Menkes and Knight, 2002) | | | |
| sunitinib (Aparicio-Gallego et al., 2011) | As above. | Cardiac hypertrophy | In an animal model of isoproterenol-induced cardiac hypertrophy, use of sEH inhibitors protected in rats (Althurwi et al., 2013). |
| 5-fluorouracil (Alter et al., 2006) | Angina, myocardial infarction, arrhythmia and heart failure. | Vasoconstriction | 11,12-EET caused relaxation of rat coronary arteries and renal and cerebral arteries of rats and rabbits. (Larsen et al., 2006, J. D. Imig et al., 2001, Fisslthaler et al., 1999, Dimitropoulou et al., 2007, Campbell et al., 1996) |
| cyclosporine A (Rezzani et al., 2005) | As above. | Increase in intracellular calcium concentration through the calcium sensing receptor (CaSR) | No evidence to date |
| eperisone (Yamagiwa et al., 2014, Saegusa et al., 1991) | QTc interval prolongation | Inhibition of nicotinic and muscarinic receptors | No evidence to date |

Other cardiotoxic drugs such as the anti-arrhythmic drug amiodarone have been shown to alter apoptotic pathways, increasing caspase 3 activity leading to an increase in apoptosis and cell death in h9c2 cells (Isomoto et al., 2006). The addition of exogenous EETs *in vitro* has been shown to boost activity of the pro-survival enzyme phosphoinositide 3 kinase (PI3K) and inhibit pro-apoptotic pathways in primary cardiomyocytes derived from a rat heart hypoxia/reperfusion model (Dhanasekaran et al., 2008).

Cardiotoxic drugs also impact haemodynamics within the cardiovascular system. An example of detrimental effects of drugs on blood pressure is the CYP2J2 substrate 5-fluorouracil which has been shown to be vasoconstrictive through inhibition of nitric oxide synthase leading to coronary spasms, and via protein kinase C leading to vasoconstriction (Alter et al., 2006). Inhibition of sEH increased EETs and dilated human coronary arterioles through BK_{ca} channels and 11,12-EET also caused relaxation of rat coronary arteries and renal and cerebral arteries of rats and rabbits. (Larsen et al., 2006, J. D. Imig et al., 2001, Fisslthaler et al., 1999, Dimitropoulou et al., 2007, Campbell et al., 1996). Taken together, EETs have been shown to act on several pathways involved in cardiotoxicity and there is circumstantial yet plausible evidence to suggest a protective impact of CYP2J2 via EET synthesis in the heart during cardiotoxicity.

1.8 Role of CYP2J2 in doxorubicin induced cardiotoxicity

The strongest case for a role of CYP2J2 in protection against cardiotoxicity has been presented for dox. Dox is an anthracycline used for the treatment of solid tumours and haematological carcinomas which has been shown to modulate CYP2J2 production of EETs. Despite its anticancer action, the clinical value of this drug is reduced due to acute and chronic, cumulative and irreversible dose dependent cardiotoxicity (Belham et al., 2007). Cardiovascular effects include acute cardiomyopathy, chronic heart failure, ventricular dysfunction and arrhythmias (Yeh et al., 2004). Currently it is unclear whether the mechanism of cardiotoxicity is the same, when occurring acutely (within days) or chronically (years) following treatment (Takemura and Fujiwara, 2007).

Preclinically, both acute and chronic dox administration have been associated with changes in EET formation (Zordoky et al., 2010, Alsaad et al., 2012). In rats, acute dox treatment was found to alter the mRNA expression of P450 and sEH enzymes in kidney

and liver, leading to decreases in 5,6-, 8,9-, 11,12- and 14,15-EET (Zordoky et al., 2010). Ichikawa et al., (2014) found that acute dox induced cardiotoxicity was associated with generation of reactive oxygen species, cellular iron accumulation and disruption of the mitochondria which in turn initiated apoptotic pathways in isolated neonatal rat cardiomyocytes (Ichikawa et al., 2014). Previously, EETs have been shown to attenuate reactive oxygen species production and mitochondrial dysfunction in carcinoma cells treated with arsenic trioxide (L. Liu et al., 2011) and an interesting and potentially important recent study suggested that CYP2J2 mRNA expression increased in adult human ventricular myocytes in culture in response to both external oxidants and addition of doxorubicin; the latter, amongst other effects, stimulates intracellular oxidant production. Moreover, cell survival decreased with oxidant exposure when CYP2J2 was inhibited either using danazol or by siRNA for CYP2J2. Unsurprisingly, this reactive oxygen species toxicity was mitigated with the addition of exogenous EETs. Although the report is intriguing and plausible, there are limitations to be highlighted. The use of millimolar concentrations of pyruvate as the only antioxidant trialled limits mechanistic interpretation as does the use of danazol as a CYP2J2 inhibitor; however in support of CYP2J2-derived EETs as protective agents, knockdown of CYP2J2 mRNA also negatively affected cell survival following dox yet levels of CYP2J2 protein were not addressed. The relatively non-specific measurement of intracellular oxidant formation resulting from dox treatment of cells also limits interpretation of the mechanism of molecular signalling. Nevertheless, this mechanism may have implications for other cardiotoxic compounds acting, in part, via oxidant formation in cells of the cardiovascular system. If the mechanism is proven to be mediated by increased oxidants in cells then protection from these agents could also be afforded by changes in CYP2J2 gene expression and the resultant increased EET formation.

Alsaad et al. (2012) studied the effects of chronic dox cardiotoxicity in the heart on the mRNA expression of proteins involved in the formation of AA metabolites as well as levels of these metabolites via LC/MS in rats. Animals were treated with multiple intraperitoneal injections over 14 days followed by a 14 day recovery period, emulating the clinical administration (Alsaad et al., 2012). Chronic Dox treatment *in vivo* caused no change in mRNA expression of the rat analogue of CYP2J2, CYP2J3. However, it increased mRNA expression of other P450 enzymes including CYP4A3, CYP4F1 and

CYP4F5 known to produce the alternative AA metabolite, 20-HETE resulting in increased levels of 20-HETE compared with an untreated control group (Alsaad et al., 2012). The authors also observed a rise in the mRNA expression of the *EPHX2* (sEH) gene in heart in dox treated rats accompanied by the decreased EET levels and an increase in the levels of inactive DHETs. Furthermore, treatment of H9c2 cells, a rat cardiac cell line, with a sEH inhibitor (t-AUCB) in combination with dox, reduced both ANP and BNP release (markers of cardiac hypertrophy), suggesting a cardioprotective effect of sEH inhibition. Additionally, dox has been shown to upregulate levels of many P450 enzymes in this cell model including 2J3 and 2E1 (Zordoky and El-Kadi, 2008). Given the biological protective activity of EETs particularly 11,12-EET and 14,15-EET against cardiovascular disease (Sudhahar et al., 2010), it is hypothesised that EETs may provide protection against cardiotoxicity induced by a whole spectrum of xenobiotics *in vivo*.

Discrepancies in mRNA expression between acute and chronic dox administration have been documented (Zordoky et al., 2010, Alsaad et al., 2012) highlighting the caution required when interpreting studies comparing acute versus chronic dox administration. Furthermore, the treatment period used by Alsaad may not be sufficient to induce many of the characteristic features of chronic dox cardiotoxicity. A detailed assessment by Cove-Smith et al., 2014 of both cardiac morphology and function in rats for 8 weeks following 1.25 mg/kg dox demonstrated changes in cardiac function, in particularly cardiac output, stroke volume and ejection fraction from day 15. Gross morphological changes and biomarkers associated with cardiomyocyte degeneration occurred much later (Cove-Smith et al., 2014). Consequently, the changes observed after 2 weeks of dox treatment are unlikely to be a true indication of the protective role of EETs during dox cardiotoxicity and therefore the study length would need to be extended to definitively determine this. However, it is plausible to suggest that epoxygenase enzymes are involved in the cellular development of dox induced cardiotoxicity.

Using transgenic mice with cardiomyocyte specific overexpression of human CYP2J2, Zhang et al. (2009) identified the possible beneficial effects of EETs in the protection against dox-induced cardiotoxicity. Elevations in serum lactate dehydrogenase (LDH) and creatinine kinase (CK) and activation of cardiac caspase 3 and catalase caused by acute treatment with dox (0, 5 and 15 mg dox/kg/day i.p. for 3 days followed by 24 h recovery) were mitigated in mice overexpressing CYP2J2 suggesting protection against

dox induced myocardial damage. However, some of these markers are not specific to the heart and this may affect the interpretation of these findings. Following chronic treatment with dox (0, 1.5, 3 mg/kg biweekly for 5 weeks followed by a 2 week recovery) the CYP2J2 transgenic mice showed a lower heart weight to body ratio, reduced cardiac ankyrin repeat protein (CARP) and expression ratio of β MHC: α MHC and no change in LVDP compared to wild type mice. This indicates that cardiac structure and contractile function were preserved which may have been mediated by protective EETs (Y. Zhang et al., 2009). Although CARP is a specific biomarker of cardiac hypertrophy, it may not be a good biomarker of early cardiac remodelling. In fact, many of the serological, pathological and functional biomarkers of early cardiac damage during cardiotoxicity were not reported. For example, cardiac troponin which is known to be the gold standard in investigating cardiac damage, pre-clinically and clinically, was not measured (Cove-Smith et al., 2014).

Studies have found that CYP2J2 is capable of metabolising dox (Y. Zhang et al., 2009). However, as this was a CYP2J2 transgenic model and not a null model other P450 enzymes may also be responsible for the increased metabolism of dox. Furthermore, increased expression and activity of reductase in the transgenic mouse hearts may also lead to an increase in activity of many other P450 enzymes. It is known that the major metabolite of dox, doxorubicinol (DOXol) contributes to the toxicity in the myocardium, however, there is also evidence to suggest other metabolites of dox including dox deoxyglycone and DOXol hydroxyglycone may also contribute to the cardiotoxicity (Licata et al., 2000). In addition cytochrome P450 reductase can also metabolise dox to 7-deoxydoxyrubicin aglycone which has been shown to inhibit AA metabolism, reducing the production of EETs and altering the regiosomers of EETs produced (Arnold et al., 2017). Therefore, increased metabolism through CYP2J2 may have a conflicting effect on the heart, elevating levels of toxic metabolites for certain drugs but increasing protection through EETs. Other cytochrome P450 enzymes belonging to the murine CYP2J family, including CYP2J8, 2J11, 2J12 and 2J13, also have epoxidase activity towards AA. This may confound results especially as expression levels of these enzymes were not measured in the CYP2J2 transgenic mice (Graves et al., 2013). In rats, only CYP2J3 has been demonstrated to possess epoxygenase activity and so protective effects by EETs may be less apparent. In addition, the use of transgenic models where there is a genetic alteration leading to

differences in protein expression and hence activity, may not directly model pharmacological activation of CYP2J2 in the wild-type mouse (Knight and Shokat, 2007).

Taken together the limited number of studies on dox toxicity suggest CYP2J2 expression and EET production have profound cardioprotective effects, modulating dox cardiotoxicity through their influence on molecular pathways involved in apoptosis, ROS generation, hypertrophy and cardiac remodelling leading to an overall conservation of structure and function. It may be hypothesised that the cardiac potential of other drugs might be affected by CYP2J2 metabolism and/or EET formation. The effects of EETs on dox raises the possibility that the CYP2J2/EET pathway may also modulate cardiotoxicity of other drugs, working through different mechanisms.

1.9 The search for the ideal cell type for *in vitro* cardiotoxicity testing

1.9.1 HepG2 cells

The HepG2 immortalised cell line was derived from liver hepatocellular carcinoma of a 15 year old Caucasian male. The cells have an epithelial-like structure that adhere and grow in small aggregates (Bouma et al., 1989). HepG2 cells are widely used in toxicity assessment of a wide variety of chemicals and drugs due to their unlimited availability and phenotypic stability. They also display a similar genotype to normal liver cells (Gerets et al., 2012).

Although expression of drug metabolism enzymes are much lower in HepG2 cells compared to primary human hepatocytes, HepG2 cells have shown similar up-regulation of P450 enzymes compared to primary cells in response to test substances indicating their usefulness in studying regulation of drug-metabolising enzymes (Wilkening et al., 2003). To support this, studies showed upregulation of CYP2J2 in response to butylated hydroxyanisole in HepG2 cells (A. C. Lee and Murray, 2010) and impaired activation of the gene under conditions of oxidative stress (P. H. Cui et al., 2010). The presence of inducible CYP2J2 in HepG2 cells indicates an appropriate model for studying its role in cardiotoxicity and the EET formation pathway.

1.9.2 iPSC-CMs

It is also important to adopt cell types which would best mimic characteristics of cardiac cells and provide a more physiologically relevant model. Induced pluripotent stem cell derived cardiomyocytes have been a breakthrough in producing more physiologically relevant models of disease, drug discovery and drug safety screening (Maillet et al., 2016).

The high degree of homology of iPSC-CMs with human cardiomyocytes is presumably through their differentiation from induced pluripotent stem cells. These cells normally originate from a human mature cell such as a fibroblast that is reprogrammed by forced expression of four pluripotent genes, Oct3/4, Sox2 and c-Myc through viral or non-viral methods (Oldroyd et al., 2012). Once an iPSC cell line has been established they can undergo treatment with growth factors which target specific signalling pathways to produce cells of a certain lineage. Cardiovascular cells are typically generated by mimicking the Actin/Nodal/TGF- β , Wnt and BMP cellular pathway (Paige et al., 2010). To retrieve a particular cell type, for example ventricular cardiomyocytes, purification techniques such as use of cell surface markers and fluorescent probes or by modulating the retinoic acid and Wnt signaling pathways are employed (Lundy et al., 2013). Phenotypically, immature iPSC-CMs (20-40 days) are small and round with little of the structural and functional machinery commonly seen in cardiac myocytes. However once mature (80-100 days) they exhibit many of the qualities of human cardiac myocytes. They are able to form connections with other myocytes and beat in synchrony. The magnitude of contraction for early stage hiPSC-CMs was shown to be 4.95% of resting length which increased to 10.17 for mature cells (Lundy et al., 2013).

One of the major assets of mature iPSC-CMs is that they possess many of the major human structural and functional cardiac proteins. They have been shown to express sarcomeric related proteins including MYH6 and TNNT2 and also contain the same components of Ca²⁺ cell cycling machinery such as the inositol triphosphate receptor IP3R and sarcoplasmic reticulum Ca²⁺ ATPase SERCA2a together with ion channels including sodium channels and L type calcium channels (Karakikes et al., 2015). However action potentials recorded for iPSC-CMs exhibit mixed action potential phenotypes with a positive diastolic potential and slow upstroke velocity when compared to native cardiomyocytes (Lundy et al., 2013).

The correlation in structural and functional characteristics between iPSC-CMs and primary cardiomyocytes, high throughput screening capabilities and the relative inaccessibility of human cardiac tissue have meant the use of iPSC-CMs in drug assessment and disease modelling is increasingly being recognised. iPSC-CMs have been used as part of an *in vitro* model for doxorubicin (dox) cardiotoxicity. Within hours of dox treatment, toxicity markers assessed showed a significant production of reactive oxygen species (ROS), mitochondrial dysfunction and increased $[Ca^{2+}]^i$ (Maillet et al., 2016). This is consistent with the toxicity response commonly seen in the initial steps of dox cardiotoxicity indicating its use as a useful candidate cell type in *in vitro* study.

The expression levels of CYP2J2 in this cell type have not been fully understood as of yet, however preliminary data from AstraZeneca indicate that RNA expression levels are very similar to human ventricle indicating that this cell type may be a suitable model to use for the study of both cardiotoxicity and CYP2J2 expression and activity (see table 4.1).

Table 1-7 CYP2J2 next generation sequencing data

Similarities were seen in CYP2J2 expression (RNA) NGS score of human primary ventricle cardiomyocytes and human induced pluripotent stem cell derived cardiomyocytes (hiPSC-CM). MEC microvascular endothelial cells; hESC-CMs human embryonic stem cells derived cardiomyocytes. Data kindly supplied by Dr Amy Pointon, AstraZeneca.

| Tissue type | Liver | Coronary-MEC | Fetal heart | Ventricle | Cardiac-MEC | hESC-CMs | hiPS-CMs |
|--------------------------|-------|--------------|-------------|-----------|-------------|----------|----------|
| CYP2J2 expression | 65.02 | 0.30 | 46.07 | 56.63 | 0.13 | 12.04 | 55.63 |

1.9.3 Human cardiac myocytes

In addition to iPSC-CMs, a commercial human cardiac myocyte cell line is also available. The human cardiac myocytes that were purchased from Promocell were from normal human ventricle tissue of the adult heart. These cells were more amenable to long term culture compared to freshly isolated cardiomyocytes and iPSC-CMs and therefore offered an economical alternative to induced pluripotent cells. However, P450 expression in this cell line had not been investigated and so its usefulness in investigating a role for CYP2J2 in cardiotoxicity was unknown.

1.9.4 EA.hy926 cells

Besides cardiac cells, other cells in particular endothelial cells make up a large proportion of the heart. With this in mind, an endothelial cell line, EA.hy926 was also included as a possible *in vitro* cell model. EA.hy926 cells are a permanent human vascular endothelial cell line generated in 1983 by fusion of human umbilical vein endothelial cells (HUVECs) with the human lung carcinoma cell line A549 (Edgell et al., 1983). They retain many of the characteristics of HUVECs including expression of adhesion molecules ICAM, VCAM and E-selectin as well von willibrand factor (vWF) which is upregulated when stimulated with TNF- α . Phenotypically these cells have an elongated structure which forms networks with nearby cells (Bouis et al., 2001). Investigation of expression of CYP2J2 in EA.hy926 cells showed inducible expression of CYP2J2 by TLR-4 agonist LPS and in correlation and an increase in epoxygenase activity which was inhibited by the epoxygenase inhibitor MS-PPOH. In addition, sEH expression and epoxide hydrolase activity were also present in these cells (Askari et al., 2014). Thus these cells were shown to be a simple, reproducible *in vitro* cell model to investigate the potential protective effects of CYP2J2 from external stimuli e.g cardiotoxic drugs.

1.10 Candidate cardiotoxic drugs

1.10.1 Astemizole

The drugs selected as candidate drugs for initial investigation of toxicity were known cardiotoxins. Astemizole, an anti-histamine drug, is a second generation H1 receptor antagonist previously used for the treatment of allergic inflammatory conditions (Baroody and Naclerio, 2000). It undergoes rapid hepatic metabolism to produce the active metabolite desmethylastemizole by o-demethylation of the parent drug. However, it was withdrawn from the market worldwide in 1998 due to its adverse effects on the heart (Minotti, 2010). Astemizole was shown to trigger torsades de pointes arrhythmias leading to tachycardia, ventricular fibrillation and death (Baroody and Naclerio, 2000). In the UK, a study showed astemizole to have the highest relative risk of toxic ventricular arrhythmias and death compared with other anti-histamines (Minotti, 2010). The mechanisms of its toxicity centres on blocking of the Kv11.1 (hERG) potassium channel by both astemizole and desmethylastemizole equipotently with IC₅₀ values in the nanomolar range (Minotti, 2010) leading to QT prolongation. The long elimination

time of desmethylastemizole (~9-13 days) means toxicity can be harder to treat (Z. Zhou et al., 1999). Astemizole and its metabolite have also been shown to block other cardiac potassium channels including the delayed rectifier K⁺ channel (IKr) in HEK293 cells and rabbit myocytes (Z. Zhou et al., 1999). *Ex vivo* studies on rabbit purkinje fibres showed a concentration dependent prolonging effect of astemizole on final repolarisation and showed a development in early after depolarisations (EADs) (Adamantidis et al., 1995). This was corroborated *in vivo* by a study in cynomolgus monkeys where single doses of astemizole ranging from 10-60mg/kg/day showed QT prolongation (J. Lee et al., 2008).

Although mainly metabolised in the liver, Matsumoto *et al* (2002) observed that astemizole could also undergo extensive first pass metabolism in rabbit small intestine, which was orchestrated primarily by CYP2J2. Due to the high expression of CYP2J2 in the heart and the adverse cardiac effects of astemizole, it may be possible that metabolism of astemizole occurs in the heart. Furthermore, inhibition studies with recombinant CYP2J2 microsomes showed an inhibition of astemizole demethylation by arachidonic acid (Matsumoto et al., 2002). This may be seen as a positive effect as arachidonic acid epoxidation by CYP2J2 leads to protective EETs which may reduce toxic effects of astemizole. The metabolism of astemizole by CYP2J2 and its inhibition by arachidonic acid proposed an opportunity for its use to better understand drug interactions with CYP2J2 and how CYP2J2 may initiate the protective EET pathway in the presence of astemizole induced cardiotoxicity.

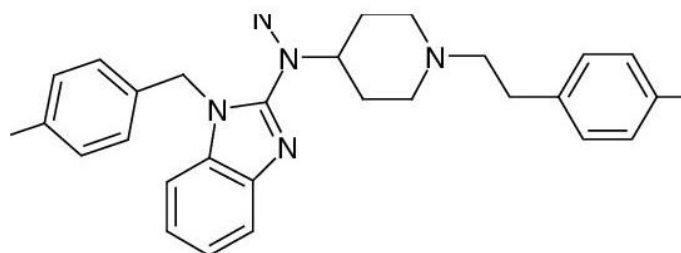


Figure 1-7 Chemical structure of astemizole (Alghamdi, 2008)

1.10.2 Doxorubicin

Dox is a quinone-containing anthracycline used for the treatment of solid tumours and haematological carcinomas. Its anti-malignancy mode of action consists of intercalation

into DNA, inhibition of topoisomerase II and generation of ROS leading to disruption of DNA crosslinking, DNA damage and apoptosis (Chatterjee et al., 2010). However the use of dox has been hampered by several toxic effects including haematopoietic suppression, extravasation, and nausea with the most severe being cardiotoxicity. Dox cardiotoxicity can have a wide range of features which occur either immediately or years after cessation of therapy. Acute dox toxicity normally occurs within 24 hours of treatment in around 11% of cancer patients. It is characterised by ECG abnormalities including QT prolongation, however this stage may also be asymptomatic. Sub-acute cardiotoxicity can occur several weeks or months after the last dose with the main symptom being pericarditis and myocardial edema (Chatterjee et al., 2010). Chronic dox toxicity may initiate 4-20 years after dox treatment (Octavia et al., 2012) and is much rarer than acute with an incidence of 1.7% related to the dosage and individual susceptibility such as age and gender. It is associated with more progressive myocardial dysfunction with reduced ventricular ejection fraction and interstitial fibrosis (Chatterjee et al., 2010).

One of the main mechanisms of dox induced cardiotoxicity appears to be the 'ROS and iron hypothesis' where accumulation of iron leads to an increased generation of ROS and toxic damage to the mitochondria of cardiomyocytes. It has been proposed that dox gets oxidised and becomes a semiquinone radical inducing reactive superoxide formation. Furthermore doxorubicin can also interact with iron forming the dox-Fe complex leading to further ROS production (Gammella et al., 2014). This hypothesis is supported by experiments *in vivo*. In a mouse model of dox toxicity where there was an increase in iron accumulation this was reduced when treated with an iron chelator which also prevented dox toxicity (Ichikawa et al., 2014). Dox may also generate ROS through interaction with eNOS where binding of dox to eNOS reductase leads to O_2^- generation. eNOS reductase reduction then forms the dox semiquinone radical which can lead to further O_2^- generation (Octavia et al., 2012).

Although cardiomyocytes are the classical cellular target for dox toxicity, the myocardium is also composed of fibroblasts, endothelial cells and vascular smooth muscle cells which may interact and play a part in dox cardiotoxicity. In particular, studies have shown that dox can inhibit proliferation, increase oxidative stress and apoptosis in cardiac progenitor cells (CPCs) (De Angelis et al., 2010). CPCs give rise to cardiomyocytes, endothelial cells and smooth muscle cells thus reducing the number

resident CPCs decreasing CPC activation and cardiomyocyte turnover in the presence of myocyte death. In addition, dox can also act on fibroblasts, transforming them to myofibroblasts with a pro-fibrotic phenotype (Cappetta et al., 2016). Dox has also been shown to disrupt the structure and function of vascular smooth muscle cells. *In vitro* smooth muscle cells enter cell cycle arrest after dox treatment and display decreased expression of adrenoreceptor protein decreasing contraction (De Angelis et al., 2016).

The metabolism of dox by CYP2J2 was observed by Zhang *et al* (2009) who observed higher rates of dox metabolism in CYP2J2 transgenic mice compared with wild type (Y. Zhang et al., 2009). However, whether there is metabolism of dox in the heart and how this may affect EET production is a question yet to be answered.

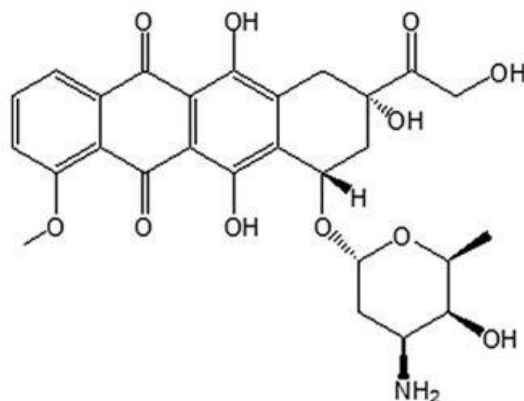


Figure 1-8 Chemical structure of doxorubicin (Senes-Lopes et al., 2018)

1.10.3 Sunitinib

Sunitinib malate is a multi- target tyrosine kinase inhibitor used in the treatment of gastrointestinal tumours and renal cell carcinoma. Its main mechanism of action is through inhibition of growth factor receptors regulating tumour cell survival, including vascular endothelial cells growth factor receptor 1-3 (VEGFR), platelet derived growth factor receptor α and β (PDGFR), stem cell factor receptor (c-KIT) and colony stimulating factor-1 receptor (CSFR-1) (Chu et al., 2007).

However, numerous studies have suggested that around 8-15% of sunitinib-treated patients show cardiac adverse effects including development of left ventricular

dysfunction, hypertension and congestive heart failure (Kerkela et al., 2009). At a cellular level, transmission electron microscopy (TEM) analysis of endomyocardial biopsy samples from patients with sunitinib induced cardiotoxicity showed cardiac hypertrophy and a disruption of mitochondrial structure with effaced cristae and membrane whorls (Chu et al., 2007). Both *in vitro* and *in vivo* models have been used to further investigate mechanisms of toxicity. Mice were given a dose of 40/mg/kg of sunitinib per day for 3 weeks to emulate levels in patients. In addition to mitochondrial swelling there was increased release of cytochrome c leading to increases in cell death particularly apoptosis (Chu et al., 2007). Sunitinib has also been associated with an impaired cardiac response to stress accompanied by microvascular dysfunction and significant depletion in coronary microvascular pericytes. These cells which have been shown to regulate capillary flow are dependent on PDGFR signalling. As PDGFR is a target for sunitinib, it has been proposed that sunitinib acts on coronary microvascular pericytes through PDGFR signalling, leading to left ventricular dysfunction and heart failure (Chintalgattu et al., 2013).

One of the proposed mechanisms of cardiotoxicity of sunitinib is through the off-target inhibition of AMP-activated protein kinase which plays a key role in regulating energy stress and is normally activated as a protective response to energy depletion, restricting energy utilisation and increasing production (Kerkela et al., 2009). Phosphorylation of AMP kinase was increased in sunitinib treated mice and determination of the IC_{50} for sunitinib against AMPK *in vitro* showed AMPK may be a target for sunitinib. In addition treatment of cardiomyocytes with compound C (AMPK inhibitor) showed a disruption in mitochondrial structure and membrane potential and induced apoptosis similar to that in sunitinib toxicity (AMPK) (Kerkela et al., 2009).

The question of whether sunitinib toxicity may be reversed with the right treatment has led to work in to new therapies. It was found that injection of fibroblast growth factor 2 (FGF2) mRNA into embryos protected cardiomyoblast H9c2 cells against sunitinib cardiotoxicity. Furthermore FGF2 did not compromise the anti-tumour action of sunitinib (G. Cui et al., 2016). Also, the use of VEGF signalling pathway inhibitors (VSP) in two severe symptomatic cases of sunitinib cardiomyopathy reversed much of the mitochondrial damage and stress, microvascular stress and hypoxic signalling (Uraizee et al., 2011).

The link between sunitinib toxicity and CYP2J2 is not clear, however investigation of the metabolic activity of 2J2 in sunitinib biotransformation in hepatocellular and renal cell carcinomas showed that CYP2J2 was highly expressed in cancer tissue and rapidly metabolised sunitinib along with other TKIs with the same efficiency as CYP3A4, a major drug metaboliser in the liver (Narjoz et al., 2014). This gives evidence for a role of CYP2J2 in drug metabolism in the liver, its role in the heart however is yet unknown.

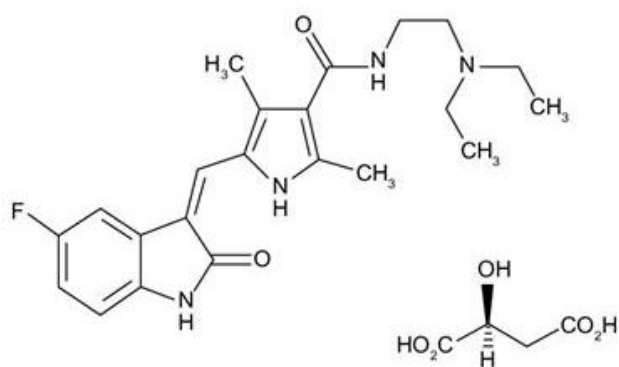


Figure 1-9 Chemical structure of sunitinib malate (Hao and Sadek, 2016)

1.11 Pharmacological inhibitors of the EET pathway

1.11.1 MS-PPOH

The acetylene N-methylsulfonyl-6-(2-propyrgyloxyphenyl) hexanamide (MSPPOH) is a potent and selective inhibitor of cytochrome P450 arachidonic acid epoxidation both *in vitro* and *in vivo* (Brand-Schieber et al., 2000). MSPPOH works as a suicide substrate by resembling the substrate such as AA and at the same time irreversibly inactivating the enzyme using the catalytic cycle. Due to the lack of specificity of MSPPOH for a particular P450 enzyme, VanAlstine *et al* (2011) studied the effects of MSPPOH on the activity of nine human and three rat recombinant P450 enzymes. MSPPOH was shown to potently inhibit CYP2C9 and 2C11 epoxygenases. However, CYP2J2 activity was not investigated (VanAlstine and Hough, 2011).

MSPPOH was shown to significantly inhibit arachidonic acid epoxidation and production of EETs in both rat renal microsomes and anaesthetised rats as measured by LC-MS. This effect lasted around 6hrs, however during that time there were no changes

seen in 20-HETE formation (Brand-Schieber et al., 2000) indicating MSPPOH did not affect hydroxylase enzyme activity. A further study in renal microsomes showed a reduction in expression of CYP2J2 in response to MSPPOH (Huang et al., 2006).

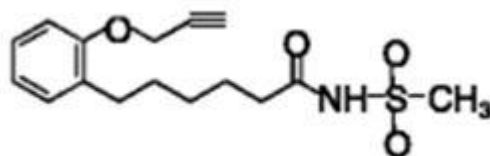


Figure 1-10 Chemical structure of MS-PPOH (Campbell and Fleming, 2010)

1.11.2 Quinacrine

Phospholipase A2 (PLA₂) releases arachidonic acid from the membrane and increases production of EETs. Quinacrine dihydrochloride is a general non-specific PLA₂ inhibitor that has been shown to reduce EET production *in vitro* in LLCPKcl4 cells (Chen et al., 1999). In isolated rat mesenteric artery EETs caused hypopolarisation of the endothelial membrane leading to release of endothelial derived hypopolarising factors and relaxation of vascular smooth muscle. In the presence of quinacrine dihydrochloride acetylcholine induced hypolarisation was attenuated and instead there was depolarisation of the membrane leading to vasoconstriction of the artery (Fulton et al., 1997).

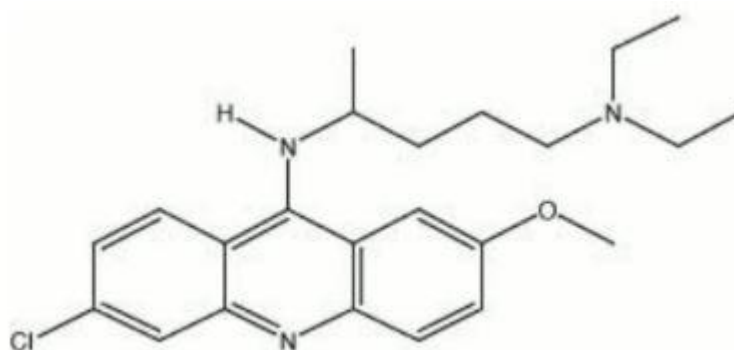


Figure 1-11 Chemical structure of quinacrine dihydrochloride (image courtesy of CAMEO online)

1.11.3 LY311727

LY311727 is a specific PLA₂ inhibitor for secretory phospholipase A₂ which has been shown to be involved in the release of fatty acids from the phospholipid membrane including arachidonic acid (AA) (Murakami et al., 1998). It is proposed that inhibition of AA release from the membrane may lead to a reduction of EET formation and signalling and exacerbation of drug induced toxicity. Although there is little evidence of the role of secretory PLA₂ in the heart, in an experimental model of ventilator induced lung injury (VILI), inhibition of sPLA₂ in the pulmonary vascular endothelium by LY311727 led to a reduction in recruitment and adhesion of inflammatory cells to the injury site (Meliton et al., 2013). This indicates there may be other more prominent pathways involved which are pro-inflammatory and counteract the protective effects of EETs. Thus it would be pertinent to see how prominent the role of EETs is in reaction to cell stress and injury in cardiac cells as well as understand the possible role of other groups of PLA₂ enzymes. For example, cytosolic phospholipase A₂ has been shown to mediate AA release in H9c2 rat cardiomyocytes in response to hydrogen peroxide, indicating PLA₂ enzymes other than sPLA₂ may also be involved in AA release.

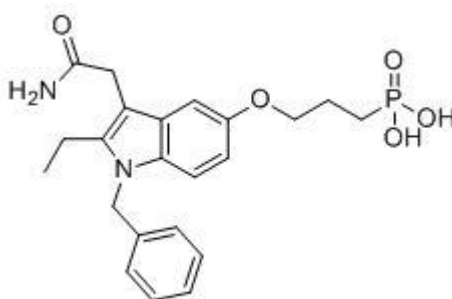


Figure 1-12 Chemical structure of LY311727 (Om, 2018)

1.12 Pharmacological facilitators of the EET pathway

1.12.1 t-AUCB

An increasing number of studies have shown the importance of the EET pathway and in particular soluble epoxide hydrolase (sEH) in cardiovascular disease and heart failure (see section 5.1). Indeed the sEH gene *EPHX2* has been identified as a susceptibility gene for heart failure (Monti et al., 2008). Animal and *in vitro* models utilising

pharmacological inhibitors of sEH have therefore become an attractive option to further investigate the role of sEH in protection.

4-[[trans-4-[[tricyclo[3.3.1.1^{3,7}]dec-1-ylamino)carbonyl]amino]cyclohexyl]oxy]-benzoic acid (t-AUCB) is a well-established inhibitor of sEH with an IC_{50} against human sEH of 1.3nM compared to other known inhibitors such as AUDA and TUPS which have IC_{50} values of 3.2 and 2.9nM respectively (J. D. Imig and Hammock, 2009). It is a urea based inhibitor which inhibits sEH by creating hydrogen bonds and salt bridges between the urea component of the inhibitor and residues on the sEH active site, resembling the intermediate formed during the EET reaction (J. D. Imig and Hammock, 2009). t-AUCB has been used widely in animal and *in vitro* models to examine the role of EETs within the heart and has been shown to successfully inhibit sEH and reverse the deleterious effects of cardiovascular disease. For example in a mouse model of atherosclerosis, treatment with t-AUCB reduced the size of the atherosclerotic plaque by promoting cholesterol efflux and increasing HDL levels (Shen et al., 2015). In addition, t-AUCB reduced the myocardium infarct size and incidence of arrhythmias in a myocardial infarction mouse model (Gui et al., 2017). Furthermore, investigation into the role of sEH in toxicity showed protective effects against hypertrophy associated with both doxorubicin and daunorubicin induced toxicity *in vitro* indicating EETs may play a major role in regulating drug induced damage to the heart (Alsaad et al., 2012, Maayah et al., 2018).

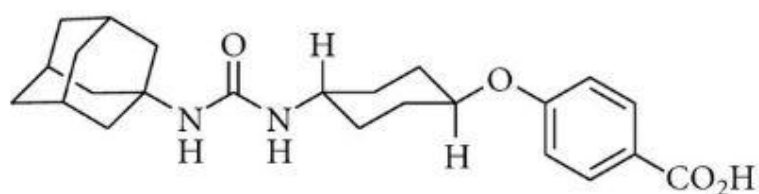


Figure 1-13 Chemical structure of t-AUCB (Iyer et al., 2012)

1.13 Conclusions

CYP2J2 is an AA and drug metabolising enzyme highly expressed in the human heart. However, the role of CYP2J2 in drug metabolism in the heart has not been well defined. Nevertheless, there is increasing awareness that many current drugs are substrates for CYP2J2. There are also substantial data suggesting that CYP2J2 along with CYP3A4 plays a significant part in the metabolism of drugs known to cause cardiotoxicity.

Therefore, changes in the expression or activity of this enzyme may alter drug concentrations in the body leading to either an ineffective drug response or increased levels of metabolites leading to potential cardiotoxicity. Known P450 inducers do not modulate CYP2J2 levels but some compounds have been recognised to induce expression and activity of CYP2J2 in adult human cardiomyocytes. In addition, several SNPs in the human CYP2J2 gene are associated with altered *in vitro* activity of the CYP2J2 enzyme, which may lead to changes in EET formation and drug metabolism, potentially altering cardiotoxicity in some individuals. As well as its role in drug metabolism, CYP2J2 derived EETs have also been shown to have a protective effect, although this has only really been reported for dox-induced cardiotoxicity. Given that our understanding of the role of CYP2J2 and EET formation is largely based on the data from this single drug and the importance of cardiotoxicity to drug development and application in man, understanding more widely the role and possible protection by CYP2J2 in the heart is worthy of further study.

Chapter 2 Hypothesis and Aims

Drug induced cardiotoxicity has been associated with pathophysiological changes which may be regulated by multiple mechanisms. CYP2J2 has been found in high levels in the heart and cardiovascular system and has been found to be involved in drug metabolism and production of endogenous protective eicosanoids called EETs. This study aimed to investigate the hypothesis that CYP2J2 may be involved in regulating *in vitro* drug cardiotoxicity through the production of EETs and drug metabolism of cardiotoxic drugs.

The aim of this study is to use cytotoxicity assays to investigate a pertinent drug cell model that could be employed as a cardiotoxicity screen to aid in the investigation of the protective capabilities of EETs towards cardiotoxicity *in vitro*. To do this we investigated:

- 1) Expression of CYP2J2 and soluble epoxide hydrolase (sEH) in human cardiac myocytes (HCMs) and Eahy.926 cells, an endothelial cell line.
- 2) Astemizole drug metabolism by CYP2J2 using LC-mass spectroscopy.
- 3) Whether CYP2J2 has a protective role in astemizole drug cardiotoxicity through the addition of 'EET modulators'.
- 4) Biomarkers of toxicity by analysing exosome release *in vitro* in response to cardiotoxic drugs.

Chapter 3 **Materials and Methods**

3.1 Cell culture and treatment reagents

3.1.1 Cell lines and primary cells

HepG2 cells were originally isolated from a human liver biopsy taken from a 15- year old male patient with hepatocellular carcinoma. The cells were purchased from ATCC as an established cell line (<https://www.lgcstandards-atcc.org/>).

HL-60 cells, a human peripheral blood cancer cell line were a generous gift from Professor Alison Goodall's group, cardiovascular science department, Glenfield hospital, Leicester, UK.

iCardiomyocytes were made by firstly inducing pluripotency in mature cells taken from adult skin or blood obtained from donors. These induced pluripotent cells were then differentiated into cardiomyocytes with the use of growth factors. The cells were generously purchased for us by AstraZeneca, Cambridge, UK from Cellular Dynamics International, Madison, Wisconsin, USA. <https://cellulardynamics.com/>.

EA.hy926 cells are a permanent human vascular endothelial cell line generated in 1983 by fusion of human umbilical vein endothelial cells (HUVECs) with the human lung carcinoma cell line A549. The cells were a generous gift from Professor Alison Goodall's group, cardiovascular science department, Glenfield hospital, Leicester, UK.

Human cardiac myocytes (HCM) originated from normal human ventricle tissue of the adult heart and were more amenable to long term culture compared to freshly isolated cardiomyocytes. The cells were purchased from PromoCell, Heidelberg, Germany.

3.1.1.1 Cell culture consumables

The stripettes were bought from Costar, Sigma-Aldrich Company Ltd, Poole, and Dorset, UK. The clear-bottom 96-well plates, 96-well white bottom plates and cell culture flasks (T25 and T75cm²) were obtained from Corning, Sigma-Aldrich Company Ltd, Pool, Dorset, UK.

3.1.1.2 Cell culture media

The media used to culture HepG2 cells, HL-60 cells and EA.hy926 cells was Dulbecco's Modified Eagle's Medium with high glucose (containing 4500mg/L glucose, 110mg/L sodium pyruvate and 4mmol/L L-glutamine) and was purchased from Gibco, Invitrogen UK Ltd, Paisley, Scotland, UK.

Specific plating medium was used for the first 24hrs after thawing iCardiomyocytes after which cells were grown in maintenance medium. Both were purchased from Cellular Dynamics International, Madison, Wisconsin, USA.

Human cardiac myocytes were grown in low serum (5% V/V) myocyte growth medium supplemented with 0.05ml/ml foetal calf serum (FCS), epidermal growth factor (0.5ng/ml), basic fibroblast growth factor (2ng/ml) and insulin (5µg/ml) purchased from PromoCell, Heidelberg, Germany.

3.1.1.3 Cell media and additives

In addition to this, heat inactivated foetal bovine serum (FBS) EU approved South American Origin, Dulbecco's phosphate buffered saline (DPBS) with calcium and magnesium, and 0.25% Trypsin/Diaminoethanetra-acetic acid (EDTA) (1X) were purchased from invitrogen, Life technologies Ltd, Paisley, Scotland UK.

Human myocyte growth medium supplement was obtained from PromoCell, Heidelberg, Germany.

3.1.1.4 Cell treatment and reagents

Trypan blue solution (0.4%), Dimethyl Sulfoxide (DMSO) and doxorubicin dihydrochloride were purchased from Sigma Aldrich. Both astemizole and sunitinib were provided by Dr Amy Pointon (AstraZeneca). CYP epoxygenase inhibitor MSPPOH (N-(methylsulfonyl)-2-(2-propynyloxy)-benzenehexanamide) was purchased from Santa Cruz Biotechnology Inc, Heidelberg, Germany. sEH inhibitor t-AUCB (4-[[*trans*-4-[[tricyclo[3.3.1.1^{3,7}]dec-1-ylamino)carbonyl]amino]cyclohexyl]oxy]-benzoic acid) and 11,12-EET (11,(12)-epoxy-5Z,8Z,14Z-eicosatrienoic acid) were purchased from Caymen Chemical, Michigan, USA.

3.1.2 Cell culture and treatment method

3.1.2.1 Culturing HepG2 cells, HL-60 cells, EA.hy926 cells and Human cardiac myocytes

HepG2 cells are adherent cells, with a morphology closely resembling epithelial cells. The cells were cultured between passages 18-22 and generally were allowed to reach a confluence of ~80% before being sub-cultured.

HL-60 cells are non-adherent cells. These cells were cultured between passages 15-20.

EA.hy926 cells are a permanent human vascular endothelial cell line generated in 1983 by fusion of human umbilical vein endothelial cells (HUVECs) with the human lung carcinoma cell line A549. They retain many of the characteristics of HUVECs. However unlike HUVECS they are contact inhibited in growth and show reduced growth factor requirements. Phenotypically these cells have a long, elongated structure which forms networks with nearby cells (Bouïs et al., 2001). These cells were cultured at a passage of 5-10 and used when at a confluence of ~90%.

After storage in liquid nitrogen, the cells were removed and thawed for 2 minutes in a 37°C water bath. Once defrosted, they were immediately pipetted into a 15ml universal tube already containing 10ml of pre-warmed (37°C) complete media. This was then centrifuged at 1000rpm for 5 minutes. The supernatant was then removed and the cell pellet was suspended in 1ml of fresh media. Cells were then stained with trypan blue and counted using a haemocytometer.

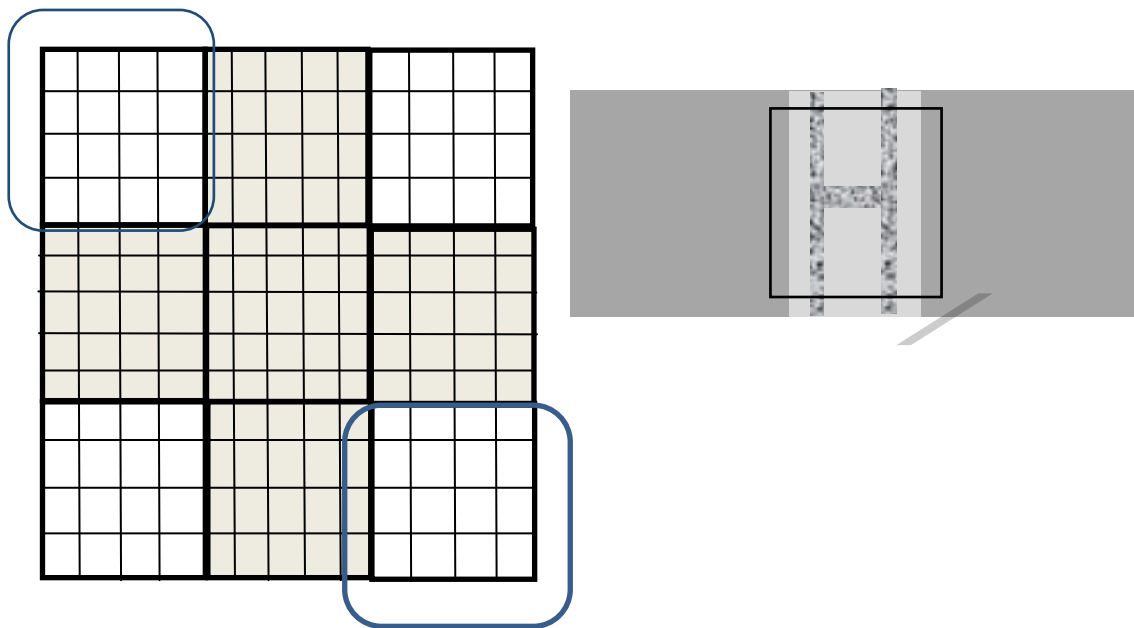


Figure 3-1 The format of a haemocytometer.

Cells were counted in the top left (n_1) and bottom right (n_2) boxes. The numbers of cells in 2ml were then found with the following calculation. $\frac{n_1+n_2}{2} \times 10,000 \times 2 = \text{Number of cells in 2ml}$.

They were then subdivided into T75 flasks to the required density.

HepG2, HL-60 cells and EA.hy926 cells were cultured in 10ml of high glucose (25mM) DMEM media containing 10% (v/v) FBS (growth media). Human cardiac myocytes were grown in myocyte growth medium supplemented with supplement mix. Cells were incubated at 37°C in an incubator with 5% (v/v) carbon dioxide (CO_2). Media was changed every 48 hours.

Once the cells had reached their intended confluence, the media was removed and 5ml of pre-warmed (37°C) trypsin-EDTA (0.25%) were added to the cell surface of the flask. The flask was then placed in a 37°C incubator for ~5 minutes until all the cells had displaced from the surface of the flask, which was ensured by firmly tapping the sides of the flask and analysing under the microscope. Immediately after this, the trypsin was neutralised with 5ml of growth media and the suspension was then transferred to a 15ml universal tube and centrifuged at 1000rpm for 5 minutes. The supernatant was then discarded and the cell pellet was resuspended in 2ml of media for counting as described above.

The remaining cells were frozen down to maintain liquid nitrogen stocks. All cells were frozen using cryopreservation media which consisted of 5% FBS, 4% media and 1% (v/v) Dimethyl Sulfoxide (DMSO). Cells were resuspended in 1ml of cryopreservation media and transferred to a cryovial. Cells were incubated at -80°C in a CoolCell®. In this way the cells were frozen down slowly at a rate of $-1^{\circ}\text{C}/\text{minute}$. After 24 hours the cells were transferred for permanent storage in liquid nitrogen.

3.1.2.2 Culturing iPSC-CMs

Cellular Dynamics iPSC derived cardiomyocytes (iCell cardiomyocytes) were obtained from AstraZeneca. They are also adherent cells that form electrically connected layers that beat in synchrony in culture. These cells do not proliferate in culture and so are not able to be sub-cultured.

Prior to defrosting cells from liquid nitrogen, a 96-well white bottom plate was coated in 0.1% (w/v) sterile gelatine solution. A $100\mu\text{l}$ of this solution was added to each well using a multichannel pipette and then left in the incubator at 37°C overnight. Immediately before plating cells the gelatin was removed. In addition icell cardiomyocyte plating medium was thawed at 4°C overnight.

To thaw cells from liquid nitrogen, a cryovial of cells were placed at 37°C in a water bath for 4 minutes, making sure not to swirl. The contents were immediately pipetted into a 50ml falcon tube. The cryovial was then rinsed with 1ml icell plating media and combined with the cell suspension in a drop-wise manner while gently swirling the tube (one drop every 4-5 seconds). A further 1ml of icell plating medium was added dropwise to the cells over 30-60 seconds and then finally a further 7ml was added over ~ 30 seconds. The cell suspension was then centrifuged at 200g for 5 minutes and the excess media was discarded. The cell pellet was resuspended in 1ml of media for staining with Trypan blue and to determine cell viability using a haemocytometer. The cardiomyocytes were then plated at a cell density of 20,000 per well in a white bottom 96 well plate in $50\mu\text{l}$ of icell plating media for 48 hours. After this point, the media from each well was pipetted up and down a few times to gently wash off the non-adherent cells and then washed twice in icell maintenance media. $50\mu\text{l}$ of icell maintenance media was then added to each well which was then replaced every 48 hours. To allow the cells to stabilise and develop a beating phenotype, the cells were used at day 10.

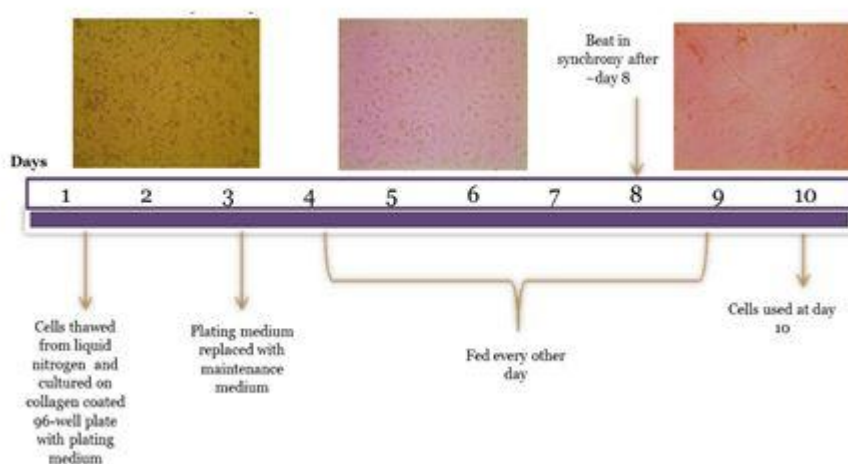


Figure 3-2 Timeline showing how iPS-CMs are cultured.

3.1.3 Treatments

HepG2 cells, EA.hy926 cells and human cardiac myocytes were seeded in 96-well white bottom plates at a density of 20,000 cells per well and grown for 24hr to 70-80% confluency. iPSC-CM were thawed and cultured in 96-well plates for 10 days. They began to beat synchronously after ~8days. Cells were treated with drugs and/or inhibitors for 30mins, 6hr and 24hr. In the case where cells were treated with a combination of both astemizole and inhibitor, there was a 1hr pretreatment with inhibitor after which cells were treated with astemizole. In addition, wells were allocated for untreated cells and a reagent blank as well as a vehicle control. After incubation the assay was conducted according to the procedure seen in section 3.1.4. Results obtained were analysed by subtracting the blank and the in cases of ATP and caspase normalising to the untreated control.

3.1.4 Markers of cell viability

3.1.4.1 ATP

ATP determination kit was purchased from Invitrogen, Life technologies Ltd, Paisley, Scotland UK.

Standard reaction solution:

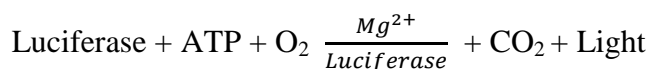
Table 3-1 The components required to make 10ml of a standard reaction solution.

This can be stored at 2–6°C protected from light for several days; however, luminescent signal diminishes with time.

| Volume | Reagent |
|--------|---------------------|
| 8.9ml | dH ₂ O |
| 0.5ml | 20X reaction buffer |
| 0.1ml | 0.1M DTT |
| 0.5ml | 10mM D-luciferin |
| 2.5µl | Firefly luciferase |

This ATP determination kit utilises the recombinant firefly luciferase and its substrate D-luciferin to provide a bioluminescent signal allowing quantitative determination of ATP.

The assay reaction is based on the principle that luciferase generates light from the reaction with ATP and luciferase.



The light intensity generated is directly proportional to the ATP concentration.

Cells were seeded in a 96 well white bottom plate and grown to confluence after which the concentrations of the reagent were made up in the relevant media and a 100µl of this was added to the cells.

After the appropriate incubation period was reached, the standard reaction solution (SRS) was made up in the dark according to the manufactures protocol and was mixed gently by inverting. After removing the media from the plates, the cells were washed first with 200µl and then with 100µl of PBS, pH 7.4. A 100µl aliquot of the SRS solution was then added to each well. A background well containing 100µl SRS without cells was included to account for luminescence produced by the SRS alone and this value was subtracted from all the other wells for subsequent analysis. A platform shaker was then used at medium speed for 1 minute at room temperature to agitate the plate after which it was incubated with the NOVOstar luminometer at the optimum temperature for this reaction (28°C). Luminescence (Relative light units per second (RLU/sec)) was measured at 30 minutes, 6 hours and 24 hours.

3.1.4.2 Caspase

The Caspase-Glo® 3/7 assay was purchased from Promega (Southampton, Hampshire, UK).

Table 3-2 Reagents supplied in the kit for measuring caspase release.

The kit was kept at -20 °C out of light as per instructions.

| Volume Supplied | Reagents |
|-----------------|--|
| 10ml | Caspase-Glo® 3/7 buffer |
| 1 bottle | Caspase-Glo® 3/7 substrate (lyophilized) |

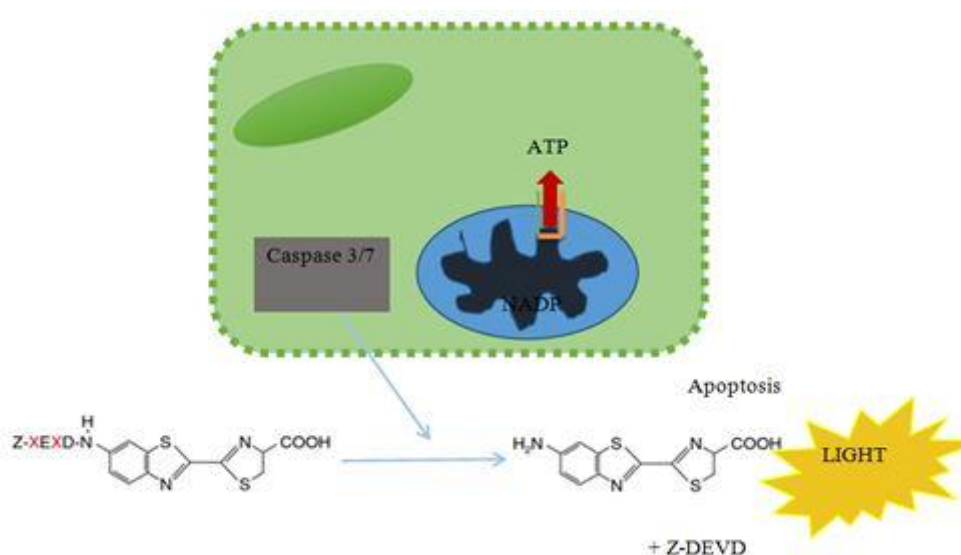


Figure 3-3 Brief diagram showing the reaction to produce luminescence, proportional to caspase 3/7 activity.

Caspases are crucial in mediating apoptosis in mammalian cells and caspase-3 in particular has been identified to be involved in chromatin condensation and DNA fragmentation (Porter and Jänicke, 1999). The Caspase-Glo® 3/7 assay uses luminescence to measure caspase-3 and 7 activities. The assay contains a luminogenic caspase 3/7 substrate which contains the tetrapeptide sequence DEVD. Caspase cleaves this sequence, releasing a substrate for luciferase resulting in the production of light.

EAhy.926 cells and human cardiac myocytes were cultured according to the sub culturing protocol previously described (3.1.2). Caspase 3/7 was measured in cells and media after incubation at 6hrs following the Promega assay protocol.

All reagents were kept on the bench for 3-4 hrs to allow slow thawing to room temperature. The Caspase-Glo® 3/7 reagent was prepared by transferring the Caspase-Glo® 3/7 buffer to the Caspase-Glo® 3/7 substrate and mixing the contents until all substrate was dissolved to for the reagent.

After incubation of cells for the desired test exposure period, assay plates were removed from 37°C and allowed to reach room temperature for ~20 minutes. 100µl of Caspase-Glo® 3/7 reagent was added to each well of the 96-well plate. 1µl of recombinant caspase 3 enzyme was added to each well of the positive control wells. A blank reaction with no cells and media and reagent was made up. The contents were then mixed using a plate shaker for 30 seconds at 300-500rpm. The plate was incubated at room temperature for ~2hours after which luminescence was read with a plate reader. The results were calculated by minusing the blank.

3.1.4.3 MTS assay

The RealTime-Glo MT cell viability assay was purchased from Promega (Southampton, Hampshire, UK).

Table 3-3 Reagents supplied in the kit for measuring metabolism of cells.

The kit was kept at -20°C out of light as per instructions.

| Volume Supplied | Reagents |
|------------------------|-------------------------------------|
| 10µl | MT cell viability substrate, 1,000X |
| 10µl | NanoLuc enzyme, 1,000X |

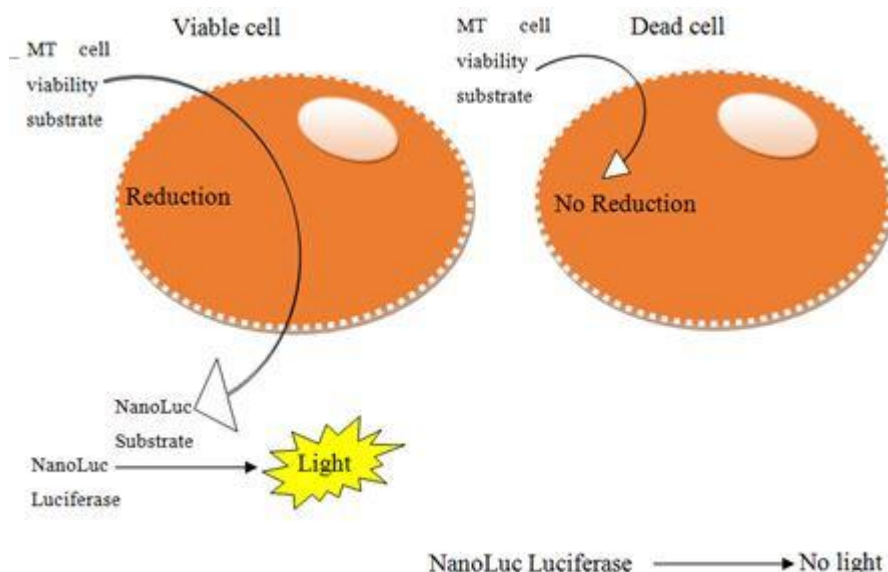


Figure 3-4 Mechanism of detection of viable cells using the MT cell viability substrate.

EAhy.926 cells and human cardiac myocytes were cultured according to the sub culturing protocol previously described in 3.1.2.

MT cell viability substrate and NanoLuc enzyme was incubated to 37°C. RealTime-Glo reagent was prepared by diluting MT cell viability substrate and NanoLuc enzyme in culture medium to form a 2x concentration for each reagent. An equal volume of 2x RealTime-Glo reagent was added to the cells and incubated 30 minutes at 37°C. The luminescence was then read using the Novostar plate reader.

3.1.4.4 Hoechst 33342 staining

Hoechst 33342 nuclear stain was purchased from Applied Biosystems Inc, California, USA.

Hoechst nucleic acid stain was used to distinguish cell viability both qualitatively and quantitatively. The Hoechst stain dye stock solution was first prepared in 10ml deionised water to create a 10mg/ml (16.23mM) solution. Once cells had been cultured, the media was removed and dye solution was added to the cell enough to cover the well. Cells were then incubated with the Hoechst stain for 10 minutes in foil. After incubation the stain was removed and cells were washed 3 times with PBS after which they were visualised using a fluorescent microscope (excitation/emission 350/461nm).

3.1.4.5 LDH assay

The CytoTox-ONE Homegenous Membrane Integrity Assay was purchased from Promega (Southampton, Hampshire UK).

Table 3-4 Reagents supplied in the kit for measuring LDH release.

The kit was kept as -20°C out of light as per instructions.

| Volume Supplied (ml) | Reagents |
|----------------------|-------------------------|
| n/a | Substrate mix (2 vials) |
| 24 | Assay buffer |
| 0.5 | Lysis solution |
| 11 | Stop solution |

Cell viability was assessed with the CytoTox LDH assay (Promega, Southampton, Hampshire UK), which allows the measurement of LDH release from cells. When membrane integrity is compromised, LDH and other enzymes are leaked from cells into the extracellular space and so are commonly used as a marker of cell viability.

The CytoTox-ONE Membrane Integrity Assay uses the conversion of Rezazurin to Resorufin to quantitatively dictate LDH release as seen in figure 3.5.

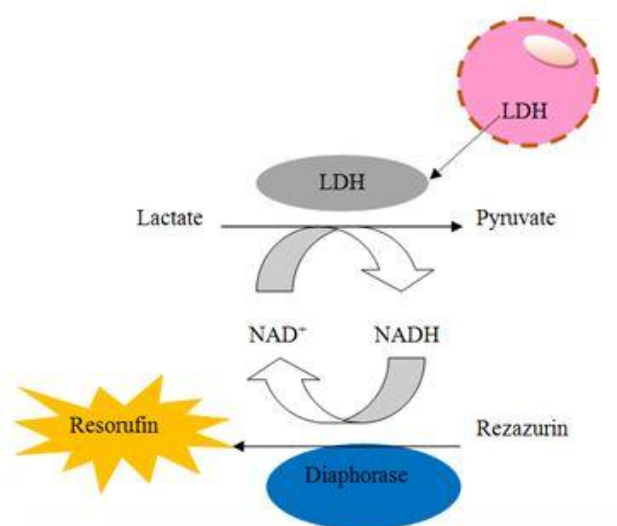


Figure 3-5 Leaked LDH from damaged cells react with lactate and NAD^+ to create Pyruvate and NADH.

NADH is utilised in the reduction reaction to produce Resorufin. Resorufin is a fluorescent product which is proportional to amount of LDH.

EAhy.926 cells were cultured according to the sub culturing protocol previously described (3.1.2). LDH was then measured in the media from these cells at following the Promega cytotoxicity assay protocol. All reagents were kept on the bench for 3-4hrs to allow slow thawing to room temperature. CytoTox-ONE reagent was made up by adding 11ml of assay buffer to a vial of substrate mix and gently mixing to dissolve. After incubation of cells for the desired test exposure period, assay plates were removed from 37°C and allowed to reach room temperature for ~20 minutes. A maximum LDH release control was set up where 2µl of lysis solution was added to positive control wells. A 100µl of cell culture medium was taken from each well of the 96 well plate and pipetted into a separate black walled 96 well plate. To this an equal volume of CytoTox reagent was added with a multi-channel pipette and the plate was shaken for 30 seconds using a plate shaker. The culture medium was then allowed to incubate with the reagent for 10mins at room temperature. 50µl of stop solution was carefully added to each well using a multi-channel pipette making sure to add stop solution in the same order CytoTox reagent was added. The plate was then shaken for 10 seconds and fluorescence was read with a plate reader at an excitation wavelength of 560nm and emission wavelength of 590nm. To calculate results the following formula was used:

Percentage Cytotoxicity

$$= 100 \times \frac{\text{Experimental} - \text{Culture Medium Background}}{\text{Maximum LDH Release} - \text{Culture Medium Background}}$$

3.1.5 Molecular biology techniques

3.1.5.1 Ribonucleic acid (RNA) extraction and quantification

The steps involved in the isolation of RNA involved a combination of the RNeasy mini kit and RNase free DNase kit. RNase free DNase I set and RNeasy mini kit were both purchased from Qiagen, Manchester, Lancashire, England, UK.

The RNeasy mini kit contains the following reagents:

Table 3-5 The components provided in the RNeasy mini kit needed for the RNA extraction of cells.

| Volume Supplied (ml)/ Number | Reagents |
|-------------------------------------|--------------------------|
| 50 | RNeasy Mini spin columns |
| 50 | Collection tubes (1.5ml) |
| 50 | Collection tubes (2ml) |
| 45ml | Buffer RLT |
| 45ml | Buffer RW1 |
| 11ml | Buffer RPE (concentrate) |
| 10ml | RNase free water |

4 volumes of 100% ethanol were added to RPE buffer to obtain the final working solution.

The components of the RNase free DNase I set were:

Table 3-6 The DNase I reagents required for DNase treatment.

| Volume Supplied (ml)/ Number | Reagents |
|-------------------------------------|-----------------------------------|
| 1500 Kunitz units | DNase I, RNase-free (lyophilized) |
| 2x2ml | Buffer RDD |
| 1.5ml | RNase-free water |

Extra components used for the RNA extraction general protocol include Kimtech Science Kimwipes purchased from Kimberley Clark Professional, West Malling, Kent, England, UK and RNase Zap™ which was purchased from Sigma Aldrich Ltd Dorset, UK.

3.1.5.1.1 Before starting

The entire workstation and all the equipment was first decontaminated with IMS followed by RNase Zap™ solution. In addition, the Gilson's pipettes were exposed to UV radiation for sterilisation. The buffer RLT and Qiagen DNase reagents were prepared as was detailed in the manufacturer's instructions.

To prepare the cells for RNA extraction the cells were first washed gently in 1XPBS. After removing the PBS thoroughly, the cells were detached with trypsin/EDTA solution and incubated at 37°C for ~3 minutes. The flask was tapped firmly until the cells were detached and the trypsin was neutralised with complete DMEM media and cells centrifuged at 1,000rpm at room temperature for 5 minutes. Without disturbing the pellet, all the suspension was removed and 1ml of RLT buffer with 10µl β-mercaptoethanol was added and the suspension was pipetted up and down to mix thoroughly.

3.1.5.1.2 Additional RNA separation step for iPSC-CMs

The cardiomyocyte lysate was loaded on to a QIAshredder spin column placed in a 2ml collection tube, and centrifuged at full speed for 2 minutes. After transferring the cardiomyocyte lysate to a new 1.5ml RNase-free tube, it was diluted with 295µl of RNase-free water. To this mixture 5µl of 20mg/ml proteinase K were added. This was then incubated on a heated block for 10 minutes at 55 °C. The lysate was then processed through the RNA extraction protocol detailed below.

3.1.5.1.3 Washing and elution

The RNA lysate was mixed with an equal volume of 70% ethanol and mixed well by pipetting. The sample were then added to an RNeasy spin column and centrifuged at 10,000rpm for 2 minutes. The flow through was discarded at this stage and a new collection tube was used. The sample was washed in an ethanol based RW1 buffer (350µl) and centrifuged at 10,000rpm for 2 minutes and the flow through discarded. DNase (80µl) was added directly to the spin-column and left to incubate for 30 minutes at room temperature after which another wash with RW1 buffer (350µl) was performed. The collection tube was again changed and 500µl of buffer RPE were added to the spin column and left to incubate at room temperature for 5 minutes prior to centrifugation at 10,000rpm for 4 minutes. This allowed drying of the spin column and prevented solvent contamination of RNA. The flow through was then discarded and a 'dry spin' was performed at 10,000rpm for 5 minutes to further dry the spin-column membrane.

To elute the RNA 25µl of RNase-free water were added directly to the spin column and centrifuged at 10,000rpm for 2 minutes. The eluted sample was again passed through the column and centrifuged for a further 2 minutes at 10,000rpm. The eluted RNA samples were then aliquoted into 3 tubes of 10µl each, 2 of which were placed on dry

ice for long term storage at -80°C . The final 10 μl aliquot was used to analyse the sample with a UV spectrophotometer immediately.

3.1.5.1.4 Quantitation and quality control of RNA - NanoDrop ND-1000 UV spectrophotometer protocol

To ensure the RNA extracted was of a high yield and quality and to measure the level of contamination, quality control was performed using a NanoDrop ND-1000 UV spectrophotometer (Thermo Scientific, NanoDrop technologies). The software calculated the concentration as a 10mm absorbance path for convenience, displaying the concentration in ng/ μl . The purity of the RNA was determined by calculating the ratios for OD_{260/280} (260nm - peak nucleic acid absorbance, 280nm - peak protein absorbance) and OD_{260/230} (260nm - peak nucleic acid absorbance, 230nm - peak carbohydrates, peptides, phenols, aromatic compounds absorbance) (figure 3.6). A ratio of between 1.8 and 2.07 was classified as the acceptable range for 260/280, indicating RNA relatively free from protein contamination. For 260/230, a ratio of between 1.8 and 2.2 was the acceptable range and demonstrated a low level of contamination from molecules that absorb in the 230nm range. Any RNA samples outside of these ranges were discarded and an RNA re-extraction was performed from a separate sample of cells.

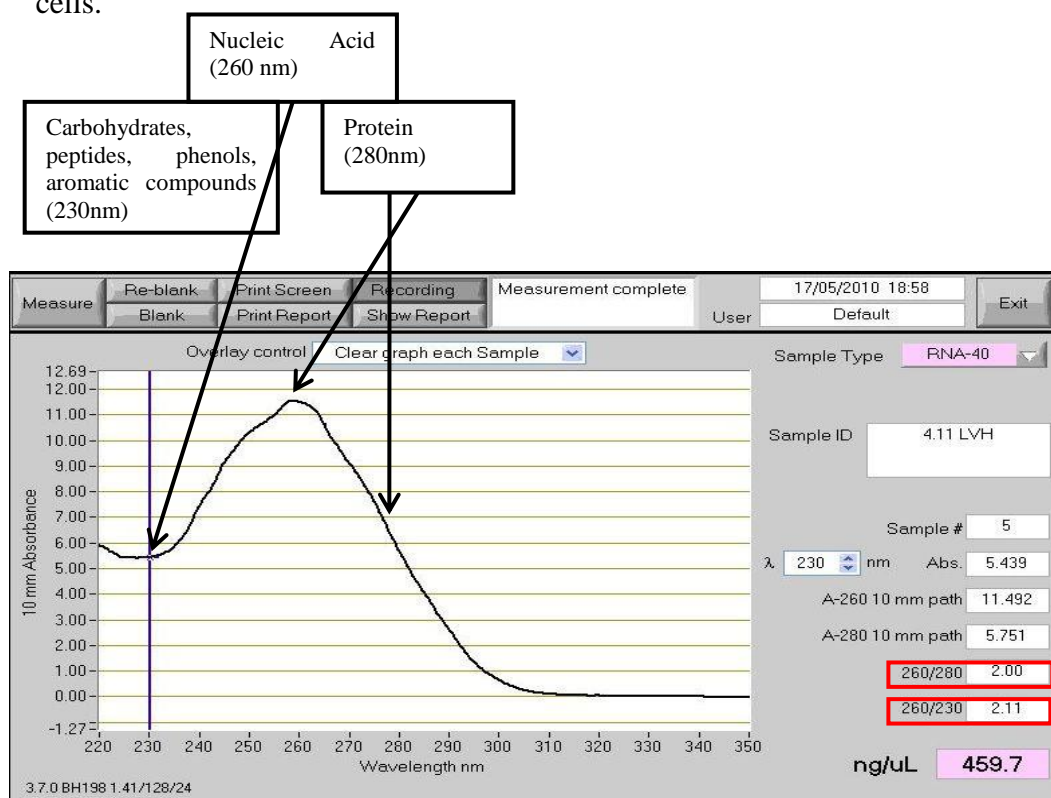


Figure 3-6 A typical nanodrop graph plot showing the significance of the peaks in the purity of the RNA

3.1.5.2 cDNA production

For the synthesis of single stranded cDNA the Applied Biosystems high capacity reverse transcriptase kit was used, Applied Biosystems Inc, California, USA.

For each 20 μ l reaction (per sample) a 2X master mix solution was made up on ice as indicated in table 3.8.

To prepare the cDNA RT reactions 10 μ l of 2X RT master mix was pipetted into each eppendorf sample tube. 10 μ l of RNA sample were then added and mixed with the master mix by pipetting up and down gently. The tubes were then centrifuged briefly to eliminate any bubbles and placed on ice.

| Component | Volume/Reaction (μ l) |
|------------------------------------|----------------------------|
| 10X RT buffer | 2.0 |
| 25X dNTP mix (100mM) | 0.8 |
| 10X RT random primers | 2.0 |
| MultiScribe™ Reverse Transcriptase | 1.0 |
| Nuclease-free H ₂ O | 4.2 |
| Total per reaction | 10.0 |

Table 3-7 Thermal cycler conditions for RT step.

To perform the reverse transcription the thermal cycler was programmed with the following conditions:

| | Step 1 | Step 2 | Step 3 | Step 4 |
|-----------------------------|---------|----------|--------|----------|
| Temperature ($^{\circ}$ C) | 25 | 37 | 85 | 4 |
| Time | 10 mins | 120 mins | 5 mins | ∞ |

Table 3-8 Composition of 2X cDNA mastermix.

The reaction volume was then set as 20 μ l, the samples were loaded and the thermal cycler started.

3.1.5.3 Gel PCR

Agarose powder was purchased from Melford Biolaboratories Ltd., Ipswich, UK. GelRed™ nucleic acid gel stain, 10,000X was purchased from Biotium Inc., California, USA. Loading buffer blue (5X) was purchased from Bioline Reagents Ltd., London, UK. PCR sizer 100pb DNA ladder was purchased from NORGEN Biotek Corp., Ontario, Canada. Gel trays, combs and tanks were purchased from Fisher Scientific, Loughborough, UK. The power supply, purchased from Bio-Rad Laboratories Ltd Hertfordshire, UK was used to run the electrophoresis in TAE buffer (table 3.9).

Table 3-9 Recipes for 10X TAE electrophoresis buffer

| Materials | Amount |
|-----------------------------|-----------|
| Tris base | 48.4g |
| Glacial acetic acid (17.4M) | 11.4ml |
| EDTA, disodium salt | 3.7g |
| Deionized water | Up to 1 L |

Primers to sEH, CYP2J2 and housekeepers were designed with the help of Laurence Hall using NCBI and Ensembl database and validated with the PrimerBlast program transcripts. In accordance with the manufacturers instructions each set of primers were then diluted to a 100µM stock solution in milliQ water as instructed on the data sheet. A working solution was made by diluting the stock solution 1 in 10 in milliQ water.

Table 3-10 CYP2J2 primer gene sequences, combinations for PCR, predicted pcr product size and annealing temperature gradient

| Primer | Sequence | Tm (°C) | Combination | Predicted pcr product size (bp) | Gradient (°C) |
|--------------------------|-------------------------|---------|-------------|---------------------------------|---------------|
| CYP2J2 transcript #1 F#1 | GAGTGGGCCACCCCTGACAC | 69 | F1+R1 #10 | 100 | 65-70 |
| CYP2J2 transcript #1 R#1 | CGAGGCATGCCCCGCTTTCCTAT | 69 | | | |
| CYP2J2 transcript #1 F#2 | ACCTGCCCAAGGGTACCATGA | 68 | F2+R2 #11 | 180 | 65-70 |
| CYP2J2 transcript #1 R#2 | GGCCAAC TGTTCCTCCGAGGCA | 69 | | | |

Table 3-11 sEH variant primer sequences, combinations for PCR and annealing temperature gradient.

| Primer | Sequence | T _m (°C) | Combination | Predicted PCR product size (bp) | Gradient (°C) |
|---------------------------|----------------------------|------------------------|-------------|--|------------------|
| sEH pan forward #1 | CAGCAGGATGGTCACTGAGG | 64.5 | #1- F1+R1 | 290 | 61-66 |
| sEH Pan Reverse #1 | GGGCCGGAATCAGGATCTTC | 64.7 | | | |
| sEH Pan Forward #2 | ACTTCGTGCTCGTTCCTCAG | 64.3 | #2- F2+R2 | 150 | 61-66 |
| sEH Pan Reverse #2 | CTCGGTTGGCTTGCCATCT | 64.6 | | | |
| sEH Transcript #1 F#1 | GGTTAGCTGCGTGCCGGGT | 69 | #3- F1+R1 | 160 | 65-70 |
| sEH Transcript #1 R#1 | GCATCATT CAGAAGTCCTCTGGGCA | 68.5 | | | |
| sEH Transcript #1 F#2 | TTCGACCTTGACGGGGTGCT | 68.4 | #4- F2+R2 | 100 | 63-68 |
| sEH Transcript #1 R#2 | CATCATTCAGAAGTCCTCTGGGCA | 66.3 | | | |
| sEH Transcript #2 F#1 | GGTTAGCTGCGTGCCGGGT | 69 | #5- F1+R1 | 160 | 65-70 |
| sEH Transcript #2_R#1 | GGTAGTGGCACCCTCTGGGCA | 70.4 | | | |
| sEH Transcript #2 F#2 | CGTCTTCGACCTTGACGGGGTG | 68.6 | #6- F2+R1 | 100 | 65-70 |
| sEH Transcript #3 F #1 | TGGCGCTGCCAGTGGATAAC | 69 | #7- F1+R1 | 150 | 65-70 |
| sEH Transcript #3 R #1 | CTGGAGCATGGGGCGGTTGA | 69 | | | |
| sEH Transcript #3 R #2 | CACGGTCGTCCAGCCAGGTGTT | 70.7 | #8-F1+R2 | 215 | 65-70 |
| sEH Transcript #4 F #1 | TGGCGCTGCCAGGACTTCTGA | 72.2 | #9-F1+R1 | 230 | 67-72 |
| sEH Transcript #4 R #1 | TGCCTGGAGCATGGGGCGGT | 70 | | | |

Table 3-12 Housekeeper primer sequences, combinations for PCR and annealing temperature gradient.

| Primer | Sequence | T _m (°C) | Combination | Predicted PCR product Size (bp) | Gradient (°C) |
|-----------------------|------------------------------|------------------------|-------------|--|------------------|
| GapDH F#1 | GCACCCCTGGCCAAGGTCAT | 69 | #12- F1+R1 | 170 | 66-71 |
| GapDH R#1 | CAGCGCCAGTAGAGGCAGGG | 69 | | | |
| GapDH F#2 | GCGACACCCACTCCTCCACC | 69 | #13- F2+R2 | 125 | 66-71 |
| GapDH R#2 | GGCCATGAGGTCCACCACCC | 69 | | | |
| βActin Forward #1 | ATATCGCCGCGCTCGTCGTC | 69 | #14- F1+R1 | 125 | 67-72 |
| βActin Reverse #1 | ACCATCACGCCCTGGTGCCT | 71 | | | |
| B Tubulin F #1 | TGGCGGAGCGTCGGTTGTAG | 69 | #15- F1+R1 | 275 | 63-70 |
| B Tubulin R #1 | GCACGTACTIONGCCGCGGT | 70 | | | |
| B Tubulin R #2 | GCTGATCACCTCCAAAACCTG GC | 68 | #16- F1+R2 | 167 | 63-70 |
| B2 Microglobulin F #1 | TGCCTGCCGTGTGAACCATGT | 69 | #17-F1+R1 | 100 | 63-70 |
| B2 Microglobulin R #1 | TGCGGCATCTTCAAACCTCCAT GA | 69 | | | |
| B2 Microglobulin R #2 | ATGCGGCATCTTCAAACCTCCA | 67 | #18- F1+R2 | 100 | 63-70 |
| TBP Forward #1 | GGGTTCAAGTGAAGTCGGGCAG | 69 | #19-F1+R1 | 110 | 63-70 |
| TBP Reverse #1 | AGTCATGGCACCCCTGGGTCA | 68 | | | |

To deduce that correct annealing temperature for the different sets of primers as well as find out which primer set showed the best expression of each gene, samples were set up for PCR, an example is shown below:

Table 3-13 An example of strip tube samples for PCR run in duplicate.

The numbers are associated with specific primer sets and the possible annealing temperatures are shown above in yellow. Possible annealing temperatures used were between $T_m -3^{\circ}\text{C}$ and $T_m +2^{\circ}\text{C}$. Most optimum annealing temperatures are found within the 63-67°C mark. T_m primer melting temperature.

| °C | | | | | | | | | | | |
|----|----|----|----|----|----|----|----|----|----|----|----|
| 61 | 62 | 63 | 64 | 65 | 66 | 67 | 68 | 69 | 70 | 71 | 72 |
| | | | | | | | | | | | |
| #1 | #1 | #1 | #1 | #1 | #1 | | | | | | |
| #1 | #1 | #1 | #1 | #1 | #1 | | | | | | |
| #2 | #2 | #2 | #2 | #2 | #2 | #9 | #9 | #9 | #9 | #9 | #9 |
| #2 | #2 | #2 | #2 | #2 | #2 | #9 | #9 | #9 | #9 | #9 | #9 |
| | | #4 | #4 | #4 | #4 | #4 | #4 | | | | |
| | | #4 | #4 | #4 | #4 | #4 | #4 | | | | |
| | | | | #3 | #3 | #3 | #3 | #3 | | | |
| | | | | #3 | #3 | #3 | #3 | #3 | | | |
| | | | | | | | | | | | |

Final mixture of each sample contained:

Table 3-14 Composition of PCR mixture.

| Reagent | μL |
|-------------------------|------|
| 5 x reaction buffer | 5 |
| Taq polymerase (25U/ml) | 0.5 |
| 10μM forward primer | 1 |
| 10μM reverse primer | 1 |
| cDNA (100ng) | 1 |
| MilliQ water | 16.5 |
| Total | 24 |

Once all reagents were added to each strip tube, a drop of mineral oil was added to each sample to avoid evaporation. The tubes were run in the G storm thermal cycler with the appropriate gradient temperature conditions. Whilst the PCR was running 4.5g of agarose was mixed with 300ml of 1XTAE in a duran bottle to make a 1.5% agarose gel. The agarose solution was then heated in the microwave for ~3mins after which it was

swirled using heat resistant gloves to facilitate dissolving. The solution was then heated for a further 1min to ensure all the agarose had dissolved. Agarose was then cooled for 15-20mins on the bench. 30µl of gel red was then added to the molten agarose which was then poured into a 16 tooth gel tray. The gel was then left to set for 30mins. Once set the combs were removed from the gel slowly and the gel was immersed in 1XTAE buffer. Each well was then loaded carefully with 30µl of sample + 1Xrunning buffer (bromophenol blue and glycerol) to ensure contents of each well fell to the bottom to avoid cross contamination. Electrophoresis was then performed for 1hr @100v for identification of bands.

3.1.5.4 Quantitative real-time PCR

SYBR green mix was purchased from Qiagen, Manchester, UK. Taqman CYP2J2 probe and TaqMan master mix were bought from Thermo Fisher scientific, Loughborough UK.

Once the desired primer set and appropriate annealing temperature had been established, gene expression was quantified with qPCR. Primers were diluted and a PCR plate was set up, an example is shown below:

Table 3-15 PCR 96 well plate with selected sEH, CY2P2J2 and housekeeping primers including non-template controls (NTC) and water controls. Gap GAPDH; β2 micro β2 microglobulin.

| | 1 | 2 | 3 | 4 | 5 | 6 | 7 | 8 | 9 | 10 | 11 | 12 |
|---|----------------|----------------|----------------|---------------|---------------|-----------------|----------------|----------------|----------------|----------------|----------------|----------------|
| A | S E H #1 F1/R1 | S E H #1 F1/R1 | S E H #1 F1/R1 | Gap F1/R1 | Gap F1/R1 | Gap F1/R1 | Gap F1/R2 | Gap F1/R2 | Gap F1/R2 | | NTC Gap F1/R1 | NTC Gap F1/R2 |
| B | B Actin F1/R1 | B Actin F1/R1 | B Actin F1/R1 | | | | B2 Micro F1/R1 | B2 Micro F1/R1 | B2 Micro F1/R1 | B2 Micro F1/R2 | B2 Micro F1/R2 | B2 Micro F1/R2 |
| C | 232 F1/R1 | 232 F1/R1 | 232 F1/R1 | 232 F1/R2 | 232 F1/R2 | 232 F1/R2 | Wat 232 F1/R2 | | | | | |
| D | 232 F1/R2 | 232 F1/R2 | 232 F1/R2 | Wat 232 F1/R1 | Wat 232 F1/R2 | Wat S E H F1/R1 | Wat Gap F1/R1 | Wat Gap F1/R2 | Wat BA F1/R1 | Wat BTub F1/R2 | Wat B2 F1/R2 | Wat B2 F1/R2 |
| E | S E H #1 F1/R1 | S E H #1 F1/R1 | S E H #1 F1/R1 | Gap F1/R1 | Gap F1/R1 | Gap F1/R1 | Gap F1/R2 | Gap F1/R2 | Gap F1/R2 | | NTC Gap F1/R1 | NTC Gap F1/R2 |
| F | B Actin F1/R1 | B Actin F1/R1 | B Actin F1/R1 | | | | B2 Micro F1/R1 | B2 Micro F1/R1 | B2 Micro F1/R1 | B2 Micro F1/R2 | B2 Micro F1/R2 | B2 Micro F1/R2 |
| G | 232 F1/R1 | 232 F1/R1 | 232 F1/R1 | 232 F2/R2 | 232 F2/R2 | 232 F2/R2 | Wat 232 F1/R2 | | | | | |
| H | 232 F1/R2 | 232 F1/R2 | 232 F1/R2 | Wat 232 F1/R1 | Wat 232 F1/R2 | Wat S E H F1/R1 | Wat Gap F1/R1 | Wat Gap F1/R2 | Wat BA F1/R1 | Wat BTub F1/R2 | Wat B2 F1/R2 | Wat B2 F1/R2 |

Each well contained the following mixture:

Table 3-16 PCR mixture per well.

| Reagent | X1 μ l |
|-----------------------------|------------|
| cDNA (100ng) | 1 |
| 2xSYBR green | 10 |
| Forward primer (10 μ M) | 1 |
| Reverse primer (10 μ M) | 1 |
| DMSO | 0.25 |
| MilliQ water | 6.5 |

Once the plate was set up, the PCR plate was covered with a plastic adhesive cover and spun for 3mins at 1200rpm before being loaded on the Vii7 real-time PCR system. Once a suitable annealing temperature had been established, gene expression was quantified with PCR set up on a 96 well plate. Once CT values were collected, data was analysed by calculating the $\Delta\Delta$ CT which normalised mRNA expression to the untreated control.

3.1.5.5 Protein extraction

Tris-base (50mM), sodium chloride (150mM), sodium deoxycholate (0.5%), hydrochloric acid (1M) and phosphatase inhibitor were purchased from Thermo Fisher Scientific. Sodium dodecyl sulphate (SDS) (0.1%), Triton-X-100 (1%) and sterile PBS was from Sigma Aldrich, Gillingham, Dorset, UK.

To prepare the cells for protein extraction the cells were first washed gently in 1XPBS. After removing the PBS thoroughly, the cells were detached with trypsin/EDTA solution and incubated at 37°C for ~3 minutes, tapping the flask firmly until the cells were detached. The trypsin was then neutralised with complete DMEM media and cells centrifuged at 1,000rpm at room temperature for 5 minutes. Without disturbing the pellet, all the suspension was removed and the pellet was resuspended with 1ml PBS and centrifuged at 1,000rpm for 5 minutes. The supernatant was removed and the pellet was suspended in 0.7 μ l protein/phosphatase inhibitor in 70 μ l RIPA buffer and left on ice for 10 minutes. The sample was centrifuged at the highest speed for 10 minutes at 4°C and the supernatant was collected and stored at -80°C.

3.1.5.6 Protein assay

Detergent compatible, (DC) protein assay kit was purchased from Bio-Rad, Hemel Hempstead, UK, containing alkaline copper tartrate solution for colorimetric assays (reagent A), dilute Folin reagent for colorimetric assays (reagent B) and surfactant solution for colorimetric assays (reagent S). Pierce™ Bovine Serum Albumin Standard Ampules, (23209 2mg/mL) was purchased from Thermo Fisher Scientific.

The DC Bio-Rad protein assay was used to dictate the concentration of protein in each sample. The standards were made up as follows:

Table 3-17 Components of protein standards used for the DC Bio-Rad protein assay.

| | [Protein] µg/µl | RIPA, µl | Pr Standard, µl |
|------------|-----------------|----------|-----------------|
| Standard 1 | 0 | 40 | 0 |
| Standard 2 | 0.35 | 30 | 10 |
| Standard 3 | 0.7 | 20 | 20 |
| Standard 4 | 1.05 | 10 | 30 |
| Standard 5 | 1.4 | 0 | 40 |

Protein samples were then diluted 1 in 5 and 5µl of this and each standard was pipetted into a 96 well plate. A, B and S solution was then added according to the manufacturer instructions and the plate was left for 10 minutes for the samples to fully change colour. Once this had occurred, absorbance readings for each well were read using the Novostar plate reader at 595nm.

3.1.5.7 Antibodies

CYP2J2 mouse monoclonal antibody was purchased from Origene, Herford, Germany. sEH rabbit polyclonal antibody was a kind gift from Professor Bruce Hammock, UCLA, CA. Monoclonal anti-β-Actin antibody, (A5441 1:2000) was from Sigma-Aldrich Company Ltd and rabbit polyclonal and rabbit anti-mouse (ab6728 1:10000) were from Abcam Ltd.

3.1.5.8 Western blotting

Western blotting reagents, 30% (W/v) acrylamide/bis solution (29:1) was purchased from Bio Rad Laboratories Ltd. Precision protein standard was purchased from Thermo Fisher scientific, Loughborough UK. Ammonium persulfate (APS), HCl, methanol,

NaCl, NaOH, 5% (W/v) trichloroacetic acid and tris were bought from Fisher Scientific UK Ltd. BSA, β -mercaptoethanol, bromophenol blue, DMSO, dithiothreitol (DTT), glycerol, glycine (electrophoresis grade), 30% (W/v) H_2O_2 , isopropanol, luminol, N,N,N',N'-tetramethylethane-1,2-diamine (TEMED) (Electrophoresis reagent), p-coumaric acid and Polyoxyethylene (20) sorbitan monolaurate (tween-20) were purchased from Sigma-Aldrich Company Ltd, Poole, and Dorset, UK.

3.1.5.8.1 Gel preparation

To produce a gel for western blot two types of gel are required, a resolving gel being the main body of the gel and the overlaying stacking gel. As resolving gel is basic (pH 8.8) compared to the stacking gel (pH 6.8) it allows for better separation of protein molecules.

The components of each are found in the table below:

Table 3-18 Gel preparation of resolving and stacking gel.

| | Resolving gel 12% | Stacking gel (4%) |
|------------------------------------|-------------------|-------------------|
| dH ₂ O water | 2.1ml | 3.675ml |
| IM Tris – HCL pH 8.8 / 6.8 | 3.75ml | 0.625ml |
| 30% Acrylamide / Bis solution 29:1 | 4ml | 0.665ml |
| 10% SDS | 100 μ l | 50 μ l |
| 10% APS | 50 μ l | 25 μ l |
| TEMED | 5 μ l | 5 μ l |

Before making the gels all glass plates, casting frames and combs were cleaned with IMS and assembled correctly to stop any leakage of gel solution. The resolving gel solution was made up in a universal tube at 12% density and 7ml was added between the short and spacer plates to form the gel cassette. The gel was then overlaid with 1ml of isopropanol and left to set for 40mins. Once set the layer of isopropanol was poured away and 4ml of stacking solution was pipetted onto the resolving gel. A comb was inserted within the stacking gel and the gel was left to solidify for 15-30 minutes. Once the gel had set the gel cast was released from the casting stand and the comb was slowly removed.

3.1.5.8.2 Electrophoresis

Once the gel was ready, protein samples were loaded onto the wells. Protein samples were made up to 70ng/ μ l of protein with loading buffer containing bromophenol blue and glycerol and water and then heated to 95^oC for 5 minutes for protein denaturation. 5 μ l of protein standard was first pipetted onto the gel followed by the protein samples in the remaining wells. The gels were then assembled in the in the electrophoresis tank and filled with 1x SDS-PAGE running buffer. The gels were then run at the lower voltage of 100V for 15 minutes after which they higher voltage of 120V was applied until the dye ran to the bottom of the gel.

Table 3-19 Components of 1X SDS-PAGE running buffer

| 1 L of 1X SDS-PAGE running buffer | Weight |
|-----------------------------------|--------|
| Tris-base | 3.03g |
| Glycine | 14.4g |
| SDS | 1g |

3.1.5.8.3 Protein transfer

Protein was transferred from the gel to the PVDF membrane using a transfer sandwich consisting of; sponge, 2 filter papers, gel, PVDF membrane, 2 filter papers and sponge. It was made sure there no air bubbles between the membrane and gel. The transfer sandwich was kept in cold transfer buffer for 90 minutes at 63V.

Table 3-20 Components of transfer buffer

| 1 L of transfer buffer | Amount |
|------------------------|--------|
| Tris-base | 3g |
| Glycine | 13.3g |
| Methanol | 100ml |
| dH2O water | 900ml |

3.1.5.8.4 Immunoblotting

Once the protein was transferred to the membrane, the membrane was blocked with 5% skimmed milk in tris-buffered saline tween-20 (TBST) for one hour to prevent any non-specific binding. Primary antibody was made also made up in 5% skimmed milk and was incubated with membrane overnight at 4⁰C on the roller rocker. After washing with TBST (3x 15 minute washes) the membrane was incubated with secondary antibody in 5% semi-skimmed milk for 1 hour. The membrane was washed a further 3 times in TBST to remove excess antibody and then incubated with ECL reagent for 5 minutes and visualised with ImageQuant.

Table 3-21 Components of ECL reagent

| ECL reagent | Amount |
|-------------------|--------|
| Reagent A | 2.2µl |
| Reagent B | 5µl |
| Hydrogen peroxide | 0.3µl |
| Tris base (8.5pH) | 10ml |

3.1.5.9 Transfections

sEH silencer select Pre-designed siRNA was purchased from Life technologies Ltd. ON-TARGETplus CYP2J2 siRNA was bought from Dharmacon, Lafayette, Colorado. Allstars scrambled siRNA control and cell death siRNA was purchased from Qiagen, Manchester, UK. RNAiMAX lipofectamine and Opti-MEM reduced serum media was purchased from Thermo Fisher Scientific UK Ltd, Loughborough UK.

SiRNA transfection was done using the lipofectamine RNAimax reverse transfection protocol. Reverse transfection differs from regular transfection in that siRNA complexes are added to the well at the same time as cells thereby giving a high-throughput transfection compared to forward transfection.

Firstly stock solutions were made of siRNA and control solutions in RNase free water. Lipofectamine and stock siRNA/control was diluted with Opti-MEM media according to manufacturer guidelines. Cells were then added at a density appropriate for the plate

type used and normal serum feeding media was then added to each well. After 24 hrs the media was changed to just normal serum feeding media and after 2 days cells were used for experiments.

3.1.6 Metabolomics

3.1.6.1 Astemizole metabolism reagents

CYP2J2 bacosomes were purchased from CYPEX, Dundee, Scotland. NADPH generation system was bought from Promega, Southampton, Hampshire, UK.

Potassium phosphate and magnesium chloride was purchased from Sigma-Aldrich Company Ltd, Poole, and Dorset, UK. Hydrochloric acid was purchased from Fisher Scientific UK Ltd.

3.1.6.2 Extraction of metabolite from cells

To prepare the cells for metabolite extraction the cells were first washed gently in 1XPBS. After removing the PBS thoroughly, the cells were detached with trypsin/EDTA solution and incubated at 37°C for ~3 minutes and the flask tapped firmly until the cells were detached. The trypsin was then neutralised with complete DMEM media and cells centrifuged at 1,000g at room temperature for 1 minute to form a pellet. As much of media pipetted off the pellet and was then resuspended in 500µl 100% methanol. The cells were then recentrifuged at 800g for 1 minute after which the supernatant was collected into a separate centrifuge tube and kept on dry-ice. The pellet was then suspended in 100% methanol and snap freezed in liquid nitrogen. The steps were then repeated: thaw cells, pellet and pool supernatant into the same tube. The cell pellet was then resuspended in 250µl ice cold milliQ water and snap freezed in liquid nitrogen. The steps were then repeated again: thaw cells, pellet and pool supernatant with the rest from earlier steps. The pooled supernatant was then centrifuged at 15,000g for 1 minute and transferred to a fresh tube. The supernatant was then dried using a centrifugal evaporator at 30°C.

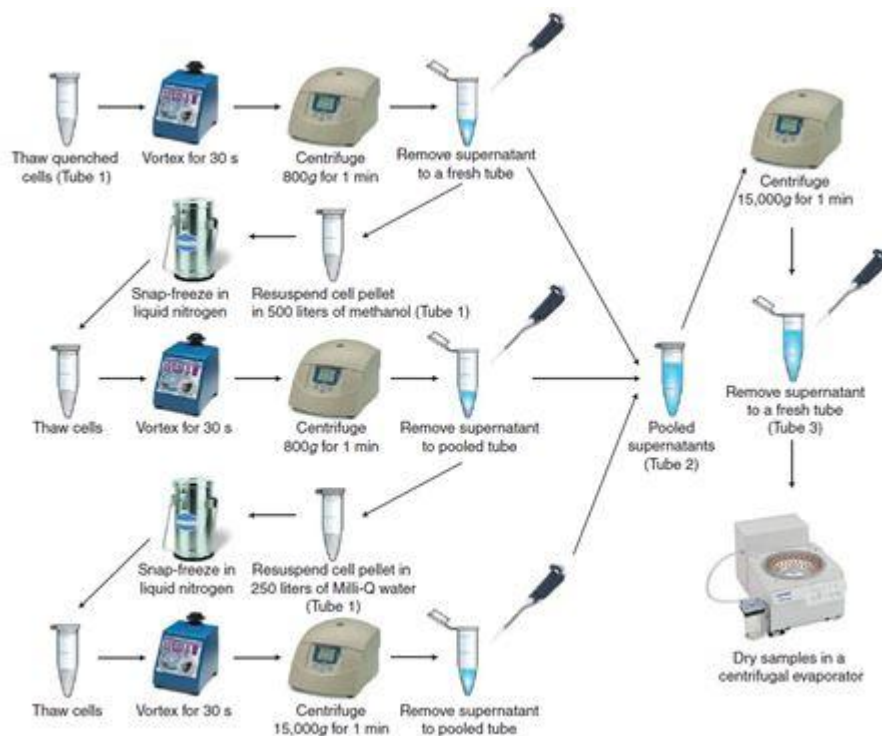


Figure 3-7 Procedure for metabolite isolation from cultured cells.

Cells were treated for 30mins, 6hrs and 24hrs before being trypsinised, centrifuged and resuspended in methanol for isolation (Diagram courtesy of Dr Rajinder Singh, University of Leicester, UK).

3.1.6.3 Astemizole metabolism by CYP2J2 recombinant bacosomes

200mM potassium phosphate buffer pH 7.4 was made up using 2.7g potassium phosphate in 50ml water and warmed until fully dissolved. This solution was then made up to 50ml with sodium hydroxide until the right pH was reached. 100 mM magnesium chloride was made up with 0.2g in 10ml water and mixed. The NADPH generation system involved preparing reagents in accordance with table 3.22. All reagents including astemizole, hydrochloric acid and the recombinant bacosomes were kept on ice.

Table 3-22 Reagents included in the NADPH generation system (Promega, Southampton, UK).

| Component | Volume per reaction (Promega instructions) | Volume needed for 1.2ml total |
|--------------|---|-------------------------------|
| water | 22ul | 1056ul |
| Solution A | 2.5ul | 120ul |
| Solution B | 0.5ul | 24ul |
| Final volume | 25ul | 1200ul |

To prepare the reaction, 2.25ml of potassium phosphate, 250µl of magnesium chloride, 500µl 100µM astemizole and either 1,5 or 10µl thawed bacosomes diluted to 1ml in water was combined in a 25ml conical flask. This was swirled gently and placed in a 37°C water bath together with the NADPH generation system vial for 4-5 min. To initiate the reaction, 1ml of pre-warmed NADPH generating system was added to the conical flask and swirled gently. The flask was then shaken in a conical flask shaker for 30 min at 37°C after which the reaction was stopped with 25µl 1M hydrochloric acid. The contents were transferred to an Eppendorf and stored in -80°C until ready to analyse.

3.1.6.3.1 Manipulating astemizole metabolism with arachidonic acid

When setting up a reaction, a standard concentration of 100µM astemizole and 0.6pmol of bacterial bacosomes was used. Aracidonic acid concentrations varied from 10, 50,100,150 and 200µM. Once the reagents were set up, the experimental procedure was undertaken as before.

3.1.6.3.2 LC-MS

The LC-ESI-MS/MS consisted of a Waters Alliance 2695 separations module with a 100 µL injection loop and Waters 2487 UV detector connected to a Micromass Quattro Platinum (Waters Ltd., Manchester, UK) tandem quadrupole mass spectrometer with an electrospray interface. The temperature of the electrospray source was maintained at 120°C and the desolvation temperature at 350°C. Nitrogen gas was used as the desolvation gas (650 L/h) and the cone gas was set to 25L/h. The capillary voltage was set at 3.20 kV. The cone and RF lens 1 voltages were 42 V and 30 V, respectively. The aperture and RF lens 2 voltages were 0.5 V and 0.8 V, respectively. The mass spectrometer was tuned by using an astemizole standard solution (50 pmol/µL) dissolved in LC-MS optima grade water/acetonitrile (90:10, v/v) introduced by continuous infusion at a flow rate of 5 µL/min with a Harvard model 22 syringe pump (Harvard Apparatus Ltd., Edenbridge, UK).

Supernatants from pelleted cell/bacteriosome samples were evaporated to dryness and re-dissolved in 50 µL of LC-MS optima grade water/acetonitrile (90:10, v/v). Following centrifugation at 14,000 rpm for 10 min the supernatants were transferred to HPLC vials. A 10 µL aliquot of the sample was injected onto a HyPurity C18 (2.1 × 150 mm, 3 µm) column connected to a HyPurity C18 (2.1 × 10 mm, 3 µm) guard cartridge

(Thermo Electron Corporation, Runcorn, UK) attached to KrudKatcher (5 μm) disposable pre-column filter. The column was eluted using a gradient with solvent A, 0.1% acetic acid and solvent B, acetonitrile (0.1% acetic acid) at a flow rate of 200 $\mu\text{L}/\text{min}$ with a run time of 30 min. The following gradient was used: 0min-10%B, 2min-10%B, 14min-90%B, 15min-90%B, 15.1min 100%B, 20min-100%B 20.1min-10%B and 30min-10%B. The column oven temperature was maintained at 30 $^{\circ}\text{C}$ and the UV detector wavelength monitored at 260nm.

The samples were analysed in positive electrospray ionization (ESI) mode with selected reaction monitoring (SRM) for the $[\text{M}+\text{H}]^{+}$ ion transitions of astemizole 459.3 to 218.2 m/z and 459.3 to 135.1 m/z plus desmethylastemizole 445.3 to 204.3 m/z and 445.3 to 121.2 m/z . The collision gas was argon (indicated cell pressure 2.5×10^{-3} mbar) and the collision energy set at 25 eV. The dwell time was set to 200 ms and the resolution was 1.0 m/z units at peak base. The data was acquired using MassLynx software (Version 4.0). The levels of astemizole and desmethylastemizole in the samples were determined from a calibration line which was constructed by the serial dilution of the astemizole standard.

3.1.7 Isolation and quantification of exosomes by Nanosight

Sepharose CL-2B was bought from GE healthcare, Uppsala, Sweden and a 10ml plastic syringe was purchased from Becton Dickinson (BD), San Jose, CA.

EA.hy 926 cells were grown in accordance with section 3.1.2. Cells were grown in T75 flasks and treated with varying concentrations of astemizole, doxorubicin and loratadine for 24 hr.

After treating cells with drug for 24hr the media was collected and spun at 1500g for 15min to remove cells. The supernatant was then collected and transferred to a separate vial and re-spun at 1500g for 15min to remove larger particles such as apoptotic bodies and samples were put on ice.

Size exclusion chromatography was used to further remove larger particles from media. A syringe stacked with Sepharose CL-2B was used to create a size exclusion chromatography column. The centrifuged media was loaded on to the column followed by PBS/0.32% citrate. The eluted sample was collected in 25 1ml fractions to be analysed by the nanosight.

The nanosight machine was prepared by first cleaning the stage with isopropanol and assembling the platform with screws. Once fluidics had been primed the camera level was set at 12, the temperature at 25⁰C and the focus at position 135. The nanosight then quantified particle concentration and size within each sample.

3.2 Equipment

Cell viability assays were read using the NOVOstar plate reader, BMG Labtech Ltd, Aylesbury, UK.

Gel PCR gels were analysed using an imaged GeneGenius Gel Imaging System and printed out using a digital graphic printer from Syngene, Cambridge, UK.

RT-qPCR was conducted on the ViiA7 real-time PCR system, Thermo Fisher Scientific UK Ltd, Loughborough UK.

Protein assays were conducted in 96 well sterile cell culture plates, flat bottom with lid were obtained from Greiner Cellstar, Sigma-Aldrich.

Western blots were visualised with the ImageQuant LAS 4000 from GE healthcare, Uppsala, Sweden.

Analysis of metabolites was done with The LC-ESI-MS/MS which consisted of a Waters Alliance 2695 separations module with a 100 µL injection loop and Waters 2487 UV detector connected to a Micromass Quattro Platinum (Waters Ltd., Manchester, UK) tandem quadrupole mass spectrometer with an electrospray interface.

Exosome quantification was done with the NanoSight nanoparticle tracking analysis (NTA) machine from NanoSight Ltd, Malvern UK

Chapter 4 **Establishing an in vitro cell model to investigate the role
of Cytochrome P450 2J2 in drug cardiotoxicity**

4.1 Background

4.1.1 A suitable cell model to investigate the role of CYP2J2 in drug cardiotoxicity

Cytochrome P450, 2J2 (CYP2J2) metabolises both exogenous and endogenous substrates and is highly expressed in the human heart. CYP2J2 has been found to be involved in phase 1 drug metabolism of a variety of structurally diverse compounds including anti histamines, anti-cancer drugs and antibiotics (C. A. Lee et al., 2010, Matsumoto et al., 2002). The significance of CYP2J2 in drug metabolism is due firstly to its expression in the intestine allowing for its involvement in first pass metabolism as well as the recent finding that this enzyme may produce unique metabolites from the metabolism of some drugs (Xie et al., 2016, C. A. Lee et al., 2010).

As well as xenobiotic metabolism, there is increasing awareness for the role of CYP2J2 in the metabolism of endogenous substrates (Solanki et al., 2018). The positive effects of CYP2J2 in combating many of the hallmarks of cardiotoxicity (Y. Zhang et al., 2009) have been attributed mainly due to its epoxygenase activity whereby it metabolises arachidonic acid producing four active metabolites known as epoxyeicosatrienoic acids or EETs. The biological effects of these EETs on the cardiovascular system are diverse due their ability to act on an assortment of cells, permitting their involvement in the protection of the heart from drug cardiotoxicity (Solanki et al., 2018). This raises the prospect that an ideal *in vitro* cell culture model would offer a better understanding of the interplay between CYP2J2 and its metabolism of both exogenous and endogenous compounds as well as investigate how the CYP2J2/EET pathway may protect against drug induced toxicity.

4.2 Aims

To establish a suitable cell type to study cardiotoxic drugs *in vitro* as well as an opportunity to investigate CYP2J2 and the protective EETs pathway.

To determine an appropriate cell type(s) and cardiotoxic drug to produce an *in vitro* model that give a consistent toxic response for further study.

To study the effects of inhibitors which modulate the CYP2J2/EET pathway on toxicity induced by astemizole in the cell models.

4.3 Results

4.3.1 Concentration response of a panel of a drugs to relevant cell types

To set a viable *in vitro* cell model of toxicity a model compound and cell culture system were investigated which would give a consistent concentration related toxicity response and allow investigation and quantification of cardiotoxic parameters in future experiments.

A concentration dependent response was evaluated for astemizole, sunitinib and doxorubicin (dox) using HepG2 cells and iPSC-CMs at 30mins, 6hr and 24hr. It was vital that concentrations used included the therapeutic and toxicity range of the drug in humans. Previous *in vitro* toxicity testing for dox used concentrations ranging from 0.1-10 μM for 24hrs when analysing apoptosis and ROS generation in mouse cardiac myocytes (Fu et al., 2010), however even lower concentrations had been reported (Xiao et al., 2017). Typically a therapeutic dose of dox lies between 0-5 μM (J. Liu et al., 2008). With regards to sunitinib, previous study into toxicity responses via cell viability and caspase activity in human cardiac myocytes showed a concentration of between 0-10 μM to be sufficient to show a concentration dependent response (Doherty et al., 2013). The therapeutic window for sunitinib was shown to be narrow and should be below 0.25 μM (Lindauer et al., 2010). Furthermore, C_{max} values for astemizole $\sim 0.74\text{ng/ml}^{-1}$ in healthy volunteers (Lefebvre et al., 1997). Thus a concentration response between 0 and 100 μM was utilised which would include both the therapeutic range and low to severe toxicity to cells.

Toxicity concentration responses to astemizole, dox and sunitinib were observed (figure 3.1). Prior to working with (expensive) iPSC-CMs the ATP method for assessment of cell viability in 96 well plate format was established in the laboratory using HepG2 cells as a preliminary cell model. For all drugs there was a decrease in ATP and hence an increase in cell death at the later timepoints of 6hr and 24hr compared with 30mins. For astemizole in HepG2 cells at 30mins there was a $\sim 40\%$ decline in ATP at the lowest concentration of 1nM compared to 100% DMSO control. The levels of ATP declined gradually until after 10 μM where there was steep decline from $\sim 50\%$ to less than 10%. At 6hrs there was a spike of ATP (1 μM) after which there was a steep decline in ATP indicating a cell stress response which was depressed by an increasing concentration of sunitinib. At 24hr the concentration response was shifted to the left (i.e toxicity at lower

concentrations of astemizole) (figure 4.1A). HepG2 cells treated with sunitinib showed an abrupt decrease in ATP at 1nM comparable to astemizole at 30mins compared to DMSO control (figure 4.1B). This may be due to an initial shock to cells. At both 30mins and 6hr there was spike of ATP at 10 μ M to 100-150% after which there was a steep decline to less than 1% control, similar to that seen for astemizole. This spike was not seen at 24hr, instead the concentration was shifted to the left with toxicity at lower concentrations of drug (figure 4.1B). For dox, there was a rapid decrease from 100% to ~50% at 1nM at 30mins. However there little change in toxicity even at the higher concentrations of 100 μ M indicating 30mins was not enough time to induce a full concentration dependent toxicity in cells. Both 6 and 24hr showed a similar trend with an initial increase in ATP to ~150% control at 10 μ M after which there was a steep decline in ATP (figure 4.1C). Due to this it was difficult to see a clear concentration dependent effect of dox.

The procedure developed successfully for HepG2 cells was applied to iPSC-CMs. iPSC-CMs showed a more traditional concentration response with all three drugs. For astemizole both 30mins and 6hr showed a similar trend with a loss of ATP proportional to the concentration of drug. This was also seen at 24 hr with a shift to the left indicating a longer drug incubation exacerbated toxicity at lower concentrations (figure 4.1D). Sunitinib showed a similar response to astemizole. Both showed a gradual decline in toxicity at lower concentrations of drug with 1-10 μ M yielding ~100% ATP after which there was a sharp decline in ATP and increased toxicity at higher concentrations of 10 and 100 μ M (figure 4.1E). With regards to dox there was little change in ATP at 30mins compared to 100% DMSO control indicating toxicity had not yet developed. At 6 and 24hr for concentrations <10 μ M there was no significant change in ATP, however between 10 and 100 μ M there was a steep decline in ATP to nominal levels suggesting there was a threshold concentration between 10 and 100 μ M at which toxicity was reached (figure 4.1F). Overall, a decrease in ATP was seen mainly at the higher drug concentrations of 1 and 10 μ M. Astemizole was seen to be a fast acting drug with toxicity apparent at 30mins. Sunitinib was found to be toxic at 10 μ M over 30mins and 24hr but required 24hr incubation to develop toxic effects at 1 μ M. As also seen in HepG2 cells, doxorubicin was the slowest acting in iPSC-CMs with significant cell death apparent at 10 μ M and above at the longer timepoints studied.

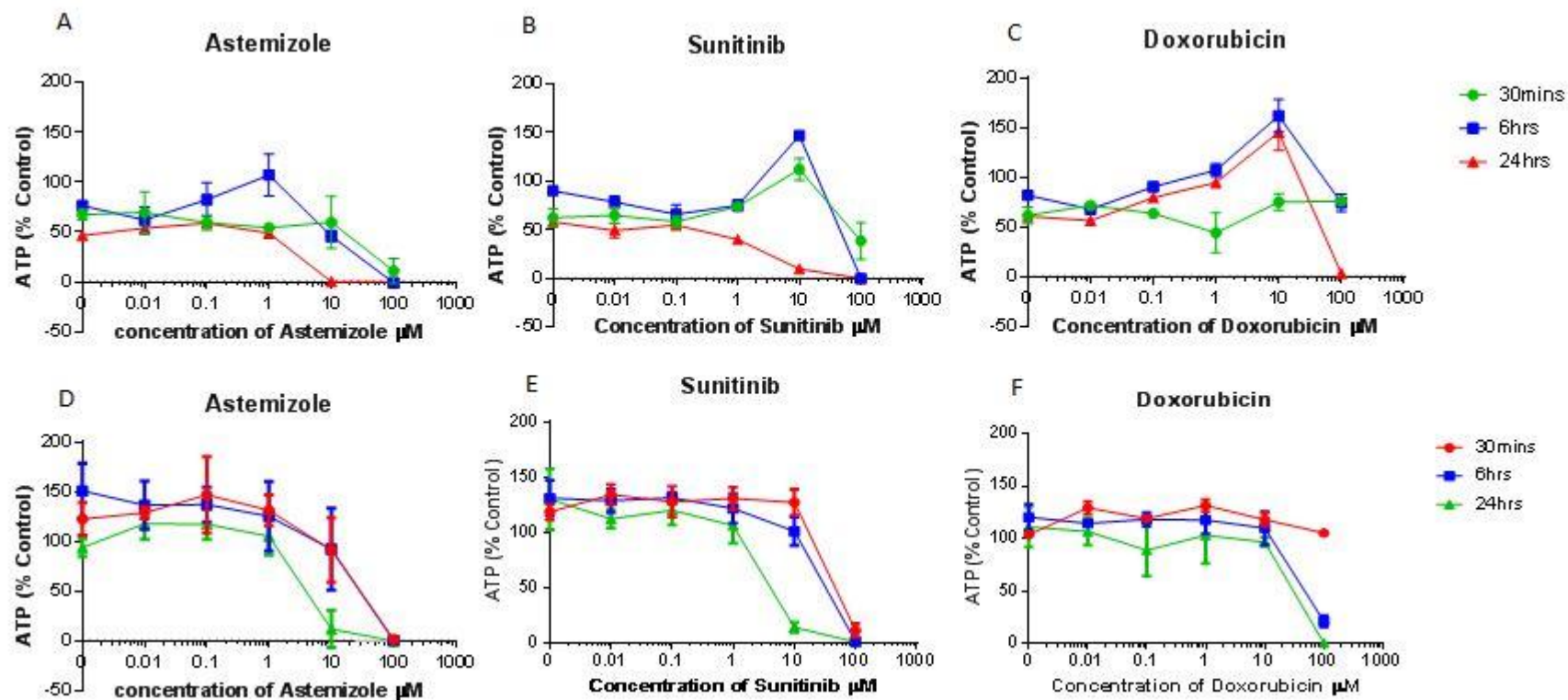


Figure 4-1 Effect of cardiotoxic compounds on ATP levels in HepG2 cells (A-C) and iPSC-CMs (D-F).

HepG2 cells and iPSC-CMs were cultured to 80-90% confluence and then treated with drugs (1nM- 100µM) for 30mins, 6hrs and 24hrs to produce a standard curve. All data (mean and SEM of 4 replicates) was normalised as a percentage of the vehicle DMSO control. DMSO was kept at a final concentration of dilution of 0.001%.

4.3.2 Concentration and time dependent toxicity response: astemizole

From the results it was inferred that astemizole gave a consistent cytotoxicity result and therefore was used for further experiments. iPSC-CMs were not used for future experiments due to expense and because cells could not be passaged. HepG2 cells showed an uncharacteristic concentration dependent response to the three drugs and it is known they lack expression and activity of many cytochrome P450 enzymes and so may not be the most appropriate model for future experiments (Gerets et al., 2012). Instead EA.hy926 cells and HCM were utilised to further ascertain the best concentration and time point to use with astemizole. ATP was assayed as a marker of toxicity to create a concentration dependent response between 1nM and 100µM at three time points (see figure 4.2). At 30mins both EA.hy926 cells and HCM showed a characteristic concentration response to astemizole. However, cells treated with astemizole showed elevated levels of ATP, 60-100% higher compared to the vehicle control suggesting there may be an alternate mechanism increasing ATP and conveying a stress response to astemizole (figure 4.2A). After 10 µM there was a steep decline in ATP in both cell types. In EA.hy926 cells ATP declined to less than 10% at 100µM, however in HCM at 100 µM ATP levels were over 50% indicating that HCM may be less prone to toxicity than EA.hy926 cells. This was reiterated at 6 hr (figure 4.2B) where levels of ATP were higher in HCM compared to control and there was a steep decline in ATP at concentrations of >10 µM. At 24 hr extensive toxicity was seen at 10µM in both cell types (figure 4.2B and 2C).

Due to a decline in ATP between 1 µM and 100 µM which made it difficult to judge the exact concentration at which toxicity was occurring, a further concentration response between 1 and 100 µM was carried out (figure 4.2D-F). At 30mins cells EA.hy926 cells showed a decline in ATP from 30µM onwards and reached full toxicity between 70-100 µM. In HCM however, ATP levels did not decline until ~70 µM and ATP was still detectable at 100 µM (figure 4.2D). At 6hr both cell types showed similar trends with a reduction in ATP ~40 µM onwards with no detectable ATP at 100 µM astemizole (figure 4.2E). This toxicity was exacerbated at 24hr where no ATP levels were detectable after 30 µM (figure 4.2F). A non-toxic dose of 25 µM (100% ATP) and a toxic dose of 50 µM (50% ATP) at a time point of 6hr for both cell types was established as suitable for further experimentation (see figure 4.2).

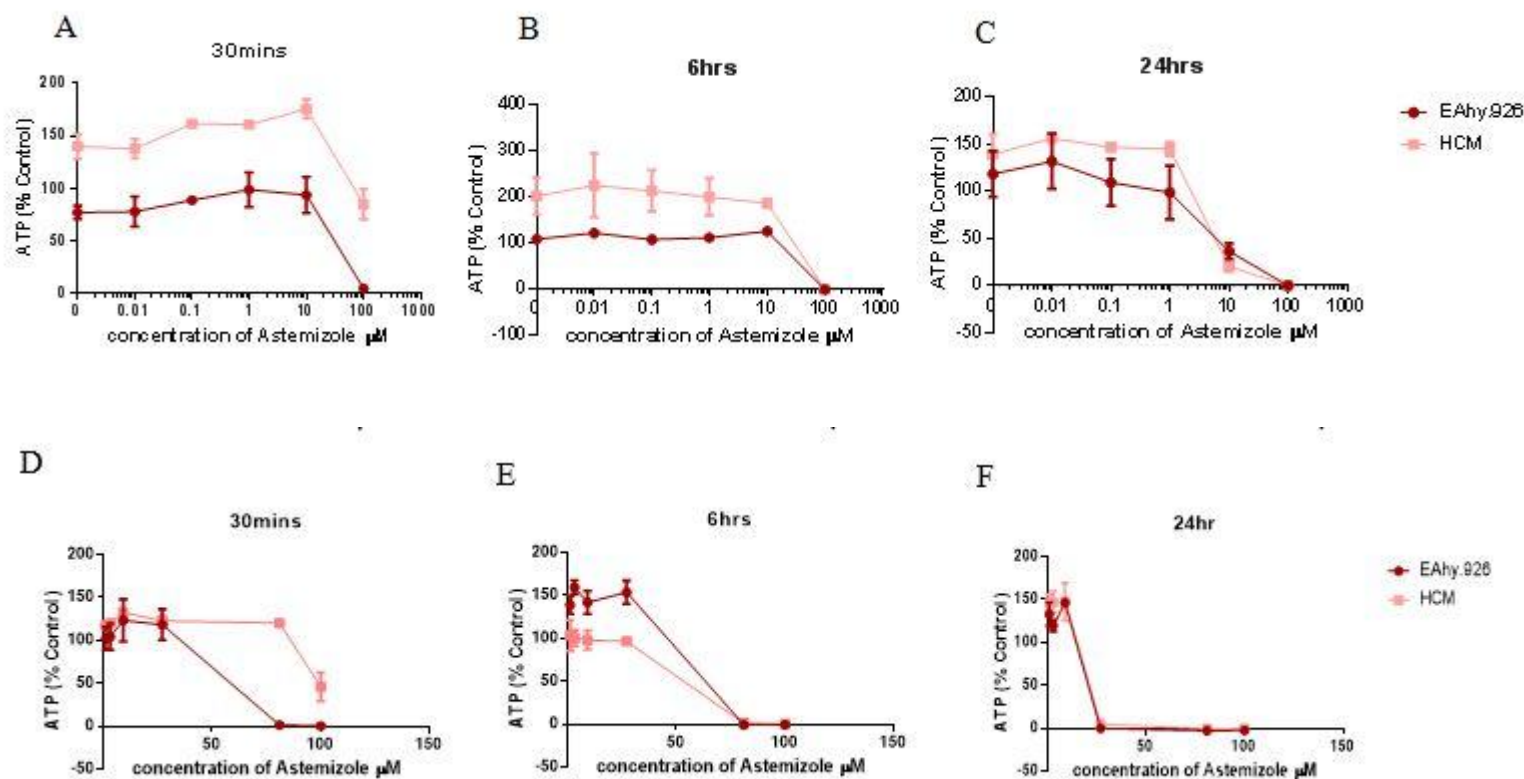


Figure 4-2 Effect of astemizole on ATP levels in EA.hy926 cells and HCM after incubation at 3 time points.

EA.hy926 cells and human cardiac myocytes were cultured to 80-90% confluence and then treated with astemizole at either 1nM-100µM (A-C) or 1-100µM (D-F) for 30mins, 6hrs and 24hrs to produce a standard curve. All data (mean and SEM of 4 replicates) was normalised as a percentage of the vehicle DMSO control. DMSO was kept at a final concentration of dilution of 0.001%.

4.3.3 Effect of EET synthesis inhibitors on astemizole toxicity

4.3.3.1 Concentration dependent response: EET inhibitors

Once a suitable concentration and timepoint had been established for astemizole, it was the aim to inhibit EET formation using inhibitors of PLA₂ (quinacrine dihydrochloride and LY311727) and the CYP epoxygenase inhibitor MSPPOH. Initially, it was important to define the toxicity caused by these inhibitors. Therefore, both cell ATP and released LDH levels were determined in EA.hy926 and HCM cell cultures after incubation with quinacrine, MSPPOH and LY311727 from 1-50 μ M at 6hr (see figure 4.3).

Overall, MSPPOH and quinacrine hydrochloride showed little toxicity with no significant change in ATP or LDH levels over the range of concentrations tested. However, LY311727 showed a concentration dependent decrease in ATP and increase in LDH showing a toxicity response which was particularly discernible at higher concentration of inhibitor. From the results a concentration which gave a 100% ATP and LDH was deduced. In further experiments, both quinacrine dihydrochloride and LY311727 were used at 25 μ M and MSPPOH was used at the lower concentration of 12.5 μ M.

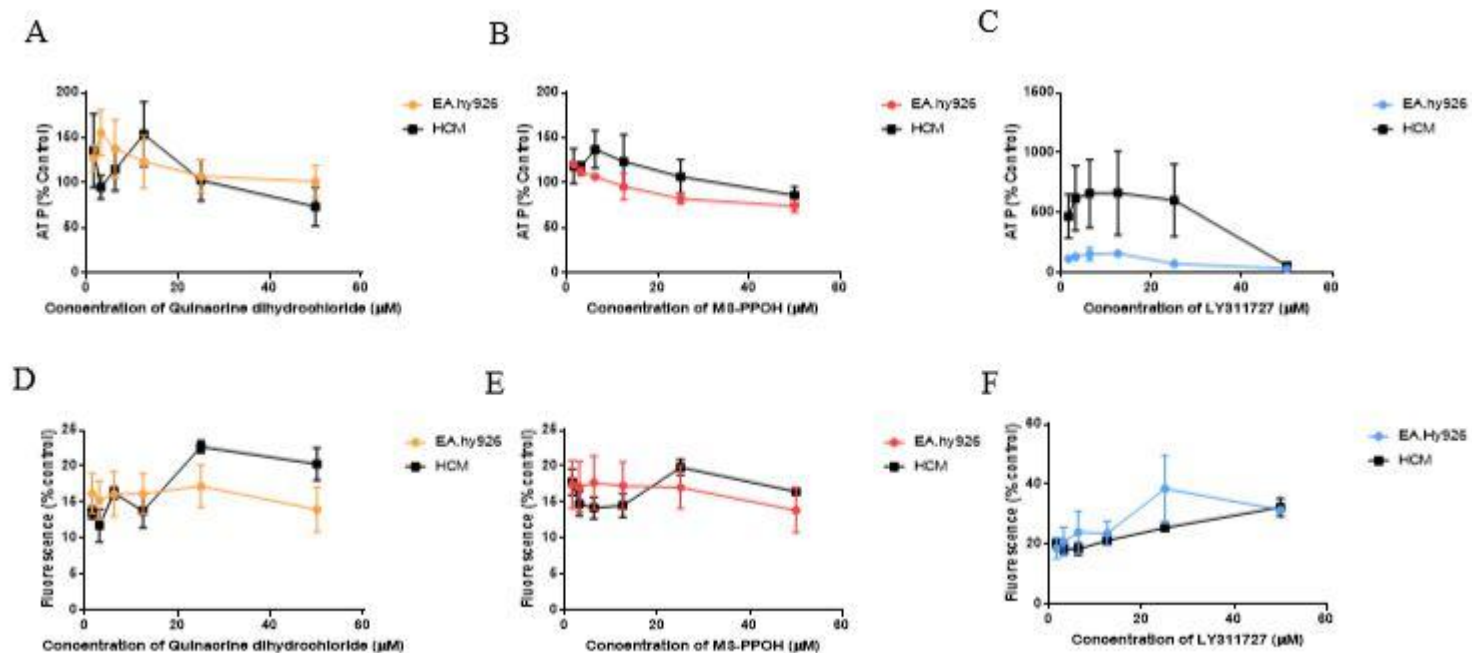


Figure 4-3 Effect of Quinacrine dihydrochloride (A,D), MSPPOH (B,E) and LY311727 (C,F) on cell viability.

EA.hy926 cells and human cardiac myocytes were cultured to 80-90% confluence and then treated with either quinacrine dihydrochloride ($25\mu\text{M}$), MSPPOH ($12.5\mu\text{M}$) and LY311727 ($25\mu\text{M}$) for 6hrs to produce a standard curve. Cellular ATP (A-C) and released LDH (D-F) levels were assessed. All data (mean and SEM of 4 replicates) was normalised as a percentage of the vehicle DMSO control. DMSO was kept at a final concentration of dilution of 0.001%.

4.3.4 Effect PLA₂ and CYP2J2 inhibitors on astemizole toxicity in EA.hy926 cells and human cardiac myocytes

EA.hy926 cells and HCM were incubated with astemizole and inhibitors for 6hr. With both cell types there was a significant decrease in ATP when cells were incubated with 50µM astemizole alone compared with vehicle control as expected (figure 4.4B, D). A concentration of 25µM was also used which had previously given ~ 100% ATP to act as a further control.

When EA.hy926 cells were incubated with both inhibitor and 25µM astemizole no significant change was seen with either quinacrine dihydrochloride or MSPPOH. However, there was a significant increase in ATP with the addition of both toxic drug and LY311727 compared to inhibitor and cells alone (figure 4.4A). Furthermore, this was also seen at 50µM astemizole (figure 4.4B) indicating a stress response by cells to these compounds. Although for EA.hy926 cells in particular, the inhibitors seemed to show evidence towards protection against ATP loss, these effects did not reach statistical significance (figure 4.4B).

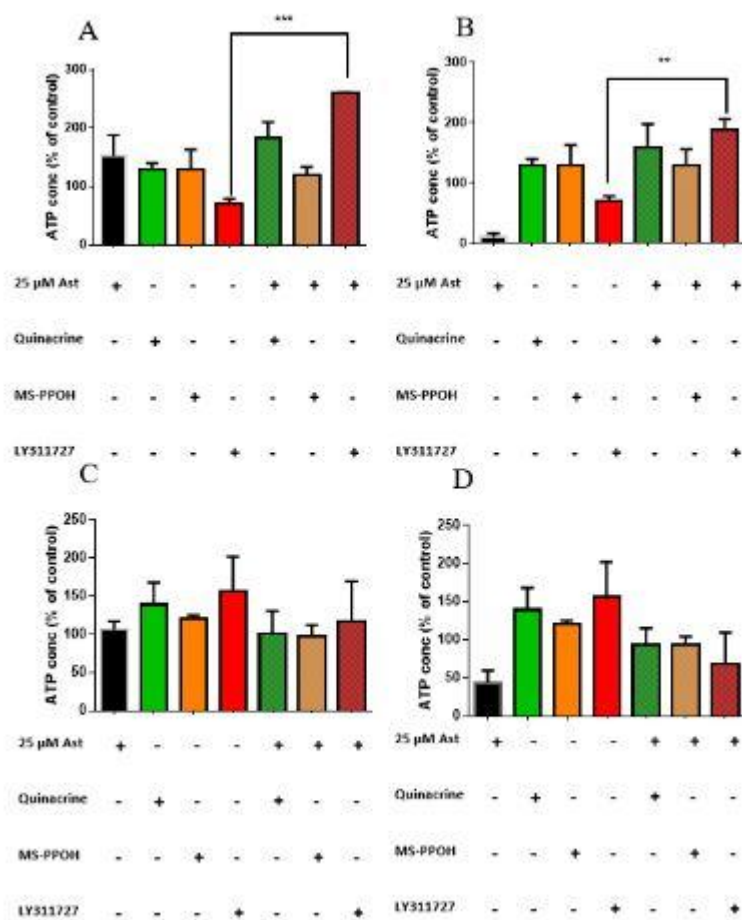


Figure 4-4 Effect of CYP epoxygenase inhibitor MSPPOH and PLA2 inhibitors quinacrine dihydrochloride and LY311727 on astemizole toxicity (ATP).

EA.hy926 cells and human cardiac myocytes were cultured to 80-90% confluence and pretreated for 1hr with MSPPOH (12.5μM), quinacrine dihydrochloride and LY311727 (25μM) after which they were incubated for 6hrs with astemizole without changing the media. Cell viability measured as cellular ATP in EA.hy926 cells (A and B) and HCM (C and D). Astemizole concentrations used were 25 μM (A and C) and 50 μM (B and D) All data (mean and SEM of 4 replicates) was normalised as a percentage of the vehicle DMSO control. DMSO was kept at a final concentration of dilution of 0.001%. .***P=0.0003, **P=0.0046

To investigate whether the LY311727 was interacting with ATP assay, an ATP assay was conducted with a mixture of LY311727 and ATP reagent with no cells. For comparison MSPPOH was also tested and normalised to ATP reagent alone. However, there was no significant change in luminescence between the two drugs and both drugs caused little change in luminescence compared to ATP reagent alone (figure 4.5).



Figure 4-5 Investigation of the effect of LY311727 on ATP reagent luminescence.

LY311727 was mixed in a plate shaker with ATP reagent in a 96 well plate with no cells and incubated for 5 min before being analysed with a plate reader. Results are a mean (+ SEM) of 3 experiments normalised to ATP reagent alone.

In addition to ATP, caspase activity was used as an alternative endpoint to measure apoptosis (see figure 4.6). Untreated cells were used as a negative control which showed negligible caspase activity and recombinant caspase-3 was used a positive control and gave a strong luminescent signal. Incubation of EA.hy926 cells with astemizole showed little change in apoptosis compared with negative control at both concentrations for both cell types. Overall there was no significant change in caspase levels and thus apoptosis when both cell types were treated with astemizole and PLA₂ inhibitors quinacrine dihydrochloride or LY311727. However there was a notable increase in caspase when EA.hy926 cells were treated with both 50uM astemizole and the CYP epoxygenase inhibitor MSPPOH compared to control which was not seen in HCM indicating a halt in EET production in EA.hy926 cells leading to increased toxicity.

Cell viability was further investigated in EA.hy926 cells using the same treatments as in Figure 4.4 with the MTS assay (see figure 4.7). Inhibitors prevented the astemizole induced loss of cell viability, so rather than exacerbating toxicity as hypothesised, these inhibitors were protective.

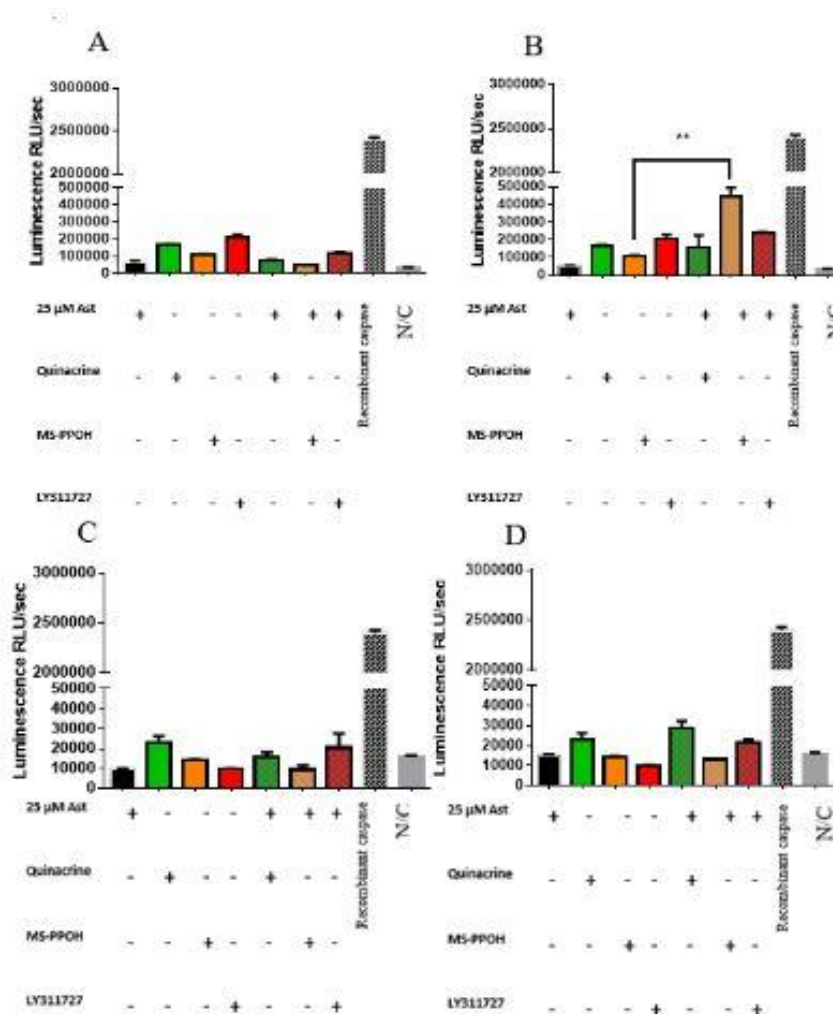


Figure 4-6 Effect of CYP epoxygenase inhibitor MSPPOH and PLA2 inhibitors quinacrine dihydrochloride and LY311727 on astemizole toxicity (Caspase 3/7).

EA.hy926 cells and human cardiac myocytes were cultured to 80-90% confluence and pretreated for 1hr with MSPPOH (12.5 μ M), quinacrine dihydrochloride and LY311727 (25 μ M) after which they were incubated for 6hrs with astemizole without changing the media. Apoptosis measured as caspase 3/7 activity in EA.hy926 cells (A and B) and HCM (C and D). Astemizole concentrations used were 25 μ M (A and C) and 50 μ M (B and D). Data was shown unnormalized. A positive control with recombinant caspase enzyme was used as well as a negative vehicle control. DMSO was kept at a final concentration of dilution of 0.001%. ** $p < 0.01$.

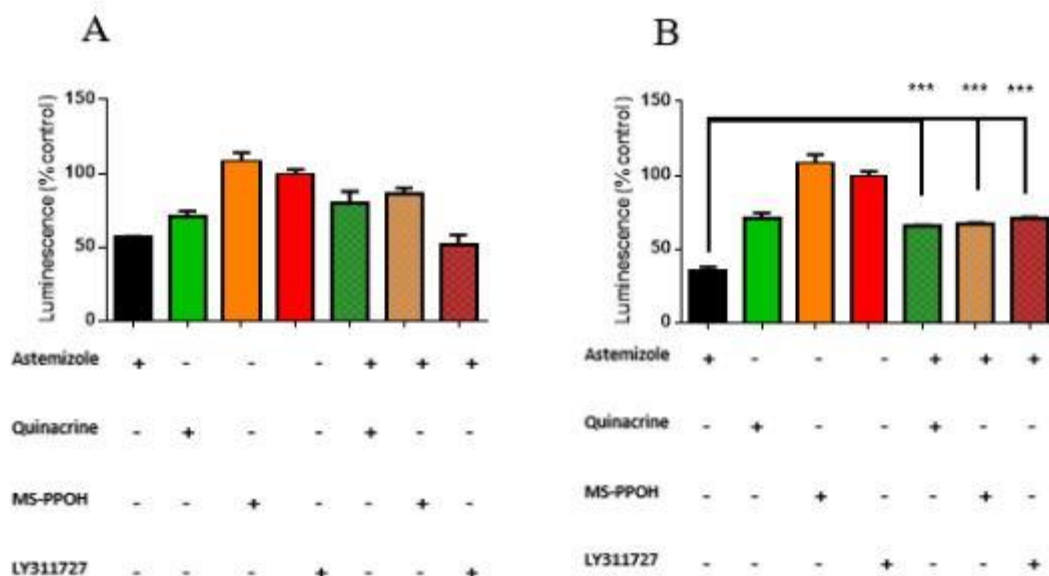


Figure 4-7 Effect of CYP epoxygenase inhibitor MSPPOH and PLA2 inhibitors quinacrine dihydrochloride and LY311727 on astemizole toxicity measured using the MTS assay in EA.hy926 cells.

EA.hy926 cells were cultured to 80-90% confluence and pretreated for 1hr with MSPPOH (12.5µM), quinacrine dihydrochloride and LY311727 (25µM) after which they were incubated for 6hrs with astemizole without changing the media. Astemizole concentrations used were 25µM (A) and 50µM (B). Cell viability was measured with the MTS assay. All data (mean and SEM of 4 replicates) was normalised as a percentage of the vehicle DMSO control. DMSO was kept at a final concentration of dilution of 0.001%. P=0.001 (quinacrine + 50uM ast), P=0.003 (MSPPOH +50uM ast) and P=<0.0001 (LY311727 +50uM ast). P=0.0001. MTS 3-(4,5-dimethylthiazol-2-yl)-5-(3-carboxymethoxyphenyl)-2-(4-sulfophenyl)-2H-tetrazolium).

Furthermore the Hoechst 33342 nuclear stain was utilised to visualise cells and further investigate cell viability. EA.hy926 cells and HCMs produced similar results. When cells were incubated with a cytotoxic concentration of astemizole there was a stark decrease in cell viability compared with a non-toxic dose of astemizole and negative control (figure 4.8).

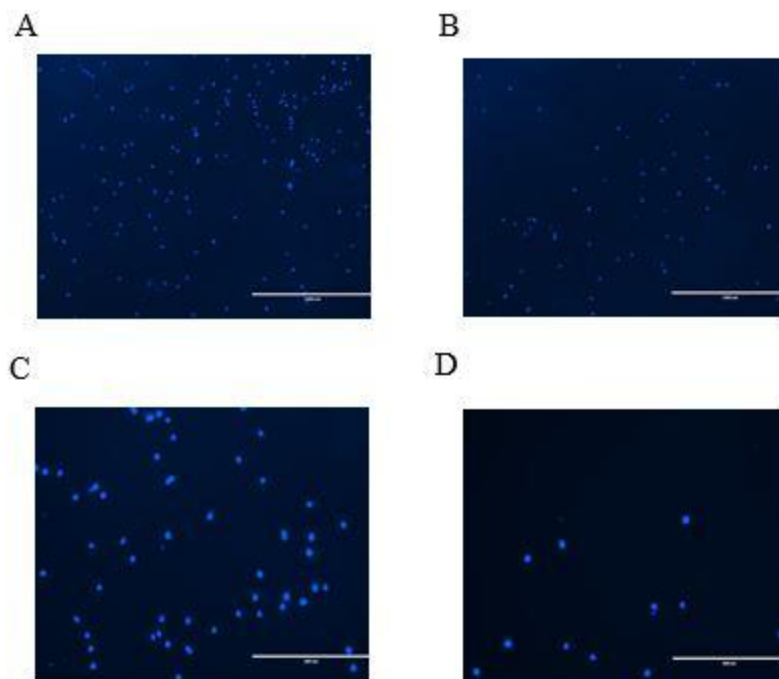


Figure 4-8 The effect of different concentrations of astemizole on cell viability through Hoechst 33342 staining.

EA.hy926 cells were cultured to 80-90% confluence and treated with a non-toxic dose (25 μ M) of Astemizole and imaged at x4 magnification (A) and x10 magnification (C). A toxic dose of Astemizole (50 μ M) was also used as a control and imaged at x40 (B) and x100 (D). Once cells had been cultured, the media was removed and dye solution (10mg/ml) was added to the cells enough to cover the well. Cells were then incubated with the Hoechst stain for 10 minutes in foil. After incubation the stain was removed and cells were visualised using a fluorescent microscope (excitation/emission 350/461nm).

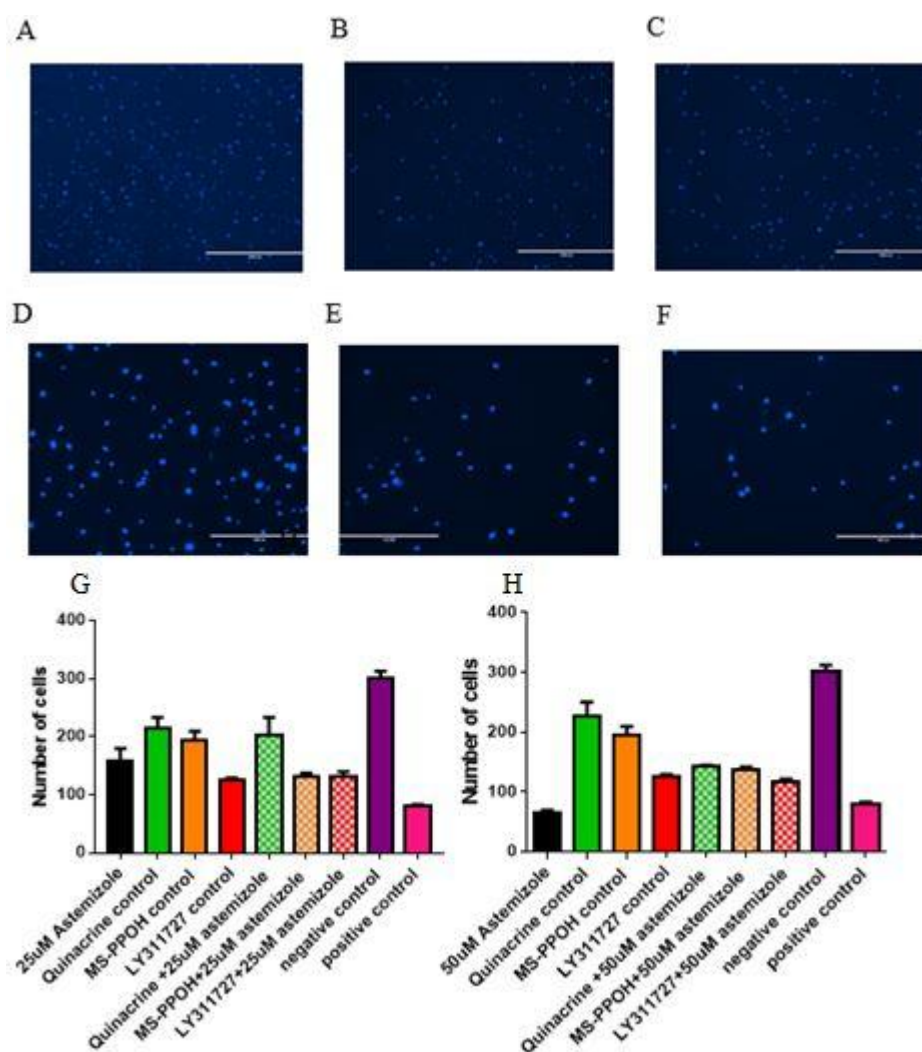


Figure 4-9 Effect of inhibitors of the EET pathway on astemizole toxicity.

Cells were treated with either 12.5 μM MSPPOH alone (A and D), 12.5 μM MSPPOH with 25 μM astemizole (B and E) or 12.5 μM MSPPOH and 50 μM astemizole (C and F) for 6hrs. Once cells had been cultured, the media was removed and dye solution (10mg/ml) was added to the cells enough to cover the well. Cells were then incubated with the Hoechst stain for 10 minutes in foil. After incubation the stain was removed and cells were visualised using a fluorescent microscope (excitation/emission 350/461nm). Cells were imaged at x4 and x10 magnification. Quantification of cytotoxic effects of astemizole and inhibitors was done by counting cells by eye in three fields of view and calculating the mean. EA.hy926 cells were cultured to 80-90% confluence and pretreated for 1hr with MSPPOH (12.5 μM), quinacrine dihydrochloride and LY311727 (25 μM) after which they were incubated for 6hrs with astemizole without changing the media. (G) Cells treated with 25 μM astemizole and (H) cells treated with 50 μM astemizole. All data (mean and SEM of 3 replicates) was normalised as a percentage of the vehicle DMSO control. Positive control was cells treated with water.

Both EA.hy926 cells and HCM were incubated with astemizole and/or inhibitors of EET formation to investigate if there were any change in cell viability. Quantification of cells within each treatment showed no exacerbation of astemizole toxicity after treatment with quinacrine dihydrochloride, instead a possible protective effect was observed when cells were treated with a toxic dose of astemizole (50 μ M) and quinacrine (figure 4.9H). Similarly, there was little change in cell viability with the alternative PLA₂ inhibitor LY311727 which showed no change in toxicity at the non-toxic dose of 25 μ M astemizole (figure 4.9G) or at 50 μ M astemizole (figure 4.9H). Similarly, cells treated with a non-toxic dose or toxic concentration of astemizole and an inhibitor of epoxygenase activity MSPPOH showed no change in cell viability compared with astemizole treatment (figure 4.9G). Overall there were no statistically significant changes in cell viability using PLA₂ and CYP epoxygenase inhibitors (figure 4.9) and therefore these data provide no convincing evidence that the inhibition of epoxidase activity or PLA₂ inhibitors affected astemizole induced cytotoxicity.

4.3.5 Effect of EET facilitators on astemizole toxicity

Both EA.hy926 cells and human cardiac myocytes were preincubated with the 100 μ M SEH inhibitor, t-AUCB, for an hour before incubation with either a non-toxic (25 μ M) or a toxic (50 μ M) dose of astemizole for 6hr. After analysing ATP levels it was found there was no significant change in ATP when cells were treated with a non-toxic dose of astemizole. However, when cells were treated with both a toxic dose of astemizole and t-AUCB, ATP was conserved to ~100% vehicle control compared to cells treated with 50 μ M astemizole alone (figure 4.10A). The evidence was even more convincing for HCM. Astemizole (50 μ M) caused a 4 fold reduction in ATP (figure 4.10B) and this toxicity was protected by t-AUCB such that ATP levels were identical to the vehicle control. This may suggest inhibiting sEH may decrease the deactivation of and lead to an increase in endogenous EETs which may have protective effects against toxicity *in vitro*.

Nuclear staining with Hoechst stain was used to further investigate cell viability. Pre-treatment with t-AUCB showed no change in the number of EA.hy926 cells in cells exposed to 25 μ M astemizole, however, against astemizole toxicity t-AUCB showed a significant protection of cells indicating a preservation of cell viability against astemizole toxicity (figure 4.11).

In addition to sEH inhibitor, exogenous EETs were also used to investigate whether EETs might be possibly responsible for protecting cells against toxicity. EA.hy926 cells were pre-treated with exogenous 11,12-EET for 1hr before being incubated with either 25 μ M or 50 μ M astemizole. ATP concentrations showed a preservation in ATP when cells were pre-treated with 11,12-EET subsequent to astemizole. This was particularly apparent and statistically significant when a cytotoxic dose of astemizole was administered (figure 4.12).

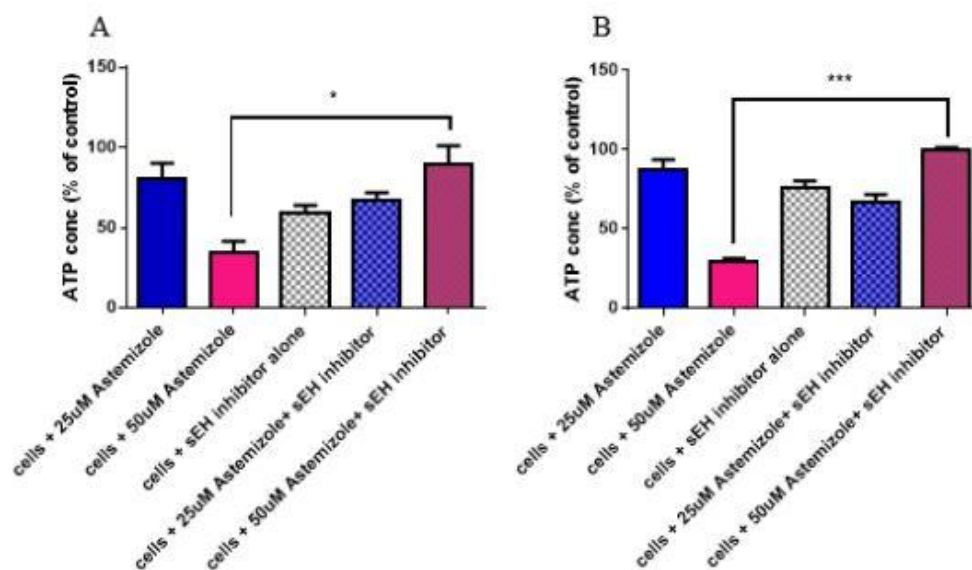


Figure 4-10 Effect of sEH inhibitor t-AUCB on astemizole toxicity assessed by measuring ATP concentrations.

EA.hy926 (A) and HCM (B) were cultured to 80-90% confluence and pretreated for 1hr with t-AUCB (100 μ M) after which they were incubated for 6hrs with astemizole (25 μ M and 50 μ M) without changing the media. Cell viability was measured with the ATP assay. All data (mean and SEM of 3 replicates) was normalised as a percentage of the vehicle DMSO control. DMSO was kept at a final concentration of dilution of 0.001%. *P<0.05, ***P=0.0002

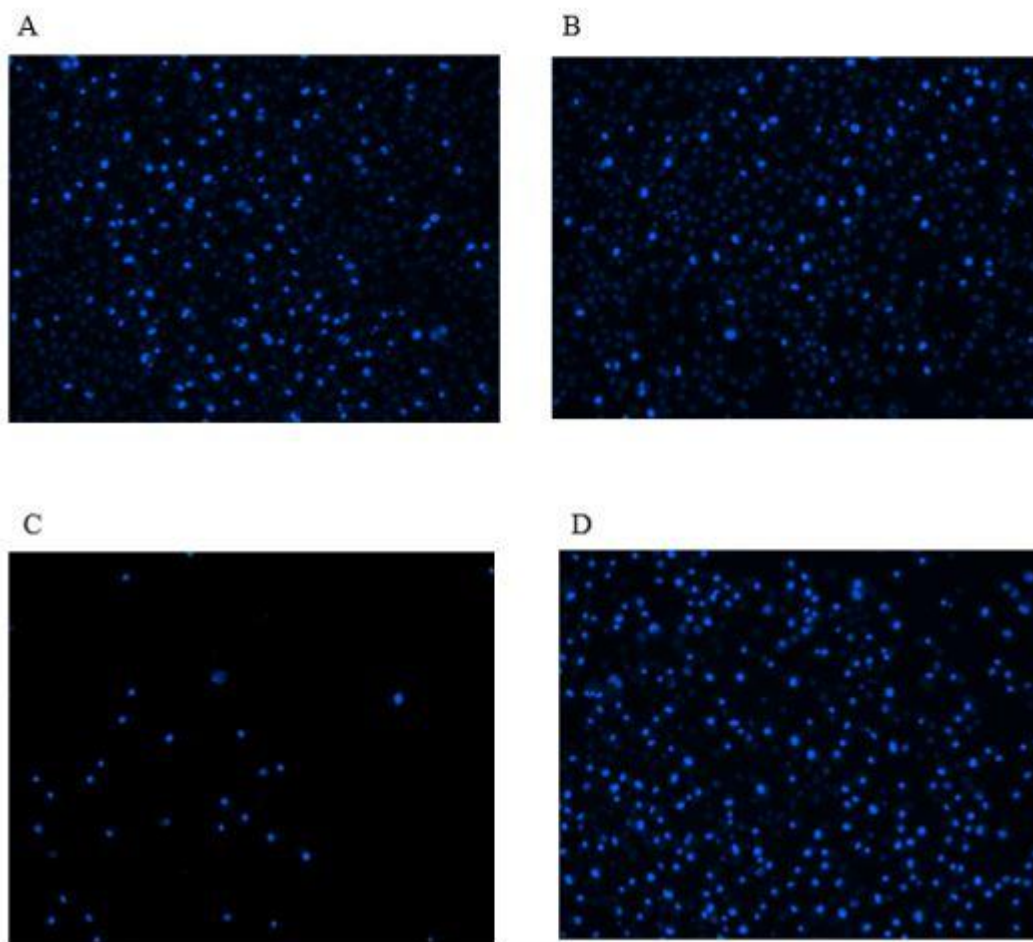


Figure 4-11 Effect of sEH inhibition on cell viability after astemizole treatment.

EA.hy926 cells were cultured and then treated with 25 μ M astemizole (A and B) and 50 μ M astemizole (C and D) for 6hr. Some cells were also pre-treated with sEH inhibitor (B and D) 1 hour before astemizole was added. The media was then removed and dye solution (10mg/ml) was added to the cells enough to cover the well. Cells were then incubated with the Hoechst stain for 10 minutes in foil. After incubation the stain was removed, and cells were visualised using a fluorescent microscope (excitation/emission 350/461nm). Cells were imaged at x10 magnification.

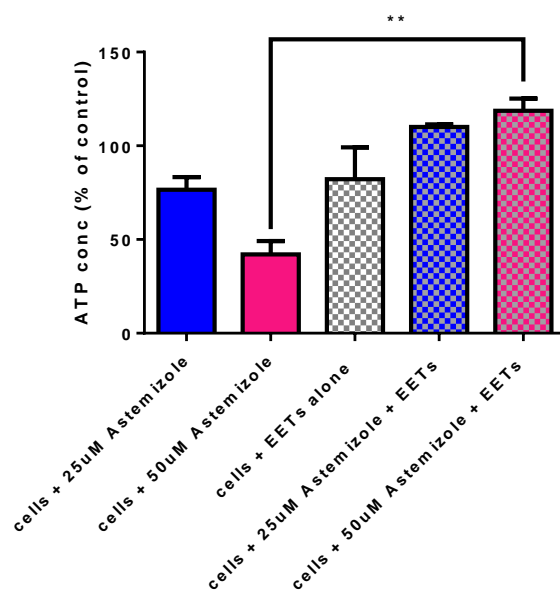


Figure 4-12 Effect of exogenous EETs on astemizole toxicity in EA.hy926 cells.

EA.hy926 cells were cultured to 80-90% confluence and pretreated for 1hr with exogenous 11,12-EET (100µM) after which they were incubated for 6hrs with astemizole (25µM and 50µM) without changing the media. Cell viability was measured with the ATP assay. All data (mean and SEM of 3 replicates) was normalised as a percentage of the vehicle DMSO control. DMSO was kept at a final concentration of dilution of 0.001%. **P<0.005.

4.4 Discussion

ATP gave a consistent response for cells incubated with a series of toxic drugs and was a good indicator of cell viability as it was proportional to the number of viable cells present as determined with Hoechst staining. Previously, ATP was used in structural profiling of cardiotoxins in the rat cell line H9C2 cells and human embryonic stem cell-derived cardiomyocytes (hESC-CMs) alongside mitochondrial membrane potential and endoplasmic reticulum stress. Cell viability measured as ATP levels agreed well with other parameters and together were predictive of cardiotoxicity *in vitro* (Pointon et al., 2013).

From the concentration response curves, the final concentrations of astemizole used were a relatively non-toxic concentration of 25 μM which resulted in 100% ATP remaining and a toxic concentration of 50 μM which caused a loss of 50% ATP relative to DMSO vehicle control. There has been little work reported on the effect of astemizole on cell viability and cell death *in vitro* and therefore there were no literature values to use as a reference. However, drug metabolism investigations with astemizole in human liver microsomes and recombinant CYP2J2 protein showed a K_m of 16 μM and V_{max} of $190\mu\text{M}^{-1}\text{min}^{-1}$ suggesting the concentrations used were appropriate to study the interaction of CYP2J2 with astemizole and may be adequate to test toxicity in cells (Uehara et al., 2016).

Contrary to the original hypothesis, which assumed inhibition of CYP2J2 or PLA₂ would inhibit the production of EETs and therefore exacerbate astemizole induced toxicity, there was an increase in ATP when cells were treated with either CYP epoxygenase inhibitor MSPPOH or PLA₂ inhibitors quinacrine dihydrochloride and LY311727 in combination with 50 μM astemizole for 6hr. This was also corroborated by Hoechst nuclear staining showing an increase in viable cells. For LY311727 this increase in ATP was particularly evident. This unexpected finding may be the result of a cell stress response leading to increases in ATP in cells. In addition, the mechanism behind how astemizole leads to cell death may involve AA, possibly producing an intermediate compound which is needed to exert its toxicity effect. Inhibiting AA release through pharmacological inhibition of PLA₂ may reduce cell death independent of the inhibition of EET production (figure 4.13).

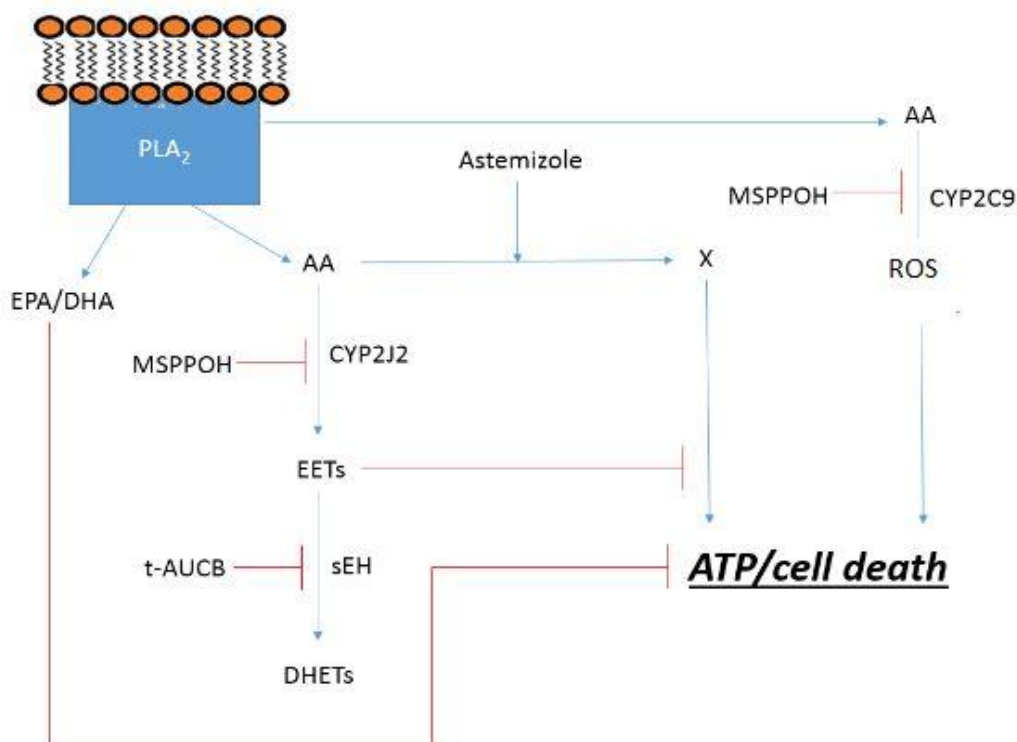


Figure 4-13 Proposed mechanism for how the CYP2J2/EET pathway may play a role in astemizole related cell death.

PLA₂ hydrolyses AA from the membrane which can be utilised to produce EETs. Inhibition of this protective pathway with PLA₂ inhibitors was shown to increase ATP in response to astemizole toxicity. A potential reason for this may be the need for AA in the initiation or execution of astemizole toxicity. Reducing AA may therefore inhibit cell death. A possible mechanism to why MSPPOH may increase ATP is that MSPPOH is a non-specific CYP epoxygenase inhibitor and can inhibit other P450 enzymes as well as CYP2J2 which may lead to non-target effects. CYP2C9 a CYP epoxygenase present in human cardiomyocytes and endothelial cells can metabolise AA to EETs. However, it has also been shown to have several detrimental effects through increasing ROS leading to oxidative stress and DNA damage. Inhibition of these pathways may account for the protective effect of MSPPOH.

Inhibition of CYP2J2 by MSPPOH in combination with a toxic dose of astemizole led to an increase in ATP compared to cells treated with astemizole alone. MSPPOH is a non-specific CYP epoxygenase inhibitor and can inhibit other P450 enzymes which may lead to non-target effects. For example CYP2C9 a CYP epoxygenase present in human cardiomyocytes and endothelial cells has the ability to metabolise AA to both EETs and 20-HETE. EETs and 20-HETE have contrasting effects on a variety of pathways. For example EETs are endothelial cell derived hypolarising factors increasing vasodilation and contributing to endothelial cell function, however 20-HETE

has been shown to be a potent vasoconstrictor. 20 HETE has also shown to contribute to vascular inflammation, oxidative stress and ischaemia-reperfusion injury all of which contrast with the known cardioprotective effects of EETs (Hoopes et al., 2015, Roman, 2002). Through this balance in EETs and HETEs, AA metabolites may modulate cardiovascular disease and cardiotoxicity (J. Imig, 2016).

Further investigation into identification and quantification of the different AA metabolites involved in the EET pathway and with a potential role in regulating toxicity *in vitro* may give an insight into how EETs and other AA metabolites may work to modulate drug-induced toxicity. Through lipidomics, isoforms of EETs and their deactivated metabolite DHETs as well as the known hydroxylated AA metabolite 20-HETE may be measured at baseline and after treatment with astemizole and/or inhibitors. Previous studies into lipidomics have found changes in the productions of specific isoforms of EETs as well as changes in the ratio of EETs to 20-HETE in both cardiovascular disease and in cardiotoxicity. Evaluation of P450-derived eicosanoids in patients with coronary artery disease showed elevated levels of EETs, versus healthy controls. However certain subsets were found to have decreased levels of EETs including those who were obese, were elderly and those who smoked. However no changes in 20-HETE were seen in all groups (Theken et al., 2012). With regards to drugs, studies into the known cardiotoxic drug fluconazole and the anti-oxidant drug resveratrol found that flucanazole inhibited the production of 8,9-, and 14,15-EET as well as 11,12 and 15-HETE with an IC₅₀ of 27, 28, 28 and 36µM respectively. In contrast the anti-oxidant drug resveratrol which has previously shown to protect in heart disease inhibited hepatic CYP4 enzymes, responsible for producing 20-HETE thus decreasing 20-HETE production (El-Sherbeni and El-Kadi, 2016). Furthermore, analysis of AA metabolites in rats with dox induced cardiotoxicity, showed a difference in EET and 20-HETE production compared to controls. Chronic dox toxicity induced gene expression of CYP4 enzymes and the sEH which was followed by an increase in 20-HETE and reduction in EETs thus suggesting an imbalance between the cardio protective EET and cardiotoxic 20-HETE pathway (Alsaad et al., 2012).

In addition, other fatty acid derivatives such as omega 3 fatty acid metabolites eicosapentaenoic acid (EPA) and docosahexaenoic acid (DHA) have been shown to share many of the protective effects of EETs and a protective role in the cardiovascular system in both experimental models and clinical trials has been demonstrated. In animal

models of cardiovascular disease, omega 3 derivatives have been found to protect against vascular inflammation (Nodari et al., 2011), atherosclerosis (Reed, 2008) and arrhythmias (Mozaffarian and Wu, 2011). The mechanism of protection is still largely unknown. However, it may be feasible to suggest that other fatty acids may be responsible for a protective effect in the astemizole induced toxicity (Figure 4.13).

In addition, to determine whether the protective effects of t-AUCB (sEH inhibitor) and exogenous 11,12-EET in EA.hy926 cells and HCM may be through the EET pathway, cells may also be incubated with the 14,15-EEZE EET receptor antagonist. 14,15-EEZE was shown to abolish the protective effects of exogenous 14,15-EET on endoplasmic reticulum stress in H9C2 cells (X. Wang et al., 2014). In a dog myocardial infarction model, 14,15-EEZE reversed the protective effect of 11,12-EET and 14,15-EET on infarct size (Gross et al., 2008) and so therefore would block any protective effects modulated specifically by EETs *in vitro* in astemizole toxicity.

It may also be pertinent to use the main metabolite of astemizole, o-desmethyl astemizole to deduce whether conversion of astemizole to its metabolite by CYP2J2 may modulate toxicity. Studies have shown there is no difference in toxicity between astemizole and o-desmethyl astemizole when measuring hERG channel inhibition (Z. Zhou et al., 1999), however the toxic effect of the metabolite on cell death *in vitro* in a different cell system may show contrasting results. If o-desmethyl astemizole is less toxic *in vitro* than astemizole then any protective effects seen in cells may be from the metabolism of astemizole by CYP2J2 to a less toxic product rather than through a potential increase in EETs.

Furthermore, in this study astemizole was the main drug investigated, however it may be useful to investigate other cardiotoxic drugs with different modes of cardiotoxicity to examine whether increasing EETs may protect against their toxic effects.

Chapter 5 **Investigating the molecular mechanism of EET
protection against astemizole induced toxicity**

5.1 Background

Soluble epoxide hydrolase (sEH) belongs to a family of enzymes which convert epoxides such as epoxyeicosatrienoic acids (EETs) to their hydrolysed derivatives i.e DHETs. Its structure consists of a C-terminal epoxide hydrolase domain that metabolises endogenous substrates such as EETs and an N-terminal phosphatase domain which is responsible for phosphorylating lipid metabolites such as cholesterol precursors (Sura et al., 2008). This enzyme is found in most tissues including liver, kidney, cardiovascular system and GI tract (Enayetallah et al., 2004). In addition, expression has been studied in the human brain where distribution of sEH was found mainly in the astrocytes, oligodendrocytes and vascular smooth muscle of arterioles (Sura et al., 2008).

EETs have been shown to have protective effects against the pathogenesis of cardiovascular disease and cardiotoxicity in experimental models (Gross and Nithipatikom, 2009). One of the major ways the EET pathway may be manipulated to increase EETs is to inhibit or knockdown the primary deactivator of EETs within cells, sEH. Pharmacological inhibitors such as t-AUCB and AUDA are commonly used to assess the protective effect of EETs in both *in vitro* and *ex vivo* models of myocardial infarction, ischaemia reperfusion injury and cardiac hypertrophy (Gui et al., 2017, Merkel et al., 2009, Gross and Nithipatikom, 2009).

In a sEH null mouse model of hypoxia reperfusion injury, sEH null mice had an improved recovery of left ventricle developed pressure (LVDP) and less infarction compared to wild type hearts after 20mins ischaemia. This protective effect was nullified with pre-treatment of the EET receptor antagonist 14,15-epoxyeicosa-5 (Z)-enoic acid (14,15-EEZE). Inhibitors of the phosphoinositide-3-kinase (PI3K) also inhibited the cardio-protective effect seen with sEH null mice suggesting the EETs may protect through the PI3K pathway (J. M. Seubert et al., 2006). In addition, other studies have shown the role of STAT3 in EET protection. Treatment of isolated cardiomyocytes from mice that had undergone hypoxia and reperfusion with 14,15-EET conferred cytoprotection from ischemia which was abolished by pharmacological inhibition of STAT3 and gene knockdown with siRNA (Merkel et al., 2009).

In addition to gene knockdown studies with pharmacological inhibition have shown similar cytoprotective and cardioprotective effects. For example, the sEH inhibitor AUDA reduced infarct size in a dog model of MI and a strengthened protective effect was observed when given in combination with exogenous 14,15-EET. These effects were replicated in mice where administration of the sEH inhibitor t-AUCB over 7 days before MI improved cardiac function and prevented development of arrhythmias compared to untreated mice (Gui et al., 2017). Furthermore, in mice with pressure overload-induced left ventricular hypertrophy, administration of the sEH inhibitors AEPU and AUDA prevented development or reversed established left-ventricular hypertrophy through the inhibition of NF- κ B (Gross and Nithipatikom, 2009). The cardioprotective effects of these inhibitors suggest the usefulness of sEH as a therapeutic target in cardiovascular disease and its potential in cardiotoxicity to combat the effects of cardiotoxic drugs.

5.2 Aims

Results in the previous chapter suggested that sEH inhibition protected against astemizole-induced cytotoxicity in both EA.hy926 cells and human cardiac myocytes. In order to further investigate possible mechanisms, the aims of the work presented in this chapter were:

1. To investigate gene expression (mRNA and protein) of sEH in the EA.hy926 endothelial cell line and human cardiac myocytes.
2. To understand the role of sEH protein in astemizole toxicity through *in vitro* knockdown.

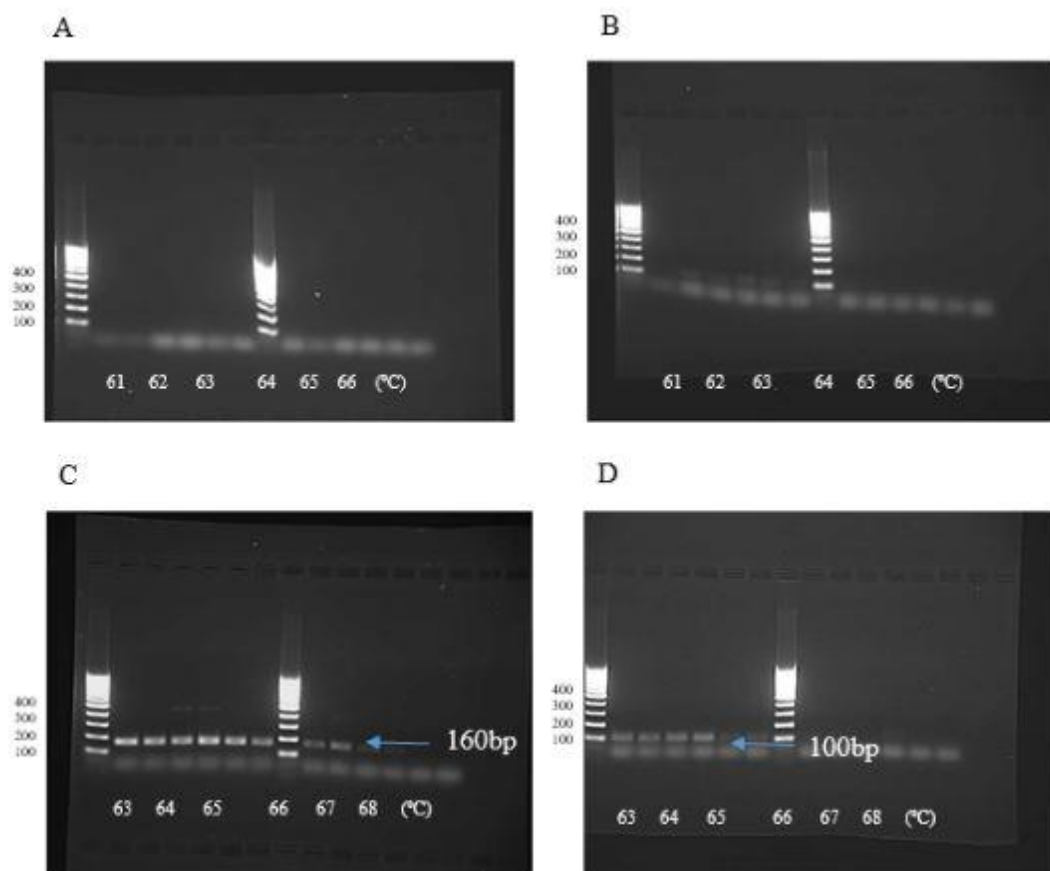
5.3 Results

5.3.1 Expression of sEH in EA.hy926 and the human cardiac myocyte cell line

5.3.1.1 Development of pcr assays for sEH mRNA expression

To conduct gene expression analysis of sEH, firstly primers were designed that were specific to this gene. From the NCBI database it was found that sEH had four variants so primers were designed that would bind to each of these as well as pan specific primers which would potentially bind to all/any sEH mRNA.

After pooling cDNA from both EA.hy926 and HCM, variants 1 and 4 gave significant amplification with the best annealing at the lower temperatures of 65-67°C. It was however further found that variants 2 and 4 had exactly the same gene sequence (<https://www.ncbi.nlm.nih.gov/gene/2053>) which may be why isoform 4 has other bands (figure 5.1).



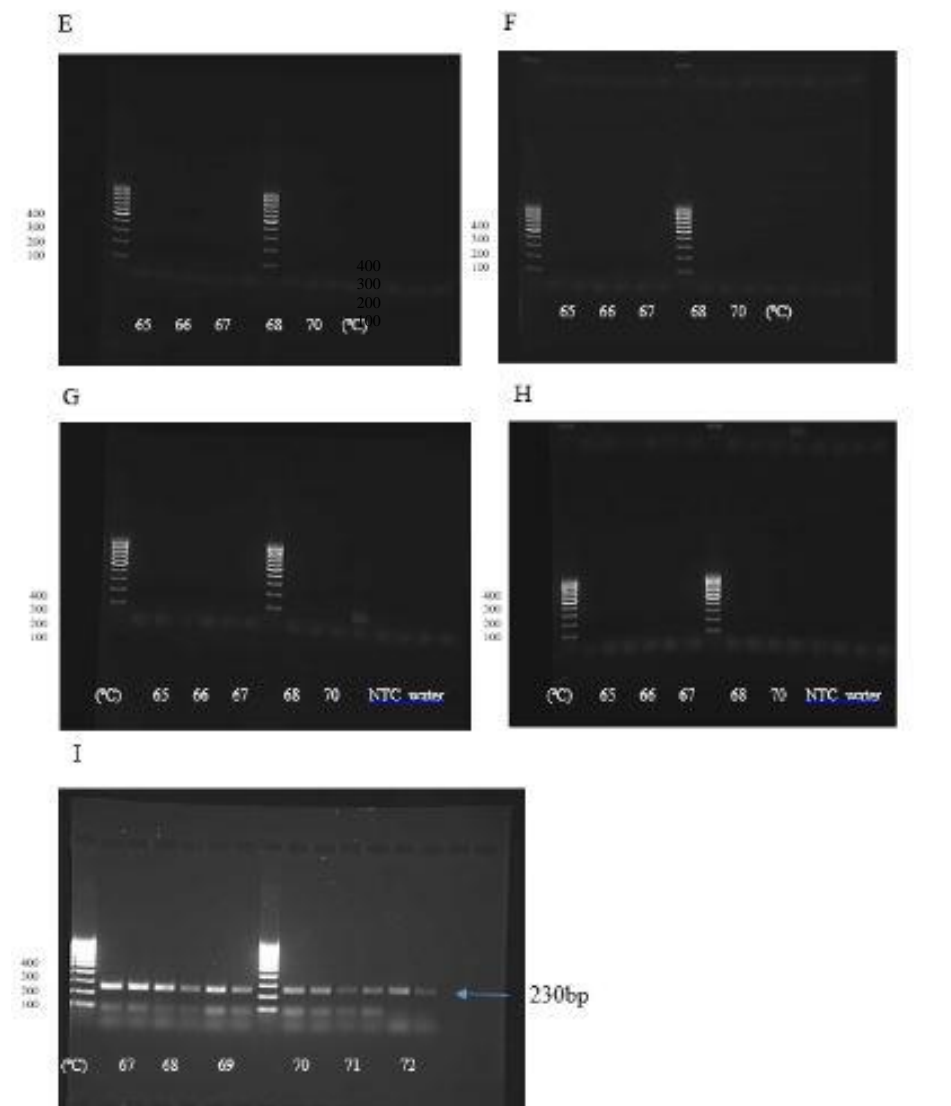


Figure 5-1. PCR products were amplified using gradient gel PCR as described in section 3.3.4.

Primers were validated and the best annealing temperature was ascertained. Primers were pan specific primers (A,B), sEH variant 1 (C,D), sEH variant 2 (E,F), sEH variant 3 (G,H) and sEH variant 4 (I). Combinations are as follows: A=#1,B=#2,C=#3,D=#4,E=#5,F=#6,G=#7, H=#8,I=#9. Different sets of primers were designed to each gene. Each gel represents a different primer combination. Primers were designed for sEH pan specific and transcript variants 1-4. A 100bp ladder was used to estimate size of PCR products.

Concomitantly, primers were designed to five housekeepers and validated with gel PCR. All PCR products were detected except for TABP (figure 5.2E) where only faint bands were seen. These primers would be used alongside the gene of interest primer for SYBR green qPCR (figure 5.2).

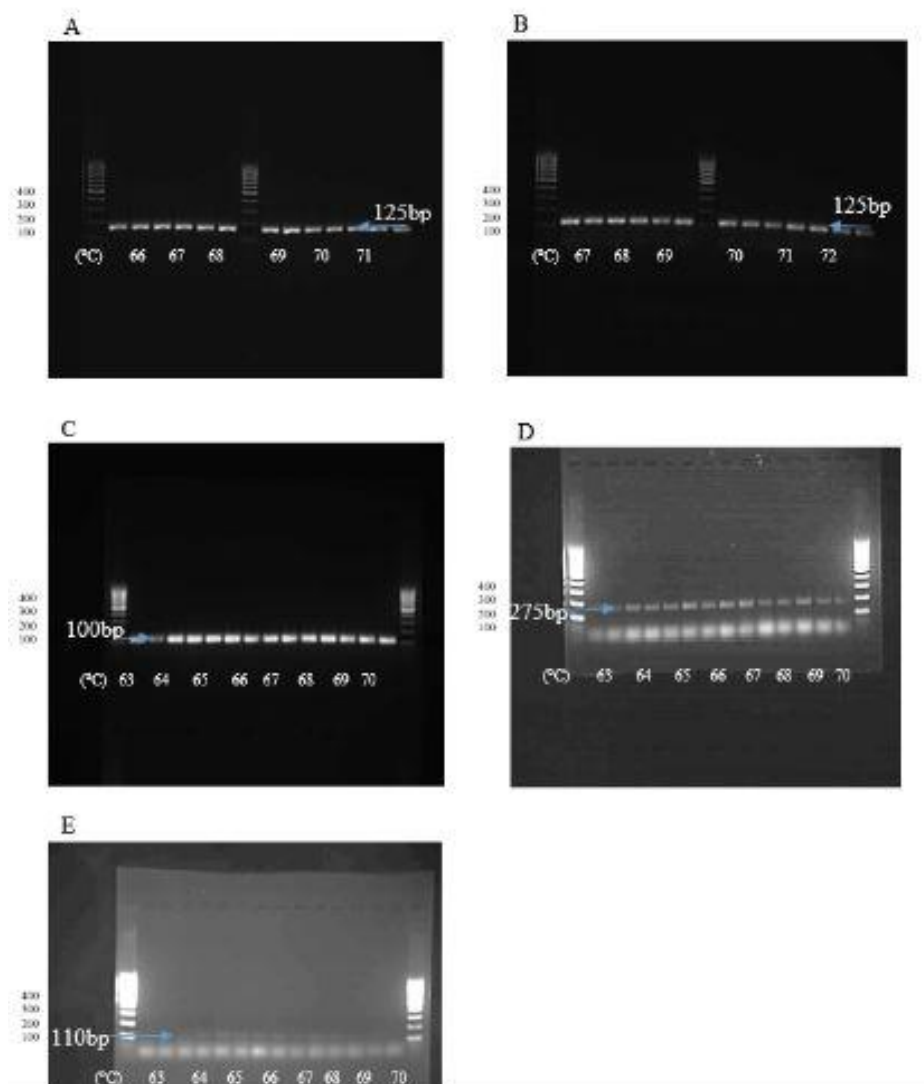


Figure 5-2 Validation of primers designed to housekeepers using gradient gel PCR.

(A) GAPDH, (B) β -actin, (C) β -microglobulin, (D) B tubulin and (E) Tata binding protein (TBP). RT-PCR was carried out as described in section 3.3.4. A temperature gradient between 60-71°C used to determine the appropriate annealing temperature for each housekeeper. Different sets of primers were designed to each gene. Each gel represents a different primer combination. A 100bp ladder was used to estimate size of PCR products.

After primers were validated using gel PCR, SYBR green PCR was undertaken using the sEH primer pair for sEH transcript 1 as this had previously given the strongest signal. Initially, all housekeepers tested earlier were used except for TABP due to lack of signal during gel PCR. In addition to housekeeping controls, water and non-template controls were used to make sure there was no interference from reagents and the sEH signal was a true representation of gene expression. To validate housekeepers the CT values were analysed to make sure they did not change significantly between cell types. Furthermore, the melt curves were observed to make sure there were no primer dimers. From these distinguishing markers β actin and $\beta 2$ microglobulin were found to be the best housekeepers for normalisation against the gene of interest. Human cardiac myocytes were found to have ~4 times more baseline expression of sEH compared to EA.hy926 cells (figure 5.3).

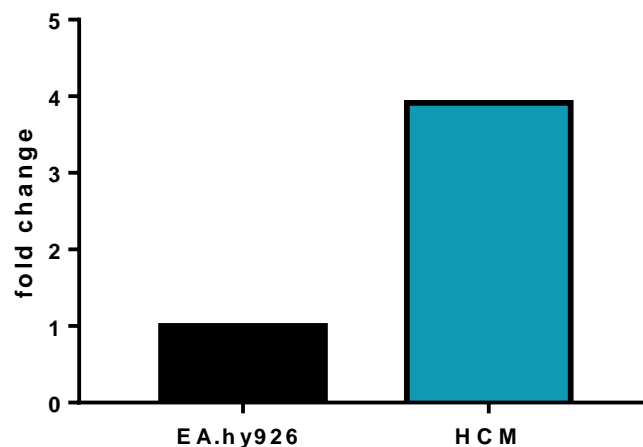


Figure 5-3 Expression of sEH mRNA in EA.hy926 cells and HCM as determined by qPCR with SYBR green detection.

EA.hy926 cells and HCM were grown to 80% confluence after which they were lysed for PCR using β actin and $\beta 2$ microglobulin as housekeeper genes. All data (mean and SEM of 3 replicates) was expressed as fold change $\Delta\Delta CT$ values.

5.3.2 Effect of astemizole on sEH mRNA and protein expression

Next, cells were treated with a ‘non-toxic’ dose of astemizole (25 μ M) for 6 and 24 hrs to observe changes in sEH expression. In EA.hy926 cells there was an initial increase in expression compared to untreated control at 6hrs. However over 24hrs this expression decreased to lower than control. In HCM there a drastic reduction in gene expression of sEH over 6 and 24 hrs (figure 5.4).

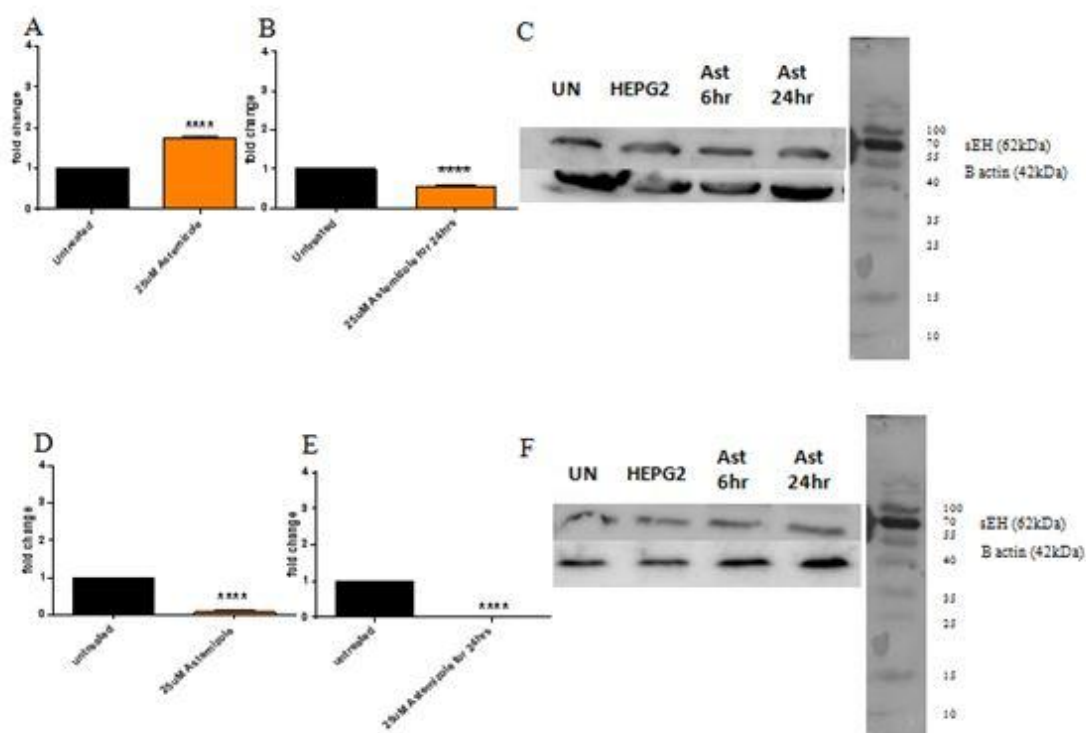


Figure 5-4 Gene expression of sEH in EA.hy926 cells (A,B) and HCM (D,E) after treatment with 25 μ M astemizole for 6h (A,D) and 24h (B,E).

EA.hy926 cells and HCM were grown to 80% confluence after which they were treated with 25 μ M astemizole for 6 and 24hrs. Cells were then lysed for PCR using β actin and $\beta 2$ microglobulin as housekeeper genes. All data (mean and SEM of 5 replicates) was expressed as fold change $\Delta\Delta$ CT values. DMSO was kept at a final concentration of dilution of 0.001%. Western blot protein expression of sEH in EA.hy926 cells (E) and HCM (F) ****P< 0.0001. Western blot protein expression of sEH in EA.hy926 cells (C) and HCM (F).

When examining protein concentrations of sEH after astemizole treatment, there was little fluctuation of protein compared to untreated control suggesting the decrease in expression of the gene was not translated to protein expression.

5.3.3 Effect of sEH and CYP epoxygenase inhibition on sEH mRNA and protein expression

To understand the mechanism by which the EET pathway may be eliciting cytoprotection against astemizole toxicity, EA.hy926 cells and HCM were incubated with 25 μ M astemizole and either the CYP epoxygenase inhibitor (MSSPOH) or the sEH inhibitor (t-AUCB).

Compared to untreated control there was an increase in sEH gene expression in EA.hy926 cells and a decrease in expression in HCM as seen in figure 5.5. When cells were treated with the CYP2J2 inhibitor MSSPOH there was no significant change in expression compared to untreated cells. However cells treated with both astemizole and MSSPOH showed a conservation of expression of sEH and opposed the increase in sEH seen with astemizole alone.

Similarly, when human cardiac myocytes were treated with both astemizole and MSSPOH, sEH expression resembled that of untreated cells. Added treatment with MSSPOH opposed the reduction in sEH expression seen in cells treated with astemizole alone. With regards to treatment with sEH inhibitor t-AUCB alone, expression of sEH did not change in either EA.hy926 cells or HCM. In EA.hy926 cells treatment with both t-AUCB and astemizole slightly reversed the increase in sEH expression seen in cells treated with astemizole alone. However, expression was still higher than both untreated control and cells with inhibitor alone. Likewise in HCM, t-AUCB maintained expression of sEH and countered the effect of astemizole. Taken together the data on t-AUCB and MSSPOH suggest that these compounds counter the effects of astemizole on sEH mRNA expression (figure 5.5A-D). Possible reasons for these findings are discussed in the discussion section 5.4.

Protein expression showed little change in expression of sEH in treatments compared with untreated cells and positive HepG2 control and normalised to β actin control indicating that although there were changes in mRNA expression, these were not

translated to protein expression (figure 5.5E,F). These effects and possible explanations are further discussed below.

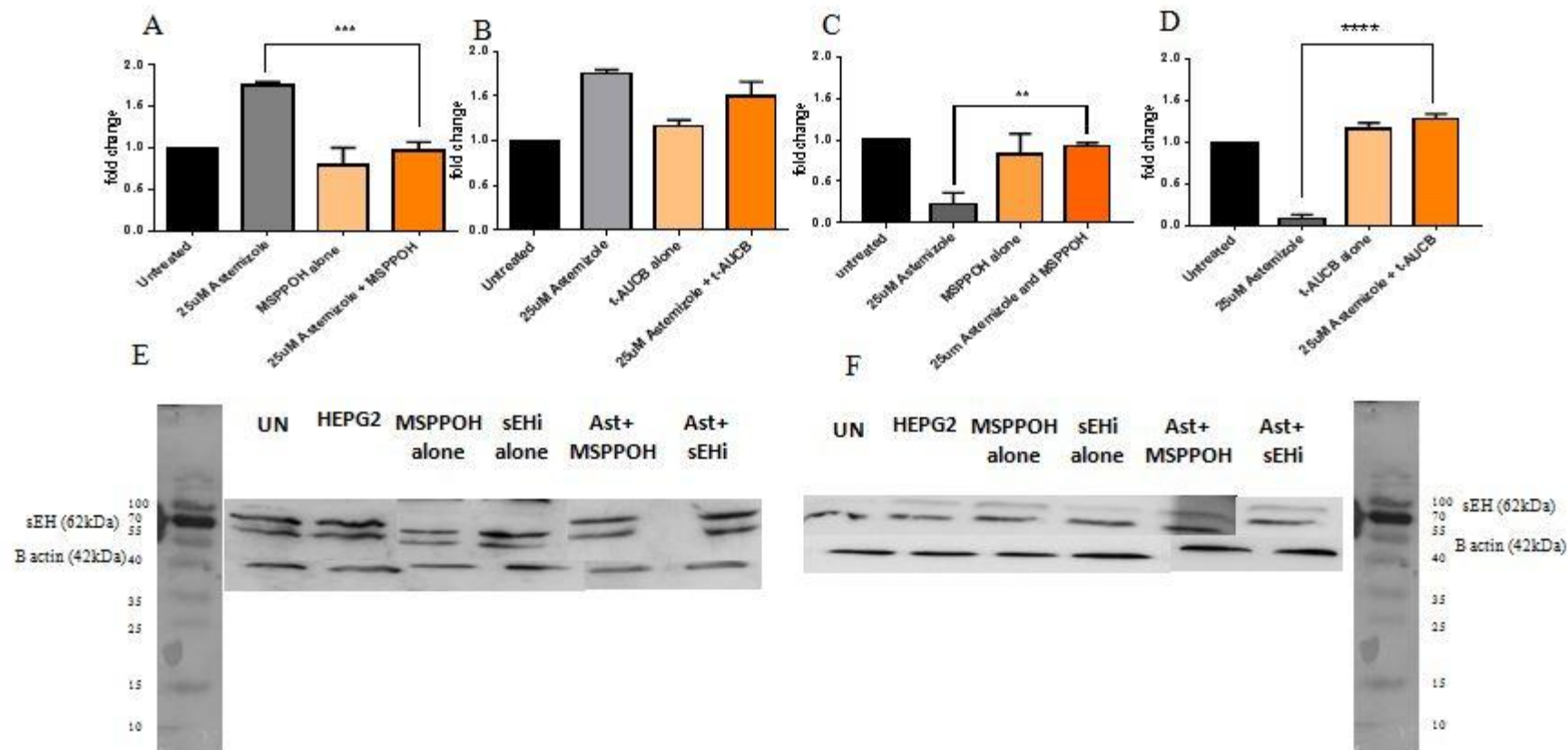


Figure 5-5 Expression of sEH in EA.hy926 cells (A and B) and human cardiac myocytes (HCM) (C and D) after treatment with 25 μ M astemizole and/or inhibitors for 6 hr.

EA.hy926 cells and HCM were grown to 80% confluence after which they were treated with 25 μ M astemizole and/or CYP epoxygenase MSPPOH (12.5 μ M) and SEH inhibitor t-AUCB (100 μ M) for 6hrs. Cells were then lysed for PCR using β actin and β 2 microglobulin as housekeeper genes. All data (mean and SEM of 5 replicates) was expressed as fold change $\Delta\Delta$ CT values. DMSO was kept at a final concentration of dilution of 0.001%. Western blot protein expression of sEH in EA.hy926 cells (E) and HCM (F) with the presence or absence of sEHi (t-AUCB) or CYP epoxygenase inhibitor (MSPPOH). **P=0.036, ***P=0.005, ****P<0.0001.

5.3.4 Effect of sEH knockdown on astemizole-induced cytotoxicity in EA.hy926 cells

To investigate the role of sEH in astemizole toxicity, an *in vitro* knockdown model was established in EA.hy926 cells. Initially, lipofectamine reagent was used for delivery of sEH siRNA into cells. In addition to cells treated with siRNA, multiple controls were used including untreated cells, cells treated with lipofectamine and opti-mem media, a negative scrambled control and a cell death control. Gene expression studies with qPCR showed a decrease in expression of sEH by sEH siRNA at gene level compared to the negative scrambled control (figure 5.6A). This was also reproduced at the transcriptional level with a decrease in the sEH protein (figure 5.6B). There was also a reduction in sEH expression when cells were treated with lipofectamine and opti-mem media or with a negative scrambled control alone.

To investigate how *in vitro* knockdown of sEH may affect astemizole induced cell death, cellular ATP was measured after knocked down cells were treated with 25 μ M astemizole and/or inhibitors of CYP2J2 or sEH for 6 hr. Data was normalised to the negative scrambled siRNA control for each treatment. There was no significant change in ATP across all treatments when sEH was knocked down compared with no knockdown (figure 5.7) indicating sEH protein/activity may still be present.

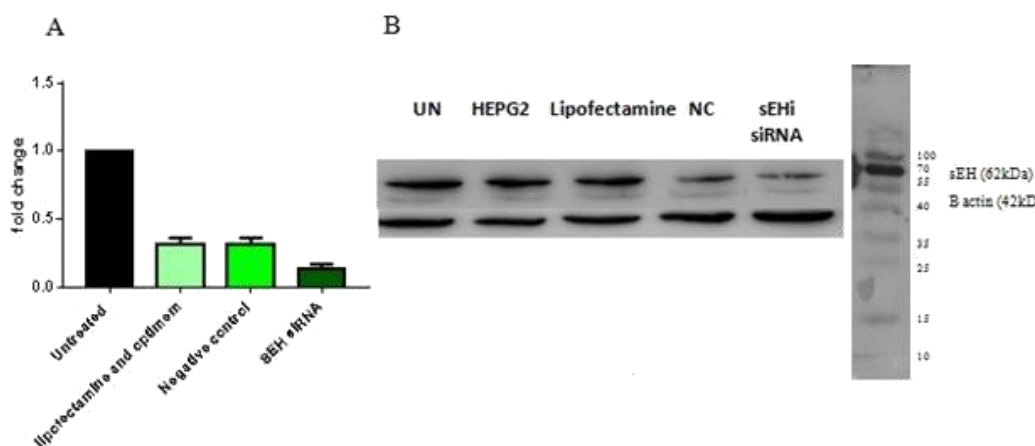


Figure 5-6 sEH gene and protein expression via RT-PCR and western blot in EA.hy926 cells.

EA.hy926 cells were cultured to 80% confluence and treated with 10nM sEH siRNA and RNAi-max Lipofectamine for 24hr after which the media was changed. In total, cells were incubated for 3 days before being lysed for PCR or western blot. Results were normalised to untreated cells (A). Values are the mean and SEM of 3 experiments expressed as fold change $\Delta\Delta$ CT values. (B) Western blot protein expression of sEH in EA.hy926 cells detected using rabbit polyclonal antibody.

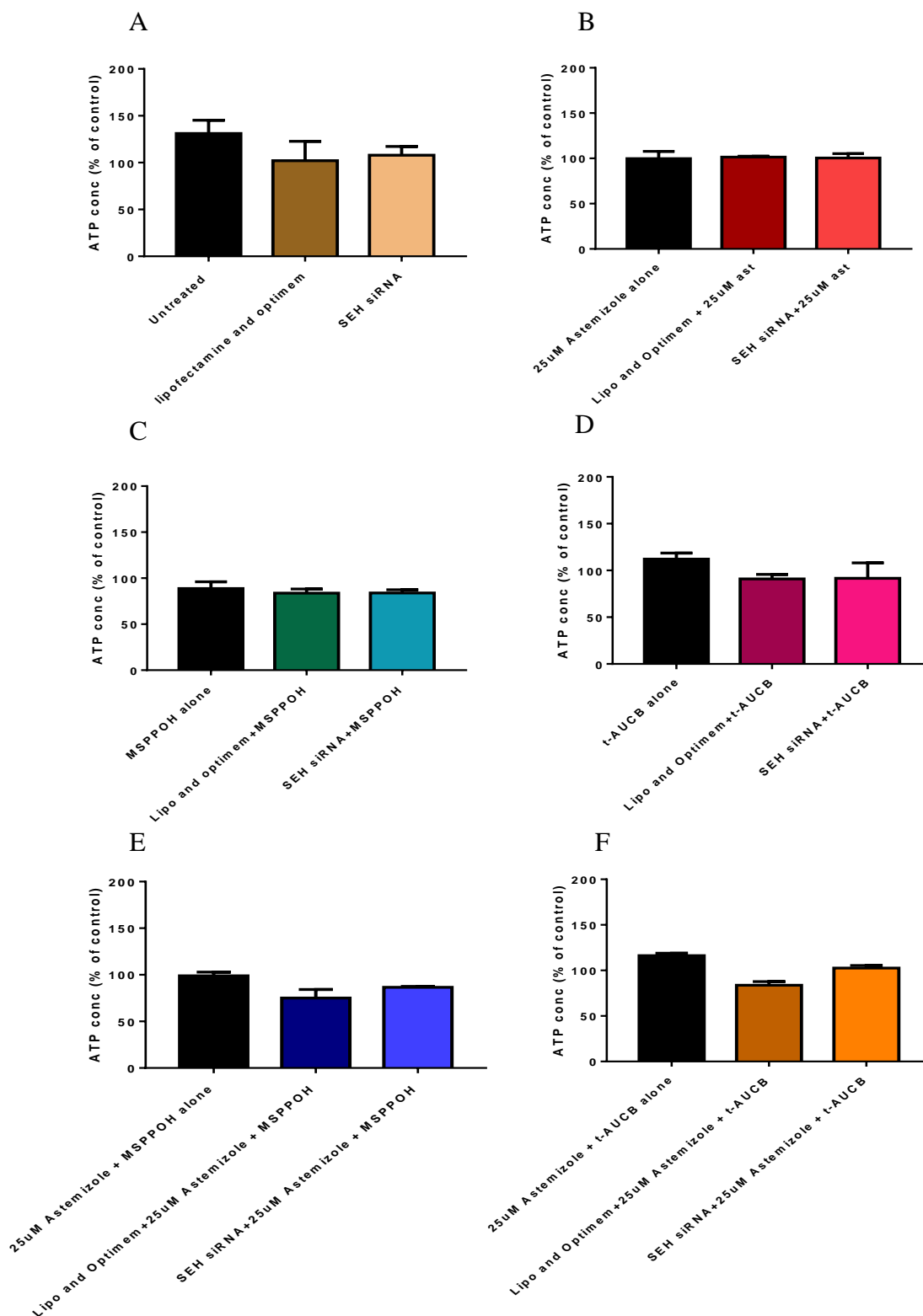


Figure 5-7 Effect of sEH knockdown and sEH and CYP2J2 inhibitor on astemizole induced cytotoxicity.

EA.hy926 cells were cultured and treated with 10nM sEH siRNA and RNAimax Lipofectamine for 24hr after which the media was changed. Knockdown cells were then treated in the following way: (A) untreated, (B) 25µM astemizole, (C) 12.5µM MSPPOH alone, (D) 100µM t-AUCB alone, (E) 25µM astemizole and MSPPOH and (F) 25µM astemizole and t-AUCB. DMSO was kept at a final concentration of dilution of 0.001%. ATP content was used a surrogate marker of cell viability and values are the mean+SEM of 3 experiments normalised to the treated scrambled oligo control.

5.4 Discussion

Initial analysis of gene expression of sEH with agarose gel PCR showed the different isoforms of sEH with isoform 1 having predominant expression, this was a novel finding as isoforms of sEH had not been identified in these cells with PCR before. It is unknown how these proteins contribute to the overall sEH activity *in vitro* and *in vivo* and thus how these other isoforms may affect toxicity.

SYBR green qPCR was used to quantify sEH gene expression which was normalised to at least two housekeepers. To investigate the most appropriate housekeepers to use for each treatment, a housekeeper screen was done with 5 housekeepers. A programme, NormFinder was then used which contained an algorithm to identify the CT values which showed the least change in response to a treatment. From this analysis β -actin and β 2 microglobulin were used in combination (table 5.8).

Table 5-8 Normfinder analysis of CT values from a housekeeper screen investigating changes in sEH expression with the treatment of astemizole in EA.hy926 cells.

RNA was extracted from EA.hy926 cells treated with astemizole for 6hrs and used for qPCR along with housekeepers for 5 genes, VCP-1, β -actin, β 2 microglobulin, 36B4 and PSMB4. The CT values were extracted and NormFinder was used to generate a stability value in response to the treatment. VCP-1 Valocin-containing protein-1; 36B4 Acidic ribosomal phosphoprotein P0; PSMB4 Proteasome subunit beta type-4.

| Gene name | Stability value | Best gene | B2 MICRO |
|-----------|-----------------|--|----------------|
| VCP-1 | 0.226 | Stability value | 0.062 |
| B | | | |
| ACTIN | 0.114 | | |
| B2 | | | B ACTIN and B2 |
| MICRO | 0.062 | Best combination of two genes | MICRO |
| | | Stability value for best combination of two genes | |
| 36B4 | 0.128 | | 0.052 |
| PSMB4 | 0.082 | | |

When investigating sEH protein expression in HCM and EA.hy926 cells a positive control was needed which would allow a validation of the Western blot and also show a comparison of protein expression between different cell types. HepG2 cells were easily obtainable and had previously been shown to constitutively express sEH (Garscha et al., 2017) making them a suitable cell type as a positive control.

Expression analysis of sEH in HCM and EA.hy926 cells showed gene expression was ~ 4 times higher in cardiac cells. Although expression of sEH has been documented in both cardiac cells and vasculature, there is little evidence for comparison of expression between different cell types. sEH expression has been found in aorta, coronary artery (Xie et al., 2016), and mesenteric artery in rodents and has been shown to be upregulated in response to external agents (Zhao et al., 2005). Treatment of HCM with 25 μ M astemizole reduced gene expression of sEH at 6hr and 24hr. In EA.hy926 cells however there was an initial increase in expression at 6hr followed by reduced expression at 24hr. These differences between cell types may be due to the baseline gene expression of sEH which was higher in HCM than in EA.hy926. In section 6.3.2 higher CYP2J2 gene expression was also seen in HCM compared to EA.hy926 cells which could indicate the importance of the CYP2J2/EET pathway in this cell type compared to endothelial cells. Previously, the sEH gene was shown to be upregulated in response to the anti-cancer drug tamoxifen in rat mesenteric artery (Mark-Kappeler et al., 2011) and in endothelial cells of the aorta of mice in response to tobacco smoke (Maresh et al., 2005). Furthermore, a link between sEH gene expression and NOS production in endothelial cells was established indicating there may be a role for sEH in regulating vascular tone in vasculature (Nayeem et al., 2011). In the heart, sEH was expressed in atrial and ventricular tissues of rodents and was found to be upregulated in cardiac hypertrophy and in response to toxic drugs including doxorubicin and arsenic (Anwar-Mohamed et al., 2012, Alsaad et al., 2012). This suggests sEH may be involved in cardiovascular toxicity and cardiovascular disease possibly through increasing the deactivation of EETs to DHETs. However, there are cases where cardiovascular pathology did not result in increases in sEH expression. For example, there was no change in protein expression in a mouse model of myocardial infarction (Li et al., 2009) and there was no change in mRNA in a rat chronic heart failure model (Merabet et al.,

2012) suggesting there may be other pathways that predominate in cardiovascular pathologies over the CYP2J2/EET pathway.

When cells were treated with a combination of astemizole and either MSPPOH or t-AUCB both cell types showed differences in expression profiles. In HCM where there was a reduction in sEH expression when cells were treated with astemizole, incubation with both astemizole and MSPPOH or t-AUCB increased sEH expression levels back to control levels. In EA.hy926 cells however the same treatment did the opposite, reducing sEH expression closer to vehicle control levels. This suggests that inhibiting CYP2J2 or sEH does affect sEH expression and may be involved in homeostatically regulating sEH expression providing further evidence that these genes may be linked.

In addition to pharmacological inhibition, sEH siRNA was used to knock down the *EPHX2* gene to further investigate the role of sEH in toxicity. A negative scrambled control and a cell death control was added to each cell plate to make sure transfection was efficient. The cell death control showed dead, floating cells after the 3 day incubation with siRNA indicating cells had taken up the siRNA (figure 5.9). Although gene and protein expression were reduced there was still some detectable sEH protein. This may be the result of not enough siRNA being transported into the cell. The cells were incubated with siRNA for 3 days, however this may not be enough to fully transfect the cells. On the other hand incubation for too long with siRNA and lipofectamine may be toxic to cells and the inhibitory effect of siRNA may also subside. Studies in adipocytes incubated with sEH siRNA for two days did show changes in lipid droplet size compared to untreated cells however, validation of knockdown with PCR was not shown (L. Liu et al., 2018). Transfection of H9c2 cells with *EPHX2* siRNA for 24 hr was shown to knockdown the gene by 50% as indicated by real-time PCR (Anwar-Mohamed et al., 2012) which when incubated in combination with arsenic trioxide further reduced sEH RNA by 62% compared to toxic drug alone. However, although ~50% gene knockdown was observed with this sEH siRNA compared to negative control, later experiments incubating EA.hy926 knockdown cells with astemizole for 6hr showed no difference in ATP. This suggests other endpoints such as PCR may be needed to fully understand the effect knockdown may be having on expression of sEH. In addition, other forms of siRNA delivery may increase the efficiency of delivery of siRNA into cells. Electroporation experiments with sEH

siRNA in the prostate cancer cell line 22RV1 cells in vitro showed 75% of cells were successfully transfected from GFP expression (Wolf, N et al 2016).

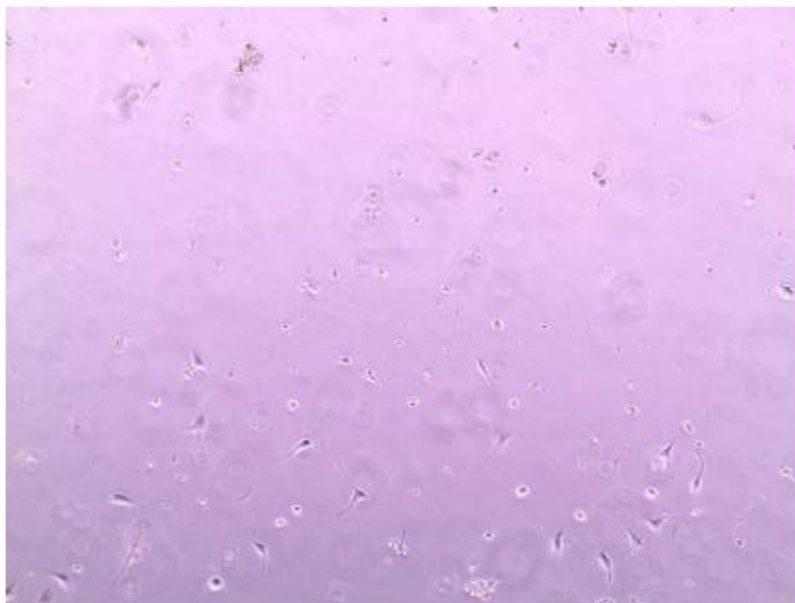


Figure 5-9 EA.hy926 cells treated with cell death siRNA after 3 days. X100 magnification.

EA.hy926 cells were cultured to 80-90% confluence and treated with 10nM AllStars Hs cell death control siRNA and RNAimax lipofectamine for 24hrs after which the media was replaced with normal cell culture media for 48hrs. Images were taken with brightfield microscopy.

Future work investigating sEH expression in other cells other than heart such as primary endothelial cells, smooth muscle cells and fibroblasts may be beneficial to understand the localisation of sEH in the heart as well as characterising the different isoforms of sEH with PCR and protein expression.

To further investigate the role of the sEH and EETs on astemizole toxicity, treatment of cells with exogenous EETs or with exogenous AA in combination with astemizole may show how increasing EETs through different means could have varying levels of protection against astemizole toxicity. Furthermore, the EET inhibitor 14,15-EEZE may elucidate a feedback mechanism between EETs and sEH expression where inhibiting EETs directly may have an opposing effect to balance the concentration of EETs.

Chapter 6 **Investigating the possible role of cytochrome P450 2J2 in
astemizole induced cytotoxicity**

6.1 Background

The CYP2J2 gene is expressed in humans and contains nine exons and eight introns; it is approximately 40.4 kb long and encodes for a protein of 58 kDa (King et al., 2002). The mRNA expression of CYP2J2 in humans is mainly confined to the cardiovascular system and liver, with predominant expression in the right ventricle of the heart (Michaud et al., 2010). Within the heart, CYP2J2 is the predominant P450 isoenzyme expressed in cardiomyocytes and human heart tissue (Evangelista et al., 2013). In addition to cardiomyocytes, CYP2J2 expression has also been observed in other cardiovascular cells. CYP2J2 is expressed in endothelial cells in a variety of vascular beds including coronary artery, aorta (Delozier et al., 2007) and in varicose veins (Bertrand-Thiebault et al., 2004). The presence of CYP2J2 in the heart leads to the hypothesis that CYP2J2 could contribute to endogenous tissue function and to cardiotoxicity through drug metabolism as well as protective effects through the formation of EETs.

CYP2J2 has been shown to possess both endogenous and exogenous activities, mediating drug biotransformation reactions with a number of exogenous substances. CYP2J2 has been shown to be the primary enzyme involved in several metabolic reactions including amiodarone 4-hydroxylation, astemizole o-demethylation and ebastine hydroxylation (Matsumoto et al., 2002, Matsumoto and Yamazoe, 2001, K. H. Liu et al., 2006). For ebastine, CYP2J2 plays a superior role in first-pass intestinal metabolism to its pharmacologically active metabolite and less toxic carebastine. The biological role of CYP2J2 appears to relate primarily to its metabolism of arachidonic acid (AA) to cardio-protective epoxyeicosatrienoic acids (EETs). However, it has been proposed that a complex interplay between EET synthesis and drug metabolism by CYP2J2 exists. Indeed Matsumoto et al (2002) showed that CYP2J2 substrates arachidonic acid (AA) and ebastine significantly inhibited astemizole o-demethylation in human small intestine and *in vitro* for recombinant CYP2J2 (Matsumoto et al., 2002) suggesting a protective mechanism of EET production predominates over toxic drug metabolism. However, Arnold et al (2017) found that through molecular dynamics simulations doxorubicin (dox) can prevent the binding of AA to CYP2J2 in a competitive way through binding to the active site (Arnold et al., 2017), thus reducing EET production indicating some drugs have more EET inhibitory potential than others.

It is likely that EET synthesis largely protects the cardiovascular system. Indeed disease states and toxicity have been shown to alter the expression of CYP2J2. For example, treatment of human cardiomyocytes with reactive oxygen species (ROS) or dox, a potent ROS stimulator, upregulated CYP2J2 expression (Evangelista et al., 2018). In addition, overexpression of CYP2J2 in experimental models has been shown to protect against cardiovascular disease. In a mouse model of ischaemia-reperfusion injury, cardiac specific expression of CYP2J2 in transgenic mice improved left ventricular functional recovery, however this protective effect was not seen in a mouse model of endothelial cell specific CYP2J2 expression indicating cardiomyocytes are the main driving force in cardioprotection through EETs (Edin et al., 2011). Furthermore, in an atherosclerosis prone apolipoprotein E-deficient mouse model CYP2J2 gene over expression deterred the development of high-fat diet induced atherosclerosis (W. Liu et al., 2016). Hypertrophy and subsequent arrhythmias are also a part of the pathogenesis of cardiovascular disease. Overexpression of CYP2J2 prevented cardiac hypertrophy in a mouse model of hypertension and the authors proposed that this protective effect was through EETs acting through downstream signalling pathways reducing NF- κ B via PPAR- γ or AMPK α 2 activation (B. Wang et al., 2016). CYP2J2 transgenic mice also had shorter action potential durations than wild type mice, however this was reversed with exposure to the CYP epoxygenase inhibitor MSPPOH (Ke et al., 2007).

Although, there are many studies involving CYP2J2 overexpression there has been little investigation into the effect of CYP2J2 downregulation on toxicity. Preliminary, *in vitro* studies in human cardiomyocytes treated with CYP2J2 silencer siRNA showed their increased susceptibility to dox compared to non-silenced cells (Evangelista et al., 2018). This indicates CYP2J2 is directly involved in modulating stresses to the heart for example during ischaemia or toxicity. It has been shown that the role of CYP2J2 in cardioprotection is due to EET production, however further study is needed to investigate signalling mechanisms which are still poorly understood.

6.2 Aims

Based on previous findings in the literature, it was hypothesised that astemizole acted via CYP2J2 to mediate its toxic effects in endothelial and HCMs. The aims of this chapter were to:

To establish gene and protein expression of CYP2J2 in the EA.hy926 endothelial cancer cell line and human cardiac myocytes.

To understand the potential role of CYP2J2 in astemizole toxicity through pharmacological inhibition and an *in vitro* knockdown model.

To analyse metabolism of astemizole by CYP2J2 and whether this metabolism may be inhibited by the alternative CYP2J2 substrate arachidonic acid.

6.3 Results

6.3.1 Expression of CYP2J2 mRNA in EA.hy926 cells and human cardiac myocytes: expression studies with TaqMan and SYBR Green qPCR

Initial investigation of CYP2J2 with TaqMan RT-PCR showed expression of CYP2J2 was increased in human cardiac myocytes (HCM) compared to EA.hy926 cells (figure 6.1A). An interesting finding in EA.hy926 cells showed expression was conserved only in lower passages of cells ≤ 10 , however at passages above p15 this expression was at undetectable levels (figure 6.2).

To conduct SYBR green RT-PCR gene expression analysis of CYP2J2, firstly primers were designed that were specific to this gene. From the NCBI database it was found that CYP2J2 had no variants so primers were designed that would bind to one isoform.

After pooling cDNA from both cell types, PCR with an annealing gradient was conducted to investigate the perfect annealing temperature for each combination of forward and reverse primers. Samples were run on an agarose gel after amplification. However, due to the low expression of CYP2J2 and the low detection capability of gel PCR, no bands were seen (figure 6.3). Due to this a T_m recommended by the manufacturer (69°C) was used for the final SYBR green experiment. SYBR green PCR reflected the TaqMan PCR results showing expression was ~ 8-9 times higher in HCM compared with EA.hy926 cells (figure 6.1).

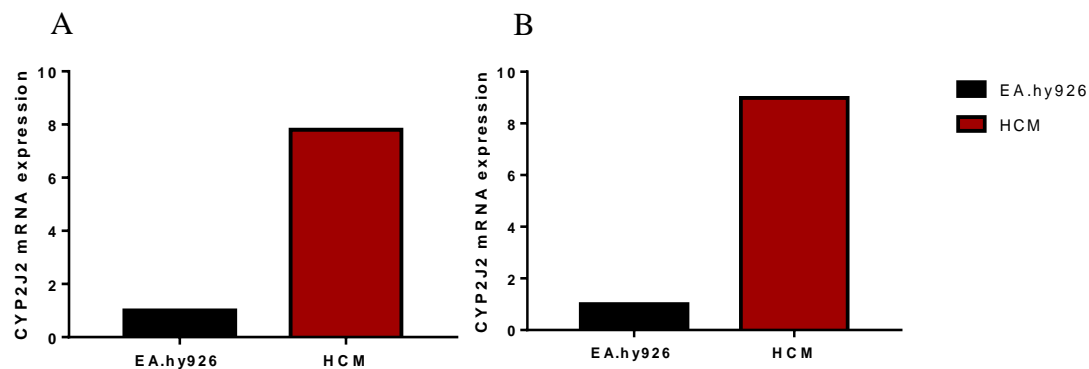


Figure 6-1 Expression of CYP2J2 mRNA in EA.hy926 cells and HCM as determined by qPCR with TaqMan and SYBR green detection.

EA.hy926 cells and HCM were grown to 80% confluence after which they were lysed for PCR. (A) Gene expression measured via TaqMan probe and (B) SYBR green RT-PCR. Expression of mRNA was calculated from average $\Delta\Delta CT$ values from 3 experiments normalised against the housekeepers GAPDH and GPI. HCM CYP2J2 expression was then normalised to EA.hy926 cell CYP2J2 expression.

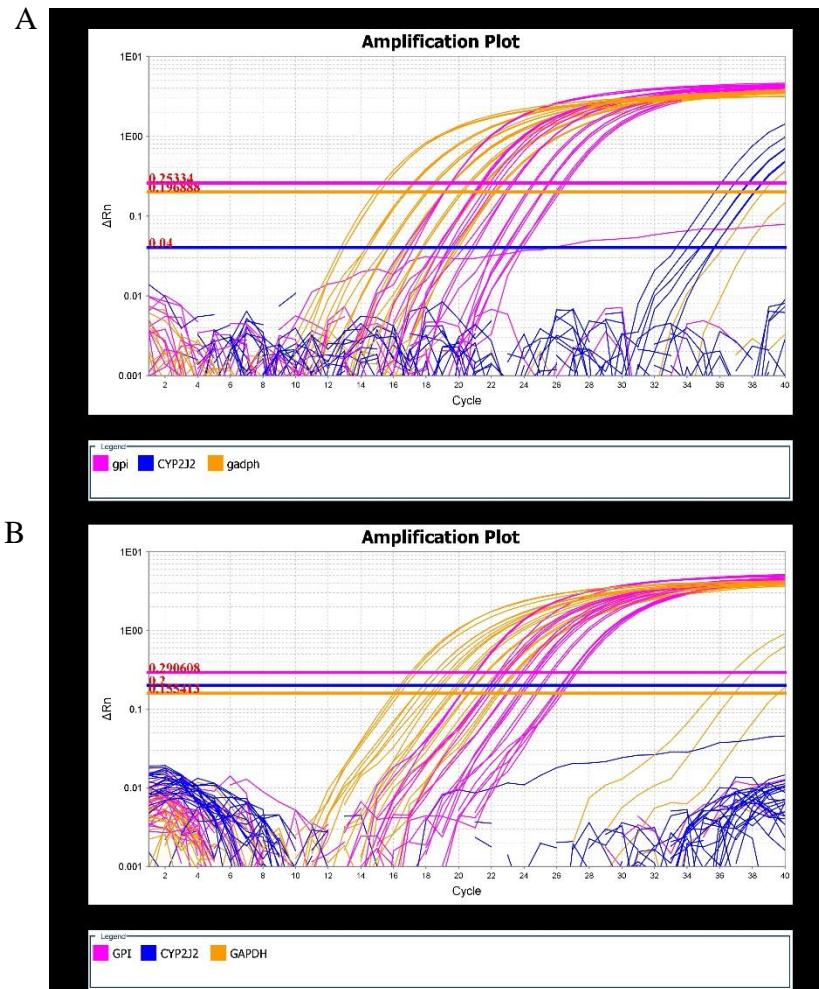


Figure 6-2 TaqMan PCR amplification.

TaqMan PCR was conducted on passage 10 (A) and 15 (B) EA.hy926 cells. A standard PCR protocol of 40 cycles was run and an amplification plot was produced. Housekeeper controls GPI (pink) and GAPDH (orange) were used to control P15 EA.hy926 cells showed undetectable expression of CYP2J2 (blue) compared to P10.

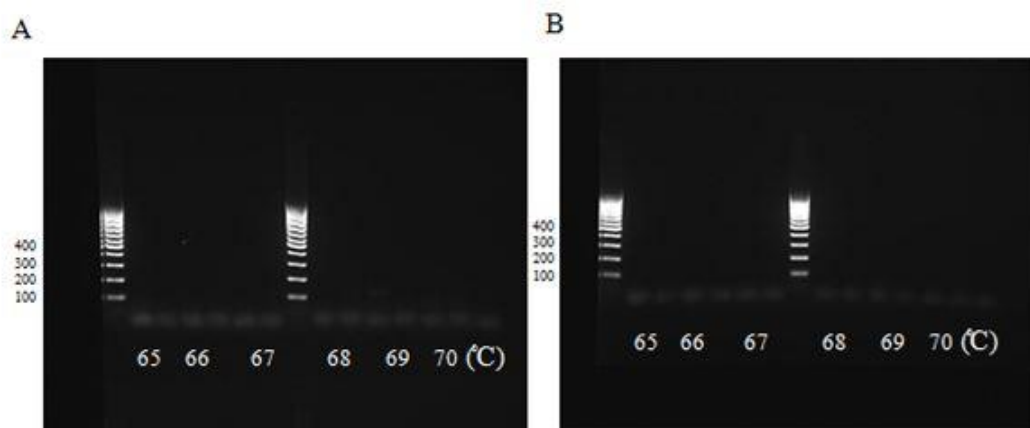


Figure 6-3 PCR products were amplified using gradient PCR and run on a gel as described in 3.1.5.3

CYP2J2 expression was undetectable using gel PCR so the best annealing temperature was ascertained according to the manufacturer. Different sets of primers were designed to each gene. Each gel represents a different primer combination. (A) Primer combination #10 (B) primer combination #11. 100bp ladder was used to estimate size of PCR products.

To further investigate the role of CYP2J2 in astemizole toxicity, cells were treated with ‘non-toxic’ concentrations of 25 μ M astemizole for 6 and 24 hr to observe changes in CYP2J2 expression. There was no change in CYP2J2 expression at 6hr in EA.hy926 cells (figure 6.4A) however expression was 3 fold higher after 24hr (figure 6.4B). At protein level the barely detectable band of CYP2J2 protein in untreated cells was noticeably increased by astemizole at 6 and 24 hr (figure 6.4C).

These results were replicated with HCM with a suggestion of a similar increase in protein expression of CYP2J2 at 6 and 24 hr and at gene and protein level at 24 hr (figure 6.4D-F).

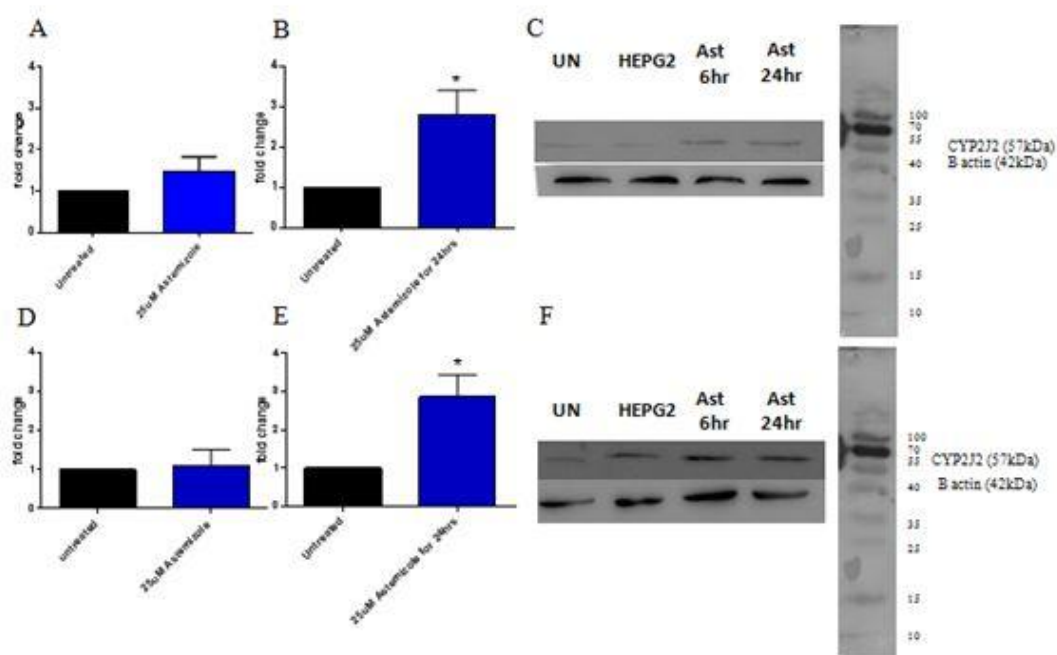


Figure 6-4 mRNA expression of CYP2J2 in EA.hy926 cells (A,B) and HCM (D,E) after treatment with 25μM astemizole for 6h (A,D) and 24h (B,E).

EA.hy926 cells and HCM were grown to 80% confluence after which they were treated with 25μM astemizole for 6 and 24hrs. Cells were then lysed for PCR using β actin and β 2 microglobulin as housekeeper genes. All data (mean and SEM of 5 replicates) was expressed as fold change $\Delta\Delta$ CT values. DMSO was kept at a final concentration of dilution of 0.001%. * $P < 0.05$. Western blot protein expression of CYP2J2 in EA.hy926 cells (C) and HCM (F) was conducted using the trueMAB mouse monoclonal CYP2J2 primary antibody from Origene.

6.3.3 Effect of sEH and CYP epoxygenase inhibitors on expression of CYP2J2 mRNA and protein

EA.hy926 and HCM cells were treated with inhibitors of sEH (t-AUCB) and CYP2J2 (MSPPOH) in the presence or absence of astemizole. In EA.hy926 cells there was a trend towards a reduction in CYP2J2 expression when cells were treated with MSPPOH in addition to astemizole for 6 hr compared to astemizole alone, however this did not reach statistical significance (figure 6.5A). When cells were treated with t-AUCB in combination with astemizole for 6 hr this reduced CYP2J2 expression compared to astemizole alone, $P < 0.001$ (figure 6.5B). Western blot also suggested a reduction in CYP2J2 protein when t-AUCB was added to cells treated with astemizole (figure 6.5E). Proof of this effect would require further experimentation.

In HCM MSPPOH had no effect on CYP2J2 expression in cells treated with astemizole at either gene or protein level (figure 6C), however, there was a reduction in CYP2J2 mRNA expression.

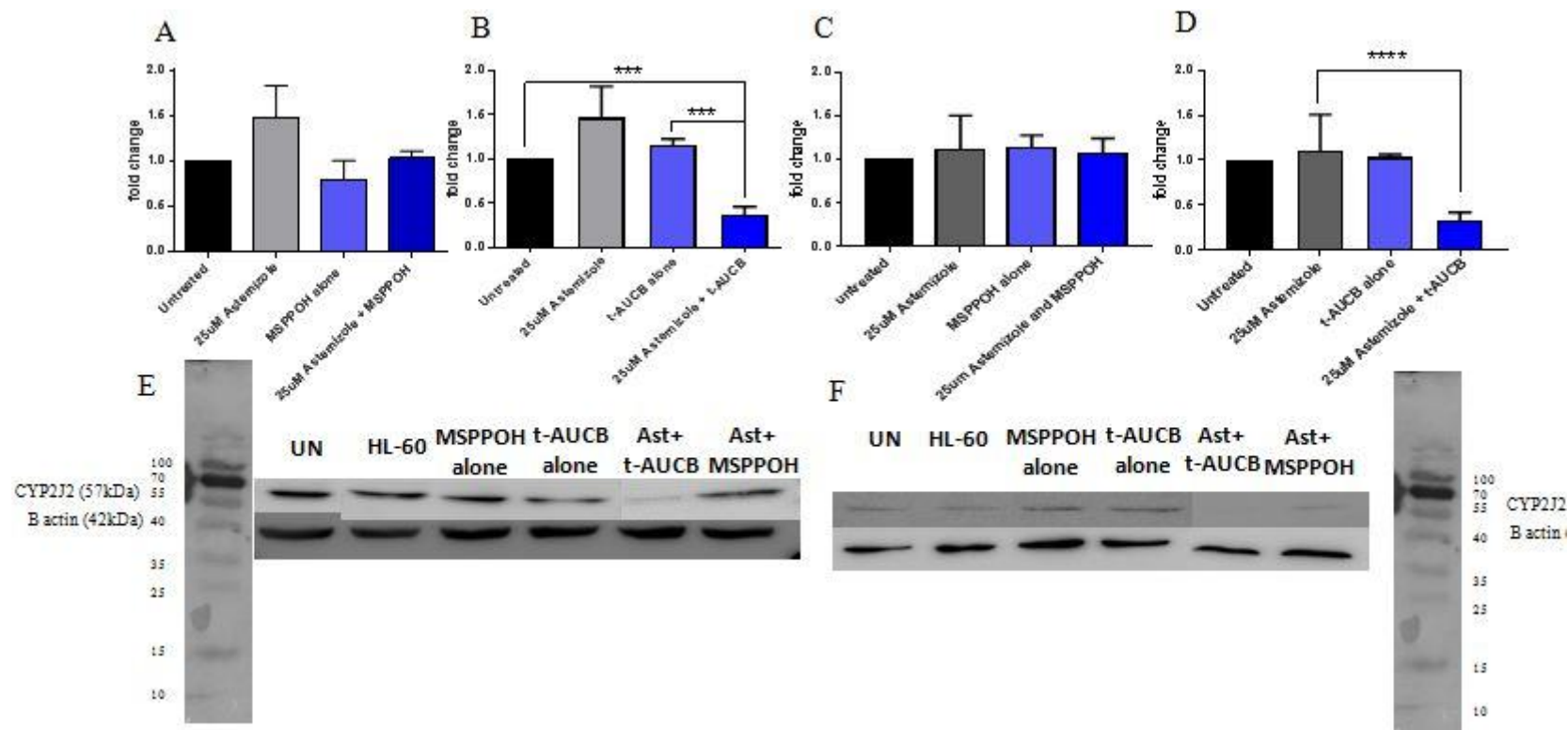


Figure 6-5 Expression of CYP2J2 mRNA in EA.hy926 cells (A and B) and human cardiac myocytes (HCM) (C and D) after treatment with 25 μ M astemizole and/or inhibitors for 6 hr.

EA.hy926 cells and HCM were grown to 80% confluence after which they were treated with 25 μ M astemizole and/or CYP epoxygenase MSPPOH (12.5 μ M) and SEH inhibitor t-AUCB (100 μ M) for 6hrs. Cells were then lysed for PCR using β actin and β 2 microglobulin as housekeeper genes. All data (mean and SEM of 5 replicates) was expressed as fold change $\Delta\Delta$ CT values. DMSO was kept at a final concentration of dilution of 0.001%. Western blot protein expression of CYP2J2 in EA.hy926 cells (E) and HCM (F) with the presence or absence of sEHi (t-AUCB) or CYP epoxygenase inhibitor (MSPPOH). ***P=0.005, ****P<0.0001.

6.3.4 Optimisation of siRNA knockdown of CYP2J2 mRNA

To further investigate role of CYP2J2 in astemizole toxicity, an *in vitro* knockdown model was attempted in EA.hy926 cells. Initially, lipofectamine reagent was used for delivery of siRNA into cells. In addition to cells treated with siRNA, untreated cells, cells treated with lipofectamine and optidem media, a negative non-template control and a cell death control were included. Gene expression studies with qPCR showed a trend towards a decrease in mRNA expression of CYP2J2 compared to the negative scrambled control, however this was not statistically significant (Figure 6.6A). This was also suggested at the protein level with a decrease in the CYP2J2 band observed by western blotting; this data was taken from a single experiment and would require further experimentation (Figure 6.6B).

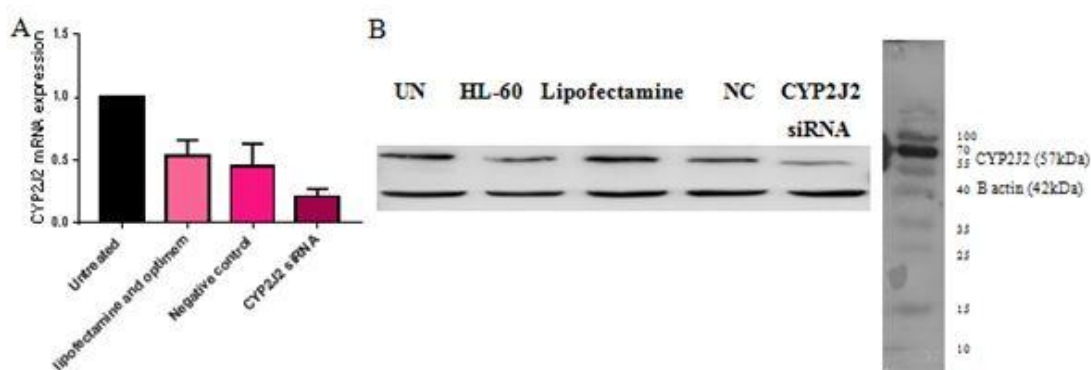
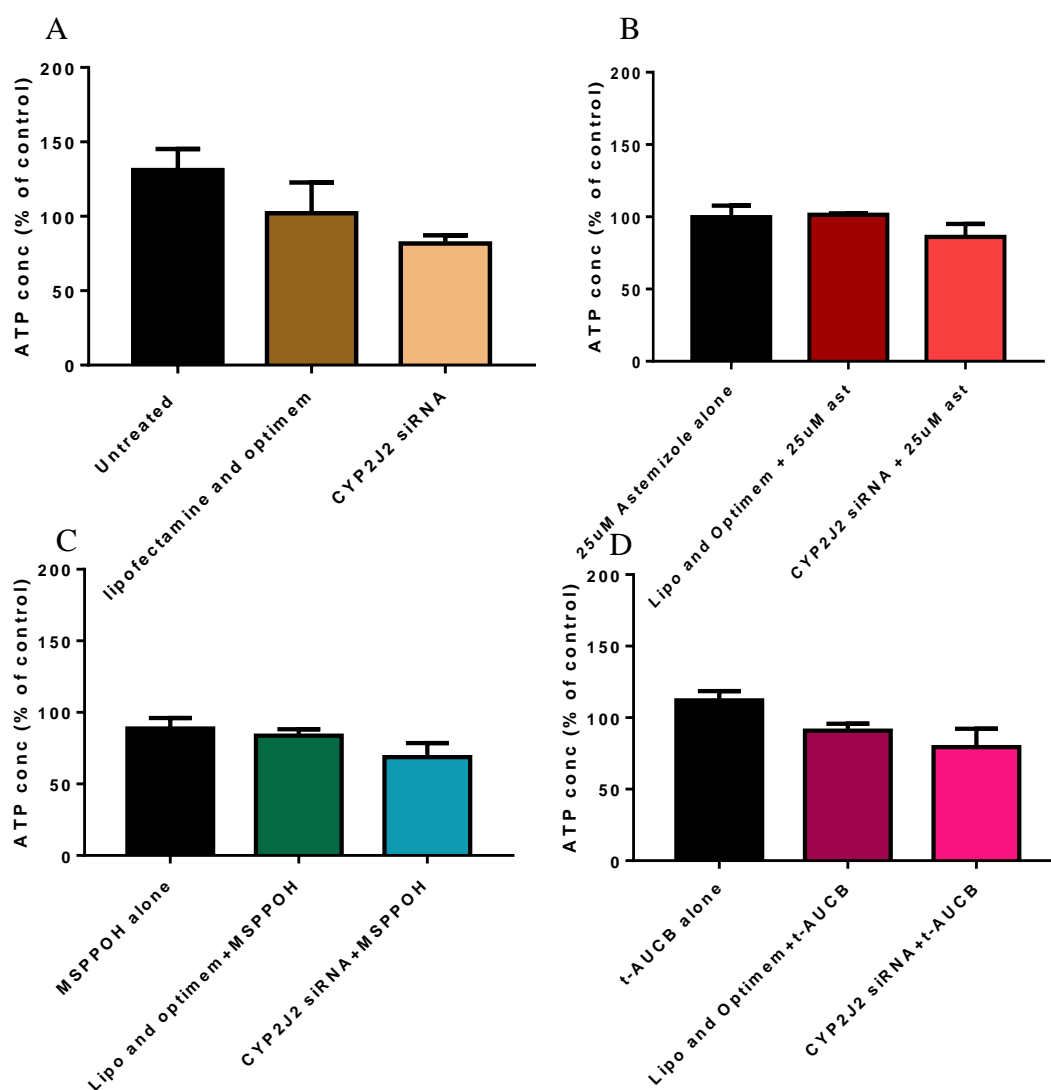


Figure 6-6 CYP2J2 mRNA knockdown in EA.hy926 cells.

Cells were treated with siRNA and lipofectamine for 24hr after which the media was changed. mRNA expression was measured by RT-PCR compared to a negative scrambled control and lipofectamine only control. In total, cells were incubated for 3 days before being lysed for PCR. Results were normalised to untreated cells. Values are the mean and SEM of 3 experiments. Expression of mRNA was calculated from average $\Delta\Delta CT$ values from 3 experiments normalised against the housekeepers B actin and B2 microglobulin. CYP2J2 expression was then normalised to untreated vehicle control CYP2J2 expression. (B) Western blot protein expression of CYP2J2 in EA.hy926 cells after incubation for 3 days.

6.3.5 Effect of knockdown of CYP2J2 mRNA and CYP2J2 and sEH inhibitors on astemizole-induced cytotoxicity

To investigate how *in vitro* knockdown of CYP2J2 may affect astemizole-induced cell death, cellular ATP was measured after knocked down cells were treated with 25 μ M astemizole and/or inhibitors of CYP2J2 or sEH for 6 hr. Data were normalised to the negative scrambled siRNA control for each treatment. There was no significant change in ATP when CYP2J2 was knocked down compared with no knockdown indicating CYP2J2 protein/activity may still be present (Figure 6.7).



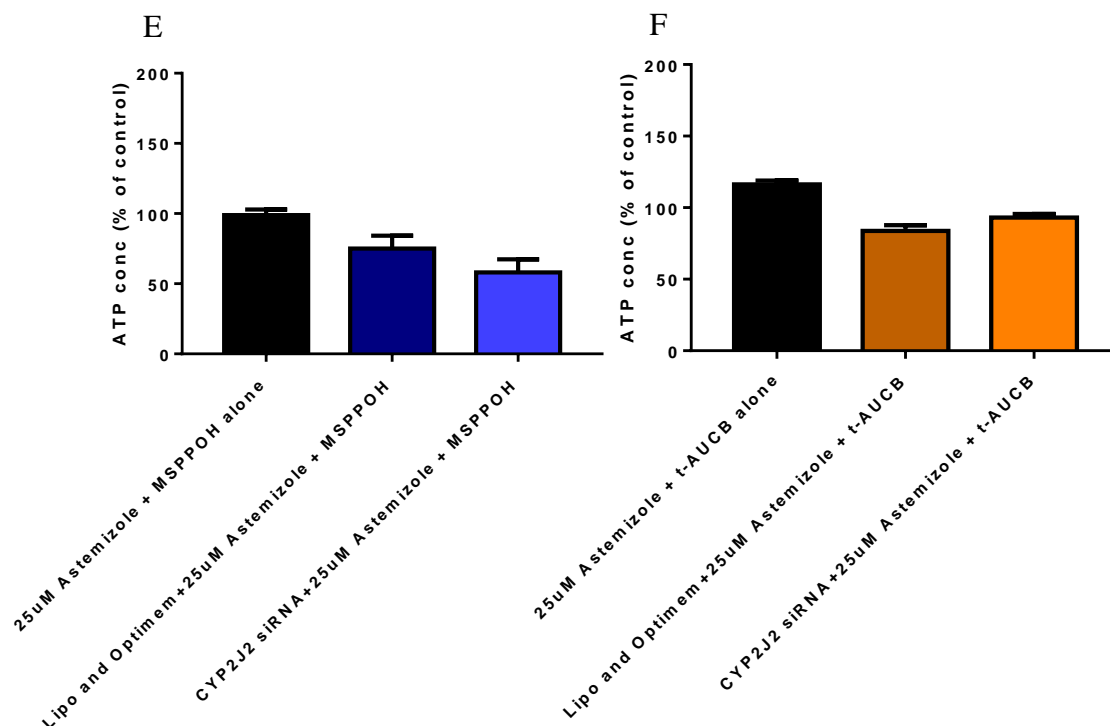


Figure 6-7 Effect of CYP2J2 knockdown and sEH and CYP2J2 inhibitors on astemizole-induced cytotoxicity.

EA.hy926 cells were cultured and treated with 10nM CYP2J2 siRNA and RNAimax Lipofectamine for 24hr after which the media was changed. Knockdown cells were then treated in the following way: (A) untreated, (B) 25µM astemizole, (C) 12.5µM MSPPOH alone, (D) 100µM t-AUCB alone, (E) 25µM astemizole and MSPPOH and (F) 25µM astemizole and t-AUCB. DMSO was kept at a final concentration of dilution of 0.001%. ATP content was used a surrogate marker of cell viability and values are the mean+SEM of 3 experiments normalised to the treated scrambled oligo control.

6.3.6 Metabolism of astemizole by cells and recombinant CYP2J2

CYP2J2 activity was investigated in EA.hy926 cells by measuring astemizole O-desmethylation. Evaluation of peak intensities showed no significant increase in the ratio of metabolite to astemizole when cells were incubated with 25 μ M astemizole for 30 min, 6 hr and 24 hr compared to the astemizole drug alone without cells (figure 6.8).

6.3.7 Metabolism of astemizole by recombinant CYP2J2 in bacosomes

To further investigate whether CYP2J2 was responsible for astemizole metabolism to its main metabolite O-desmethylastemizole, 100 μ M astemizole was incubated with recombinant CYP2J2 bacosomes over a range of bacosome concentrations. The ratio of O-desmethylastemizole: astemizole increased in a concentration dependent manner with increasing bacosome concentration (Figure 6.9). At 2 μ M bacosome concentration the metabolite ratio was less than 2% compared with 10 μ M where the metabolite: astemizole ratio was approximately 5%.

To manipulate this metabolism an alternative substrate for CYP2J2, AA was added to the reaction with a standard concentration of 10 μ M astemizole and 0.6pmol bacosomes. O-desmethylastemizole formation decreased as AA concentration increased such that at the highest AA concentration metabolite was undetectable. The IC₅₀ value was estimated as 75 μ M.

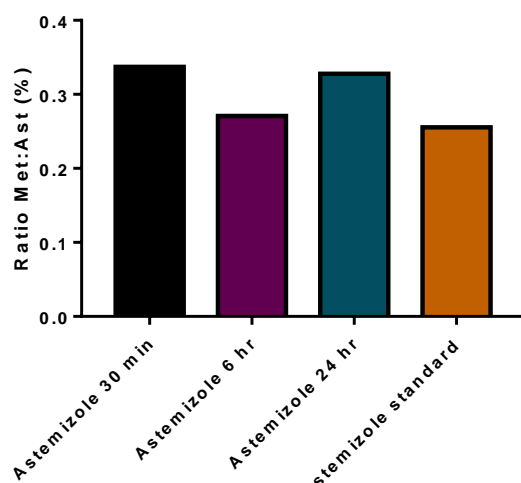


Figure 6-8 Metabolism of astemizole by EA.hy926 cells.

EA.hy926 cells were grown to 80% confluence and incubated with 25 μ M astemizole for 30 min, 6 hr and 24 hr before detached using trypin/EDTA. The pellet was resuspended in 100% methanol and snap frozen in liquid nitrogen. The steps were then repeated: thaw cells, pellet and pool supernatant into the same tube. The cell pellet was then resuspended in 250 μ l ice cold milliQ water and snap frozen in liquid nitrogen. The pooled supernatant was then centrifuged at 15,000g for 1 minute and transferred to a fresh tube. The supernatant was then dried using a centrifugal evaporator at 30 $^{\circ}$ C. O-desmethyl astemizole was quantified via LC-MS (see section 3.1.6) Values are the ratio of the mean of peak intensity values of O-desmethylastemizole and astemizole and represent the percent conversion of astemizole to o-desmethylastemizole. Astemizole standard was astemizole drug alone with no cells.

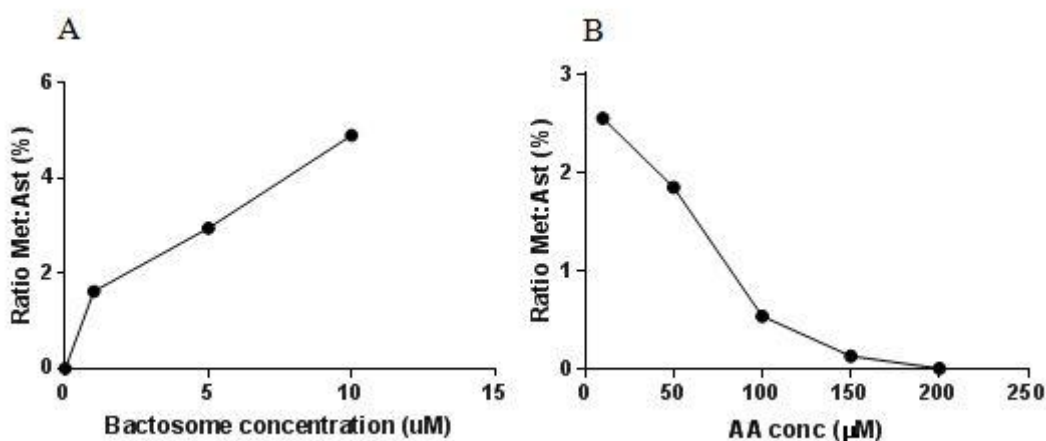


Figure 6-9 Metabolism of astemizole by recombinant CYP2J2 bacosomes.

(A) Metabolism of astemizole by recombinant CYP2J2 bacosomes and quantified via LC-MS. Bacosomes were incubated with 200mM potassium phosphate, 100mM magnesium chloride, 100 μ M astemizole and 0.6pmol thawed bacosomes diluted to 1ml in water. To initiate the reaction, 1ml of pre-warmed NADPH generating system was added to the conical flask and swirled gently. The reaction was stopped with 25 μ l 1M hydrochloric acid after 30 mins at 37 $^{\circ}$ C. Metabolism was reduced when a competing substrate for CYP2J2, AA was added. Aracidonic acid concentrations varied from 10, 50, 100, 150 and 200 μ M (B). Results were normalised to untreated cells. Values are the ratio of the mean of peak intensity values of O-desmethylastemizole and astemizole. Data are from a single experiment.

6.4 Discussion

Investigation of expression of CYP2J2 showed it was higher in HCM than in EA.hy926 cells. This corroborated with expression studies of CYP2J2 in human heart and coronary artery samples compared with other CYP epoxygenase enzymes. CYP2J2 was the highest expressed P450 enzyme in heart and a primary human cardiac cell line with 10^3 fold higher mRNA and protein expression than CYP2C9 or CYP2C8, however in coronary artery and aorta CYP2C9 mRNA was more abundant than CYP2J2 mRNA (Delozier et al., 2007, Evangelista et al., 2013).

One novel outcome when analysing baseline gene expression in cells was that cultured EA.hy926 cells were shown to have diminished expression of CYP2J2 over multiple passages. Previously it was shown that P450 gene and protein expression and activity of multiple P450 enzymes (not including CYP2J2) were reduced in cultured hepatocytes over increased culture time compared to human liver (Rodriguez-Antona et al., 2002). This may lead to the conclusion that other potential CYP enzymes including CYP2J2 may be regulated in a similar way and may be reduced in other cell types including those of cardiac origin.

When investigating an annealing temperature for CYP2J2 primers in SYBR green qPCR, no products were detected on agarose gels with any combination of CYP2J2 primers. CYP2J2 mRNA was later detected with the more sensitive SYBR green PCR. SYBR green RT-PCR has previously been compared to conventional agarose gel electrophoresis PCR and was found to be at least 10 times more sensitive than traditional gel electrophoresis detection when detecting infectious virus mRNA (Fellahi et al., 2016), corroborating the fact that CYP2J2 gene expression was only detected when using the more sensitive SYBR green method of detection.

Treatment of both EA.hy926 cells and HCM with 25 μ M astemizole showed a time-dependent increase in CYP2J2 gene expression compared to the vehicle treated control. This response may be due to a need for increased metabolism of the drug astemizole or to attenuate its toxic effects by increasing production of protective EETs. Very recently, adult ventricular myocytes treated with 5 or 20 μ M dox also showed a 2-fold increase in CYP2J2 expression after 24hr as well as other genes encoding for antioxidant proteins

indicating an increase in CYP2J2 expression may be a protective response against the toxic effects of dox (Evangelista et al., 2018).

When incubated with both astemizole and CYP epoxygenase inhibitor MSPPOH both cell types showed no change in expression of CYP2J2. This may be the result of a short incubation time of 6hr where changes in gene expression could not yet be observed. There is little evidence in the literature investigating the effect of MSPPOH on CYP epoxygenase expression in the heart however, in rat proximal tubular epithelial cells treated with high glucose to induce a diabetes-like phenotype, inhibition of EET production with MSPPOH altered protein expression of CYP epoxygenase CYP2C11 after 6hr and this was further decreased after 48hr suggesting suppression of expression is time dependent and may have different effects according to cell type (Eid et al., 2013).

In response to incubation with both astemizole and the sEH inhibitor t-AUCB for 6hr there was a reduction in CYP2J2 mRNA expression in EA.hy926 cells. Expression of sEH was previously increased in response to the same treatment indicating a possible link between the regulations of these genes, where t-AUCB increased expression of sEH yet decreased expression of CYP2J2. It is still unclear how gene expression of CYP2J2 and sEH may be linked. Studies have shown that CYP2J2 may be downregulated in HepG2 cells in response to a hypoxic environment and this is regulated by c-jun, part of the AP-1 transcription factor (Marden et al., 2003). Furthermore expression of CYP2J2 *in vitro* in HEK293 cells activated PPAR α which was also activated by CYP2J2 AA metabolites 8,9- and 11,12-EET (Wray et al., 2009).

Along with pharmacological inhibition, siRNA knockdown of the CYP2J2 gene was also conducted to further investigate the role of CYP2J2/EETs in astemizole toxicity. A mixture of siRNA and lipofectamine as the transfection reagent was used to increase the efficiency of transfection. In addition a negative scrambled control and a cell death control was added to each cell plate to make sure transfection was efficient. The cell death control showed dead, floating cells after the 3 day incubation with siRNA indicating cells had taken up the siRNA (figure 6.10).

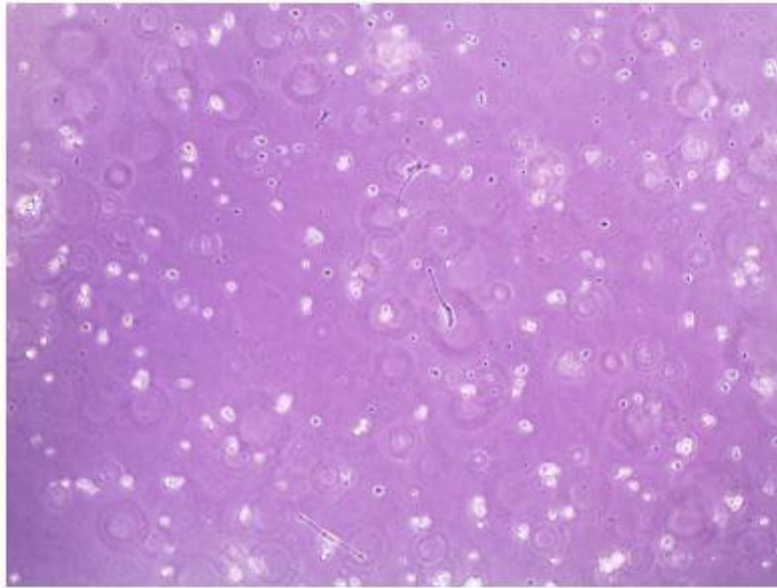


Figure 6-10 EA.hy926 cells treated with cell death siRNA after 3 days. X100 magnification.

EA.hy926 cells were grown to 80% confluence and treated with 20nM AllStars cell death siRNA and RNAimax lipofectamine in optimem media for 24hr after which the media was changed. Images were taken after 3 days with brightfield microscopy.

However, although a reduction in CYP2J2 gene and protein was found there was still protein detected indicating CYP2J2 activity may still be present. When these transfected cells were then treated with astemizole and/or inhibitors of CYP2J2 and sEH there was no change in ATP. Further work into investigation of optimisation of CYP2J2 siRNA knockdown may include incubating cells with siRNA for different timepoints as well using different modes of siRNA delivery into cells such as electroporation. A similar experiment done in adult ventricular myocytes using the cardiotoxic drug doxorubicin incubated cells with Trilencer siRNA and lipofectamine reagent for 3 days and evaluated knockdown by PCR. PCR showed a significant knockdown of CYP2J2 gene of ~90%. Investigating cell viability with a treatment with doxorubicin for 24hr showed a reduction in viability of ~50% compared with scrambled control (Evangelista et al., 2018). This suggests the 3 day protocol may be an appropriate timepoint to use for CYP2J2 knockdown, however different siRNA targeting multiple sites may be needed to fully knockdown the gene and protein. A 3 day siRNA incubation with 4 non-targeting sequences was also used in the MC47 breast cancer cell line which showed a complete knockdown of the gene as indicated with PCR (Mitra et al., 2011). However, when investigating potential pathological mechanisms of homocysteine in SMMC7721 cancer cells, cells were incubated with CYP2J2 siRNA and lipofectamine for 8hr (D.

Zhang et al., 2017). This showed a reduction in CYP2J2 gene expression by ~50% compared to control suggesting timepoints may vary possibly with cell type and type of siRNA.

To study the metabolism of astemizole by CYP2J2, EA.hy926 cells were incubated with 25µM astemizole for 30min, 6hr and 24hr. Using LC-MS the peak intensity of the O demethylated metabolite was determined. However, there very low detectable metabolism of astemizole seen at all timepoints. There may be many limitations of studying drug metabolism of astemizole in EA.hy926. As these cells are an endothelial cell line they are not primarily responsible for drug metabolism and therefore may lack some of proteins involved in drug metabolism. For example, there may be produce insufficient levels of NADPH cytochrome P450 reductase (CPR) that enable P450 enzymes to function. Furthermore, it is already known these cells have much lower expression of P450 enzymes than the heart (Delozier et al., 2007). A cell type such as human cardiac myocytes which have higher expression of CYP2J2, subsidised with the relevant proteins and enzyme systems they lack may be more adequate in showing metabolism of astemizole by CYP2J2.

To further investigate the role of CYP2J2 in astemizole drug metabolism a bacosome system with recombinant expression of CYP2J2 was found to be efficient in metabolising astemizole to O-desemthylastemizole indicating CYP2J2 activity was active in this system. To further manipulate metabolism AA was added which would potentially inhibit drug metabolism. AA was shown to inhibit astemizole drug metabolism in a concentration dependent way. Indeed Matsumoto et al (2002) showed that CYP2J2 substrates arachidonic acid (AA) and ebastine significantly inhibited astemizole O-demethylation in human small intestine and *in vitro* for recombinant CYP2J2 (Matsumoto et al., 2002). This suggests a protective mechanism of EET production predominates over toxic drug metabolism. Further work into drugs other than astemizole would be useful in understanding the role of CYP2J2 in balancing both exogenous and endogenous metabolism.

Future advances may be made by investigating CYP2J2 expression in cells other than heart such as primary endothelial cells, smooth muscle cells and fibroblasts which may be beneficial to understand the localisation of CYP2J2 in the heart.

It may also be of interest to show how over expression of CYP2J2 may protect against astemizole toxicity. Over expression of the CYP2J2 gene has already shown to be protective in a variety of animal models of disease so it may be feasible to suggest that protection may also be afforded against astemizole toxicity (Ma et al., 2013, W. Liu et al., 2016, Deng et al., 2011, J. Seubert et al., 2004).

Chapter 7 **Investigation of biomarkers of astemizole induced
cardiotoxicity**

7.1 Background

Extracellular vesicles can be released by eukaryotic and prokaryotic cells into the extracellular environment (Yáñez-Mó et al., 2015) and can be classified into 3 main types, exosomes, microvesicles and apoptotic bodies which are differentiated according to their size, lineage and function (Valadi et al., 2007).

Exosomes, the smallest of these with a size of around 30-150nm, are secreted by most cells types and are present in biological fluids including blood, urine and culture medium (van der Pol et al., 2012). They are enclosed in a lipid membrane and are released by exocytosis by two main mechanisms, either through the classic or direct pathway. The classic pathway involves the production of intraluminal vesicles (ILVs) within the multi vesicular endosomes (MVEs). When MVEs fuse with the cell membrane the ILVs or exosomes are released. Alternatively, the direct pathway involves the direct fusion of vesicles with membrane where they are released as exosomes (van der Pol et al., 2012).

Exosomes carry unique substances including proteins, mRNA and miRNA which can then function as signalling mediators, crossing the cell membrane to transfer information to nearby cells (Boriachek et al., 2018). Proteins within exosomes are unique to the cell they originate from. The protein content of exosomes include transmembrane and membrane transport proteins, proteins involved in apoptosis, those involved in transporting exosomes and enzymes involved in intracellular signalling such as GTPase which promotes the fusion of membranes (Boriachek et al., 2018). In addition to proteins, RNA is transported in exosomes and translated to proteins within target cells thus potentially manipulating chemical signalling processes within the cell. It's unclear what mechanisms are involved in dictating which RNA sequences are found in exosomes, however studies have found the presence of short sequence motifs (EXOMotifs) on miRNA may be involved in the encapsulation and exportation into exosomes. Exosomes are also able to transport lipids such as cholesterol, sphingolipids and prostaglandins to target cells (Boriachek et al., 2018).

Due to the role of exosomes in modulating major cell processes it's not surprising that they have been shown to modulate the pathology of cancer (Skog et al., 2008), infections (Pegtel et al., 2010), cardiovascular disease (Kuwabara et al., 2011) and cardiotoxicity (Yarana et al., 2017). Microparticles such as exosomes have been found

as effectors of cardiovascular inflammation by transporting bioactive molecules, leading to an increase in adhesion molecules and cytokine release. For example, investigation of microparticles produced from angiotensin-activated endothelial cells showed an increase in ROS formation. Furthermore, when thrombin upregulated TNF-related apoptosis-inducing ligand (sTRAIL), this increased release of exosomes from human umbilical vein endothelial cells (HUVECs) leading to increases in inflammatory regulators such as ICAM-1 and IL-8. (Andriantsitohaina et al., 2012) Exosomes isolated from hypertensive patients attenuated proliferation of endothelial cells and increased cellular senescence compared to individuals with hypertension and normal albuminuria (Berezin et al., 2015). A high number of exosomes have also been associated with atherosclerosis and myocardial infarction compared to healthy controls indicating exosomes may be promising biomarkers for cardiovascular disease (Tushuizen et al., 2011).

Recently their role has also been studied in drug induced toxicity. Investigation of extracellular vesicles from hepatocytes treated with hepatotoxic drugs such as acetaminophen and diclofenac showed drug specific increases in several mRNA coding for proteins including albumin, guanine nucleotide binding protein (G protein), beta polypeptide 2-like 1 (Gnb21) and retinol binding protein 4 (RBP4). In addition, analysis of miRNA in patients with acetaminophen toxicity showed specific changes in their miRNA profile compared to healthy controls. Of all the miRNAs, MiR-122-5p increased substantially and was shown to be more sensitive than alanine aminotransferase (ALT) in reporting liver injury (Palomo et al., 2018). Similarly biomarkers of doxorubicin induced cardiotoxicity were also assessed in extracellular vesicles released by cardiomyocytes in a dox-induced cardiotoxicity mouse model. Dox treated rats had increasing circulating exosomes compared with controls. Proteomic analysis showed the presence of brain/heart, skeletal muscle and liver glycogen phosphorylase (PYGB) which correlated with a reduction in PYGB in the heart. Furthermore, the extracellular vesicles containing PYGB were released before cardiac troponin in response to dox related injury indicating this may be a sensitive biomarker to detect early tissue injury (Yarana et al., 2017). Thus, it is realistic to suggest astemizole toxicity may also increase exosomes *in vitro* and may be investigated for possible biomarkers.

The gold standard of exosome isolation is differential centrifugation which requires low speed centrifugation to remove cells and apoptotic bodies, a high speed spin to abolish larger vesicles and high speed centrifugation to precipitate exosomes. However this form of exosome isolation has reduced sample purity and increasing contamination with larger artefacts. Another more recent method is size exclusion chromatography which relies on porous polymer beads in a column to separate protein molecules according to their size. As the samples pass through the column it is collected in fractions for further analysis. Size exclusion chromatography has been shown to remove most of the abundant proteins contained in body fluids, as well as maintaining structure and conformation of exosomes increasing the purity and viability of the sample (Gómez-Valero et al., 2016). The quantification of microparticles can be done with nanoparticle tracking analysis which simultaneously determines the size and number of particles by light scattered from each particle in motion. It overcomes many of the limitations of other techniques of analysis as it is relatively quick and easy and is more sensitive towards smaller molecules (Dragovic et al., 2011).

7.2 Aims

To isolate and investigate exosome release from EA.hy926 cells after astemizole induced toxicity and compare with this exosome release from other cardiotoxic and non-cardiotoxic drugs.

7.3 Results

7.3.1 The effect of serum free media on EA.hy926 cells treated with astemizole

To investigate exosomes released in response to astemizole, the use of serum free media was pertinent to minimise contamination from proteins in serum including albumin. Therefore, firstly cells were incubated with astemizole at timepoints of 24, 48 and 72hr with FBS serum or serum free DMEM media. With serum media there was no change cell viability as measured with trypan blue staining (figure 7.1A). However, when cells were incubated with serum free media there was a marked reduction in cell viability at both 48 and 72hr compared to the DMSO control. This was more prominent at 72hr where there was reduction in cell viability of ~20% (figure 7.1B).

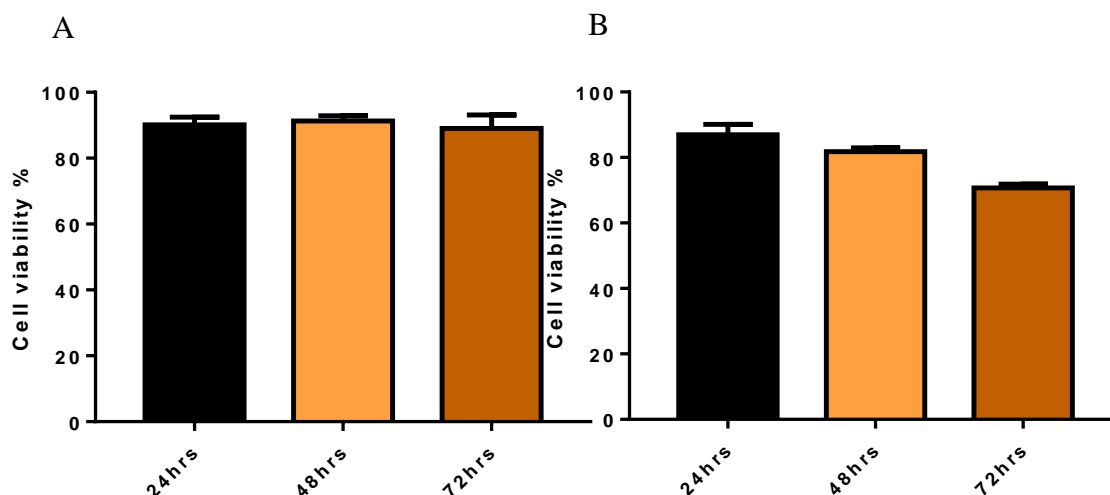


Figure 7-1 The effect of serum free media on EA.hy926 cells.

EA.hy926 cells were grown to ~80% confluence and cultured in serum supplemented media (A) or serum free media (B) for 24, 48 and 72hr. Cell viability was assessed using trypan blue cell stain. Values are the mean and SEM of 3 experiments normalised to serum cells.

Once a suitable timepoint had been found, an appropriate concentration of astemizole was investigated which would give release of exosomes but would not be toxic to cells. Therefore, lower concentrations of astemizole between 5-25 μ M were used to investigate cell viability and then release of exosomes. Investigation of cell viability showed a concentration dependent decrease in cell viability with a stark decrease in viable cells from 10, 15 and 25 μ M. Therefore, a concentration between 2-10 μ M was used to further investigate particle concentration and specifically exosomes stimulated from EA.hy926 cells (figure 7.2).

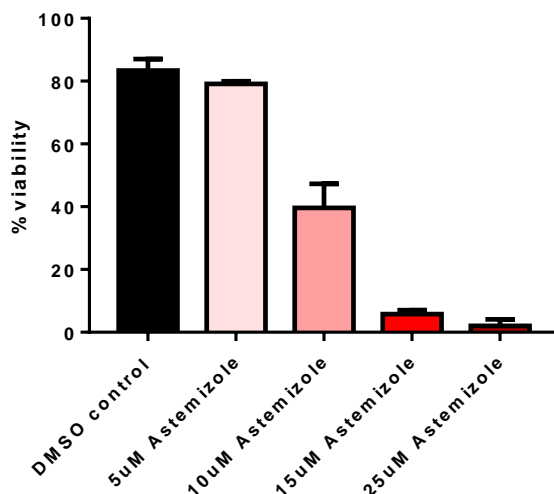


Figure 7-2 The effect of astemizole on EA.hy926 cell viability

EA.hy926 cells were grown to ~80% confluence and were treated with 5, 10, 15 and 25µM astemizole for 24hr in serum free media. Cell viability was assessed using trypan blue cell stain. Values are the mean and SEM of 3 experiments and were normalised to the DMSO control which was kept at 0.01%.

The NanoSight nanoparticle tracker was used to determine the concentration and size of particles in media from EA.hy926 cells stimulated with astemizole. Exosomes are typically between 30-100nm (van der Pol et al., 2012). With larger particles being larger microvesicles and apoptotic bodies. From the graph, it was proposed that untreated cells and lower concentrations of astemizole between 2-4µM gave mostly larger particles >100nm indicating a lower concentration of exosomes. However at samples treated with 6, 8, 10µM there was a peak in concentration of particles at a lower particle size <100nm as well as at larger particle sizes indicating a mixture of both small and larger microparticles present in the sample (figure 7.3A). In addition, the NanoSight identified that the concentrations of particles increased in a concentration dependent way proportional to increased concentrations of astemizole (figure 7.3B).

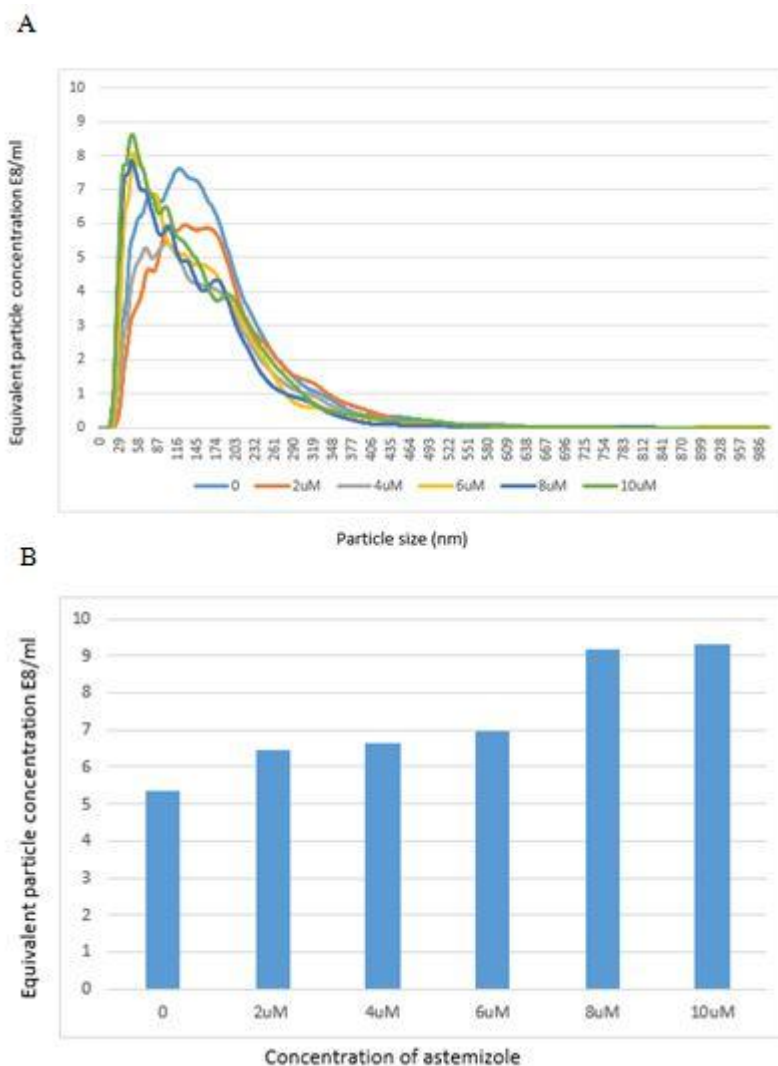


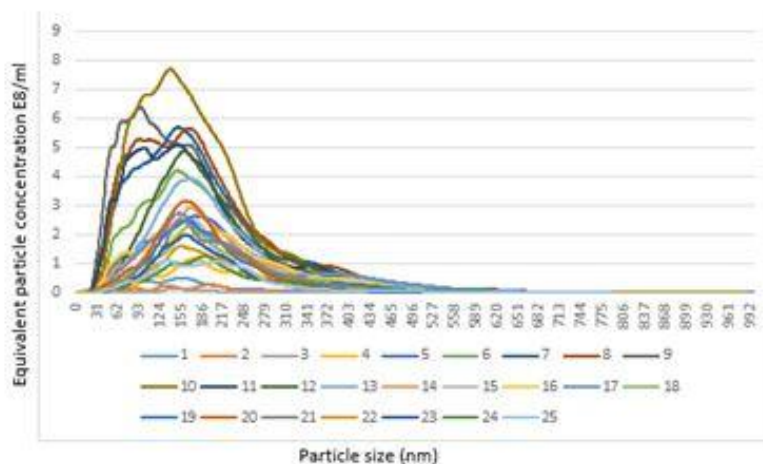
Figure 7-3 Particle size distribution (A) and particle concentration (B) in cells treated with varying concentrations of astemizole for 24hr.

EA.hy926 cells were grown to ~80% confluence after which they were treated with varying concentrations of astemizole (2, 4, 6, 8 10 μ M) for 24hr in serum free media. The media was then obtained and used for NanoSight analysis.

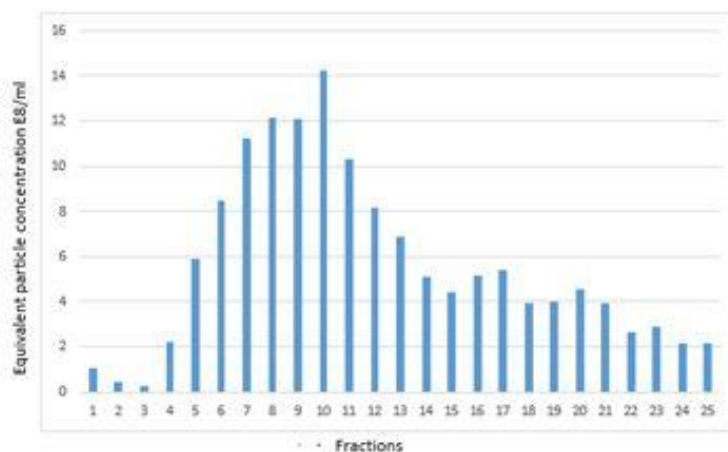
To further isolate exosomes from larger microparticles, a size exclusion chromatography column was used which utilised porous polymer beads to separate molecules according to size with larger molecules traveling faster down the column and smaller molecules isolated later. An astemizole concentration of 10 μ M was used as this had shown to stimulate the release of smaller exosomes as well as an untreated vehicle control sample. 25 1ml fractions were collected for each sample and analysed using the NanoSight to determine the ~concentration of exosomes and purity of the sample.

Media from astemizole treated cells showed that the highest concentration of particles were seen at fractions between 6 and 12 indicating these fractions may have an increased concentration of exosomes, however at the earlier and later fractions there was hardly any particles detected (figure 7.4B). Fraction 8,9,10 and 11 also gave a peak concentration of particles at a smaller particle size indicating these fractions yielded the most exosomes. However all fractions analysed had a peak at larger particle sizes indicating contamination with larger particles (figure 7.4A). Fractions from untreated samples showed a lower concentration of particles compared with treated cells with the highest equivalent particle concentration at fraction 12, 13 and 14 peaking at around 2 to 3 compared to treated cells with a peak concentration of between 12 and 14 (figure 7.4D). This was further seen when investigating the size distribution of particles in each fraction. The peak concentration of all fractions were low and veered towards the bigger particle sizes indicating cells may not be stimulated to release exosomes (figure 7.4C).

A



B



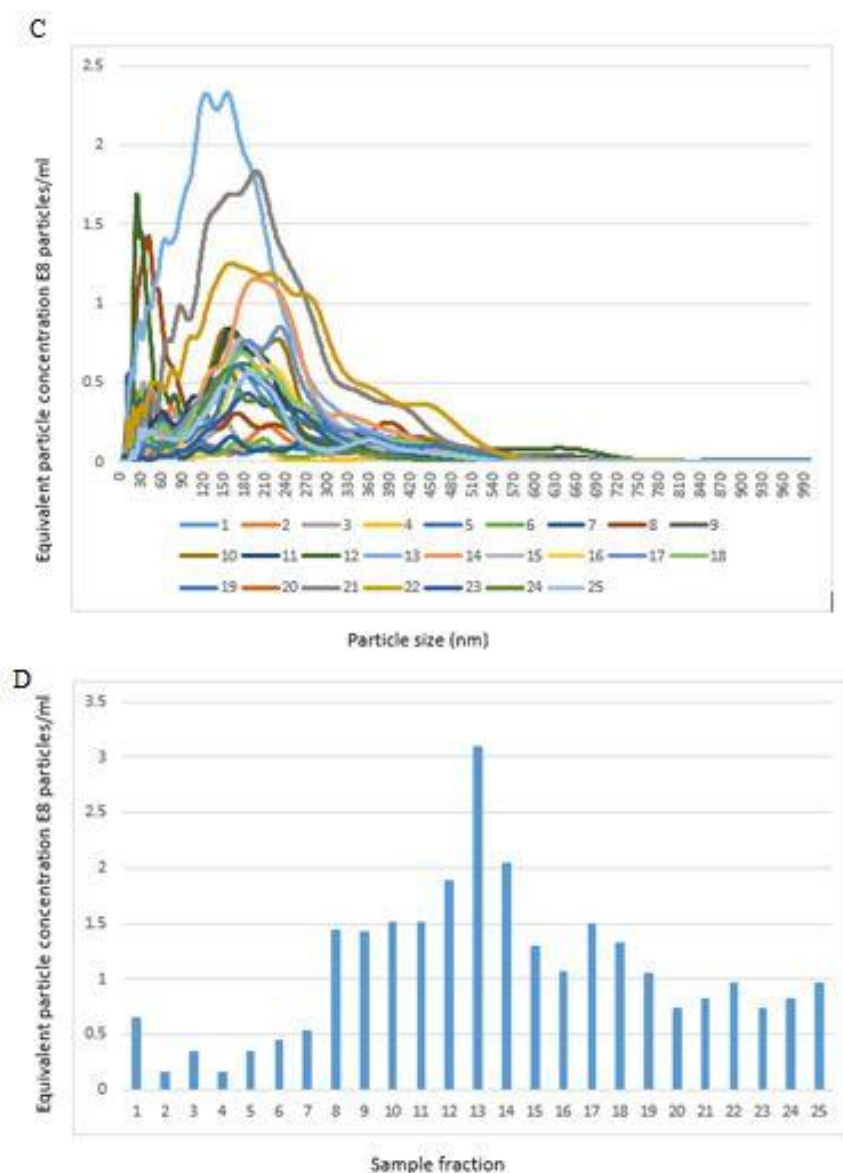


Figure 7-4 Particle size distribution and particle concentration in cells treated with astemizole and untreated EA.hy926 cells.

EA.h926 cells were grown to ~80% confluence and treated with 10 μ M astemizole (A,B) in serum free media or untreated serum free media (C,D) for 24hr. The media was then isolated and used for NanoSight analysis.

7.3.2 The effect of serum free media on EA.hy926 cells treated with doxorubicin

To understand whether the effects seen with cells stimulated with astemizole was a drug specific effect, another cardiotoxic drug, doxorubicin was utilised. Firstly, an appropriate concentration was investigated which would give release of exosomes but would not be toxic to cells. Therefore, lower concentrations of dox between 5-25 μ M were used to investigate cell viability and then release of exosomes. Investigation of cell viability showed a ~20% decrease when cells were treated with dox at any

concentration between 5-25 μ M indicating toxicity was not concentration dependent (figure 7-5). Therefore, a lower concentration range between 2-10 μ M was used to further investigate particle concentration and specifically exosomes stimulated in EA.hy926 cells.

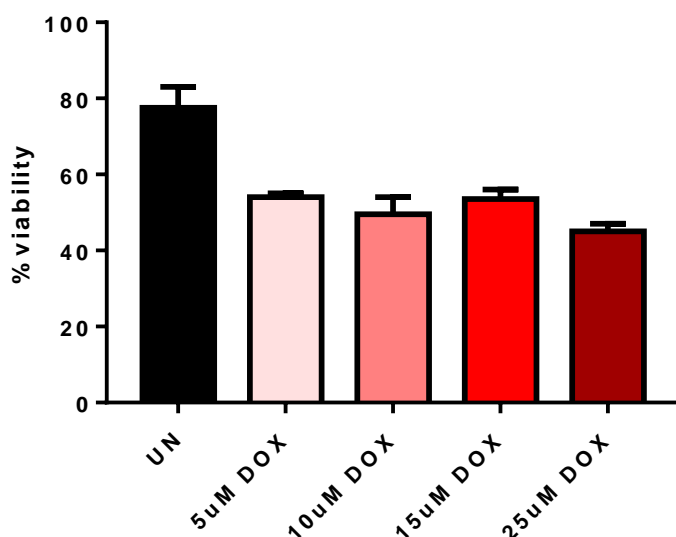
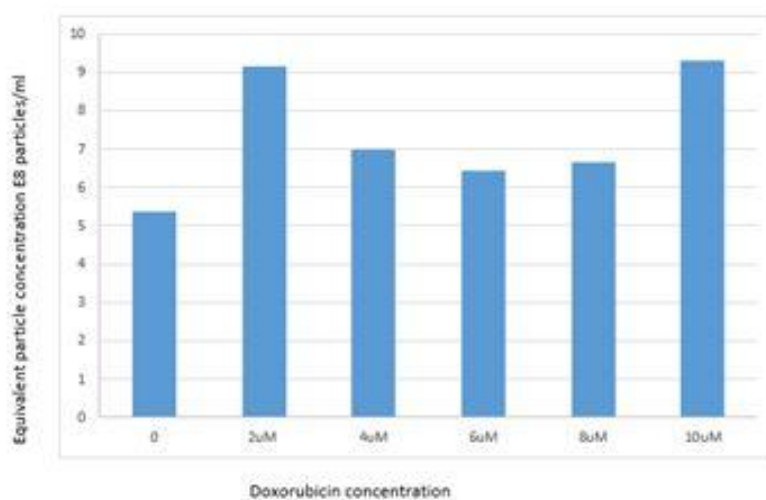


Figure 7-5 The effect of doxorubicin on EA.hy926 cell viability

EA.hy926 cells were grown to ~80% confluence and were treated with 5, 10, 15 and 25 μ M dox for 24hr in serum free media. Cell viability was assessed using trypan blue cell stain. Values are the mean and SEM of 3 experiments and were normalised to the DMSO control which was kept at 0.01%.

Stimulation of cells with dox between 2-10 μ M did not show a concentration dependent increase in particles as with astemizole. A 2 fold increase in particle concentration was seen at 2 and 10 μ M dox with all other concentrations showing a modest increase in particle concentration compared to untreated (figure 7.6A). Further investigation of the particle size distribution of particles within each sample showed all samples had a similar size distribution and peak particle concentration. Furthermore, compared to astemizole there was a shift in particle size distribution to the right when EA.hy926 cells were treated with dox with larger particles (>100nm) predominating within each sample. This suggested that dox was not stimulating the release of exosomes or at least not to the extent of astemizole (figure 7.6B).

A



B

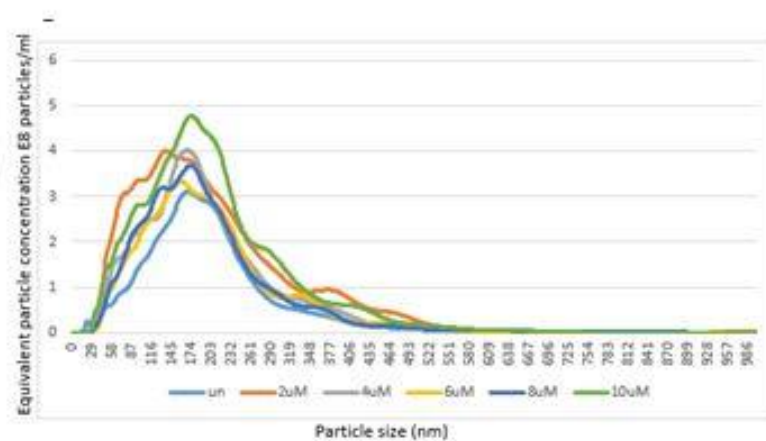
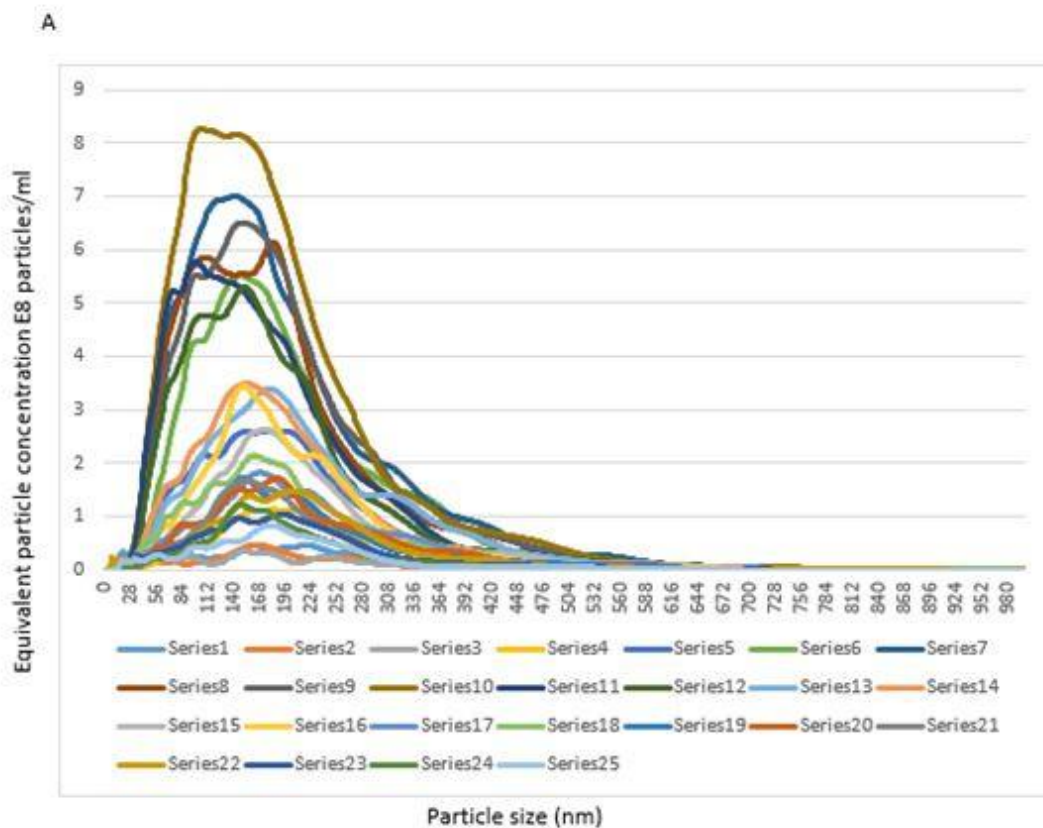


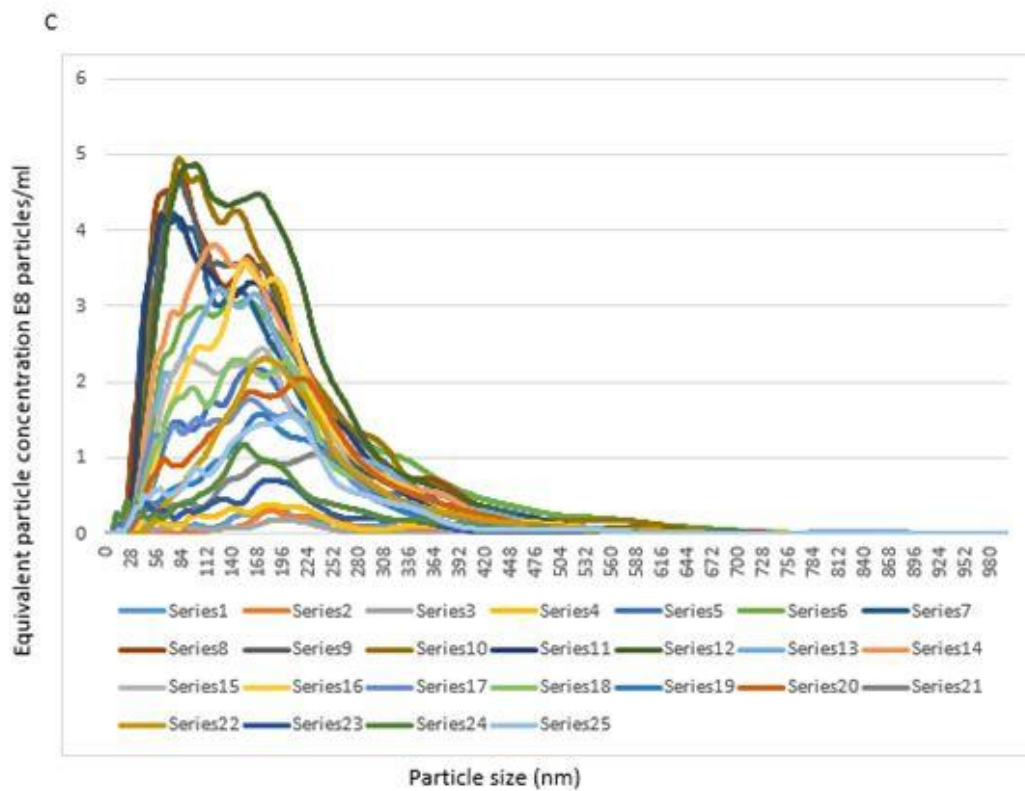
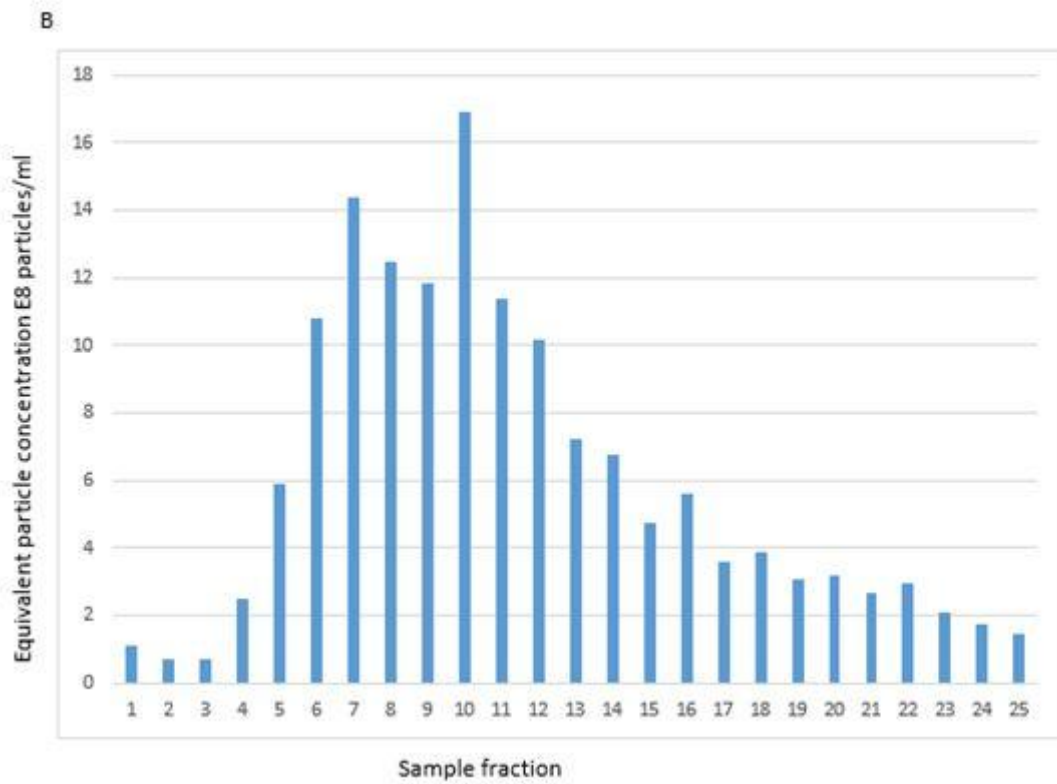
Figure 7-6 Particle size distribution (A) and particle concentration (B) in cells treated with varying concentrations of doxorubicin for 24hr.

EA.hy926 cells were grown to ~80% confluence after which they were treated with varying concentrations of dox (2, 4, 6, 8 10µM) for 24hr in serum free media. The media was then obtained and used for NanoSight analysis.

To further investigate whether dox was releasing exosomes and to isolate them from larger microparticles, a size exclusion chromatography column was used. A concentration of 2 μ M was used as this was non-toxic and had increased the concentration of microparticles previously. 25 1ml fractions were collected for each sample and analysed using the NanoSight to determine the concentration of exosomes and purity of the sample.

Media from dox treated cells showed a large size distribution curve suggesting that although separation through the column had occurred there was still contamination with different microparticles. However, compared to untreated cells there was an increase in overall particle concentration suggesting dox may stimulate the release of microparticles and possibly microsomes (figure 7.7)





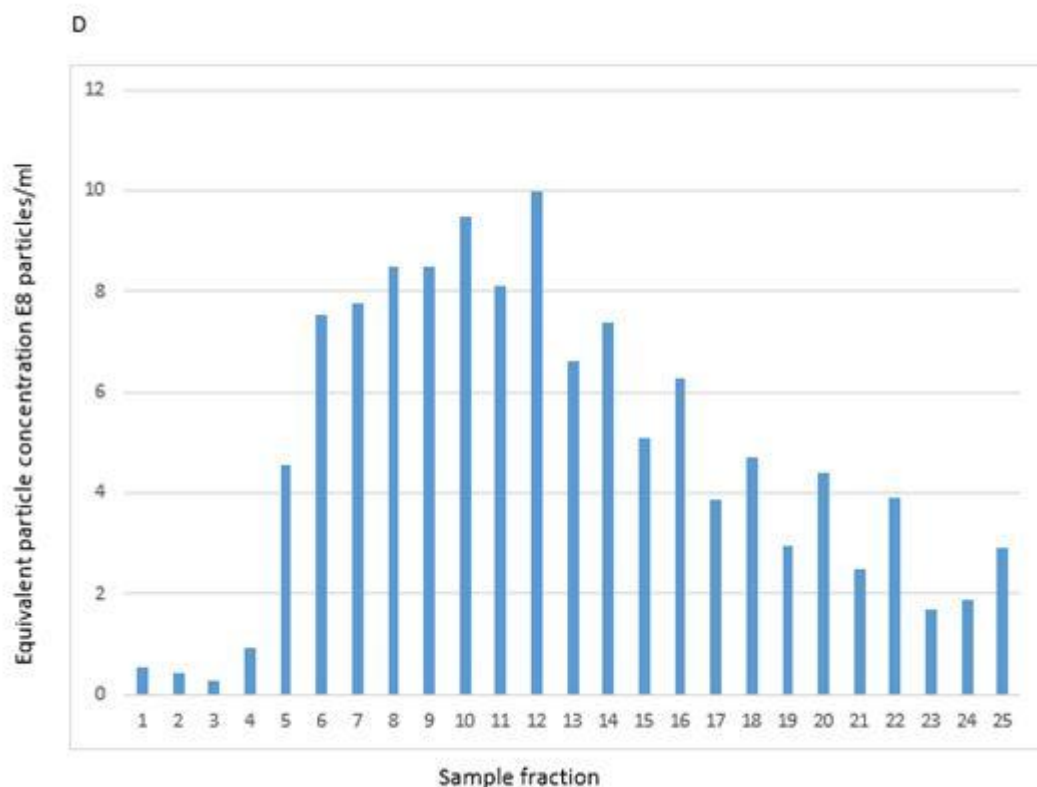


Figure 7-7 Particle size distribution and particle concentration in cells treated with dox and untreated EA.hy926 cells.

EA.hy926 cells were grown to ~80% confluence and treated with 2 μ M dox (A,B) in serum free media or untreated serum free media (C,D) for 24hr. The media was then isolated and used for NanoSight analysis.

7.3.3 The effect of serum free media on EA.hy926 cells treated with loratadine

To investigate whether the release of exosomes was an effect seen only with cardiotoxic drugs a non cardiotoxic drug, loratadine, from the same family as the anti-histamine astemizole was investigated for its exosome releasing effects. Firstly, an appropriate concentration was investigated which would give release of exosomes but would not be toxic to cells. As loratadine had none of the reported toxic effects of astemizole, initially a higher concentration range between 12.5-100 μ M was used to investigate cell viability in serum free media. However these concentrations were too toxic for EA.hy926 cells in serum free media (figure 7.8) and so a lower concentration range between 5-25 μ M was assessed. This concentration showed a concentration dependent decrease in cell viability with increasing concentrations of loratadine. A 20% decrease in cell viability compared with vehicle control was seen at 10 μ M. At higher concentrations cell viability was

negligible. However, 5 μ M loratadine showed a promising preservation of cell viability compared to DMSO control, therefore a low concentration range of between 2-10 μ M was used to assess the concentration of microparticles and potential presence of exosomes (figure 7.8).

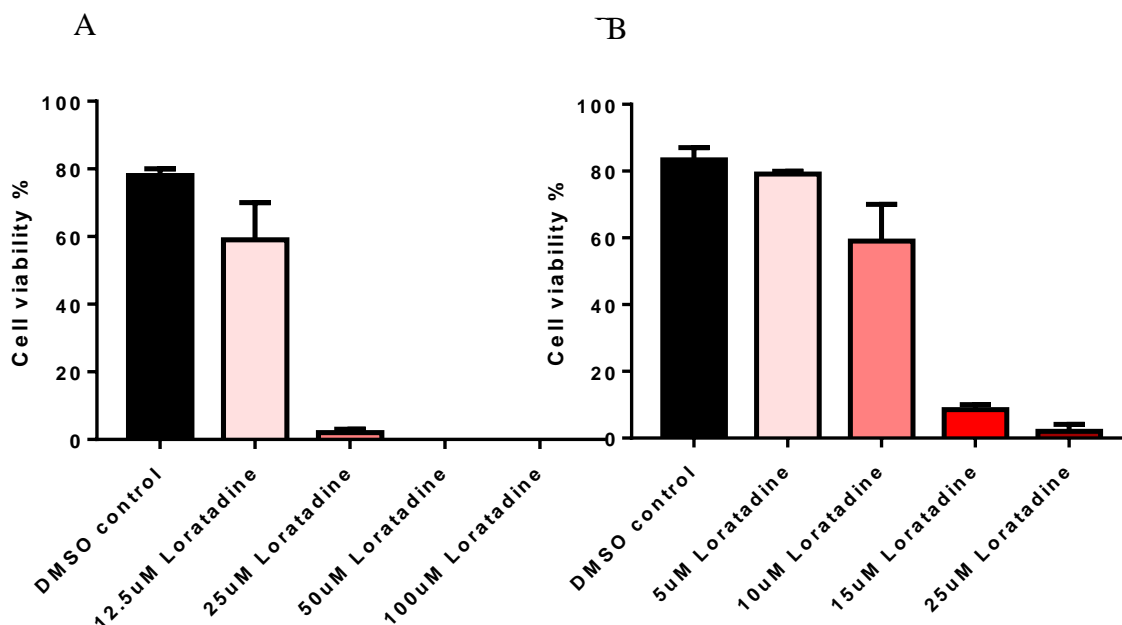


Figure 7-8 The effect of loratadine on EA.hy926 cells over different concentrations at 24hr.

EA.hy926 cells were grown to ~80% confluence and were treated with concentrations ranging from 12.5-100 μ M (A) and 5-25 μ M (B) loratadine for 24hr. Cell viability was assessed using trypan blue cell stain. Values are the mean and SEM of 3 experiments and were normalised to the DMSO control which was kept at 0.01%.

Media from cells treated with Loratadine showed microparticles levels lower than both astemizole and dox and no change in the equivalent particle concentration over increasing concentrations indicating there was no release of extra microparticles in response to loratadine. Size distribution curves showed a wide particle distribution size for all concentration apart from 10 μ M which showed a peak at particle size between 29-100nm indicating at the potential presence of exosomes at 10 μ M (Figure 7.9).

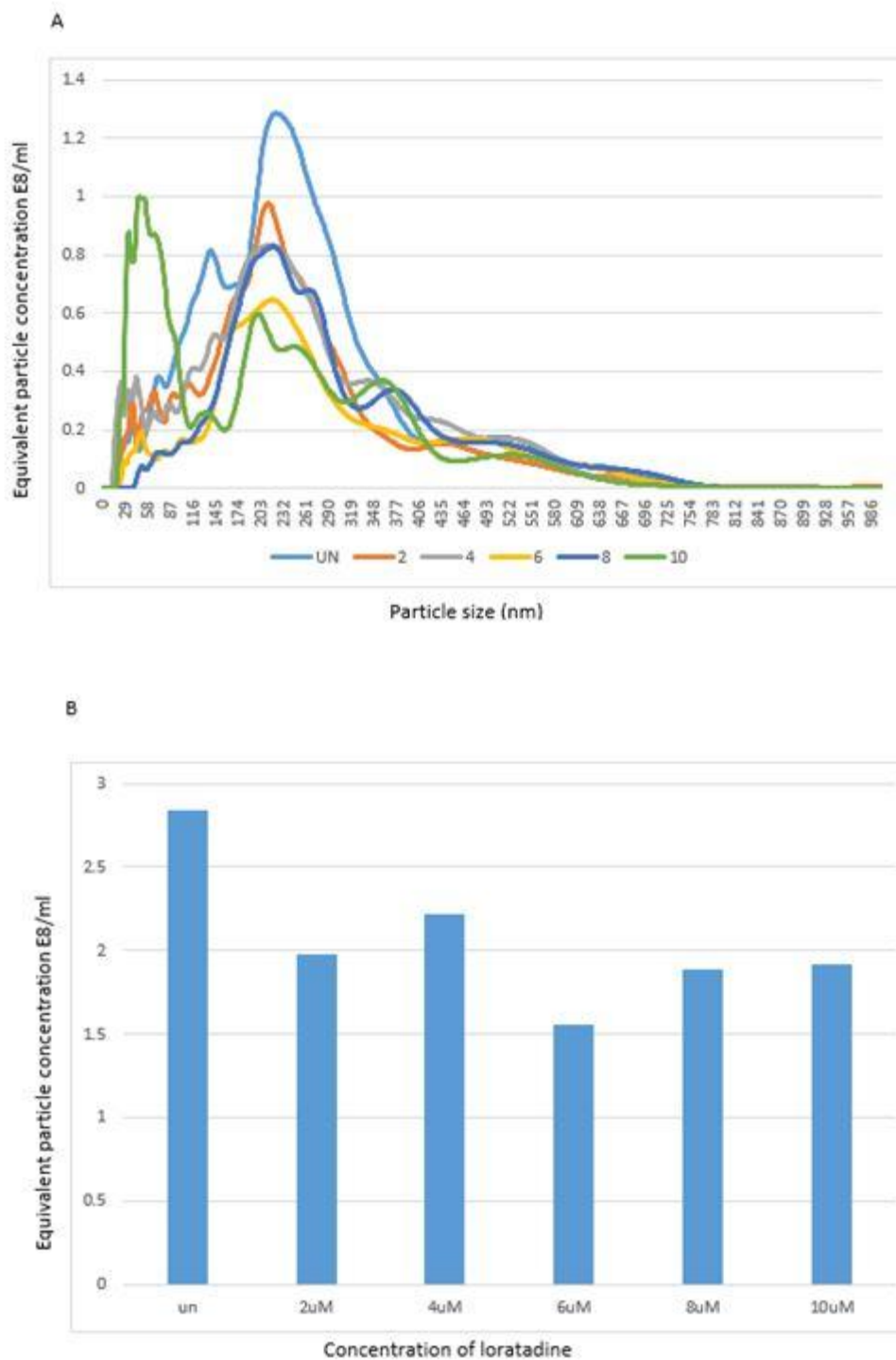


Figure 7-9 Particle size distribution (A) and particle concentration (B) in cells treated with varying concentrations of loratadine for 24hr.

EA.hy926 cells were grown to ~80% confluence after which they were treated with varying concentrations of loratadine (2, 4, 6, 8 10 μ M) for 24hr in serum free media. The media was then obtained and used for NanoSight analysis.

7.4 Discussion

The NanoSight nanotracking analysis device was found to be good predictor of microparticle size and concentration in cell culture media samples. Samples with higher microparticle concentrations generally correlated with increased exosome concentrations which were indicated by the size distribution curve peaking at a lower particle size, thus the NanoSight was a good indication of whether exosomes may be present in the sample. However it is important to note that in addition to exosomes, low density lipoproteins such as chylomicrons (100-600nm) and very low density lipoproteins (VLDL) (30-80nm) may contaminate samples and cause false positive results on the NanoSight.

Size exclusion chromatography was used to increase the purity of the cell culture media and exclude larger particles leaving exosomes. In theory this should yield a higher exosome concentration meaning there may be a lower concentration of overall microparticles but the size distribution curve would indicate more particles in the 30-100nm range. However, size exclusion chromatography column did not increase the exosomes yield as hoped. Although it has shown to perform well in isolating larger plasma proteins from plasma samples, size exclusion chromatography does have several limitations which may compromise the purity of the sample and the lower concentration of exosomes isolated. Firstly, isolation of exosomes is limited by the pore size of the matrix used. For example CL-2B Sepharose has a pore size of 70nm which means it can only isolate vesicles larger than this size. Exosomes range from 30-100nm which means smaller exosomes may not be isolated efficiently. Furthermore, due to the manual collection of sample fractions from the column there may be variability between samples due to human error. The samples are also diluted as they pass through the column often leading to a reduced, less concentrated yield of exosomes (Stranska et al., 2018).

To enhance the exosome yield from cell culture media a previous ultrafiltration step may be used to exclude larger particles. This was shown by Benedikter *et al* (2017) who showed culture media samples which had undergone ultrafiltration and size exclusion chromatography had a higher yield and EV-to-protein ratio compared to ultra-centrifugation alone (Benedikter et al., 2017). In addition to size exclusion

chromatography, other size exclusion techniques may be more efficient at separating exosomes. A new method is the membrane affinity spin column method which works on the principle that distinguishes exosomes by the biochemical features of vesicles and was shown to produce a purer sample than size exclusion chromatography alone (Stranska et al., 2018).

Astemizole increased microvesicle release in a concentration dependant way with an increase in exosomes specifically at higher concentration of 10 μ M suggesting exosomes may be involved in the pathogenesis of astemizole toxicity or at least may be used as a biomarker at sub-toxic concentrations.

Doxorubicin increased concentrations of extracellular vesicles compared to untreated cells, however this was not concentration dependent. Furthermore, the size distribution did not show an increase in exosomes. *In vivo* studies in rats have previously shown increased circulating exosomes compared with controls (Yarana et al., 2017). However due to the differences between *in vitro* and *ex vivo* models there may be variances between exosome release and concentrations. Furthermore, astemizole and dox may be eliciting toxicity through different mechanisms. For example in a study related to drug induced liver injury elicited by acetaminophen, there was no increase in exosomes *ex vivo* in rats or *in vitro* in primary human hepatocytes. However, the concentration of exosomal albumin mRNA and miR-122 were increased. Both these exosomal contents have been shown to trigger immunoligcal responses in other cell types (Holman et al., 2016). This suggests that an increase in exosome concentrations may not be a direct indicator of toxicity; rather it may be more pertinent to investigate exosomal contents which may be involved in toxicity.

A non toxic drug loratadine was used a potential control to investigate if an increase in exosomes were toxicity dependent. Loratadine showed a decrease in extracellular vesicle concentration at all concentrations, and this was not concentration dependent. However, similar to astemizole, loratadine showed a difference in subsets of extracellular vesicles with higher concentrations of the drug producing high exosome contents. Both astemizole and loratadine are H1 antihistamines which may suggest why they have a similar exosome profile albeit with different levels of exosomes.

Further work with proteomics and PCR arrays to identify changes in specific proteins and RNA may identify biomarkers of toxicity common between astemizole and dox which do not change with non-toxic drugs such as loratadine.

Chapter 8 **General discussion and future work**

The aim of this study was to investigate the role of CYP2J2 in regulating drug induced toxicity through potential EET formation and drug metabolism. An *in vitro* cell model was established in a relevant cell type to measure cellular and biochemical changes associated with astemizole drug induced toxicity. The effects of EET modulation on toxicity were also investigated. From this work, further work extends towards investigating EET formation and quantification of EETs in response to toxicity *in vitro* and uncovering future biomarkers for the detection of early toxicity.

8.1 EA.hy926 cells and human cardiac myocytes (HCM) as an *in vitro* model to study the cellular effects of drug toxicity

Both EA.hy926 cells and HCM showed classic phenotypic characteristics of endothelial cells and human cardiac myocytes respectively. However as EA.hy926 cells are a cancer cell line, cells showed increased replication. This allowed them to be easier to conduct experiments on but may have compromised their cellular integrity particularly after higher passages. Furthermore, the commercially bought HCM cell line did not beat and so did not share all functional characteristics with primary human cardiac myocytes. Gene and protein expression showed the presence of CYP2J2 and sEH, two of the most fundamental enzymes in the regulation of EET production. Gene expression was higher in HCM than in EA.hy926 cells and so allowed comparison between cell types.

Investigating cell viability in both cell types in response to varying concentrations of astemizole toxicity showed consistent changes in ATP, caspase and LDH suggesting these cells were worthy of investigating structural toxicity. Current drug testing for astemizole has tested toxicity only in the context of hERG channel inhibition (Z. Zhou et al., 1999) which does not take into context other biochemical changes. Furthermore, pharmaceutical companies usually use animal derived cells or *ex vivo* studies which do not fully represent toxicity in man. It is therefore pertinent that an *in vitro* cell model which is physiologically relevant to humans and can be manipulated for study is investigated

Due to the drawbacks of using animals for drug testing and the increased number and diversity of compounds that need to be tested in recent years, the occurrence of research

into new *in vitro* paradigms has become more pronounced, leading the way to new high-throughput and physiological accurate *in vitro* drug testing models.

To tackle the downside of the current *in vitro* cultures new 3D cultures and perfusion cultures are being developed. Current 2D test cultures, although relatively inexpensive, can result in false results when predicting tissue-specific responses due to limited cell-cell and cell-matrix interactions (Basu and Yang, 2005). Various 3D cultures have been developed to combat this. 3D cultures are multi-layer cells or aggregate clusters in a 3D scaffold (S. T. Yang et al., 2008). 3D cultures show morphology very similar to *in vivo* allowing for more accurate analysis of cell-cell interactions, cell migration and cell-morphogenesis. Overall they can repeat the *in vivo* cellular responses to drug treatment and have potential to be a superior platform for drug toxicity testing (S. T. Yang et al., 2008). Widely used static cultures do not fully correlate with conditions *in vivo* and cannot support long term cell culture as they often become contaminated. With microfluidic technology, perfusion cultures have been generated which are modified multiwell plates with the integration of microfluidic systems (Lob et al., 2007). These systems can maintain the cell culture for longer allowing for the evaluation of long term drug effects. As well as this, microchannels keep conditions more stable as cells are constantly being provided with nutrients and waste is constantly removed. In regards to toxicity screening, microfluidics can be used to generate gradients of drug concentrations (M. Wu et al., 2010). The combination of both 3D culture and microfluidics characteristics would also be desirable and various natural and synthetic hydrogels have been incorporated into microfluidic cell culture systems to support cells in 3D (Zang et al., 2012). Wen *et al* developed a microbioreactor assay that has the capability of perfusion of high density 3D cell culture. Cell proliferation is measured non-invasively and time dependently through a plate reader (Wen et al., 2010).

The types of cells used are just as important and many drug companies are veering towards a more common cell type to be used for all kinds of toxicity testing. Human derived cells are fast becoming a must for *in vitro* drug toxicity testing as they provide a more realistic interpretation of toxicity in man and express the same drug metabolising enzymes and drug transporters. In this way they overcome the limitations of animal models. Induced pluripotent stem cell derived cardiomyocytes (iPSC-CMs) are a recent breakthrough in the formation of physiologically relevant cell lines. These cells are derived from mature human cells which have been reverted back to their stem cell

phenotype before being differentiated into cardiomyocytes. The advantages of these cells are that, compared with human embryonic stem cell derived cardiomyocytes (hESC-CM), they have no ethical issues associated with their use and they allow generation of PSCs and their derivatives from any individual of choice (Davis et al., 2011). In addition to this, iPSC-CMs could also increase the safety and predictability of repeat dose testing (RDT), an integral part of the drug safety screening. Currently RDT is done *in vivo*, in rodent and non-rodent animals which commonly give false negative results, however, *in vitro* testing protocols using PSC-CMs are very complimentary to the existing RDT procedures as they allow many of the same endpoints to be analysed. These include action potential parameters, metabolic activity, and energy content and intracellular calcium handling (Laustriat et al., 2010). Already multi electrode arrays are being used to measure action potentials as well as fluorescence imaging plate reader (FLIPR) for calcium flux. High content biology has also been used for the analysis of structural cardiotoxicity as seen in fig 8.1. (Pointon et al., 2013).

Future *in vitro* testing may include a step to investigate not only early toxicity but also potential protection with protective EETs, thus allowing potential application of these protective EETs in protecting against unknown side effects of drugs.

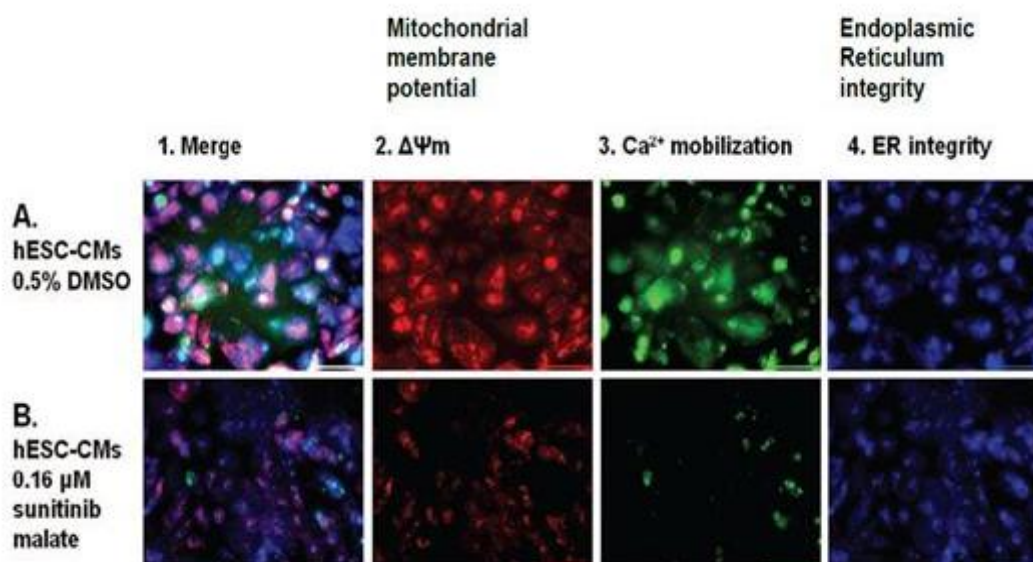


Figure 8-1 High content biology used to analyse structure and function.

High content biology used to analyse structure and function of hESC-CMs (A and B) and H9c2 cells (C and D) after treatment with 0.5% DMSO (vehicle) and 0.16 μ M Sunitinib Malate (Pointon et al., 2013).

8.2 Mechanism of CYP2J2/ EETs in regulating astemizole induced toxicity

Inhibition of EET production through either pharmacologically inhibiting CYP2J2 or PLA₂ did not exacerbate astemizole toxicity as expected. Instead, there was an increase in ATP which was also corroborated by Hoechst nuclear staining showing an increase in viable cells. This unexpected finding may therefore be the result of a non-specific cell stress response leading to increases in ATP in cells. Another conclusion may include the involvement of AA in producing a toxic intermediate compound from astemizole leading to cell death. Inhibiting AA release through pharmacological inhibition of PLA₂ may reduce cell death independent of the inhibition of EET production. MSPPOH is a non-specific CYP epoxygenase inhibitor and is able to inhibit other P450 enzymes which may lead to non-target effects. For example CYP2C9 a CYP epoxygenase present in human cardiomyocytes and endothelial cells has the ability to increase ROS production which have detrimental effects including inducing apoptosis and mitochondrial damage. As EETs and ROS, they may modulate cardiovascular disease and cardiotoxicity (Chaudhary et al., 2009).

Gene and protein expression correlated with this hypothesis with no change in expression of CYP2J2 when cells were incubated with both astemizole and CYP epoxygenase inhibitor MSPPOH compared with astemizole alone. Treatment of both EA.hy926 cells and HCM with 25µM astemizole showed a time-dependent increase in CYP2J2 gene expression compared to the vehicle treated control. This may be the result of a short incubation time of 6hr where changes in gene expression could not yet be observed. There is little evidence in the literature investigating the effect of MSPPOH on CYP epoxygenase expression in the heart however, in rat proximal tubular epithelial cells treated with high glucose to induce a diabetes-like phenotype, inhibition of EET production with MSPPOH altered protein expression of CYP epoxygenase CYP2C11 after 6hr and was this further decreased after 48hr suggesting suppression of expression is time dependent and may have different effects according to cell type (Eid et al., 2013). In response to incubation with both astemizole and the sEH inhibitor t-AUCB for 6hr there was a reduction in CYP2J2 mRNA expression in EA.hy926 cells. Expression of sEH was previously increased in response to the same treatment indicating a possible

link between the regulations of these genes, where t-AUCB increased expression of sEH yet decreased expression of CYP2J2.

Increasing the production of EETs through inhibition of sEH protected cells from cell death and preserved cell viability induced by astemizole. This protective effect was replicated when cells were treated with exogenous 11,12-EET suggesting increasing available EETs protects against toxicity *in vitro*. Gene and protein expression showed that in HCM where there was a reduction in sEH expression when cells were treated with astemizole, incubation with both astemizole and MSPPOH or t-AUCB increased sEH expression levels back to control levels. In EA.hy926 cells however the same treatment did the opposite, reducing sEH expression closer to vehicle control levels. This suggests that inhibiting CYP2J2 or sEH does affect sEH expression and may be involved in homeostatically regulating sEH expression providing further evidence that these genes may be linked.

8.3 Exosomes and future biomarkers of drug induced cardiotoxicity

Drug induced cardiotoxicity accounts for many new drugs failing in the pre-clinical and clinical phase of drug testing. Currently cardiotoxicity is monitored by cardiac imaging techniques and serum protein biomarkers such as CK, LDH and cardiac troponin. However recent advances in exosome derived miRNA molecules have shown they may be early indicators of drug cardiotoxicity (W. Wang et al., 2015). For example increased levels of plasma miR-208 were seen in rats with isoproterenol-induced myocardial injury and was shown to be better than cardiac troponin in detecting toxicity earlier (Ji et al., 2009). In addition to cardiotoxicity their use in cardiovascular disease has shown that in myocardial infarction there were increased levels of miR-1, miR-133 and miR-499 in patients within 4hr compared to healthy controls. Furthermore, miR-423-5p has been shown to be a good predictor of heart failure in patients (Tijsen et al., 2010). The work in this study has shown increased levels of exosomes compared to untreated cells and a non-cardiotoxic drug after 24 hr. This may lead to further work into investigating specific biomarkers that can detect effectively drug toxicity, possibly in animal models of toxicity.

Bibliography

Adamantidis MM, Lacroix DL, Caron JF, and Dupuis BA. (1995) Electrophysiological and arrhythmogenic effects of the histamine type 1-receptor antagonist astemizole on rabbit Purkinje fibers: clinical relevance. *Journal of Cardiovascular Pharmacology* 26:319-327.

Akhnokh MK, Yang FH, Samokhvalov V, Jamieson KL, Cho WJ, Wagg C, Takawale A, Wang X, Lopaschuk GD, and Hammock BD. (2016) Inhibition of soluble epoxide hydrolase limits mitochondrial damage and preserves function following ischemic injury. *Frontiers in Pharmacology* 7.

Alghamdi AH. (2008) Square-wave adsorptive stripping voltammetric determination of an antihistamine drug astemizole. *Chemical Papers* 62:339-344.

Alsaad AM, Zordoky BN, Tse MM, and El-Kadi AO. (2013) Role of cytochrome P450-mediated arachidonic acid metabolites in the pathogenesis of cardiac hypertrophy. *Drug Metabolism Reviews* 45:173-195.

Alsaad AM, Zordoky BN, El-Sherbeni AA, and El-Kadi AO. (2012) Chronic doxorubicin cardiotoxicity modulates cardiac cytochrome P450-mediated arachidonic acid metabolism in rats. *Drug Metabolism and Disposition* 40:2126-2135.

Alter P, Herzum M, Soufi M, Schaefer J, and Maisch B. (2006) Cardiotoxicity of 5-fluorouracil. *Cardiovascular & Hematological Agents in Medicinal Chemistry (Formerly Current Medicinal Chemistry-Cardiovascular & Hematological Agents)* 4:1-5.

Althurwi HN, Tse MM, Abdelhamid G, Zordoky BN, Hammock BD, and El-Kadi AO. (2013) Soluble epoxide hydrolase inhibitor, TUPS, protects against isoprenaline-induced cardiac hypertrophy. *British Journal of Pharmacology* 168:1794-1807.

Anandan S, Webb HK, Chen D, Wang YJ, Aavula BR, Cases S, Cheng Y, Do ZN, Mehra U, and Tran V. (2011) 1-(1-Acetyl-piperidin-4-yl)-3-adamantan-1-yl-urea (AR9281) as a potent, selective, and orally available soluble epoxide hydrolase inhibitor with efficacy in rodent models of hypertension and dysglycemia. *Bioorganic and Medicinal Chemistry Letters* 21:983-988.

Andriantsitohaina R, Gaceb A, Vergori L, and Martínez MC. (2012) Microparticles as regulators of cardiovascular inflammation. *Trends in Cardiovascular Medicine* 22:88-92.

Anwar-Mohamed A, El-Sherbeni AA, Kim SH, Althurwi HN, Zordoky BN, and El-Kadi AO. (2012) Acute arsenic toxicity alters cytochrome P450 and soluble epoxide

hydrolase and their associated arachidonic acid metabolism in C57Bl/6 mouse heart. *Xenobiotica* 42:1235-1247.

Arnold WR, Baylon JL, Tajkhorshid E, and Das A. (2017) Arachidonic Acid Metabolism by Human Cardiovascular CYP2J2 is Modulated by Doxorubicin. *Biochemistry (N Y)* 56:6700-6712.

Askari AA, Thomson S, Edin ML, Lih FB, Zeldin DC, and Bishop-Bailey D. (2014) Basal and inducible anti-inflammatory epoxygenase activity in endothelial cells. *Biochemical and Biophysical Research Communications* 446:633-637.

Barau C, Ghaleh B, Berdeaux A, and Morin D. (2015) Cytochrome P450 and myocardial ischemia: potential pharmacological implication for cardioprotection. *Fundamental and Clinical Pharmacology* 29:1-9.

Baroody F and Naclerio R. (2000) Antiallergic effects of H1- receptor antagonists. *Allergy* 55:17-27.

Basu S and Yang S. (2005) Astrocyte growth and glial cell line-derived neurotrophic factor secretion in three-dimensional polyethylene terephthalate fibrous matrices. *Tissue Engineering* 11:940-952.

Belham M, Kruger A, Mephram S, Faganello G, and Pritchard C. (2007) Monitoring left ventricular function in adults receiving anthracycline- containing chemotherapy. *European Journal of Heart Failure* 9:409-414.

Benedikter BJ, Bouwman FG, Vajen T, Heinzmann AC, Grauls G, Mariman EC, Wouters EF, Savelkoul PH, Lopez-Iglesias C, and Koenen RR. (2017) Ultrafiltration combined with size exclusion chromatography efficiently isolates extracellular vesicles from cell culture media for compositional and functional studies. *Scientific Reports* 7:15297.

Berezin A, Zulli A, Kerrigan S, Petrovic D, and Kruzliak P. (2015) Predictive role of circulating endothelial-derived microparticles in cardiovascular diseases. *Clinical Biochemistry* 48:562-568.

Berlin DS, Sangkuhl K, Klein TE, and Altman RB. (2011) PharmGKB summary: cytochrome P450, family 2, subfamily J, polypeptide 2: CYP2J2. *Pharmacogenetics and Genomics* 21:308-311.

Bernstrom K, Kayganich K, Murphy RC, and Fitzpatrick FA. (1992) Incorporation and distribution of epoxyeicosatrienoic acids into cellular phospholipids. *Journal of Biological Chemistry* 267:3686-3690.

Bertrand- Thiebault C, Ferrari L, Bouterin- Falson O, Kockx M, Desquand- Billiard S, Fichelle J, Nottin R, Renaud J, Batt A, and Visvikis S. (2004) Cytochromes P450 are differently expressed in normal and varicose human saphenous veins: linkage with varicosis. *Clinical and Experimental Pharmacology and Physiology* 31:295-301.

- Boriachek K, Islam MN, Möller A, Salomon C, Nguyen N, Hossain MSA, Yamauchi Y, and Shiddiky MJ. (2018) Biological functions and current advances in isolation and detection strategies for exosome nanovesicles. *Small* 14:1702153.
- Bouïs D, Hospers GA, Meijer C, Molema G, and Mulder NH. (2001) Endothelium in vitro: a review of human vascular endothelial cell lines for blood vessel-related research. *Angiogenesis* 4:91-102.
- Bouma M, Rogier E, Verthier N, Labarre C, and Feldmann G. (1989) Further cellular investigation of the human hepatoblastoma-derived cell line HepG2: morphology and immunocytochemical studies of hepatic-secreted proteins. *In Vitro Cellular & Developmental Biology* 25:267-275.
- Brand-Schieber E, Falck J, and Schwartzman M. (2000) Selective inhibition of arachidonic acid epoxidation in vivo. *Journal of Physiology and Pharmacology* 51.
- Brutsaert DL. (2003) Cardiac endothelial-myocardial signaling: its role in cardiac growth, contractile performance, and rhythmicity. *Physiology Reviews* 83:59-115.
- Bylund J, Bylund M, and Oliw EH. (2001) cDNA cloning and expression of CYP4F12, a novel human cytochrome P450. *Biochemical and Biophysical Research Communications* 280:892-897.
- Bystrom J, Wray JA, Sugden MC, Holness MJ, Swales KE, Warner TD, Edin ML, Zeldin DC, Gilroy DW, and Bishop-Bailey D. (2011) Endogenous epoxygenases are modulators of monocyte/macrophage activity. *PLoS One* 6:e26591.
- Campbell WB and Fleming I. (2010) Epoxyeicosatrienoic acids and endothelium-dependent responses. *Pflügers Archiv-European Journal of Physiology* 459:881-895.
- Campbell WB, Gebremedhin D, Pratt PF, and Harder DR. (1996) Identification of epoxyeicosatrienoic acids as endothelium-derived hyperpolarizing factors. *Circulation Research* 78:415-423.
- Cappetta D, Esposito G, Piegari E, Russo R, Ciuffreda LP, Rivellino A, Berrino L, Rossi F, De Angelis A, and Urbanek K. (2016) SIRT1 activation attenuates diastolic dysfunction by reducing cardiac fibrosis in a model of anthracycline cardiomyopathy. *International Journal of Cardiology* 205:99-110.
- Chatterjee K, Zhang J, Honbo N, and Karliner JS. (2010) Doxorubicin cardiomyopathy. *Cardiology* 115:155-162.
- Chaudhary KR, Batchu SN, and Seubert JM. (2009) Cytochrome P450 enzymes and the heart. *IUBMB Life* 61:954-960.
- Chen JK, Wang DW, Falck JR, Capdevila J, and Harris RC. (1999) Transfection of an active cytochrome P450 arachidonic acid epoxygenase indicates that 14,15-epoxyeicosatrienoic acid functions as an intracellular second messenger in response to epidermal growth factor. *Journal of Biological Chemistry* 274:4764-4769.

- Chintalgattu V, Rees ML, Culver JC, Goel A, Jiffar T, Zhang J, Dunner K, Pati S, Bankson JA, and Pasqualini R. (2013) Coronary microvascular pericytes are the cellular target of sunitinib malate-induced cardiotoxicity. *Science Translational Medicine* 5:187ra69-187ra69.
- Chu TF, Rupnick MA, Kerkela R, Dallabrida SM, Zurakowski D, Nguyen L, Woulfe K, Pravda E, Cassiola F, and Desai J. (2007) Cardiotoxicity associated with tyrosine kinase inhibitor sunitinib. *The Lancet* 370:2011-2019.
- Cove-Smith L, Woodhouse N, Hargreaves A, Kirk J, Smith S, Price SA, Galvin M, Betts CJ, Brocklehurst S, Backen A, Radford J, Linton K, Roberts RA, Schmitt M, Dive C, Tugwood JD, Hockings PD, and Mellor HR. (2014) An integrated characterization of serological, pathological, and functional events in doxorubicin-induced cardiotoxicity. *Toxicological Sciences* 140:3-15.
- Cui G, Chen H, Cui W, Guo X, Fang J, Liu A, Chen Y, and Lee SMY. (2016) FGF2 prevents sunitinib-induced cardiotoxicity in zebrafish and cardiomyoblast H9c2 cells. *Cardiovascular Toxicology* 16:46-53.
- Cui PH, Lee AC, Zhou F, and Murray M. (2010) Impaired transactivation of the human CYP2J2 arachidonic acid epoxygenase gene in HepG2 cells subjected to nitrate stress. *British Journal of Pharmacology* 159:1440-1449.
- Dai M, Wu L, He Z, Zhang S, Chen C, Xu X, Wang P, Gruzdev A, Zeldin DC, and Wang DW. (2015) Epoxyeicosatrienoic Acids Regulate Macrophage Polarization and Prevent LPS- Induced Cardiac Dysfunction. *Journal of Cellular Physiology* 230:2108-2119.
- Davis RP, van den Berg, Cathelijne W, Casini S, Braam SR, and Mummery CL. (2011) Pluripotent stem cell models of cardiac disease and their implication for drug discovery and development. *Trends in Molecular Medicine* 17:475-484.
- De Angelis A, Urbanek K, Cappetta D, Piegari E, Ciuffreda LP, Rivellino A, Russo R, Esposito G, Rossi F, and Berrino L. (2016) Doxorubicin cardiotoxicity and target cells: a broader perspective. *Cardio-Oncology* 2:2.
- De Angelis A, Piegari E, Cappetta D, Marino L, Filippelli A, Berrino L, Ferreira-Martins J, Zheng H, Hosoda T, Rota M, Urbanek K, Kajstura J, Leri A, Rossi F, and Anversa P. (2010) Anthracycline cardiomyopathy is mediated by depletion of the cardiac stem cell pool and is rescued by restoration of progenitor cell function. *Circulation* 121:276-292.
- Deb A and Ubil E. (2014) Cardiac fibroblast in development and wound healing. *Journal of Molecular Cell Cardiology* 70:47-55.
- Delozier TC, Kissling GE, Coulter SJ, Dai D, Foley JF, Bradbury JA, Murphy E, Steenbergen C, Zeldin DC, and Goldstein JA. (2007) Detection of human CYP2C8, CYP2C9, and CYP2J2 in cardiovascular tissues. *Drug Metabolism and Disposition* 35:682-688.

- Deng Y, Edin ML, Theken KN, Schuck RN, Flake GP, Kannon MA, DeGraff LM, Lih FB, Foley J, Bradbury JA, Graves JP, Tomer KB, Falck JR, Zeldin DC, and Lee CR. (2011) Endothelial CYP epoxygenase overexpression and soluble epoxide hydrolase disruption attenuate acute vascular inflammatory responses in mice. *FASEB Journal* 25:703-713.
- Dhanasekaran A, Gruenloh SK, Buonaccorsi JN, Zhang R, Gross GJ, Falck JR, Patel PK, Jacobs ER, and Medhora M. (2008) Multiple antiapoptotic targets of the PI3K/Akt survival pathway are activated by epoxyeicosatrienoic acids to protect cardiomyocytes from hypoxia/anoxia. *American Journal of Physiology- Heart and Circulatory Physiology* 294:H724-35.
- Dimitropoulou C, West L, Field MB, White RE, Reddy LM, Falck JR, and Imig JD. (2007) Protein phosphatase 2A and Ca²⁺-activated K⁺ channels contribute to 11, 12-epoxyeicosatrienoic acid analog mediated mesenteric arterial relaxation. *Prostaglandins Other Lipid Mediators* 83:50-61.
- Dixon K, Thanavaro J, Thais A, and Lavin MA. (2013) Amiodarone surveillance in primary care. *The Journal for Nurse Practitioners* 9:46-54.
- Doherty KR, Wappel RL, Talbert DR, Trusk PB, Moran DM, Kramer JW, Brown AM, Shell SA, and Bacus S. (2013) Multi-parameter in vitro toxicity testing of crizotinib, sunitinib, erlotinib, and nilotinib in human cardiomyocytes. *Toxicology and Applied Pharmacology* 272:245-255.
- Dragovic RA, Gardiner C, Brooks AS, Tannetta DS, Ferguson DJ, Hole P, Carr B, Redman CW, Harris AL, and Dobson PJ. (2011) Sizing and phenotyping of cellular vesicles using Nanoparticle Tracking Analysis. *Nanomedicine: Nanotechnology, Biology and Medicine* 7:780-788.
- Dutheil F, Dauchy S, Diry M, Sazdovitch V, Cloarec O, Mellottee L, Bieche I, Ingelman-Sundberg M, Flinois JP, de Waziers I, Beaune P, Decleves X, Duyckaerts C, and Lorient MA. (2009) Xenobiotic-metabolizing enzymes and transporters in the normal human brain: regional and cellular mapping as a basis for putative roles in cerebral function. *Drug Metabolism and Disposition* 37:1528-1538.
- Edgell CJ, McDonald CC, and Graham JB. (1983) Permanent cell line expressing human factor VIII-related antigen established by hybridization. *PNAS Journal* 80:3734-3737.
- Edin ML, Wang Z, Bradbury JA, Graves JP, Lih FB, DeGraff LM, Foley JF, Torphy R, Ronnekleiv OK, Tomer KB, Lee CR, and Zeldin DC. (2011) Endothelial expression of human cytochrome P450 epoxygenase CYP2C8 increases susceptibility to ischemia-reperfusion injury in isolated mouse heart. *FASEB Journal* 25:3436-3447.
- Eid S, Maalouf R, Jaffa AA, Nassif J, Hamdy A, Rashid A, Ziyadeh FN, and Eid AA. (2013) 20-HETE and EETs in diabetic nephropathy: a novel mechanistic pathway. *PLoS One* 8:e70029.

- El-Kadi AO and Zordoky BN. (2008) Modulation of cardiac and hepatic cytochrome P450 enzymes during heart failure. *Current Drug Metabolism* 9:122-128.
- El-Sherbeni AA and El-Kadi AO. (2016) Repurposing resveratrol and fluconazole to modulate human cytochrome P450-mediated arachidonic acid metabolism. *Molecular Pharmaceutics* 13:1278-1288.
- Enayetallah AE, French RA, Thibodeau MS, and Grant DF. (2004) Distribution of soluble epoxide hydrolase and of cytochrome P450 2C8, 2C9, and 2J2 in human tissues. *Journal of Histochemistry and Cytochemistry* 52:447-454.
- Evangelista EA, Lemaitre RN, Sotoodehnia N, Gharib SA, and Totah RA. (2018) CYP2J2 Expression in Adult Ventricular Myocytes Protects Against Reactive Oxygen Species Toxicity. *Drug Metabolism and Disposition* 46:380-386.
- Evangelista EA, Kaspera R, Mokadam NA, Jones JP,3rd, and Totah RA. (2013) Activity, inhibition, and induction of cytochrome P450 2J2 in adult human primary cardiomyocytes. *Drug Metabolism and Disposition* 41:2087-2094.
- Fava C, Montagnana M, Almgren P, Hedblad B, Engstrom G, Berglund G, Minuz P, and Melander O. (2010) The common functional polymorphism -50G>T of the CYP2J2 gene is not associated with ischemic coronary and cerebrovascular events in an urban-based sample of Swedes. *Journal of Hypertension* 28:294-299.
- Feenstra J, Grobbee DE, Remme WJ, and Stricker BHC. (1999) Drug-induced heart failure. *Journal of American College of Cardiology* 33:1152-1162.
- Fellahi S, El Harrak M, Kuhn JH, Sebbar G, Khataby K, Fihri OF, El Houadfi M, and Ennaji MM. (2016) Comparison of SYBR green I real-time RT-PCR with conventional agarose gel-based RT-PCR for the diagnosis of infectious bronchitis virus infection in chickens in Morocco. *BMC Research Notes* 9:231.
- Fisslthaler B, Popp R, Kiss L, Potente M, Harder DR, Fleming I, and Busse R. (1999) Cytochrome P450 2C is an EDHF synthase in coronary arteries. *Nature* 401:493-497.
- Fleming I. (2001) Cytochrome p450 and vascular homeostasis. *Circulatory Research* 89:753-762.
- Fu Z, Guo J, Jing L, Li R, Zhang T, and Peng S. (2010) Enhanced toxicity and ROS generation by doxorubicin in primary cultures of cardiomyocytes from neonatal metallothionein-I/II null mice. *Toxicology in Vitro* 24:1584-1591.
- Fulton D, McGiff J, Wolin M, Kaminski P, and Quilley J. (1997) Evidence against a cytochrome P450-derived reactive oxygen species as the mediator of the nitric oxide-independent vasodilator effect of bradykinin in the perfused heart of the rat. *Journal of Pharmacological Experimental Therapeutics* 280:702-709.
- Gaedigk A, Baker DW, Totah RA, Gaedigk R, Pearce RE, Vyhldal CA, Zeldin DC, and Leeder JS. (2006) Variability of CYP2J2 expression in human fetal tissues. *Journal of Pharmacological Experimental Therapeutics* 319:523-532.

Gámez-Valero A, Monguió-Tortajada M, Carreras-Planella L, Beyer K, and Borràs FE. (2016) Size-Exclusion Chromatography-based isolation minimally alters Extracellular Vesicles' characteristics compared to precipitating agents. *Scientific Reports* 6:33641.

Gammella E, Maccarinelli F, Buratti P, Recalcati S, and Cairo G. (2014) The role of iron in anthracycline cardiotoxicity. *Frontiers in Pharmacology* 5:25.

Garscha U, Romp E, Pace S, Rossi A, Temml V, Schuster D, König S, Gerstmeier J, Liening S, and Werner M. (2017) Pharmacological profile and efficiency in vivo of diflapolin, the first dual inhibitor of 5-lipoxygenase-activating protein and soluble epoxide hydrolase. *Scientific Reports* 7:9398.

Gerets H, Tilmant K, Gerin B, Chanteux H, Depelchin B, Dhalluin S, and Atienzar F. (2012) Characterization of primary human hepatocytes, HepG2 cells, and HepaRG cells at the mRNA level and CYP activity in response to inducers and their predictivity for the detection of human hepatotoxins. *Cellular Biology Toxicology* 28:69-87.

Gonzalez FJ, Fang Z, and Ma X. (2015) Transgenic mice and metabolomics for study of hepatic xenobiotic metabolism and toxicity. *Expert Opinion on Drug Metabolism & Toxicology* 11:869-881.

Graves JP, Edin ML, Bradbury JA, Gruzdev A, Cheng J, Lih FB, Masinde TA, Qu W, Clayton NP, Morrison JP, Tomer KB, and Zeldin DC. (2013) Characterization of four new mouse cytochrome P450 enzymes of the CYP2J subfamily. *Drug Metabolism and Disposition* 41:763-773.

Gross GJ, Gauthier KM, Moore J, Falck JR, Hammock BD, Campbell WB, and Nithipatikom K. (2008) Effects of the selective EET antagonist, 14, 15-EEZE, on cardioprotection produced by exogenous or endogenous EETs in the canine heart. *American Journal of Physiology-Heart and Circulatory Physiology* 294:H2838-H2844.

Gross GJ and Nithipatikom K. (2009) Soluble epoxide hydrolase: a new target for cardioprotection. *Current Opinion in the Investigation of Drugs* 10:253-258.

Gui Y, Yang T, Liu Q, Liao C, Chen J, Wang Y, Hu J, and Xu D. (2017) Soluble epoxide hydrolase inhibitors, t-AUCB, regulated microRNA-1 and its target genes in myocardial infarction mice. *Oncotarget* 8:94635.

Hao Z and Sadek I. (2016) Sunitinib: the antiangiogenic effects and beyond. *Oncotargets and Therapy* 9:5495-5505.

Harmon SD, Fang X, Kaduce TL, Hu S, Gopal VR, Falck JR, and Spector AA. (2006) Oxygenation of ω -3 fatty acids by human cytochrome P450 4F3B: Effect on 20-hydroxyeicosatetraenoic acid production. *Prostaglandins, Leukotrienes and Essential Fatty Acids* 75:169-177.

Hartung T and Daston G. (2009) Are in vitro tests suitable for regulatory use? *Toxicological Sciences* 111:233-237.

Heijman J, Heusch G, and Dobrev D. (2013) Pleiotropic effects of antiarrhythmic agents: dronedarone in the treatment of atrial fibrillation. *Clinical Medicine Insights. Cardiology* 7:127.

Hoffmann MM, Bugert P, Seelhorst U, Wellnitz B, Winkelmann BR, Boehm BO, and Marz W. (2007) The -50G>T polymorphism in the promoter of the CYP2J2 gene in coronary heart disease: the Ludwigshafen Risk and Cardiovascular Health study. *Clinical Chemistry* 53:539-540.

Holman NS, Mosedale M, Wolf KK, LeCluyse EL, and Watkins PB. (2016) Subtoxic alterations in hepatocyte-derived exosomes: an early step in drug-induced liver injury? *Toxicological Sciences* 151:365-375.

Hoopes SL, Garcia V, Edin ML, Schwartzman ML, and Zeldin DC. (2015) Vascular actions of 20-HETE. *Prostaglandins Other Lipid Mediators* 120:9-16.

Huang H, Chang H, Xu Y, Reddy DS, Du J, Zhou Y, Dong Z, Falck JR, and Wang M. (2006) Epoxyeicosatrienoic acid inhibition alters renal hemodynamics during pregnancy. *Experimental Biological Medicine* 231:1744-1752.

Hwang SH, Weckler AT, Zhang G, Morisseau C, Nguyen LV, Fu SH, and Hammock BD. (2013) Synthesis and biological evaluation of sorafenib-and regorafenib-like sEH inhibitors. *Bioorganic and Medicinal Chemistry Letters* 23:3732-3737.

Ichikawa Y, Ghanefar M, Bayeva M, Wu R, Khechaduri A, Prasad SVN, Mutharasan RK, Naik TJ, and Ardehali H. (2014) Cardiotoxicity of doxorubicin is mediated through mitochondrial iron accumulation. *Journal of Clinical Investigation* 124:617-630.

Imig J. (2016) Epoxyeicosatrienoic acids and 20-hydroxyeicosatetraenoic acid on endothelial and vascular function, in *Advances in Pharmacology*(Anonymous) pp 105-141, Elsevier.

Imig JD and Hammock BD. (2009) Soluble epoxide hydrolase as a therapeutic target for cardiovascular diseases. *Nature Reviews Drug Discovery* 8:794.

Imig JD, Zhao X, Falck JR, Wei S, and Capdevila JH. (2001) Enhanced renal microvascular reactivity to angiotensin II in hypertension is ameliorated by the sulfonimide analog of 11, 12-epoxyeicosatrienoic acid. *Journal of Hypertension* 19:983-992.

Isomoto S, Kawakami A, Arakaki T, Yamashita S, Yano K, and Ono K. (2006) Effects of antiarrhythmic drugs on apoptotic pathways in H9c2 cardiac cells. *Journal of Pharmacological Sciences* 101:318-324.

Iyer A, Kauter K, Alam MA, Hwang SH, Morisseau C, Hammock BD, and Brown L. (2012) Pharmacological inhibition of soluble epoxide hydrolase ameliorates diet-induced metabolic syndrome in rats. *Experimental Diabetes Research* 2012:758614.

Jenkins CM, Cedars A, and Gross RW. (2009) Eicosanoid signalling pathways in the heart. *Cardiovascular Research* 82:240-249.

- Ji X, Takahashi R, Hiura Y, Hirokawa G, Fukushima Y, and Iwai N. (2009) Plasma miR-208 as a biomarker of myocardial injury. *Clinical Chemistry* 55:1944-1949.
- Jiang JG, Chen CL, Card JW, Yang S, Chen JX, Fu XN, Ning YG, Xiao X, Zeldin DC, and Wang DW. (2005) Cytochrome P450 2J2 promotes the neoplastic phenotype of carcinoma cells and is up-regulated in human tumors. *Cancer Research* 65:4707-4715.
- Jie Z, Hong K, Jianhong T, Biao C, Yongmei Z, and Jingchuan L. (2010) Haplotype analysis of the CYP2J2 gene associated with myocardial infarction in a Chinese Han population. *Cellular and Biochemical Function* 28:435-439.
- Kang W, Elitzer S, Noh K, Bednarek T, and Weiss M. (2011) Myocardial pharmacokinetics of ebastine, a substrate for cytochrome P450 2J, in rat isolated heart. *British Journal of Pharmacology* 163:1733-1739.
- Karakikes I, Ameen M, Termglinchan V, and Wu JC. (2015) Human induced pluripotent stem cell-derived cardiomyocytes: insights into molecular, cellular, and functional phenotypes. *Circulatory Research* 117:80-88.
- Karkhanis A, Tram NDT, and Chan ECY. (2017) Effects of dronedarone, amiodarone and their active metabolites on sequential metabolism of arachidonic acid to epoxyeicosatrienoic and dihydroxyeicosatrienoic acids. *Biochemical Pharmacology* 146:188-198.
- Karkhanis A, Lam HY, Venkatesan G, Koh SK, Chai CLL, Zhou L, Hong Y, Kojodjojo P, and Chan ECY. (2016) Multiple modes of inhibition of human cytochrome P450 2J2 by dronedarone, amiodarone and their active metabolites. *Biochemical Pharmacology* 107:67-80.
- Kaspera R, Kirby BJ, Sahele T, Collier AC, Kharasch ED, Unadkat JD, and Totah RA. (2014) Investigating the contribution of CYP2J2 to ritonavir metabolism in vitro and in vivo. *Biochemical Pharmacology* 91:109-118.
- Ke Q, Xiao YF, Bradbury JA, Graves JP, Degraff LM, Seubert JM, and Zeldin DC. (2007) Electrophysiological properties of cardiomyocytes isolated from CYP2J2 transgenic mice. *Molecular Pharmacology* 72:1063-1073.
- Kerkela R, Woulfe KC, Durand J, Vagnozzi R, Kramer D, Chu TF, Beahm C, Chen MH, and Force T. (2009) Sunitinib- induced cardiotoxicity is mediated by off- target inhibition of AMP- activated protein kinase. *Clinical and Translational Science* 2:15-25.
- Kimes B and Brandt B. (1976) Properties of a clonal muscle cell line from rat heart. *Experimental Cell Research* 98:367-381.
- King LM, Ma J, Srettabunjong S, Graves J, Bradbury JA, Li L, Spiecker M, Liao JK, Mohrenweiser H, and Zeldin DC. (2002) Cloning of CYP2J2 gene and identification of functional polymorphisms. *Molecular Pharmacology* 61:840-852.

Knight ZA and Shokat KM. (2007) Chemical genetics: where genetics and pharmacology meet. *Cell* 128:425-430.

Kuwabara Y, Ono K, Horie T, Nishi H, Nagao K, Kinoshita M, Watanabe S, Baba O, Kojima Y, and Shizuta S. (2011) Increased microRNA-1 and microRNA-133a levels in serum of patients with cardiovascular disease indicate myocardial damage. *Circulation: Genomic and Precision Medicine* 4:446-454.

Larsen BT, Campbell WB, and Gutterman DD. (2007) Beyond vasodilatation: non-vasomotor roles of epoxyeicosatrienoic acids in the cardiovascular system. *Trends in Pharmacological Sciences* 28:32-38.

Larsen BT, Miura H, Hatoum OA, Campbell WB, Hammock BD, Zeldin DC, Falck JR, and Gutterman DD. (2006) Epoxyeicosatrienoic and dihydroxyeicosatrienoic acids dilate human coronary arterioles via BK(Ca) channels: implications for soluble epoxide hydrolase inhibition. *American Journal of Physiology- Heart Circulatory Physiology* 290:H491-9.

Laustriat D, Gide J, and Peschanski M. (2010) Human pluripotent stem cells in drug discovery and predictive toxicology. *Biochemical Society Transactions* 38:1051.

Lavery H, Benson C, Cartwright E, Cross M, Garland C, Hammond T, Holloway C, McMahon N, Milligan J, and Park B. (2011) How can we improve our understanding of cardiovascular safety liabilities to develop safer medicines? *British Journal of Pharmacology* 163:675-693.

Lazaar AL, Yang L, Boardley RL, Goyal NS, Robertson J, Baldwin SJ, Newby DE, Wilkinson IB, Tal- Singer R, and Mayer RJ. (2016) Pharmacokinetics, pharmacodynamics and adverse event profile of GSK2256294, a novel soluble epoxide hydrolase inhibitor. *British Journal of Clinical Pharmacology*.

Lee J, Kim D, Seo J, Lee H, Oh J, Shin H, Yoon S, and Kim C. (2008) Assessment of General and Cardiac Toxicities of Astemizole in Male Cynomolgus Monkeys: Serum Biochemistry and Action Potential Duration. *Toxicological Research* 24:289-295.

Lee AC and Murray M. (2010) Up-regulation of human CYP2J2 in HepG2 cells by butylated hydroxyanisole is mediated by c-Jun and Nrf2. *Molecular Pharmacology* 77:987-994.

Lee CA, Neul D, Clouser-Roche A, Dalvie D, Wester MR, Jiang Y, Jones JP,3rd, Freiwald S, Zientek M, and Totah RA. (2010) Identification of novel substrates for human cytochrome P450 2J2. *Drug Metabolism and Disposition* 38:347-356.

Lee SS, Jeong HE, Liu KH, Ryu JY, Moon T, Yoon CN, Oh SJ, Yun CH, and Shin JG. (2005) Identification and functional characterization of novel CYP2J2 variants: G312R variant causes loss of enzyme catalytic activity. *Pharmacogenet Genomics* 15:105-113.

Lefebvre RA, Van Peer A, and Woestenborghs R. (1997) Influence of itraconazole on the pharmacokinetics and electrocardiographic effects of astemizole. *British Journal of Clinical Pharmacology* 43:319-322.

- Li N, Liu J, Timofeyev V, Qiu H, Hwang SH, Tuteja D, Lu L, Yang J, Mochida H, and Low R. (2009) Beneficial effects of soluble epoxide hydrolase inhibitors in myocardial infarction model: Insight gained using metabolomic approaches. *Journal of Molecular Cell Cardiology* 47:835-845.
- Licata S, Saponiero A, Mordente A, and Minotti G. (2000) Doxorubicin metabolism and toxicity in human myocardium: role of cytoplasmic deglycosidation and carbonyl reduction. *Chemical Research in Toxicology* 13:414-420.
- Lindauer A, Di Gion P, Kanefendt F, Tomalik-Scharte D, Kinzig M, Rodamer M, Dodos F, Sörgel F, Fuhr U, and Jaehde U. (2010) Pharmacokinetic/pharmacodynamic modeling of biomarker response to sunitinib in healthy volunteers. *Clinical Pharmacology & Therapeutics* 87:601-608.
- Liu J, Zheng H, Tang M, Ryu Y, and Wang X. (2008) A therapeutic dose of doxorubicin activates ubiquitin-proteasome system-mediated proteolysis by acting on both the ubiquitination apparatus and proteasome. *American Journal of Physiology-Heart and Circulatory Physiology* 295:H2541-H2550.
- Liu L, Puri N, Raffaele M, Schragenheim J, Singh SP, Bradbury JA, Bellner L, Vanella L, Zeldin DC, and Cao J. (2018) Ablation of Soluble Epoxide Hydrolase reprogram white fat to beige-like fat through an increase in mitochondrial integrity, HO-1-adiponectin in vitro and in vivo. *Prostaglandins and Other Lipid Mediators*.
- Liu JY, Park SH, Morisseau C, Hwang SH, Hammock BD, and Weiss RH. (2009) Sorafenib has soluble epoxide hydrolase inhibitory activity, which contributes to its effect profile in vivo. *Molecular Cancer Therapeutics* 8:2193-2203.
- Liu KH, Kim MG, Lee DJ, Yoon YJ, Kim MJ, Shon JH, Choi CS, Choi YK, Desta Z, and Shin JG. (2006) Characterization of ebastine, hydroxyebastine, and carebastine metabolism by human liver microsomes and expressed cytochrome P450 enzymes: major roles for CYP2J2 and CYP3A. *Drug Metabolism and Disposition* 34:1793-1797.
- Liu L, Chen C, Gong W, Li Y, Edin ML, Zeldin DC, and Wang DW. (2011) Epoxyeicosatrienoic acids attenuate reactive oxygen species level, mitochondrial dysfunction, caspase activation, and apoptosis in carcinoma cells treated with arsenic trioxide. *Journal of Pharmacology and Experimental Therapy* 339:451-463.
- Liu W, Wang T, He X, Liu X, Wang B, Liu Y, Li Z, Tan R, Ding C, Wang H, and Zeng H. (2016) CYP2J2 Overexpression Increases EETs and Protects Against HFD-Induced Atherosclerosis in ApoE^{-/-} Mice. *Journal of Cardiovascular Pharmacology* 67:491-502.
- Lob V, Geisler T, Brischwein M, Uhl R, and Wolf B. (2007) Automated live cell screening system based on a 24-well-microplate with integrated micro fluidics. *Medical and Biological Engineering and Computing* 45:1023-1028.
- Lu HR, Hermans AN, and Gallacher DJ. (2012) Does terfenadine-induced ventricular tachycardia/fibrillation directly relate to its QT prolongation and Torsades de Pointes? *British Journal of Pharmacology* 166:1490-1502.

- Lundy SD, Zhu W, Regnier M, and Laflamme MA. (2013) Structural and functional maturation of cardiomyocytes derived from human pluripotent stem cells. *Stem Cells and Development* 22:1991-2002.
- Ma B, Xiong X, Chen C, Li H, Xu X, Li X, Li R, Chen G, Dackor RT, and Zeldin DC. (2013) Cardiac-specific overexpression of CYP2J2 attenuates diabetic cardiomyopathy in male streptozotocin-induced diabetic mice. *Endocrinology* 154:2843-2856.
- Maayah ZH, Ansari MA, El Gendy MA, Al-Arifi MN, and Korashy HM. (2014) Development of cardiac hypertrophy by sunitinib in vivo and in vitro rat cardiomyocytes is influenced by the aryl hydrocarbon receptor signaling pathway. *Archives of Toxicology* 88:725-738.
- Maayah ZH, Abdelhamid G, Elshenawy OH, El-Sherbeni AA, Althurwi HN, McGinn E, Dawood D, Alammari AH, and El-Kadi AO. (2018) The Role of Soluble Epoxide Hydrolase Enzyme on Daunorubicin-Mediated Cardiotoxicity. *Cardiovascular Toxicology* 18:268-283.
- Maillet A, Tan K, Chai X, Sadananda SN, Mehta A, Ooi J, Hayden MR, Pouladi MA, Ghosh S, and Shim W. (2016) Modeling doxorubicin-induced cardiotoxicity in human pluripotent stem cell derived-cardiomyocytes. *Scientific Reports* 6:25333.
- Marden NY, Fiala-Beer E, Xiang SH, and Murray M. (2003) Role of activator protein-1 in the down-regulation of the human CYP2J2 gene in hypoxia. *Biochemical Journal* 373:669-680.
- Maresh JG, Xu H, Jiang N, Gairola CG, and Shoheit RV. (2005) Tobacco smoke dysregulates endothelial vasoregulatory transcripts in vivo. *Physiological Genomics* 21:308-313.
- Mark-Kappeler CJ, Martin DS, and Eyster KM. (2011) Estrogens and selective estrogen receptor modulators regulate gene and protein expression in the mesenteric arteries. *Vascular Pharmacology* 55:42-49.
- Matsumoto S and Yamazoe Y. (2001) Involvement of multiple human cytochromes P450 in the liver microsomal metabolism of astemizole and a comparison with terfenadine. *British Journal of Clinical Pharmacology* 51:133-142.
- Matsumoto S, Hirama T, Matsubara T, Nagata K, and Yamazoe Y. (2002) Involvement of CYP2J2 on the intestinal first-pass metabolism of antihistamine drug, astemizole. *Drug Metabolism and Disposition* 30:1240-1245.
- Meliton AY, Muñoz NM, Meliton LN, Birukova AA, Leff AR, and Birukov KG. (2013) Mechanical induction of group V phospholipase A2 causes lung inflammation and acute lung injury. *American Journal of Physiology-Lung Cellular and Molecular Physiology* 304:L689-L700.
- Menkes DB and Knight JC. (2002) Cardiotoxicity and prescription of thioridazine in New Zealand. *Australian and New Zealand Journal of Psychiatry* 36:492-498.

- Merabet N, Bellien J, Glevarec E, Nicol L, Lucas D, Remy-Jouet I, Bounoure F, Dreano Y, Wecker D, and Thuillez C. (2012) Soluble epoxide hydrolase inhibition improves myocardial perfusion and function in experimental heart failure. *Journal of Molecular Cell Cardiology* 52:660-666.
- Mercurio G, Cadeddu C, Piras A, Dessi M, Madeddu C, Deidda M, Serpe R, Massa E, and Mantovani G. (2007) Early epirubicin-induced myocardial dysfunction revealed by serial tissue Doppler echocardiography: correlation with inflammatory and oxidative stress markers. *Oncologist* 12:1124-1133.
- Merkel MJ, Liu L, Cao Z, Packwood W, Young J, Alkayed NJ, and Van Winkle DM. (2009) Inhibition of soluble epoxide hydrolase preserves cardiomyocytes: role of STAT3 signaling. *American Journal of Physiology-Heart and Circulatory Physiology* 298:H679-H687.
- Michaels S and Wang MZ. (2014) The revised human liver cytochrome P450 "Pie": absolute protein quantification of CYP4F and CYP3A enzymes using targeted quantitative proteomics. *Drug Metabolism and Disposition* 42:1241-1251.
- Michaud V, Frappier M, Dumas M, and Turgeon J. (2010) Metabolic activity and mRNA levels of human cardiac CYP450s involved in drug metabolism. *PLoS one* 5:e15666.
- Minotti G. (2010) *Cardiotoxicity of Non-Cardiovascular Drugs* John Wiley & Sons.
- Mitra R, Guo Z, Milani M, Mesaros C, Rodriguez M, Nguyen J, Luo X, Clarke D, Lamba J, Schuetz E, Donner DB, Puli N, Falck JR, Capdevila J, Gupta K, Blair IA, and Potter DA. (2011) CYP3A4 mediates growth of estrogen receptor-positive breast cancer cells in part by inducing nuclear translocation of phospho-Stat3 through biosynthesis of (+/-)-14,15-epoxyeicosatrienoic acid (EET). *Journal of Biological Chemistry* 286:17543-17559.
- Miyata N, Seki T, Tanaka Y, Omura T, Taniguchi K, Doi M, Bandou K, Kametani S, Sato M, Okuyama S, Cambj-Sapunar L, Harder DR, and Roman RJ. (2005) Beneficial effects of a new 20-hydroxyeicosatetraenoic acid synthesis inhibitor, TS-011 [N-(3-chloro-4-morpholin-4-yl) phenyl-N'-hydroxyimido formamide], on hemorrhagic and ischemic stroke. *Journal of Pharmacology and Experimental Therapy* 314:77-85.
- Monti J, Fischer J, Paskas S, Heinig M, Schulz H, Gösele C, Heuser A, Fischer R, Schmidt C, and Schirdewan A. (2008) Soluble epoxide hydrolase is a susceptibility factor for heart failure in a rat model of human disease. *Nature Genetics* 40:529.
- Mozaffarian D and Wu JH. (2011) Omega-3 fatty acids and cardiovascular disease: effects on risk factors, molecular pathways, and clinical events. *Journal of American College of Cardiology* 58:2047-2067.
- Murakami M, Shimbara S, Kambe T, Kuwata H, Winstead MV, Tischfield JA, and Kudo I. (1998) The functions of five distinct mammalian phospholipase A2S in regulating arachidonic acid release. Type IIa and type V secretory phospholipase A2S

are functionally redundant and act in concert with cytosolic phospholipase A2. *Journal of Biological Chemistry* 273:14411-14423.

Narjoz C, Favre A, McMullen J, Kiehl P, Montemurro M, Figg WD, Beaune P, de Waziers I, and Rochat B. (2014) Important role of CYP2J2 in protein kinase inhibitor degradation: A possible role in intratumor drug disposition and resistance. *PLoS one* 9:e95532.

Nayeem MA, Zeldin DC, Boegehold MA, and Falck JR. (2011) Salt modulates vascular response through adenosine A2A receptor in eNOS-null mice: role of CYP450 epoxygenase and soluble epoxide hydrolase. *Molecular Cell Biochemistry* 350:101-111.

Nebert DW, Wikvall K, and Miller WL. (2013) Human cytochromes P450 in health and disease. *Philosophical Transactions of the Royal Society B: Biological Sciences* 368:20120431.

Nelson DR. (2009) The cytochrome p450 homepage. *Human Genomics* 4:59.

Nelson DR, Zeldin DC, Hoffman SM, Maltais LJ, Wain HM, and Nebert DW. (2004) Comparison of cytochrome P450 (CYP) genes from the mouse and human genomes, including nomenclature recommendations for genes, pseudogenes and alternative-splice variants. *Pharmacogenetics and Genomics* 14:1-18.

Newman JW, Morisseau C, and Hammock BD. (2005) Epoxide hydrolases: their roles and interactions with lipid metabolism. *Progress in Lipid Research* 44:1-51.

Nishimuta H, Sato K, Mizuki Y, Yabuki M, and Komuro S. (2011) Species differences in intestinal metabolic activities of cytochrome P450 isoforms between cynomolgus monkeys and humans. *Drug Metabolism and Pharmacokinetics* 26:300-306.

Nodari S, Triggiani M, Campia U, Manerba A, Milesi G, Cesana BM, Gheorghide M, and Dei Cas L. (2011) Effects of n-3 polyunsaturated fatty acids on left ventricular function and functional capacity in patients with dilated cardiomyopathy. *Journal of American College of Cardiology* 57:870-879.

Node K, Huo Y, Ruan X, Yang B, Spiecker M, Ley K, Zeldin DC, and Liao JK. (1999) Anti-inflammatory properties of cytochrome P450 epoxygenase-derived eicosanoids. *Science* 285:1276-1279.

Octavia Y, Tocchetti CG, Gabrielson KL, Janssens S, Crijns HJ, and Moens AL. (2012) Doxorubicin-induced cardiomyopathy: from molecular mechanisms to therapeutic strategies. *Journal of Molecular Cell Cardiology* 52:1213-1225.

Oldroyd KG, Berry C, and Bartunek J. (2012) Myocardial repair and regeneration: bone marrow or cardiac stem cells? *Molecular Therapy* 20:1102-1105.

Om P. (2018) Substrate selective synthesis of indole, tetrahydroquinoline and quinoline derivatives via intramolecular addition of hydrazones and imines. *Organic Chemistry Frontiers* 5:1170-1175.

Paige SL, Osugi T, Afanasiev OK, Pabon L, Reinecke H, and Murry CE. (2010) Endogenous Wnt/ β -catenin signaling is required for cardiac differentiation in human embryonic stem cells. *PloS one* 5:e11134.

Paine MF, Hart HL, Ludington SS, Haining RL, Rettie AE, and Zeldin DC. (2006) The human intestinal cytochrome P450 "pie". *Drug Metabolism and Disposition* 34:880-886.

Palomo L, Mleczko JE, Azkargorta M, Conde- Vancells J, González E, Elortza F, Royo F, and Falcon- Perez JM. (2018) Abundance of Cytochromes in Hepatic Extracellular Vesicles Is Altered by Drugs Related With Drug- Induced Liver Injury. *Hepatology Communications*.

Pegtel DM, Cosmopoulos K, Thorley-Lawson DA, van Eijndhoven MA, Hopmans ES, Lindenberg JL, de Gruijl TD, Wurdinger T, and Middeldorp JM. (2010) Functional delivery of viral miRNAs via exosomes. *Proc Natl Acad Sci U S A* 107:6328-6333.

Piccini JP, Hasselblad V, Peterson ED, Washam JB, Califf RM, and Kong DF. (2009) Comparative efficacy of dronedarone and amiodarone for the maintenance of sinus rhythm in patients with atrial fibrillation. *Journal of American College of Cardiology* 54:1089-1095.

Pointon A, Abi-Gerges N, Cross MJ, and Sidaway JE. (2013) Phenotypic profiling of structural cardiotoxins in vitro reveals dependency on multiple mechanisms of toxicity. *Toxicological Sciences* 132:317-326.

Porter AG and Jänicke RU. (1999) Emerging roles of caspase-3 in apoptosis. *Cell Death and Differentiation* 6:99.

Potente M, Fisslthaler B, Busse R, and Fleming I. (2003) 11,12-Epoxyeicosatrienoic acid-induced inhibition of FOXO factors promotes endothelial proliferation by down-regulating p27Kip1. *Journal of Biological Chemistry* 278:29619-29625.

Preissner SC, Hoffmann MF, Preissner R, Dunkel M, Gewiess A, and Preissner S. (2013) Polymorphic cytochrome P450 enzymes (CYPs) and their role in personalized therapy. *PloS one* 8:e82562.

Redfern W, Ewart L, Hammond T, Bialecki R, Kinter L, Lindgren S, Pollard C, Roberts R, Rolf M, and Valentin J. (2010) Impact and frequency of different toxicities throughout the pharmaceutical life cycle. *Toxicologist* 114:1081.

Reed DR. (2008) Animal models of gene–nutrient interactions. *Obesity* 16:S23-S27.

Rezzani R, Giugno L, Buffoli B, Bonomini F, and Bianchi R. (2005) The protective effect of caffeic acid phenethyl ester against cyclosporine A-induced cardiotoxicity in rats. *Toxicology* 212:155-164.

Rodriguez-Antona C, Donato M, Boobis A, Edwards R, Watts P, Castell JV, and Gómez-Lechón M. (2002) Cytochrome P450 expression in human hepatocytes and

hepatoma cell lines: molecular mechanisms that determine lower expression in cultured cells. *Xenobiotica* 32:505-520.

Roman RJ. (2002) P-450 metabolites of arachidonic acid in the control of cardiovascular function. *Physiology Reviews* 82:131-185.

Saegusa K, Furukawa Y, Akahane K, Haniuda M, and Chiba S. (1991) Anti-nicotinic and anti-muscarinic actions of eperisone in the isolated canine atrium. *The Japanese Journal of Pharmacology* 56:187-193.

Senes-Lopes TF, López JA, do Amaral VS, Brandao-Neto J, de Rezende AA, da Luz, Jefferson Romáryo Duarte, Guterres Zdr, and Almeida MdG. (2018) Genotoxicity of *Turnera subulata* and *Spondias mombin* × *Spondias tuberosa* Extracts from Brazilian Caatinga Biome. *Journal of Medicinal Food* 21:372-379.

Seubert J, Yang B, Bradbury JA, Graves J, Degraff LM, Gabel S, Gooch R, Foley J, Newman J, Mao L, Rockman HA, Hammock BD, Murphy E, and Zeldin DC. (2004) Enhanced postischemic functional recovery in CYP2J2 transgenic hearts involves mitochondrial ATP-sensitive K⁺ channels and p42/p44 MAPK pathway. *Circulatory Research* 95:506-514.

Seubert JM, Sinal CJ, Graves J, DeGraff LM, Bradbury JA, Lee CR, Goralski K, Carey MA, Luria A, Newman JW, Hammock BD, Falck JR, Roberts H, Rockman HA, Murphy E, and Zeldin DC. (2006) Role of soluble epoxide hydrolase in postischemic recovery of heart contractile function. *Circulatory Research* 99:442-450.

Shen L, Peng H, Peng R, Fan Q, Zhao S, Xu D, Morisseau C, Chiamvimonvat N, and Hammock BD. (2015) Inhibition of soluble epoxide hydrolase in mice promotes reverse cholesterol transport and regression of atherosclerosis. *Atherosclerosis* 239:557-565.

Sidorik L, Kyyamova R, Bobyk V, Kapustian L, Rozhko O, Vigontina O, Ryabenko D, Danko I, Maksymchuk O, and Kovalenko V. (2005) Molecular chaperone, HSP60, and cytochrome P450 2E1 co-expression in dilated cardiomyopathy. *Cell Biology International* 29:51-55.

Skog J, Würdinger T, Van Rijn S, Meijer DH, Gainche L, Curry Jr WT, Carter BS, Krichevsky AM, and Breakefield XO. (2008) Glioblastoma microvesicles transport RNA and proteins that promote tumour growth and provide diagnostic biomarkers. *Nature Cell Biology* 10:1470.

Solanki M, Pointon A, Jones B, and Herbert K. (2018) Cytochrome P450 2J2: Potential Role in Drug Metabolism and Cardiotoxicity. *Drug Metabolism and Disposition* 46:1053-1065.

Spector AA, Fang X, Snyder GD, and Weintraub NL. (2004) Epoxyeicosatrienoic acids (EETs): metabolism and biochemical function. *Progress in Lipid Research* 43:55-90.

Spector AA and Norris AW. (2007) Action of epoxyeicosatrienoic acids on cellular function. *American Journal of Physiology and Cell Physiology* 292:C996-1012.

- Spiecker M, Darius H, Hankeln T, Soufi M, Sattler AM, Schaefer JR, Node K, Borgel J, Mugge A, Lindpaintner K, Huesing A, Maisch B, Zeldin DC, and Liao JK. (2004) Risk of coronary artery disease associated with polymorphism of the cytochrome P450 epoxygenase CYP2J2. *Circulation* 110:2132-2136.
- Stranska R, Gysbrechts L, Wouters J, Vermeersch P, Bloch K, Dierickx D, Andrei G, and Snoeck R. (2018) Comparison of membrane affinity-based method with size-exclusion chromatography for isolation of exosome-like vesicles from human plasma. *Journal of Translational Medicine* 16:1.
- Sudhahar V, Shaw S, and Imig JD. (2010) Epoxyeicosatrienoic acid analogs and vascular function. *Current Medical Chemistry* 17:1181-1190.
- Sura P, Sura R, EnayetAllah AE, and Grant DF. (2008) Distribution and expression of soluble epoxide hydrolase in human brain. *Journal of Histochemistry & Cytochemistry* 56:551-559.
- Takemura G and Fujiwara H. (2007) Doxorubicin-induced cardiomyopathy: from the cardiotoxic mechanisms to management. *Progress in Cardiovascular Diseases* 49:330-352.
- Tan FL, Moravec CS, Li J, Apperson-Hansen C, McCarthy PM, Young JB, and Bond M. (2002) The gene expression fingerprint of human heart failure. *PNAS U S A* 99:11387-11392.
- Tang Z, Salamanca-Pinzón SG, Wu Z, Xiao Y, and Guengerich FP. (2010) Human cytochrome P450 4F11: heterologous expression in bacteria, purification, and characterization of catalytic function. *Archives of Biochemistry and Biophysics* 494:86-93.
- Taniyama Y and Griendling KK. (2003) Reactive oxygen species in the vasculature: molecular and cellular mechanisms. *Hypertension* 42:1075-1081.
- Theken KN, Schuck RN, Edin ML, Tran B, Ellis K, Bass A, Lih FB, Tomer KB, Poloyac SM, and Wu MC. (2012) Evaluation of cytochrome P450-derived eicosanoids in humans with stable atherosclerotic cardiovascular disease. *Atherosclerosis* 222:530-536.
- THUM T and BORLAK J. (2002) Testosterone, cytochrome P450, and cardiac hypertrophy. *The FASEB Journal* 16:1537-1549.
- Tijssen AJ, Creemers EE, Moerland PD, de Windt LJ, van der Wal, Allard C, Kok WE, and Pinto YM. (2010) MiR423-5p as a circulating biomarker for heart failure. *Circulatory Research* 106:1035.
- Tushuizen ME, Diamant M, Sturk A, and Nieuwland R. (2011) Cell-derived microparticles in the pathogenesis of cardiovascular disease: friend or foe? *Arteriosclerosis, Thrombosis and Vascular Biology* 31:4-9.

- Uehara S, Uno Y, Inoue T, Okamoto E, Sasaki E, and Yamazaki H. (2016) Marmoset cytochrome P450 2J2 mainly expressed in small intestines and livers effectively metabolizes human P450 2J2 probe substrates, astemizole and terfenadine. *Xenobiotica* 46:977-985.
- Uehara S, Murayama N, Nakanishi Y, Nakamura C, Hashizume T, Zeldin DC, Yamazaki H, and Uno Y. (2015) Immunochemical quantification of cynomolgus CYP2J2, CYP4A and CYP4F enzymes in liver and small intestine. *Xenobiotica* 45:124-130.
- Uno Y, Hosaka S, Matsuno K, Nakamura C, Kito G, Kamataki T, and Nagata R. (2007) Characterization of cynomolgus monkey cytochrome P450 (CYP) cDNAs: Is CYP2C76 the only monkey-specific CYP gene responsible for species differences in drug metabolism? *Archives of Biochemistry and Biophysics* 466:98-105.
- Uraizee I, Cheng S, and Moslehi J. (2011) Reversible cardiomyopathy associated with sunitinib and sorafenib. *New England Journal of Medicine* 365:1649-1650.
- Valadi H, Ekström K, Bossios A, Sjöstrand M, Lee JJ, and Lötvall JO. (2007) Exosome-mediated transfer of mRNAs and microRNAs is a novel mechanism of genetic exchange between cells. *Nature Cell Biology* 9:654.
- van der Pol E, Boing AN, Harrison P, Sturk A, and Nieuwland R. (2012) Classification, functions, and clinical relevance of extracellular vesicles. *Pharmacology Reviews* 64:676-705.
- VanAlstine MA and Hough LB. (2011) Effects of acetylenic epoxygenase inhibitors on recombinant cytochrome p450s. *Drug Metabolism and Disposition* 39:1221-1226.
- Virkel G, Lifschitz A, Sallovitz J, Pis A, and Lanusse C. (2004) Comparative hepatic and extrahepatic enantioselective sulfoxidation of albendazole and fenbendazole in sheep and cattle. *Drug Metabolism and Disposition* 32:536-544.
- Wang B, Zeng H, Wen Z, Chen C, and Wang DW. (2016) CYP 2J2 and its metabolites (epoxyeicosatrienoic acids) attenuate cardiac hypertrophy by activating AMPK α 2 and enhancing nuclear translocation of Akt1. *Aging Cell* 15:940-952.
- Wang C, Hung W, Yu T, Chiu C, Lu L, Chung F, Hung C, Shin S, Chen H, and Lee Y. (2010) Genetic variation in the G-50T polymorphism of the cytochrome P450 epoxygenase CYP2J2 gene and the risk of younger onset type 2 diabetes among Chinese population: potential interaction with body mass index and family history. *Experimental and Clinical Endocrinology & Diabetes* 118:346-352.
- Wang H, Zhang D, Zeng X, Mu J, Yang H, Lu L, and Zhang L. (2012) Upregulation of cytochrome P450 2J3/11, 12-epoxyeicosatrienoic acid inhibits apoptosis in neonatal rat cardiomyocytes by a caspase-dependent pathway. *Cytokine* 60:360-368.
- Wang W, Shi Q, Mattes WB, Mendrick DL, and Yang X. (2015) Translating extracellular microRNA into clinical biomarkers for drug-induced toxicity: from high-throughput profiling to validation. *Biomarkers in Medicine* 9:1177-1188.

Wang SY, Xing PF, Zhang CY, and Deng BQ. (2017) Association of CYP2J2 gene polymorphisms with ischemic stroke and stroke subtypes in Chinese population. *Medicine (Baltimore)* 96:e6266.

Wang X, Ni L, Yang L, Duan Q, Chen C, Edin ML, Zeldin DC, and Wang DW. (2014) CYP2J2-derived epoxyeicosatrienoic acids suppress endoplasmic reticulum stress in heart failure. *Molecular Pharmacology* 85:105-115.

Wen Y, Zhang X, and Yang S. (2010) Microplate- reader compatible perfusion microbioreactor array for modular tissue culture and cytotoxicity assays. *Biotechnology Progress* 26:1135-1144.

Wilkening S, Stahl F, and Bader A. (2003) Comparison of primary human hepatocytes and hepatoma cell line Hepg2 with regard to their biotransformation properties. *Drug Metabolism and Disposition* 31:1035-1042.

Wray JA, Sugden MC, Zeldin DC, Greenwood GK, Samsuddin S, Miller-Degraff L, Bradbury JA, Holness MJ, Warner TD, and Bishop-Bailey D. (2009) The epoxygenases CYP2J2 activates the nuclear receptor PPAR α in vitro and in vivo. *PloS one* 4:e7421.

Wu M, Huang S, and Lee G. (2010) Microfluidic cell culture systems for drug research. *Lab on a Chip* 10:939-956.

Wu S, Zhang Y, Gardner CO, Chen Q, Li Y, Wang G, Gao P, and Zhu D. (2007) Evidence for association of polymorphisms in CYP2J2 and susceptibility to essential hypertension. *Annals of Human Genetics* 71:519-525.

Wu S, Moomaw CR, Tomer KB, Falck JR, and Zeldin DC. (1996) Molecular cloning and expression of CYP2J2, a human cytochrome P450 arachidonic acid epoxygenase highly expressed in heart. *Journal of Biological Chemistry* 271:3460-3468.

Wu S, Chen W, Murphy E, Gabel S, Tomer KB, Foley J, Steenbergen C, Falck JR, Moomaw CR, and Zeldin DC. (1997) Molecular cloning, expression, and functional significance of a cytochrome P450 highly expressed in rat heart myocytes. *Journal of Biological Chemistry* 272:12551-12559.

Wu Z, Lee D, Joo J, Shin JH, Kang W, Oh S, Lee do Y, Lee SJ, Yea SS, Lee HS, Lee T, and Liu KH. (2013) CYP2J2 and CYP2C19 are the major enzymes responsible for metabolism of albendazole and fenbendazole in human liver microsomes and recombinant P450 assay systems. *Antimicrobial Agents and Chemotherapy* 57:5448-5456.

Xiao S, Zhang J, Liu M, Iwahata H, Rogers HB, and Woodruff TK. (2017) Doxorubicin has dose-dependent toxicity on mouse ovarian follicle development, hormone secretion, and oocyte maturation. *Toxicological Sciences* 157:320-329.

Xie F, Ding X, and Zhang Q. (2016) An update on the role of intestinal cytochrome P450 enzymes in drug disposition. *Acta Pharmaceutica Sinica B* 6:374-383.

- Xu M, Ju W, Hao H, Wang G, and Li P. (2013) Cytochrome P450 2J2: distribution, function, regulation, genetic polymorphisms and clinical significance. *Drug Metabolism Reviews* 45:311-352.
- Xu X, Zhang XA, and Wang DW. (2011) The roles of CYP450 epoxygenases and metabolites, epoxyeicosatrienoic acids, in cardiovascular and malignant diseases. *Advances in Drug Delivery Reviews* 63:597-609.
- Xu D, Li N, He Y, Timofeyev V, Lu L, Tsai HJ, Kim IH, Tuteja D, Mateo RK, Singapuri A, Davis BB, Low R, Hammock BD, and Chiamvimonvat N. (2006) Prevention and reversal of cardiac hypertrophy by soluble epoxide hydrolase inhibitors. *PNAS U S A* 103:18733-18738.
- Yamagiwa T, Morita S, Amino M, Miura N, Saito T, and Inokuchi S. (2014) Serum concentration of eperisone hydrochloride correlates with QT interval. *American Journal of Emergency Medicine* 32:75-77.
- Yan H, Kong Y, He B, Huang M, Li J, Zheng J, Liang L, Bi J, Zhao S, and Shi L. (2015) CYP2J2 rs890293 polymorphism is associated with susceptibility to Alzheimer's disease in the Chinese Han population. *Neuroscience Letters* 593:56-60.
- Yáñez-Mó M, Siljander PR, Andreu Z, Bedina Zavec A, Borràs FE, Buzas EI, Buzas K, Casal E, Cappello F, and Carvalho J. (2015) Biological properties of extracellular vesicles and their physiological functions. *Journal of Extracellular Vesicles* 4:27066.
- Yang L, Ni L, Duan Q, Wang X, Chen C, Chen S, Chaugai S, Zeldin D, Tang JR, and Wang DW. (2015) CYP epoxygenase 2J2 prevents cardiac fibrosis by suppression of transmission of pro-inflammation from cardiomyocytes to macrophages. *Prostaglandins and Other Lipid Mediators* 116:64-75.
- Yang S, Wei S, Pozzi A, and Capdevila JH. (2009) The arachidonic acid epoxygenase is a component of the signaling mechanisms responsible for VEGF-stimulated angiogenesis. *Archives in Biochemistry and Biophysics* 489:82-91.
- Yang L, Cheriyan J, Gutterman DD, Mayer RJ, Ament Z, Griffin JL, Lazaar AL, Newby DE, Tal-Singer R, and Wilkinson IB. (2017) Mechanisms of Vascular Dysfunction in COPD and Effects of a Novel Soluble Epoxide Hydrolase Inhibitor in Smokers. *Chest* 151:555-563.
- Yang ST, Zhang X, and Wen Y. (2008) Microbioreactors for high-throughput cytotoxicity assays. *Current Opinion in Drug Discovery and Development* 11:111-127.
- Yarana C, Carroll D, Chen J, Chaiswing L, Zhao Y, Noel T, Alstott M, Bae Y, Dressler EV, and Moscow JA. (2017) Extracellular vesicles released by cardiomyocytes in a doxorubicin-induced cardiac injury mouse model contain protein biomarkers of early cardiac injury. *Clinical Cancer Research*. 2046.2017.
- Yeh ET, Tong AT, Lenihan DJ, Yusuf SW, Swafford J, Champion C, Durand JB, Gibbs H, Zafarmand AA, and Ewer MS. (2004) Cardiovascular complications of cancer therapy: diagnosis, pathogenesis, and management. *Circulation* 109:3122-3131.

- Zang R, Li D, Tang I, Wang J, and Yang S. (2012) Cell-based assays in high-throughput screening for drug discovery. *International Journal of Biotechnology for Wellness Industries* 1:31-51.
- Zanger UM and Schwab M. (2013) Cytochrome P450 enzymes in drug metabolism: regulation of gene expression, enzyme activities, and impact of genetic variation. *Pharmacology Therapeutics* 138:103-141.
- Zeldin DC, Foley J, Boyle JE, Moomaw CR, Tomer KB, Parker C, Steenbergen C, and Wu S. (1997) Predominant expression of an arachidonate epoxygenase in islets of Langerhans cells in human and rat pancreas. *Endocrinology* 138:1338-1346.
- Zeldin D, Wu S, and Ma J. (1997) CYP 2 J subfamily P 450 s: Physiologically relevant hemoproteins active in the metabolism of arachidonic acid in hepatic and extrahepatic tissues. *Reviews in Toxicology* 1:1-32.
- Zeldin DC, Foley J, Ma J, Boyle JE, Pascual JM, Moomaw CR, Tomer KB, Steenbergen C, and Wu S. (1996) CYP2J subfamily P450s in the lung: expression, localization, and potential functional significance. *Molecular Pharmacology* 50:1111-1117.
- Zhang Q, Ding X, and Kaminsky LS. (1997) cDNA cloning, heterologous expression, and characterization of rat intestinal CYP2J4. *Archives of Biochemistry and Biophysics* 340:270-278.
- Zhang D, Lou J, Zhang X, Zhang L, Wang F, Xu D, Niu N, Wang Y, Wu Y, and Cui W. (2017) Hyperhomocysteinemia results from and promotes hepatocellular carcinoma via CYP450 metabolism by CYP2J2 DNA methylation. *Oncotarget* 8:15377-15392.
- Zhang G, Panigrahy D, Hwang SH, Yang J, Mahakian LM, Wettersten HI, Liu JY, Wang Y, Ingham ES, Tam S, Kieran MW, Weiss RH, Ferrara KW, and Hammock BD. (2014) Dual inhibition of cyclooxygenase-2 and soluble epoxide hydrolase synergistically suppresses primary tumor growth and metastasis. *PNAS U S A* 111:11127-11132.
- Zhang LN, Vincelette J, Cheng Y, Mehra U, Chen D, Anandan SK, Gless R, Webb HK, and Wang YX. (2009) Inhibition of soluble epoxide hydrolase attenuated atherosclerosis, abdominal aortic aneurysm formation, and dyslipidemia. *Arteriosclerosis, Thrombosis and Vascular Biology* 29:1265-1270.
- Zhang Y, El-Sikhry H, Chaudhary KR, Batchu SN, Shayeganpour A, Jukar TO, Bradbury JA, Graves JP, DeGraff LM, Myers P, Rouse DC, Foley J, Nyska A, Zeldin DC, and Seubert JM. (2009) Overexpression of CYP2J2 provides protection against doxorubicin-induced cardiotoxicity. *American Journal of Physiology and Heart Circulatory Physiology* 297:H37-46.
- Zhao X, Dey A, Romanko OP, Stepp DW, Wang M, Zhou Y, Jin L, Pollock JS, Webb RC, and Imig JD. (2005) Decreased epoxygenase and increased epoxide hydrolase expression in the mesenteric artery of obese Zucker rats. *American Journal of Physiology-Regulatory, Integrative and Comparative Physiology* 288:R188-R196.

Zhou J, Xu Z, Li N, Zhao Y, Wang Z, and Xiao W. (2016) Identification of cardioprotective agents from traditional Chinese medicine against oxidative damage. *Molecular Medicine Reports* 14:77-88.

Zhou Z, Vorperian VR, Gong Q, Zhang S, and January CT. (1999) Block of HERG potassium channels by the antihistamine astemizole and its metabolites desmethylastemizole and norastemizole. *Journal of Cardiovascular Electrophysiology* 10:836-843.

Zhu Q, Fu Z, Ma Y, Yang H, Huang D, Xie X, Liu F, Zheng Y, and Cha E. (2013) A novel polymorphism of the CYP2J2 gene is associated with coronary artery disease in Uygur population in China. *Clinical Biochemistry* 46:1047-1054.

Zordoky BN and El-Kadi AO. (2008) Induction of several cytochrome P450 genes by doxorubicin in H9c2 cells. *Vascular Pharmacology* 49:166-172.

Zordoky BN, Anwar-Mohamed A, Aboutabl ME, and El-Kadi AO. (2010) Acute doxorubicin cardiotoxicity alters cardiac cytochrome P450 expression and arachidonic acid metabolism in rats. *Toxicology and Applied Pharmacology* 242:38-46.